ROLE OF VIRAL GENETICS IN DENGUE EPIDEMIOLOGICAL FITNESS

GAYATHRI MANOKARAN

B.Science (Hons), Monash University

A THESIS SUBMITTED

FOR THE DEGREE OF DOCTOR OF PHILOSOPHY

DEPARTMENT OF MICROBIOLOGY

YONG LOO LIN SCHOOL OF MEDICINE

NATIONAL UNIVERSITY OF SINGAPORE

2014

DECLARATION

I hereby declare that this thesis is my original work and it has been written by me in its entirety. I have duly acknowledged all the sources of information which have been used in the thesis.

This thesis has also not been submitted for any degree in any university previously.

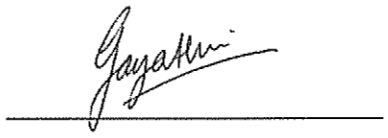

Gayathri Manokaran

11th December 2014

Acknowledgements

I would like to express my heartfelt gratitude to Associate Professor Ooi Eng Eong for his patient guidance, invaluable advice and encouragement throughout my research. His continued support and mentorship significantly aided the progress of the project. I would also like to thank Professor Mariano Garcia-Blanco for his scientific guidance and kind encouragement.

To Professor Duane Gubler: A big thank you for having the hindsight of collecting the clinical isolates used in this study and the generosity to allow me to work with them. My sincere appreciation is also extended to the rest of my thesis advisory committee, Professor David Virshup, Assistant Professor Manoj Krishnan and Professor Naoki Yamamoto for the stimulating discussions and critical suggestions during my research.

Special thanks to Esteban Finol, Eugenia Ong, Justin Bahl, Dr Alex Ward, Dr Katell Bidet, Tan Hwee Cheng and Summer Zhang for providing technical assistance and support in my research. And not forgetting colleagues from Duke-NUS who have made this a very conducive environment for scientific research.

Lastly, I would like to thank my mum, dad, sister and dog for their love, encouragement and support all these years. This work would not have been possible without them. “The more I study science, the more I believe in God” – Albert Einstein. With that, I’ll like to extend a final thank you to God for His continued presence throughout these grueling PhD years.

Table of Contents

Summary

The staggeringly large number of dengue virus (DENV) infections around the globe has led to increasing viral genetic diversity, some of which appears to be associated with greater epidemic potential. The underlying mechanisms of viral fitness in an epidemiological setting, however, remain poorly defined. We conducted *in vitro* studies and identified a determinant of fitness in a foreign dominant (PR-2B) DENV-2 clade, which emerged during the 1994 epidemic in Puerto Rico and replaced an endemic (PR-1) DENV-2 clade. The PR-2B DENV-2 produced increased levels of subgenomic relative to genomic RNA during replication. The subgenomic RNA bound and inhibited de-ubiquitylation of tripartite motif 25 (TRIM25), which is needed to activate its E3 ligase activity critical for sustained and amplified RIG-I induced type-I interferon expression. Our findings demonstrate a unique viral RNA-host protein interaction to evade the innate immune response for increased epidemiological fitness.

List of Tables

List of Figures

List of Abbreviations

ADE	Antibody-dependent enhancement
AP-1	Activating protein 1
ATCC	American Type Culture Collection
BSA	Bovine serum albumin
C	Capsid
CDC	Centers for Disease Control and Prevention
CVD	ChimeriVax-DENV
DALYs	Disability-adjusted life years
DC-SIGN	Dendritic cell-specific intercellular adhesion molecule-3-grabbing non-integrin
DENV	Dengue virus
E	Envelope
ER	Endoplasmic reticulum
FcγR	Fragment crystallisable receptors
GAPDH	Glyceraldehyde-3-phosphate dehydrogenase
gRNA	Genomic RNA

HRP	Horseradish peroxidase
IFIT	Interferon induced proteins with tetratricopeptide repeats
IFITM	Interferon-induced transmembrane protein
IFN	Interferon
IFNα	Interferon alpha
IFNβ	Interferon beta
IFNγ	Interferon gamma
IFNAR	IFN-α/β receptor
IgG	Immunoglobulin G
IgM	Immunoglobulin M
IKK	IκB kinase
IL	Interleukin
IRF	Interferon-regulatory factor
ISG	Interferon stimulated genes
ISRE	IFN-stimulated response elements
JAK	Janus kinase

JEV	Japanese encephalitis virus
KUNV	Kunjin virus
LAV	Live attenuated viruses
LILRB-1	Leukocyte Ig-like receptor-B1
LIV	Louping ill virus
M	Membrane
MDA5	Melanoma Differentiation-Associated protein 5
min	Minutes
MOI	Multiplicity of infection
MVEV	Murray valley encephalitis virus
MMLV	Montana myotis leukoencephalitis virus
MODV	Modoc virus
ORF	Open reading frame
PB	Processing bodies
PBMC	Peripheral blood mononuclear cells
PBS	Phosphate buffered solution
PKR	Protein kinase R

polyIC	Polyinosinic-polycytidylic acid
prM	Premembrane
PRNT	Plaque reduction neutralization test
miRNA	MicroRNA
NEMO	NFκB essential modulator
NHG	National Healthcare Group
NKV	Viruses with no known vector
nm	Nanometers
NS	Non-structural
PBMC	Peripheral blood mononuclear cells
PBS	Phosphate-buffered saline
PBS-T	PBS in 0.05% Tween 20
pfu	Plaque forming units
pfu/ml	Plaque forming units per ml
PKR	Double-stranded RNA activated protein kinase
PRR	Pattern recognition receptors
PVDF	Polyvinylidene fluoride

qRT-PCR	Quantitative Real-time quantitative PCR
RdRp	RNA-dependent RNA polymerase
RNA	Ribonucleic acid
RNAi	RNA interference
RIG-I	Retinoic acid-inducible gene
RIP	RNA- immunoprecipitation
RISC	RNA-induced silencing complex
SDS-PAGE	Sodium dodecyl sulfate polyacrylamide gel electrophoresis
sfRNA	Subgenomic flavivirus RNA
SH	Shimodaira-Hasegawa
SILAC	Stable isotope labeling by amino acids in cell culture
siRNA	Small interfering RNA
SL	Stemloop
STAT	Signal transducer and activator of transcription
Syk	Spleen tyrosine kinase
TANK	TRAF family member-associated NFκB activator

TAK1	Transforming growth factor beta-activated kinase
TBEV	Tick-borne encephalitis virus
TBK-1	TANK-binding kinase
TLR	Toll-like receptor
TRAF	Tumour Necrosis Factor (TNF)-receptor-associated factors
TRIF	TIR-domain-containing adapter-inducing interferon β
TRIM	Tripartite motif
Tyk	Tyrosine kinase
UB	Ubiquitin
μm	micrometers
μl	microlitres
USP15	Ubiquitin-specific peptidase 15
UTR	Untranslated region
WHO	World Health Organization
WNV	West Nile virus
YFV	Yellow fever virus

List of Publications

Manuscript in Review

Manokaran, G., Finol, E., Wang, C.L., Gunaratne, J., Bahl, J., Ong, E.Z., Tan, H.C., Sessions, O.M., Ward, A.M., Gubler, D.J., Harris, E., Garcia-Blanco, M.A., and Ooi, E.E. Subgenomic RNA of dengue-2 virus binds tripartite motif 25 protein to inhibit interferon expression providing a mechanism for epidemiological fitness.

Previous Publications

Manokaran, G., Lin, Y.N., Soh, M.L., Lim, E.A., Lim, C.W., and Tan, B.H. (2008). Detection of porcine circovirus type 2 in pigs imported from Indonesia. Vet Microbiol *132*, 165-170.

CHAPTER 1:

An Introduction to the role of viral genetics in dengue epidemiological fitness.

1.1 Dengue Virus

1.1.1 Virus Structure and genome organization

Dengue virus (DENV) is a member of the genus *Flavivirus* within the family *Flaviviridae* (Lindenbach, 2007). Flaviviruses are enveloped, positive single-stranded RNA viruses that replicate in the cytoplasm of arthropods and infected mammalian cells (Lindenbach, 2007). This genus can be subdivided into three groups, namely (1) mosquito-borne (2) tick-borne and (3) viruses with no known vector (NKV) (Figure 1.1) (Charlier et al., 2004; Lindenbach, 2007). Many clinically important viruses such as the yellow fever virus (YFV), Japanese encephalitis virus (JEV), tick-borne encephalitis virus (TBEV) and the West Nile virus (WNV) belong to *Flavivirus* (Figure 1.1) (Charlier et al., 2004; D.J. Gubler, 2007; St John et al., 2013).

A

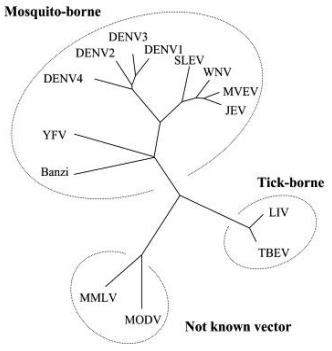

Charlier et. al., 2004

B

Flavivirus species	Prominent pathologies during human infection
Dengue virus (DENV1–DENV4)	Fever–arthralgia–rash syndrome, plasma leakage, haemorrhage and severe disease associated with organ failure All four serotypes can cause a spectrum of illness ranging from asymptomatic to severe and fatal disease, as determined by a complex interaction of the virus with the innate immune response of the individual host; the strain of virus, the previous infection history and age of the host, and host genetics all influence disease severity.
Yellow fever virus	Fever, nausea, abdominal pain, jaundice and haemorrhage
West Nile virus	Fever, myalgia, encephalitis and long-term neurological defects
Japanese encephalitis virus	Fever, encephalitis and long-term neurological defects
Tick-borne encephalitis virus	Meningitis, encephalitis, mild fever and long-term neurological defects

St John et. al., 2013

Figure 1.1 Flaviviruses and medically important viruses within the genus (A) Phylogenetic tree displaying the subgroups among Flavivirus. DENV: dengue virus; WNV: west nile virus; MVEV: murray valley encephalitis virus; JEV: japanese encephalitis virus; YFV: yellow fever virus; LIV: louping ill virus; TBEV: tick-borne encephalitis virus; MMLV: montana myotis leukoencephalitis virus; MODV: modoc virus (B) Clinical manifestations during infection.

Among the flaviviruses, DENV is one of the most prevalent causing an estimated 390 million infections annually and with over 3 billion people at risk (Figure 1.2) (Bhatt et al., 2013; Gubler, 2002).

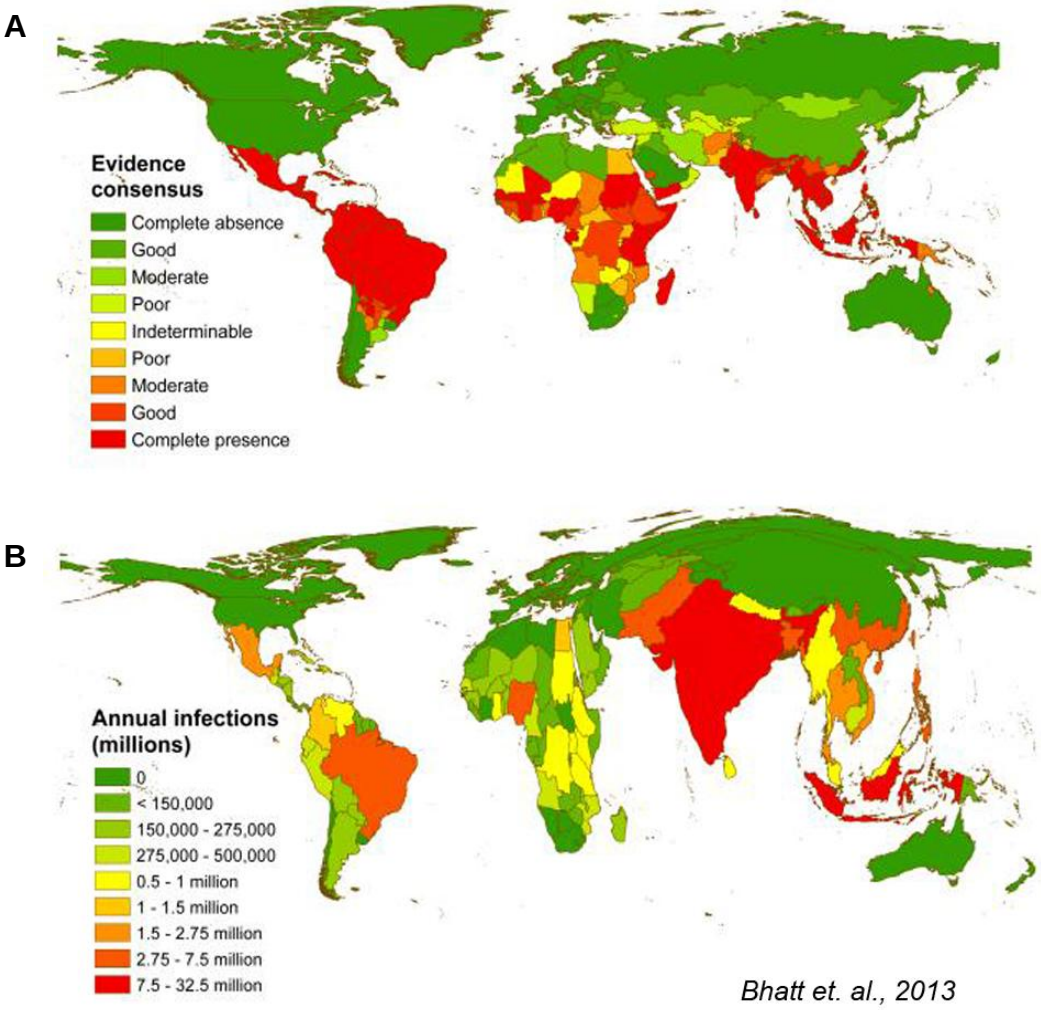

Figure 1.2 Global evidence consensus and burden of dengue in 2010 (A) National and subnational evidence on dengue. Red indicates complete presence through to green indicating complete absence. (B) Cartogram of annual number of infections for all ages as a proportion of national or sub-national (China) geographical area.

There are four serotypes of DENV (DENV-1, DENV-2, DENV-3, DENV-4) that are immunologically distinct but antigenically related, 65-70% homology in amino acid sequence (Guzman et al., 2010). Despite these

differences, each serotype circulates in the same ecological niche and causes almost identical syndromes in humans (Halstead, 2008).

The dengue virion comprises a spherical particle, 40-50nm in diameter and is composed of a single, positive-stranded RNA genome that is packaged by the virus capsid (C) protein and surrounded by an envelope (Figure 1.3) (Kuhn et al., 2002; Zhang et al., 2004).

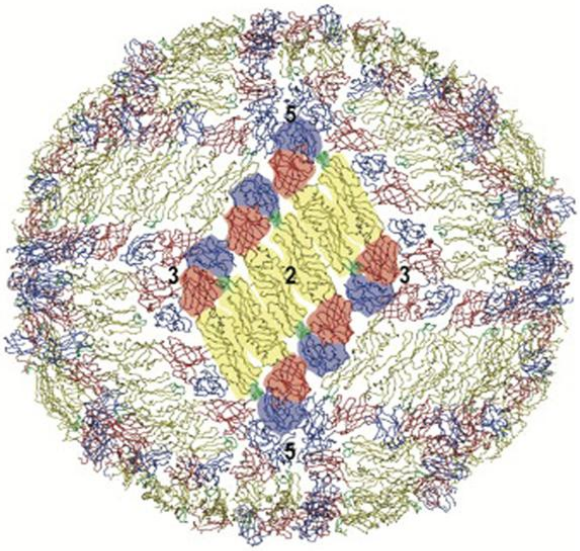

Zhang et. al., 2004

Figure 1.3 Structure of the mature dengue virion arrangement of the envelope (E) protein subunits on the surface is shown. E proteins exist as homodimers arranged as 30 "rafts" organized into a herringbone pattern. Domains I, II and III of E proteins are coloured red, yellow and blue respectively. Fusion peptides are shown in green.

The envelope (E) protein consists of 180 monomers organized into 90 tightly packed dimers that lie flat on the surface of the viral membrane (Kuhn et al., 2002; Zhang et al., 2004). The ~ 11 kb DENV genome consists of a single open reading frame (ORF) flanked by highly structured untranslated regions (UTRs) that is capped at the 5'end but lacks a polyA tail (Figure 1.4) (Guzman et al., 2010; Pastorino et al., 2010). The type 1 cap is a modified guanine nucleoside methylated at the N-7 and 2'-O positions identical to that of cellular messenger RNAs (mRNAs) (Saeedi and Geiss, 2013). The genome is translated to produce a

single polyprotein which is cleaved co- and post-translationally by viral and cellular proteases into three structural (C, membrane (M), E) and seven nonstructural (NS1, NS2A, NS2B, NS3, NS4A, NS4B, NS5) proteins that are essential for viral RNA replication, virus assembly and modulation of the host cell responses (Figure 1.4) (Guzman et al., 2010; Pastorino et al., 2010).

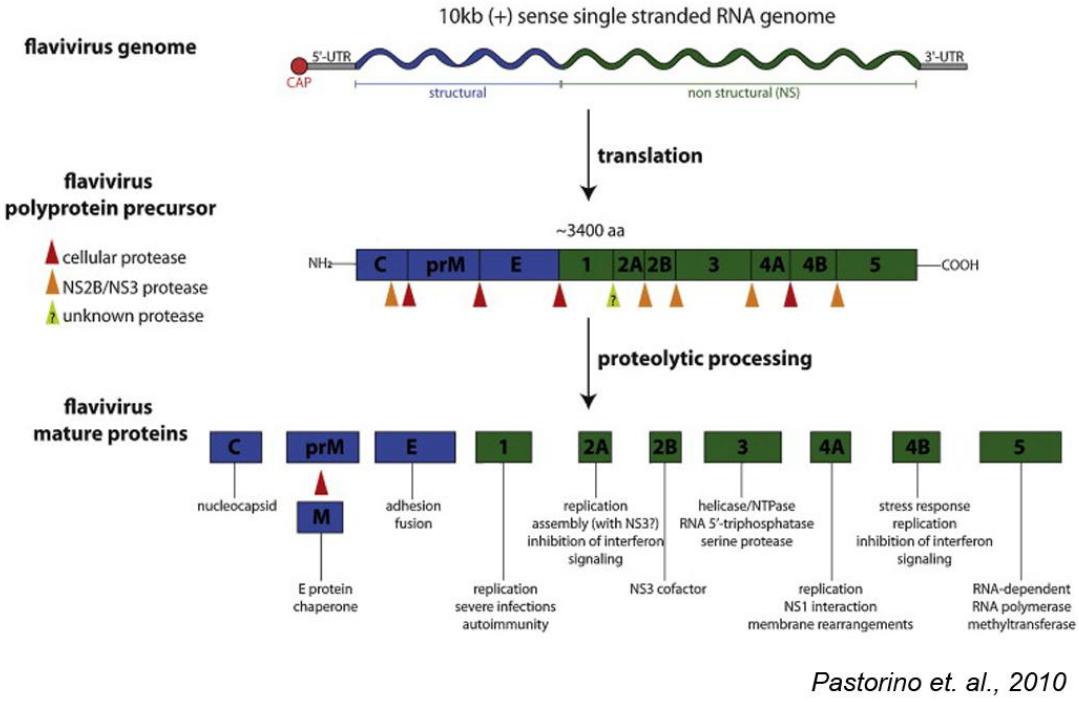

Figure 1.4 Flavivirus genome and polyprotein organization The single open reading frame (ORF) (~11kb) is depicted with the structural and non-structural protein coding regions highlighted in blue and green respectively. This ORF has a 5'cap and is flanked by the 5'and 3'untranslated regions (UTRs). It encodes an immature polyprotein precursor that is co- and post- translationally cleaved into three structural proteins (C, M, E) and seven non-structural proteins (NS1, NS2A, NS2B, NS3, NS4A, NS4B, NS5). Cleavage sites for cellular proteases, NS2B/NS3 and unknown protease are indicated. Putative functions of these proteins are described.

1.1.2 Lifecycle of dengue virus

Dengue virus particles bind to a ubiquitous, low-affinity receptor on the cell surface and enter cells through receptor-mediated endocytosis. Although various mammalian cell receptors have been proposed including heparan sulfate (Chen et al., 1997), heat shock protein 90 (Valle et al., 2005), CD14 (Chen et al., 1999), C-type lectins CLEC5A (Chen et al., 2008b) and the mannose receptor (Miller et al., 2008), the best characterized interaction is between DENV and DC-specific intercellular adhesion molecule 3 (ICAM-3)-grabbing nonintegrin (DC-SIGN) (Tassaneetrithep et al., 2003).

Besides direct interaction with a cellular receptor, DENV has an alternative mechanism of entry into monocytes/macrophages. In the presence of dengue-specific antibodies, antibody opsonization of DENV results in the formation of immune complexes. These immune complexes can bind to Fcγ receptors (FcγR) on the surface of myeloid cells resulting in increased entry and infection via FcγR-mediated phagocytosis (Figure 1.5) (Chan et al., 2011; Chawla et al., 2013; Halstead and O'Rourke, 1977; van der Schaar et al., 2009; Whitehead et al., 2007).

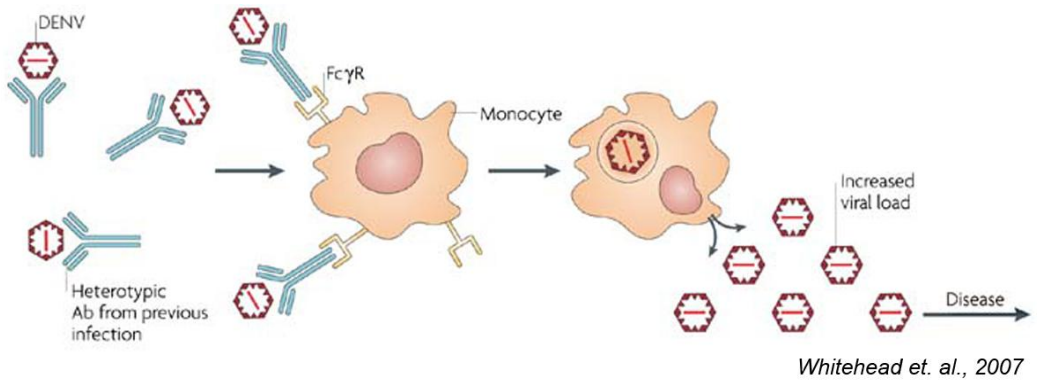

Figure 1.5 Antibody-dependant enhancement of dengue virus replication In the presence of heterotypic antibodies, either from previous infections or maternal transfer, the infecting dengue virus can be opsonized to form immune complexes. These immune complexes are able to engage Fcγ receptors (FcγR) facilitating increased viral entry and subsequent infection, leading to the potential for more severe disease.

Upon entry into cells, acidification of the late endosomes triggers trimerization of the E protein, inducing fusion of viral and cell endosomal membranes, thus allowing the viral nucleocapsid to uncoat (Kuhn et al., 2002; Li et al., 2008; van der Schaar et al., 2008). The DENV genome is then released into cells and translated. Once the viral replication complex is synthesized by viral and co-opted host proteins, RNA synthesis begins in DENV-induced replication compartments within the endoplasmic reticulum (ER).

A full-length complementary minus strand RNA, termed an antisense intermediate is first synthesized by the viral RNA-dependent RNA polymerase (RdRp). This RNA, acting as a replicative intermediate, is then used as a template for multiple rounds of positive sense genomic RNA (gRNA) synthesis. Subsequently, successive rounds of translation generate large quantities of viral proteins and immature virions assemble in the ER

with the prM acting as a scaffold to prevent premature virus fusion. These immature virions are then transported to the trans-Golgi network where premembrane (prM) is cleaved into pr and M by furin. Mature infectious particles are thus formed and egress cells via the host secretory pathway leading to new rounds of infection (Figure 1.6) (Fernandez-Garcia et al., 2009; Mukhopadhyay et al., 2005; Pastorino et al., 2010).

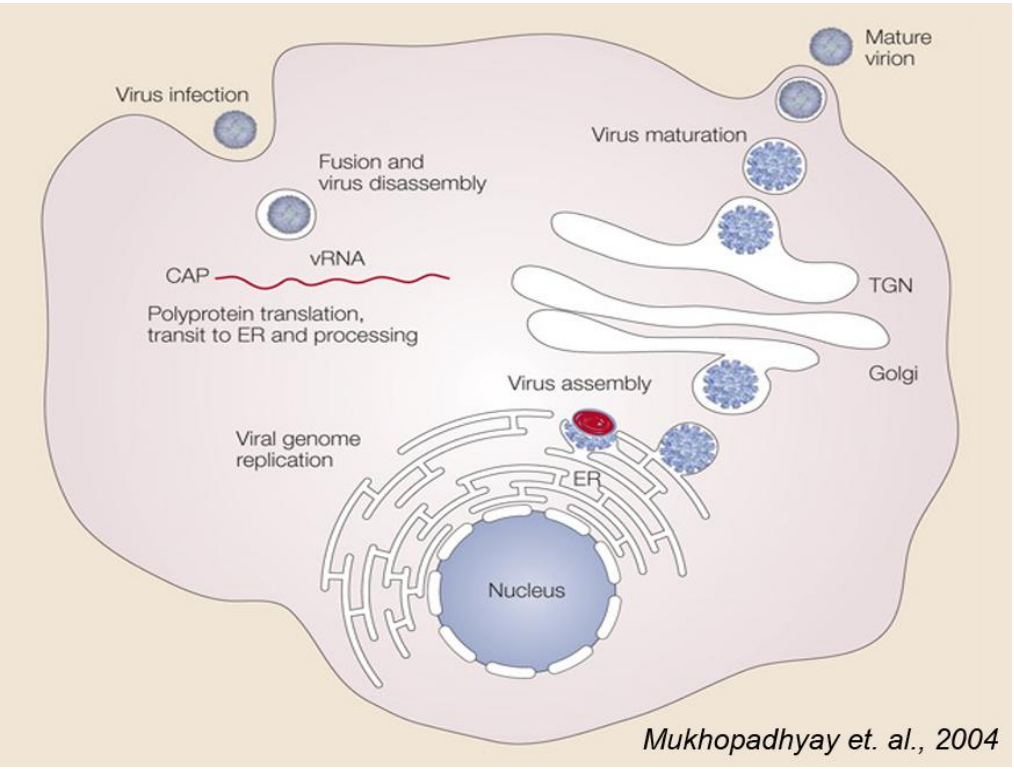

Figure 1.6 Lifecycle of dengue virus After binding to its receptor on target cells, dengue virus enters through receptor-mediated endocytosis. The acidic pH in the endosomal compartments causes a conformational change of the virus and viral fusion occurs. Once the nucleocapsid is released, uncoating follows and RNA is released into the cytoplasm where it undergoes the first round of translation. Viral and host proteins are involved in the formation of ER membrane-bound compartments wherein replication occurs. After several rounds of replication and translation, progeny virions are assembled in the ER and transported to Golgi where they are cleaved by furin to form mature particles. Mature viruses leave the cell by exocytosis.

1.1.3 Virus Transmission

Dengue, an arthropod-borne virus, is spread to humans through a human-mosquito-human cycle of transmission. The virus is transmitted to humans by *Aedes* mosquitoes (Monath, 1994). Dengue is most widely transmitted by its main vector, *Aedes aegypti.* The *Aedes albopictus* mosquito and other *Aedes* species transmit dengue in specific geographical regions where they are found. For instance, *Aedes polynesiensis* plays an important role in dengue transmission in the Pacific islands (Rosen et al., 1954). *Aedes aegypti*, a highly domesticated mosquito is the principal vector of dengue because of its close contact with humans in urban areas as it breeds in domestic and peridomestic water containers (Gubler, 1998a; Platt et al., 1997). In a single gonotrophic cycle, *Aedes aegypti* is known to feed on multiple human hosts for a blood meal.

The secondary vector, *Aedes albopictus*, is also of increasing importance in dengue transmission and is responsible for endemic transmission of dengue in Asia and for epidemic spread in circumstances where *A. aegypti* is absent or in low density (Lambrechts et al., 2010). Since these mosquitoes originated from forests, a sylvatic cycle for dengue transmission has been documented in Africa (Diallo et al., 2003) and southeast Asia (Wolfe et al., 2001). However, the contribution of the sylvatic cycle of dengue transmission to human infection has only been dissected recently with studies showing that sylvatic DENV may have an equal or

greater potential to cause dengue as compared to established urban DENV genotypes (Vasilakis et al., 2010; Vasilakis et al., 2008).

1.1.4. Clinical presentation and progression

Typically, someone bitten by an infected mosquito may develop symptoms of acute dengue 3-14 days later. A range of clinical manifestations has been reported, ranging from mild flu-like illness to severe disease and death. Majority of the patients are diagnosed with dengue fever which presents as a self-limiting febrile illness. Most common signs and symptoms include high fever (>38°C), leukopenia and rash (Snow et al., 2014). Headache, retro-orbital pain, petechiae, myalgia, arthralgia, flushing of the face, anorexia, abdominal pain and nausea are some of the other symptoms. A very low percentage of patients experience nosebleed. Macular rash can be observed during fever defervescence and majority of the patients recover without complications about a week after disease onset (Simmons et al., 2012).

A small proportion of infected individuals may progress to more severe dengue. Around the time of fever defervescence some patients develop signs of thrombocytopenia (platelet count ≤ 100,000/mm^3), hemorrhagic manifestations and enhanced vascular permeability with leakage of intravascular fluid (Gubler, 1998a). The fluid leakage through increased vascular permeability may lead to shock when a critical volume of plasma is lost into the extravascular space and cardiac output becomes

insufficient to maintain the necessary blood pressure. Prolonged shock may result in organ hypoperfusion leading to progressive organ impairment, metabolic acidosis and disseminated intravascular coagulation (Figure 1.7) (WHO, 2009). Without proper treatment, a stage of profound shock may set in, causing death within 12 to 36 hours after shock onset. It is thus important to detect patients progressing from non-severe to severe disease early as intravenous rehydration can reduce case fatality rates to less than 1% of severe cases (Simmons et al., 2012).

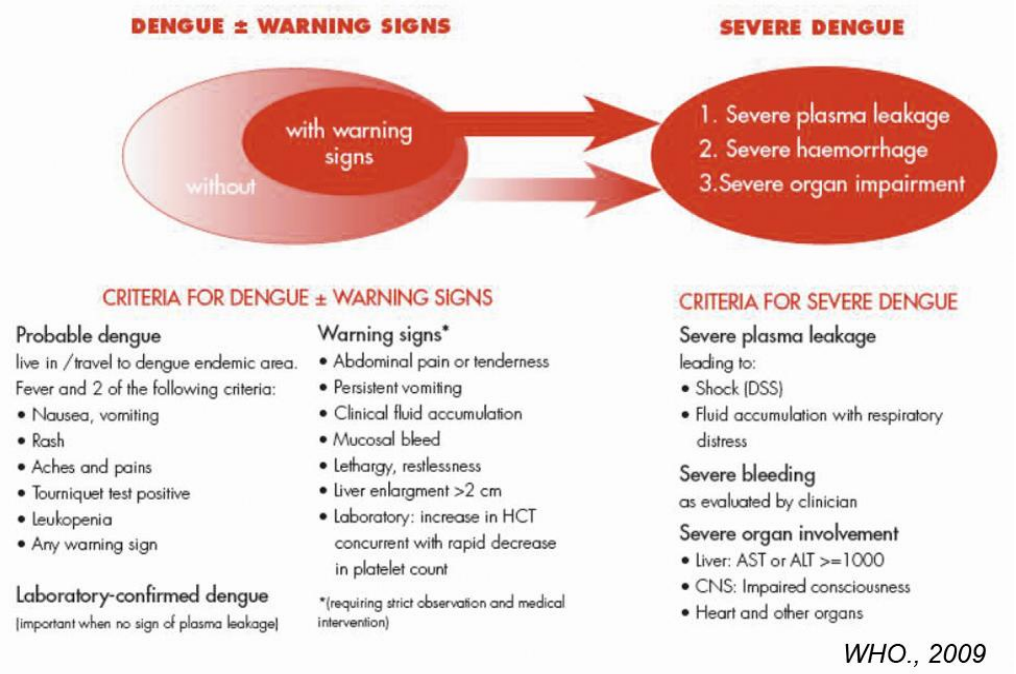

Figure 1.7 World Health Organization (WHO) dengue case classification and levels of severity

Despite being a disease complex in its manifestations, clinical management of dengue is not difficult, inexpensive and highly effective provided timely appropriate interventions are provided. Treatment plans for

dengue are provided by the latest WHO guidelines based on the severity of clinical manifestations (WHO, 2012; Wright and Pritt, 2012).

Supportive care such as analgesics, acetaminophen, fluid replacement, and bed rest is usually sufficient for classic dengue cases. These patients can be successfully managed as outpatients. For patients with warning signs of severe dengue, hospitalization with sufficient fluid replacement, proactive treatment of hemorrhage and supportive medical care is recommended (WHO, 2012; Wills et al., 2005). Frequent and regular measurement of the patient's hemocrit is crucial as a heightened hemocrit precedes plasma leakage, indicating potential hemorrhagic complications (WHO, 2009). Besides hematocrit, plasma leakage could also be monitored using ultra sonography of the gall bladder wall or pleural cavity. Another warning sign is when patients have moderate to severe thrombocytopenia (platelet count of below 100,000 cells per cubic millimeter) (Halstead, 2007; Lye et al., 2009; WHO, 2009).

Although these clinical parameters can be monitored for development of severe dengue, timely intervention is not always possible as the clinical outcome of dengue infections is often unpredictable. Despite close monitoring, some cases have progressed to severe disease without any warning signs. Hence, prevention and control of dengue transmission may be a better prospect than case management in reducing the overall burden of dengue.

1.1.5 Prevention and control of dengue

There is currently no licensed dengue vaccine or anti-viral drug available. To reduce morbidity rates, effective prevention of dengue transmission and thus vector control remains important (Eisen et al., 2009; Guzman and Kouri, 2002). Historically, prevention and control of dengue has relied on control of the main vector, *Aedes aegypti*. Unfortunately, most countries do not have intensive dengue preventative programs. There are multiple reasons for this, which include misguided public health policies, the lack of resources for mosquito control, lack of political will, and lack of research along with the global trend of unprecedented population growth, unplanned urbanization and globalization (Gubler and Clark, 1994).

1.1.5.1 Vector control Programs

The first vector control program was instituted in Central and South America by the Pan American Sanitory Board in the 1950s-1960s. Highly successful, it depended on a multifaceted approach which included surveillance, constant inspection, chemical control and community involvement (Schliessmann, 1967).

Another instance of a vector control program being successful was in Cuba, where a national campaign to eradicate *Aedes aegypti* was started in 1981. Intense insecticidal treatment along with source reduction brought the epidemic under control in about four months (Kouri et al., 1989). In Singapore, a successful reduction of *Aedes aegypti* from 16% to 2% was

observed with the initiation of a similar program in 1970 (Ooi et al., 2006). This was followed by a 15 year period of low dengue incidence.

Despite the initial success of all the above programs, none of them were sustainable mainly due to the lack of long-term political and financial support. Other reasons such as over-reliance of chemical control and "passive" community participation also contributed to the non-sustainability of vector control (Gubler, 1989). A resurgence of dengue was even observed in Singapore probably due to lowered herd immunity (Goh, 1995), shift in virus transmission from domestic to non-domestic settings (Ooi et al., 2001) and change in surveillance emphasis of the program (Yew et al., 2009). Thus, vector control is ultimately unreliable as a method for dengue prevention leading to considerable interest in the development of a dengue vaccine.

1.1.5.2 Vaccines in clinical development

Although much progress has been made in the development of a dengue vaccine, it has been considerably challenging as there is a need to immunize against all four DENV serotypes simultaneously. Moreover, to minimize the risk of vaccine-induced ADE (Figure 1.5) of dengue infection, it is necessary to develop tetravalent dengue vaccines that induce balanced immune responses to all four serotypes (Table 1.1) (Guzman and Harris, 2014). Despite this difficulty, currently there are live attenuated viruses, inactivated viruses, recombinant proteins and DNA vaccines under development as dengue vaccine candidates (Table 1.1) (Guzman and Harris, 2014; Thomas and Endy, 2011).

Table 1.1 Candidate dengue vaccines

	Description	Clinical trial status
Chimeric live-attenuated vaccine		
YF17D/dengue chimeric vaccine	Recombinant infectious cDNA clone of yellow fever 17D vaccine strain as a backbone, substituting prM and E protein genes with those of the four dengue virus serotypes	Phase 3
Live-attenuated vaccine		
Tetravalent live attenuated virus	Attenuation by serial passage in PDK cells	Phase 1/2
Dengue virus infectious clone live-attenuated vaccine		
Chimeric recombinant attenuated vaccine	Attenuated DENV 2 infectious clone containing prM/M and E of DENV 1, DENV 3, and DENV 4	Phase 2
3′-UTR deletion mutant attenuated vaccine	Attenuating deletion of a 30 nucleotide sequence in 3′-UTR of DENV 1, DENV 3 and DENV 4; production of chimera with DENV 2 prM/M and E in a DENV 4-attenuated backbone	Phase 1/2
DNA		
D1ME	prM and E protein genes	Phase 1
Protein		
r80E	Expression of N-terminal 80% E protein in insect cells	Phase 1
cEDIII	Domain III of E protein gene fused to p64K protein of *Neisseria meningitides* and expressed in *Escherichia coli*	Preclinical
Inactivated		
Purified inactivated dengue virus	Whole purified inactivated virus	Phase 1
Virus-like particle		
EDIII-capsid protein	Chimeric protein comprising domain III of E protein and the capsid protein of DENV 1–4	Preclinical
Virus vector		
Alphavirus VRP	Alphavirus replicon particles expressing two configurations of dengue virus E antigen (subviral particles [prME] and soluble E dimers [E85])	Preclinical
Adenovirus	Tetravalent formulation combining two bivalent adenovirus constructs	Preclinical
Measles virus	Expression of dengue virus antigen by a vector derived from live-attenuated measles vaccine	Preclinical

PDK=primary dog kidney. DENV=dengue virus. 3′-UTR=3′-untranslated region.

Table 1: Candidate dengue vaccines — Guzman and Harris, 2014

The Sanofi Pasteur ChimeriVax-DENV (CVD) vaccine, which has recently completed Phase III clinical trials, is the most advanced vaccine candidate to date. A chimeric vaccine, it consists of the structural genes (prM and E) from all four DENV serotypes inserted into the backbone of the yellow fever virus 17D vaccine strain (Guirakhoo et al., 2001). Results from the phase I and II trials have shown the vaccine to be safe and immunogenic (Dayan et al., 2013a; Dayan et al., 2013b; Guy et al., 2010; Guy et al., 2008; Sabchareon et al., 2012). The recent phase III trials in Southeast Asia demonstrated the clinical efficacy of this vaccine to be 59% in preventing acute dengue caused by any of the four serotypes (Capeding et al., 2014). Similar trends have also been observed in the (Guzman and Vazquez, 2010; Halstead, 1974) phase III trial in Latin America with the vaccine being 60.8% efficacious against dengue fever and severe dengue as compared to the placebo group (Villar et al., 2014). However, serotype-specific efficacy varies significantly, with DENV4 and DENV2 having the highest and lowest efficacy, respectively (Capeding et al., 2014; Sabchareon et al., 2012; Villar et al., 2014). Overall, the trials have shown collectively that this vaccine has a good safety profile although the efficacy in preventing disease is less than ideal (Capeding et al., 2014).

The low efficacy of the CVD vaccine for DENV-2 as seen in the phase II and III trials poses several questions. Firstly, it suggests that the neutralizing antibody titers might be insufficient for protection against that specific strain of DENV-2 (Mullard, 2014). Alternatively, the plaque reduction neutralization

test (PRNT), used as an immune correlate to predict dengue infection outcome might not be an accurate measure because of the discrepancy with trial results. Furthermore, other vital immune correlates of protection might have been ignored. For instance, recent evidence has suggested a protective role for CD8+ T cells response in dengue infection (Yauch et al., 2009). The specificity of this response was mapped to epitopes on the DENV nonstructural proteins. Since the CVD vaccine is based on a yellow fever virus backbone, it lacks the epitopes required to induce cell-mediated immunity during an infection.

Yet another major limitation of this vaccine is the requirement of an extended dosing schedule of 3 doses at intervals of 6 months. This could potentially lead to major compliance issues or problems related to ADE in endemic areas as the waning immunity over such an extended interval might cause severe dengue. Therefore, it is highly recommended that further studies be conducted to assess the long-term effects of this vaccine and to completely prove its clinical effectiveness and the robustness of its immunogenicity (da Costa et al., 2014).

Other vaccines in development include the live attenuated vaccine (LAV), TV003 by the National Institutes of Health (Whitehead et al., 2003) and DENVax produced by CDC-Inviragen (Osorio et al., 2011), now a part of Takeda. TV003 is a tetravalent formulation comprising of DENV-1Δ30, DENV-2/4Δ30, DENV-3Δ30/31 and DENV4Δ30. Except for DENV-2/4Δ30 that has a

recombinant genome consisting of DENV-2 structural genes inserted into an attenuated DENV-4 backbone, the remaining serotypes are attenuated by a 30-nucleotide deletion in the 3'UTR. A single dose of this LAV induced a trivalent or better neutralizing antibody response in 75-90% of vaccinees (Durbin et al., 2013). Based on the promising phase I trial results, this vaccine is currently undergoing a phase II trial. Similarly, DENVax has also entered phase II trials (Osorio et al., 2011). The genomic backbone of DENVax consists of a DENV-2 strain (16681-PDK53) serially passaged in primary dog kidney cells. The DENV-2 prM and E genes were substituted with those from DENV-1, DENV-3 and DENV-4 to form chimeras which formulated the rest of this tetravalent vaccine.

Despite considerable progress made in dengue vaccine development, much still remains to be understood about protective immune responses against DENV (Webster et al., 2009). The lack of an ideal animal model for DENV infection or a well-characterized human infection model also means that the study of DENV pathogenesis is limited. Thus, an improved understanding of disease pathogenesis and immune protection will greatly help in the design of a safe and effective DENV vaccine (Thomas, 2014).

1.2 Disease Pathogenesis

1.2.1. Factors contributing to dengue pathogenesis

The pathogenesis of severe dengue disease is highly complex and multifactorial. Unfortunately, the lack of a good animal model hampers the study of dengue pathogenesis. However, it remains crucial to attain a better understanding of the underlying mechanisms leading to severe disease for the development of prognostic markers, novel diagnostics, therapeutics and a safe vaccine. High viremia has been shown by several studies to be directly correlated with severe dengue disease (Libraty et al., 2002; Vaughn et al., 2000; Wang et al., 2003). However, there are two main bodies of thought as to what might cause an increase in viral load. These are: (1) Secondary infection or immune enhancement (Halstead et al., 1970) (2) Viral virulence (Gubler, 1998a). These theories are not mutually exclusive and could be equally valid as shown by multiple clinical and epidemiological observations. This section aims to highlight the complex interplay of host immunity and viral factors in dengue pathogenesis.

1.2.1.1Role of secondary infection in severe dengue pathogenesis

The assumption that neutralizing or non-neutralizing antibodies control, eliminate and protect against viral infection holds true in most infection models. Nonetheless, a detrimental role for virus specific antibodies has been described for dengue where the subsequent infection of preimmune individuals to a different DENV serotype would exacerbate rather than

mitigate dengue disease due to the presence of enhancing concentrations of antibodies. This phenomenon is termed antibody-dependant enhancement (ADE).

After a primary DENV infection, immunoglobulin M (IgM) antibodies are first generated and decline to undetectable levels over the following 2-3 months (Guzman et al., 2010). Towards the end of the first week of illness, immunoglobulin G (IgG) antibodies are generated. Majority of these antibodies act against NS1, E and prM proteins (de Alwis et al., 2011). Anti-E antibodies are protective and produced at levels sufficient for efficient neutralization against all four DENV serotypes during early convalescence after acute infection (Sabin, 1952; Zompi et al., 2012). Subsequently, antibody levels decline and only serotype-specific antibodies retain the capability to protect the host from re-infection (Guzman and Vazquez, 2010; Halstead, 1974).

When antibody levels decline to sub-neutralizing levels, infection with a heterologous DENV serotype can result in more severe disease. Both sub-neutralizing and cross reactive antibodies can opsonize DENV to enhance infection through entry via Fc gamma receptors (FcγR) (Figure 1.8) (Halstead and O'Rourke, 1977). However, infection enhancement is peculiar as cross-linking of FcγRs induces type I interferon-stimulated gene expression which would create an unfavourable intracellular environment for DENV replication (Dhodapkar et al., 2007). To resolve this question, a

study recently showed that antibody-opsonized DENV co-ligates leukocyte Ig-like receptor-B1 (LILRB1) to inhibit FcγR signaling for ISG expression

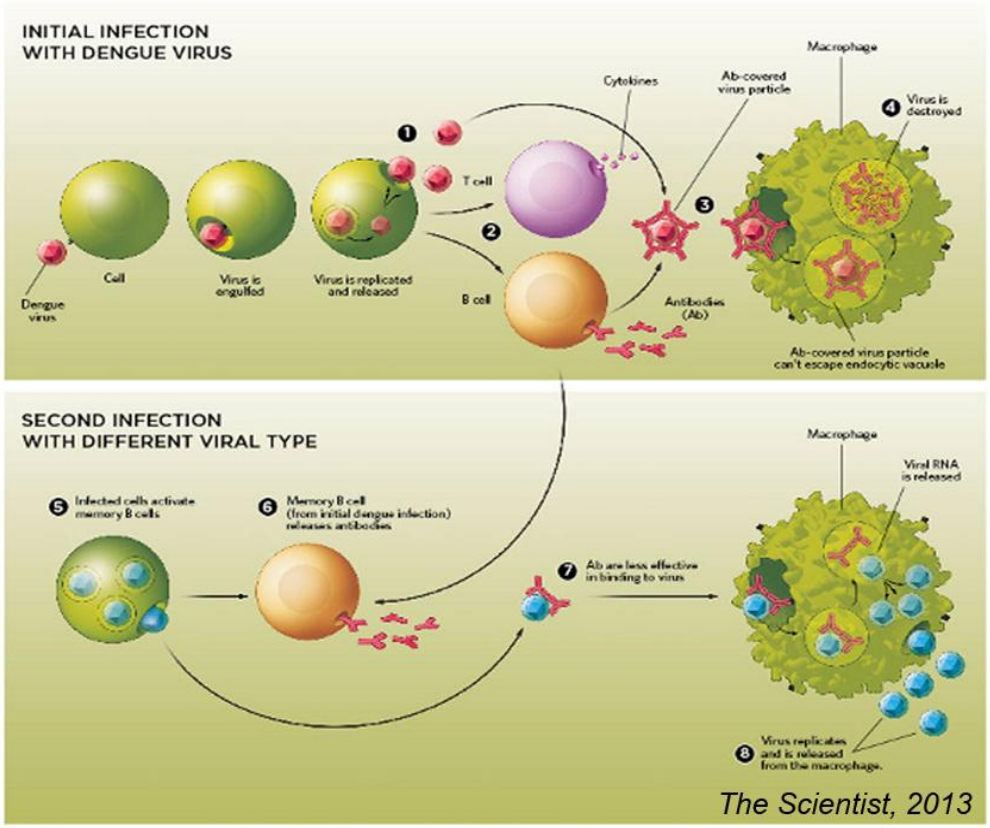

Figure 1.8 Antibody-dependant Enhancement Dengue virus infects by attachment to the cell surface followed by engulfment through endocytosis. The virus rearranges its coat proteins to bind to the endosome, releasing its genome into the cytoplasm where replication and release of new progeny virions occur. (1) The infected cell triggers an immune response. (2) T cells are recruited and release pro-inflammatory cytokines and antibodies. (3) Virus specific antibodies bind and cover the virus, leading to (4) clearance of the virus by immune cells. (5) Upon infection with a second serotype, memory B cells created during the first infection get activated (6), releasing antibodies to the first serotype. (7) These are less effective to binding to the second serotype but allow efficient uptake into mononuclear cells through entry via Fc receptors. (8) This leads to enhanced replication in macrophages and monocytes resulting in an increased viral load.

through spleen tyrosine kinase (Syk) dephosphorylation (Chan et al., 2014). Therefore, ADE not only facilitates viral entry process, but also modulates innate and adaptive intracellular antiviral mechanisms, resulting in unrestricted DENV replication. Signaling from the immunoreceptor tyrosine inhibitory motif of LILRB1 may also modify other processes in the cell for enhanced DENV infection. Further work will need to be carried out to identify these modified processes.

The abovementioned study is consistent with the concept labeled "intrinsic ADE" (Halstead et al., 2010). "Intrinsic ADE" suggests that besides providing an alternative and perhaps a more efficient mode of entry into monocytes, FcγR signaling also modifies the antiviral immune mechanisms to create an intracellular environment favorable for enhanced replication and infection (Halstead et al., 2010). Indeed, DENV infection via ADE caused suppression of IL-12, IFNγ production and the Jak/STAT signaling pathway (Chareonsirisuthigul et al., 2007).

Prior infection thus, through ADE, could potentially cause an enhanced viral load in mononuclear cells in patients. Infected mononuclear cells also produce and secrete vasoactive mediators that increase vascular permeability, causing severe dengue disease. Indeed, studies have shown that plasma leakage, the hallmark of severe disease generally occurs at or near defervesence, suggesting that disease pathogenesis is primarily mediated by host immune response (Vaughn et al., 2000; Vaughn et al., 1997).

Epidemiologically, the role of secondary infection in severe dengue has been described. Sera from mothers whose infants developed severe dengue upon a primary infection, contained sub-neutralizing levels of dengue-specific antibodies, suggesting that maternal transfer of antibodies to the infants had enhanced the disease outcome (Kliks et al., 1988). Likewise, 65% of Vietnamese infants that experienced severe dengue had sub-neutralizing levels of maternally transferred dengue-specific antibodies (Simmons et al., 2007). Another study showed an approximately 15-80 fold increase in risk of hemorrhagic manifestations upon secondary infection with another serotype (Thein et al., 1997). A prospective study in Yogyakarta, Indonesia on dengue in young children showed that all the children who had to be hospitalized for severe disease had secondary infection (Graham et al., 1999). In Rayong, the biggest risk factor for severe clinical outcome was secondary infection with DENV-2 (Sangkawibha et al., 1984).

Nonetheless, not all severe dengue cases are caused by secondary infection alone and not all secondary infections lead to severe dengue disease outcome (Watts et al., 1999). A prospective study on primarily DENV-3 infections in infants showed no significant association between levels of maternal antibodies at disease onset and the development of severe disease (Libraty et al., 2009). Moreover, a severe dengue outbreak occurred in Niue in 1972 where many children died of severe disease {Barnes and Rosen, 1974 #424}. Since Niue had been free of dengue for the preceding 25 years, it

is highly unlikely that secondary infection resulted in severe disease, thus suggesting that other factors such as differential virulence of DENV strains may also contribute to disease pathogenesis (Barnes and Rosen, 1974; Rosen, 1977)

1.2.1.2 Viral virulence contributes to pathogenesis

Support for the differential virulence of DENV strains began as early as the 1950s with Sabin's experimental infections of human volunteers (Sabin, 1952). Subcutaneous inoculation of the Hawaii DENV strain into subjects resulted in more severe disease as compared to inoculation with the New Guinea strain, proving the existence of "multiple immunological types" of dengue, as noted by Sabin.

Based on nucleotide variations, the four DENV serotypes can be further subdivided into many genotypes and according to the viral virulence hypothesis, some DENV strains are responsible for more severe disease (Figure 1.9) (Holmes and Burch, 2000). The selection of more virulent dengue strains occurs in nature and analysis of DENV genomes has shown that dengue virus is continually evolving even during epidemics (Chen et al.,

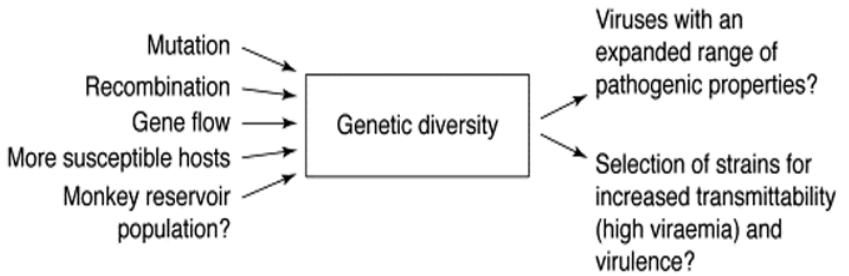

Figure 1.9 Processes that led to an increase in DENV genetic diversity and two likely consequences

2008a; Rico-Hesse, 1990; Rodriguez-Roche et al., 2005).

In the Western Hemisphere, although dengue was circulating prior to 1981, the first outbreak of severe disease only occurred in 1981 when the American genotype DENV-2 was displaced by the more virulent Southeast Asian DENV-2 genotype (Cologna et al., 2005; Rico-Hesse et al., 1997). In Cuba, towards the end of the 1981 DENV-2 epidemic, the severity of disease and case fatality rates increased, suggesting that the circulating DENV-2 might have become more virulent (Kouri et al., 1987). This was observed again during the 1997 Cuban epidemic (Guzman et al., 2000). Similarly, during the 1992 dengue epidemic in Australia, the number of cases with spontaneous hemorrhagic manifestations increased as the epidemic progressed, thus implying that the virus might have evolved due to selection pressure to become more virulent (Streatfield et al., 1993). Collectively, these epidemiological studies show that viral genetics contributes to dengue disease pathogenesis.

In addition, *in vitro* studies that examined the attenuation of viral strains for vaccine production have suggested that viral genetic differences can lead to variations in DENV infectivity and/or virulence (Brault et al., 2011; Hanley et al., 2004; Kelly et al., 2011). In a comparison of live attenuated DENV-2 viral strain PDK-50 and its parent strain, thirteen attenuating amino acid mutations were identified in prM, E, NS1, NS2A, NS2B, NS4B genes and 5'UTR (Kelly et al., 2011). Another study investigated the genetic basis for the impaired replication of a vaccine candidate and

found substitutions in NS1, NS3 and 5'UTR responsible (Brault et al., 2011). Furthermore, attenuating mutations introduced into the 3'UTR of a dengue vaccine candidate resulted in decreased replication in rhesus monkeys (Hanley et al., 2004). Thus, DENV can be attenuated by mutations in its genome which suggests that genetic mutations could also conversely increase its virulence.

In mice, a single nucleotide substitution in the E protein gene resulted in increased neurovirulence (Sanchez and Ruiz, 1996). Mutations engineered into the 5'UTR of a DENV-2 infectious clone also showed differences in replication and variability in neurovirulence in mice (Sirigulpanit et al., 2007). Yet another study looking into mouse-adapted DENV-4 strains, identified the E protein to be an important determinant of mouse neurovirulence with mutations in this region significantly changing the DENV-4 phenotype (Kawano et al., 1993). Collectively, these aforementioned studies suggest that a small number of genetic changes in the DENV genome can lead to significant phenotypic differences, including increased replication, viremia and disease severity.

In an attempt to directly study viral factors contributing to severe disease, dengue viral RNA sequences were isolated from patients with dengue fever and severe dengue, sequenced and compared (Leitmeyer et al., 1999). Results showed multiple amino acid changes in the proteins along with several sequence variations in both the 5' and 3' noncoding regions.

Although suggestive, this data is not compelling as not all variations were conserved among the viruses in both the dengue fever and severe dengue groups. Furthermore, host genetics may have played a role as these viruses were isolated from patients living in two different locales: Thailand and Americas.

Hence, disease outcome cannot always be attributed to DENV sequence variations. For instance, in Singapore, a major outbreak took place in 2005, during which both DENV-1 and DENV-3 were co-circulating and genomic analysis confirmed that there was no connection between viral sequences and disease outcome (Schreiber et al., 2009). Rather, this study pointed out that ecological or immunological factors were the main determinants of the epidemic. Likewise, there may be other secondary factors such as age, host genetics contributing to disease pathogenesis as well (Watts et al., 1999).

In summary, increased viral replication caused by both secondary infection or virus virulence will lead to a higher antigenic stimulation of host cells. This will result in greater levels of pro-inflammatory immune responses in the host which then leads to more severe dengue disease outcome (Devignot et al., 2010). The next section will thus explore the immune responses upon dengue infection.

1.2.2 Immune responses to dengue infection

Being a human disease that has no known animal reservoirs, dengue virus has developed sophisticated mechanisms to evade human immune responses, especially innate antiviral immunity. This section focuses on mechanisms of innate antiviral responses against dengue and how the virus evades immune responses (Figure 1.10).

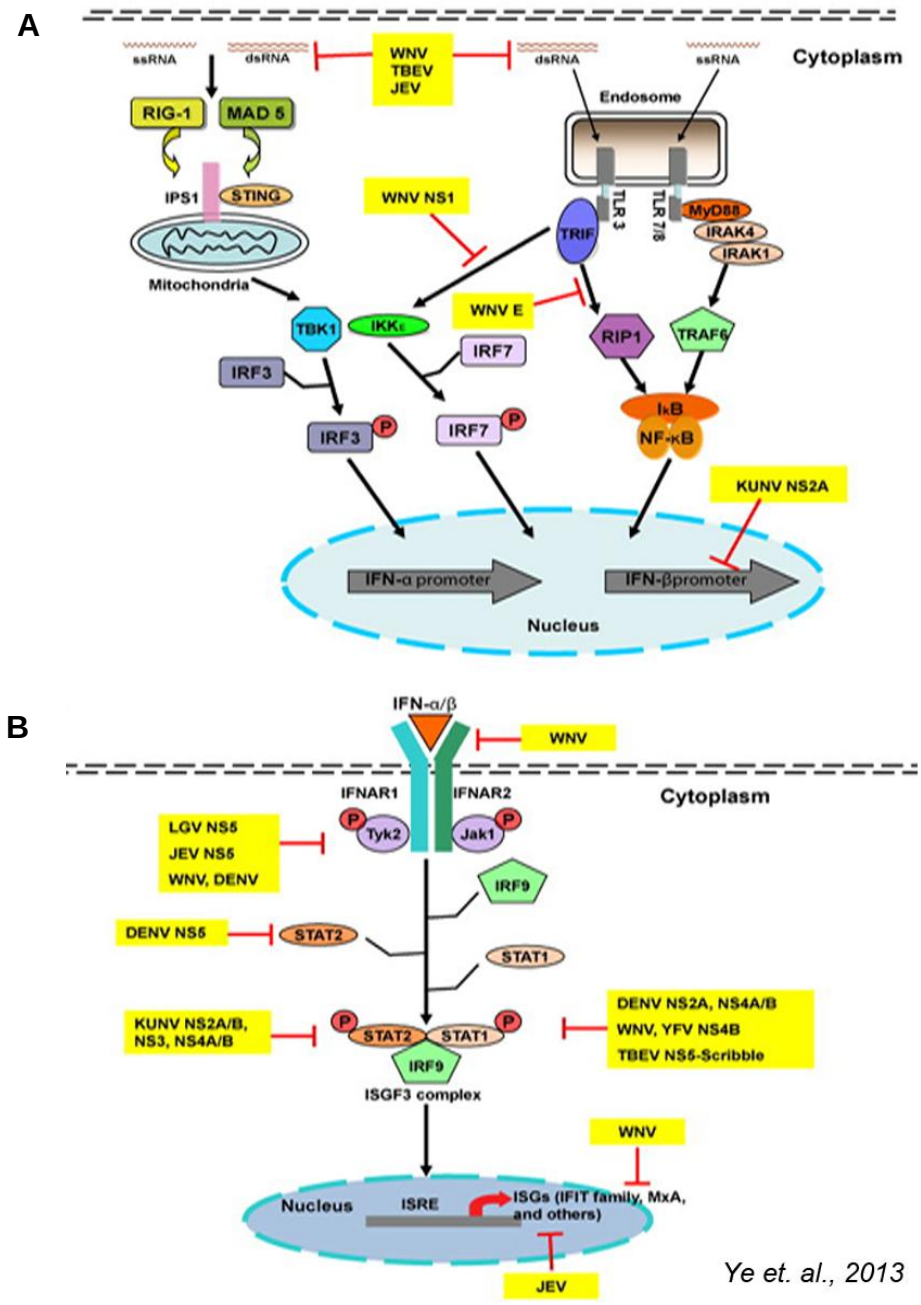

Figure 1.10 Type I interferon signal pathway and evasion strategies of flaviviruses (A) Pattern recognition receptors (PRR) (RIG-I and TLR3/7) sense flavivirus dsRNA and ssRNA structures. These receptors activate their adaptor molecules initiating signaling cascades that activate IRF3, IRF7, and NF-κB, leading to IFN-α/β gene transcription. Mechanisms of evasion at this stage include: a delay in recognition of viral RNA by PRRs; impairment of RIG-I signaling by high mannose carbohydrates on the structural E protein; attenuation of TLR3 signaling by the NS1 protein; and reduction in IFN-β gene transcription by NS2A protein. (B) Activation of JAK/STAT pathway by binding of type I IFN to the IFN-α/β receptor (IFNAR). This results in generation, phosphorylation, and assembly of the trimeric ISGF3 transcription factor complex, which consists of a STAT1-STAT2 heterodimer and IRF9. This is followed by nuclear translocation of this complex and binding to IFN-stimulated response elements (ISREs). The production of ISGs is induced. The evasion mechanisms of flaviviruses consist of: blockade of phosphorylation of Tyk2 and Jak1 by NS5; reduction in STAT2 gene and protein expression by NS5; inhibition of STAT signaling by non-structural proteins; down-regulation of the IFNAR through virus-induced redistribution of cellular cholesterol and impairment of ISG functions.

1.2.2.1 Host innate immune response against dengue

The host cell's first line of defense starts with innate immune recognition of dengue viral RNA by pattern recognition receptors (PRRs). PRRs important for RNA viruses include toll-like receptors (TLRs), particularly TLR-3, TLR-7, TLR-8, intracellular sensors such as the DExE/H box and RNA helicases such as retinoic acid-inducible gene (RIG-I) and melanoma differentiation-associated protein 5 (MDA5) (Green et al., 2014)

After endosomal acidification, one of the TLRs, involved in dengue viral recognition, TLR-3, recognizes DENV RNA and induces strong IL-8 and interferon α/β responses (Lee et al., 2012a; Tsai et al., 2009). This results in phosphorylation of TIR-domain-containing adapter-inducing interferon β (TRIF). Following phosphorylation, TRIF interacts with both TNF-receptor-associated factors TRAF3 and TRAF6. Interaction of TRAF3 with TANK binding kinase 1 and Ik kinase 1(Ikk1) cause interferon regulatory factor (IRF)-3 phosphorylation while TRAF6 signals through association with TAK1, leading to activation of activator protein 1 (AP-1), initiation of Ikk1/Ikk2 dephosphorylation of IkB and finally NFkB (nuclear factor kappa-light-chain-enhancer of activated B cells) activation. Production of IFNs, interferon stimulation genes (ISGs) and chemokines is then induced following nuclear translocation of IRF3, AP-1, and NFkB. Administration of TLR-3 and TLR-7/TLR-8 agonists resulted in significantly decreased viral replication along

with increased production of pro-inflammatory chemokines, thus revealing a protective role for TLRs during dengue infection (Sariol et al., 2011).

In conjunction with TLRs, RNA helicases such as RIG-I and MDA5 sense the intracellular viral RNA during infection and are induced leading to IFN-β production (Loo et al., 2008; Nasirudeen et al., 2011). Both RIG-I and MDA5 signal through the mitochondrial antiviral signaling protein (MAVS) present on the mitochondria which interacts with the stimulator of interferon genes (STING). Upon activation, mitochondrial antiviral signaling protein (MAVS) oligomerizes and attracts many ubiquitin E3 ligases such as TRAF3 and TRAF6 which activate intracellular signaling cascade that results in the transcription and production of interferon (IFN) α/β.

Interferons promote the intracellular antiviral responses and initiate the adaptive immune responses throughout the course of dengue infection. When secreted by infected cells, IFN-α/β triggers warning signals to adjacent cells that an infection is in progress and acts as an autocrine or paracrine induction of cellular antiviral responses. IFN-α/β binds to the IFN-α/β receptor (IFNAR), activating the JAK/STAT pathway via phosphorylation of the adaptor molecules tyrosine kinase 2 (TYK2) and janus kinase 1 (JAK1) (Darnell et al., 1994; Velazquez et al., 1992). This results in the phosphorylation and dimerization of various signal transducer and activator of transcription (STAT) molecules. In response to IFNAR activation, the interferon stimulating gene factor 3 complex (STAT1, STAT2, IRF9) is one

important signaling complex formed that migrates to the nucleus and binds to IFN-stimulated response elements located in the promoter region of IFN stimulated genes (ISG). This binding induces the production of multiple antiviral proteins including interferon-induced transmembrane (IFITM) proteins, viperin, ISG20, double-stranded RNA activated protein kinase R (PKR) and pro-inflammatory cytokines (Platanias, 2005). All these ISGs are known to restrict dengue infection by either preventing viral entry or replication (Chan et al., 2012; Jiang et al., 2010). In addition, IFNAR signaling induces alternative signaling cascades, such as the mitogen-activated protein kinase p38 cascade and the phosphatidylinositol 3 kinase cascade that lead to production of pro-inflammatory cytokines and chemokines.

Thus, interferons have been demonstrated to be highly effective against DENV infection (Diamond et al., 2000; Johnson and Roehrig, 1999). In response, DENV has developed many ways to manipulate the cellular antiviral responses and directly inhibit cellular signaling cascades.

1.2.2.2 Subversion of innate immune responses by dengue

As interferons are such strong inhibitors of dengue infection, DENV has evolved several strategies to attenuate the induction of IFN and its effector responses (Morrison et al., 2012). Dengue virus is able to inhibit IFN at various steps of the signaling cascade. Such a multifaceted approach is likely important to ensure that if one evasion strategy fails, yet another can aid in downregulation of IFN during dengue infection. This review shall focus

on the role of dengue coding and noncoding regions in subversion of IFN response during infection.

1.2.2.2.1 Role of dengue coding regions

The coding regions of the dengue genome are translated to produce viral proteins, essential for the various stages of DENV lifecycle and as numerous studies have shown, important for the inhibition of innate immune responses during infection (Figure 1.11) (Green et al., 2014).

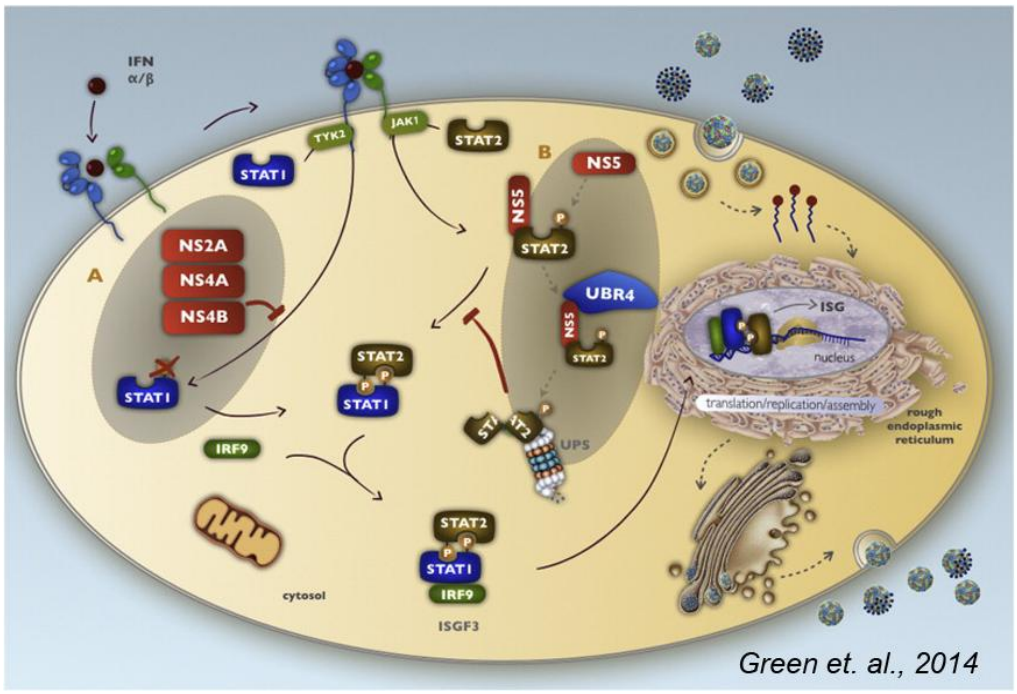

Figure 1.11 Dengue virus interference with IFN-α/β signaling The DENV non-structural proteins impede IFN-α/β signaling in infected cells. (A) NS2A, NS4A and NS4B complex together to prevent STAT1 phosphorylation, nuclear translocation and transcriptional activation of ISGs. (B) DENV NS5 binds and degrades human STAT2, targeting it toward the proteasomal degradation pathway. This prevents the formation of the STAT1/STAT2 heterodimer and its transcriptional ISG induction.

Firstly, DENV non-structural proteins can act directly as IFN antagonists on distinct components of the signaling cascade. Flaviviral NS1 can mediate the inhibition of TLR3-dependant responses during infection (Wilson et al., 2008). A transmembrane receptor, TLR3 interacts with an

adaptor molecule to induce activation of kinases, phosphorylation and nuclear translocation of IRF3. Its signaling leads to activation of transcription factors such as NF-κB and subsequent IFN-β promoter transcriptional activation. In West Nile virus infection, NS1 was found to inhibit TLR3 induced transcriptional activation of promoters by preventing nuclear translocation of IRF3, thus interfering with the type 1 interferon pathway and TLR3-dependent establishment of an antiviral state in cells.

Recently, three independant reports have also shown that the enzymatically active DENV NS2B/3 protease abrogates the IFN production in a species-specific manner by directly cleaving the STING protein (Aguirre et al., 2012; Rodriguez-Madoz et al., 2010; Yu et al., 2012). A key adapter protein in the type 1 interferon pathway, STING induces interferon production when cells are infected with pathogens through TANK-binding kinase (TBK-1) phosphorylation and subsequent activation of transcription factors IRF3/7 and NFκB. The cleavage site of STING was mapped to the NS2B/NS3 protease, thus identifying one other mechanism of how dengue subverts the host innate immunity (Aguirre et al., 2012; Yu et al., 2012).

In addition, NS2B, NS4A and NS4B are able to block the nuclear localization of STAT1 and transcriptional activation of the IFN promoters leading to inhibition of IFN signaling and hence downregulation of ISG expression (Grant et al., 2011; Munoz-Jordan et al., 2005; Munoz-Jordan et al., 2003). Interestingly, proper proteolytic processing of NS4A/4B is required for this anti-interferon function (Munoz-Jordan et al., 2005).

Even if ISG expression were to occur, DENV is still able to overcome some of their effects. One mechanism of subversion is through the 2′-*O* methylation of the viral mRNA cap structure by the dengue NS5 protein (Daffis et al., 2010; Dong et al., 2012). Since cellular messenger RNA (mRNAs) are similarly methylated at the 2'-O positions of the 5' guanosine cap, by "camouflaging" as host mRNA, dengue RNA avoids MDA5 recognition and host restriction via interferon induced proteins with tetratricopeptide repeats (IFIT)-1 dependent and IFIT1-independent mechanisms (Daffis et al., 2010; Dong et al., 2012).

In addition, dengue NS5 has also been shown to bind and reduce the expression of STAT-2 protein (Ashour et al., 2009; Mazzon et al., 2009). Upon binding of IFN to IFN receptors on cell surfaces, STAT2 gets phosphorylated, activating the IFN signaling pathway leading to cells attaining an antiviral state to prevent viral replication. Thus, STAT2 plays an important role in IFN signaling. However, dengue antagonizes STAT2 by the binding of proteolytically processed mature NS5 (Ashour et al., 2009). This binding subsequently results in STAT2 degradation via the proteosomal pathway. Hence, NS5 is a potent and specific antagonist of the Type 1 IFN pathway. Interestingly, although NS5 alone can bind and inhibit phosphorylation of STAT2, its degradation is induced only when all nonstructural proteins are present (Mazzon et al., 2009).

1.2.2.2.2 Role of dengue noncoding regions - sfRNA

More recently, the 3'UTR of the DENV and other flaviviral genomes has been shown to play a critical role in regulating the host immune responses through the production of an abundant, highly structured noncoding RNA species of 0.3-0.7 kb in length termed subgenomic flavivirus RNA (sfRNA) (Roby et al., 2014). Remarkably, sfRNA is detected in abundance in cytoplasm of infected cells, not packaged into virions and is highly conserved among all members of the genus *Flavivirus* but not the family *Flaviviridae* (Pijlman et al., 2008). This suggests that it plays a vital and conserved role in flaviviral infections.

Interestingly, the start of sfRNA remains remarkably conserved even amongst different flaviviruses and corresponds to stemloop SL-II (or its equivalent structure) at the 5'end of the 3'UTR (Figure 1.12) (Chapman et al., 2014a; Funk et al., 2010; Pijlman et al., 2008). The formation of sfRNA is vastly dependent on the presence of conserved pseudoknot structures and does not require viral proteins nor viral replication. In 2010, two groups presented a model in which sfRNA is generated by the incomplete degradation of uncapped viral genomes by the cellular 5'-3' exonuclease XRN1 which cannot progress through the pseudoknot structures in SL-II (Funk et al., 2010; Silva et al., 2010). For DENV-2 however, the pseudoknot in SL-II does not appear necessary for sfRNA production but conserved residues within the SL-II stem may play an analogous role by forming XRN1 resistant structures (Chapman et al., 2014b).

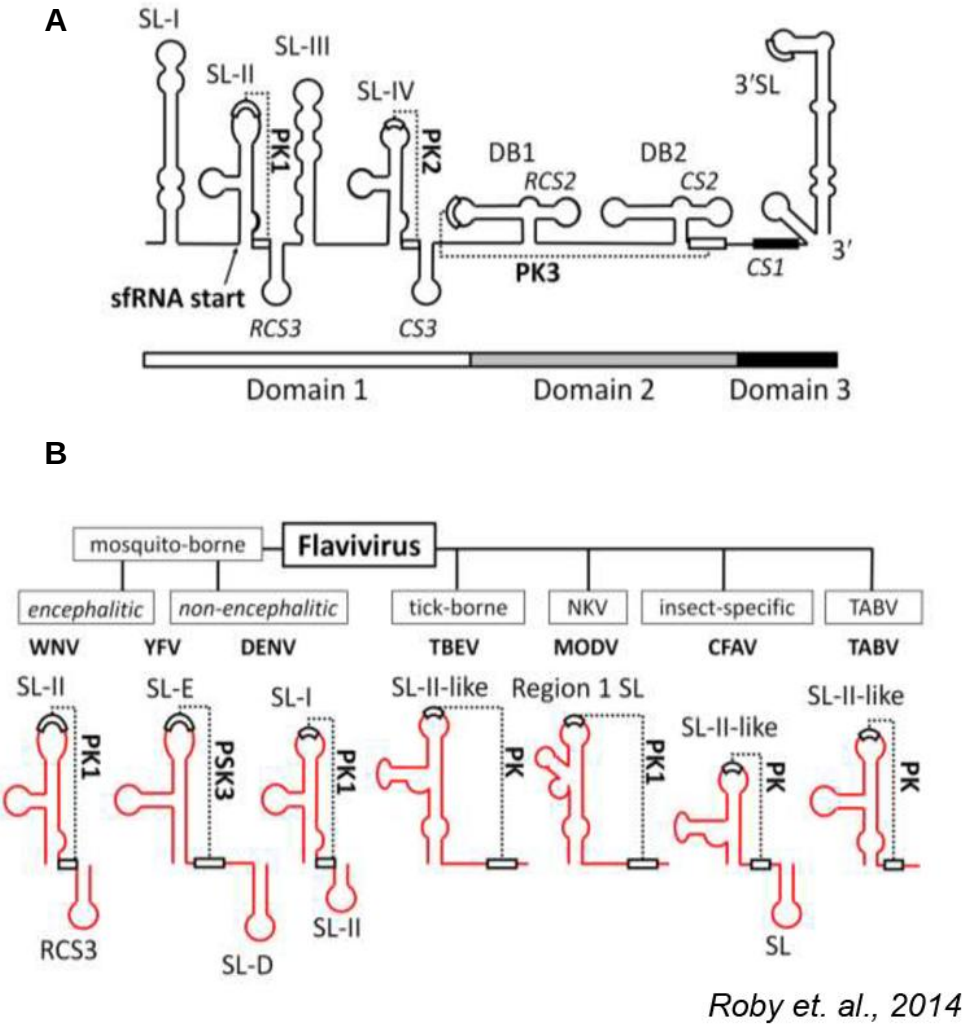

Figure 1.12 The 3'UTR structure of west nile virus and conservation of SL-II within the genus Flavivirus (A) Schematic representation of the 3'UTR demonstrating the arrangement of stemloops (SL) and pseudoknots (PK) and the sfRNA start site. (B) Schematic representation showing the predicted conservation of the SL-II/PK1-like RNA structure within the 3'UTR of divergent members of the genus Flavivirus.

The proportion of sfRNA is greater than viral genomes in both infected mammalian and mosquito cells with ratios ranging from 10:1. sfRNA could thus play a critical role in regulating the flaviviral life cycle (Fan et al., 2011; Funk et al., 2010; Lin et al., 2004; Liu et al., 2010; Pijlman et al., 2008; Silva et al., 2010). Surprisingly, functional studies using mutants showed that viral replication is not abrogated when sfRNA is not produced (Funk et al., 2010; Liu et al., 2014; Pijlman et al., 2008; Silva et al., 2010). Although there was a delay in replication, viruses deficient in sfRNA could still reach peak titers as compared to wild type viruses. Consistent with this finding, when sfRNA formation was compromised, there was no effect on translation, RNA synthesis or packaging of reporter constructs (Pijlman et al., 2008). However, presence of sfRNA is absolutely vital to viral cytopathogenicity suggesting that sfRNA is critical for virus-host interactions (Liu et al., 2014; Pijlman et al., 2008; Silva et al., 2010).

Although sfRNA was first observed in Murray Valley encephalitis (Urosevic et al., 1997), Japanese encephalitis (Lin et al., 2004) and West Nile viruses (Scherbik et al., 2006), the mechanism of sfRNA generation and its importance in pathogenicity remained highly elusive till recent years. Since then, it has been shown to play a multifaceted role in modulating the host antiviral response, although many underlying mechanisms remain incompletely understood (Figure 1.13) (Bidet and Garcia-Blanco, 2014).

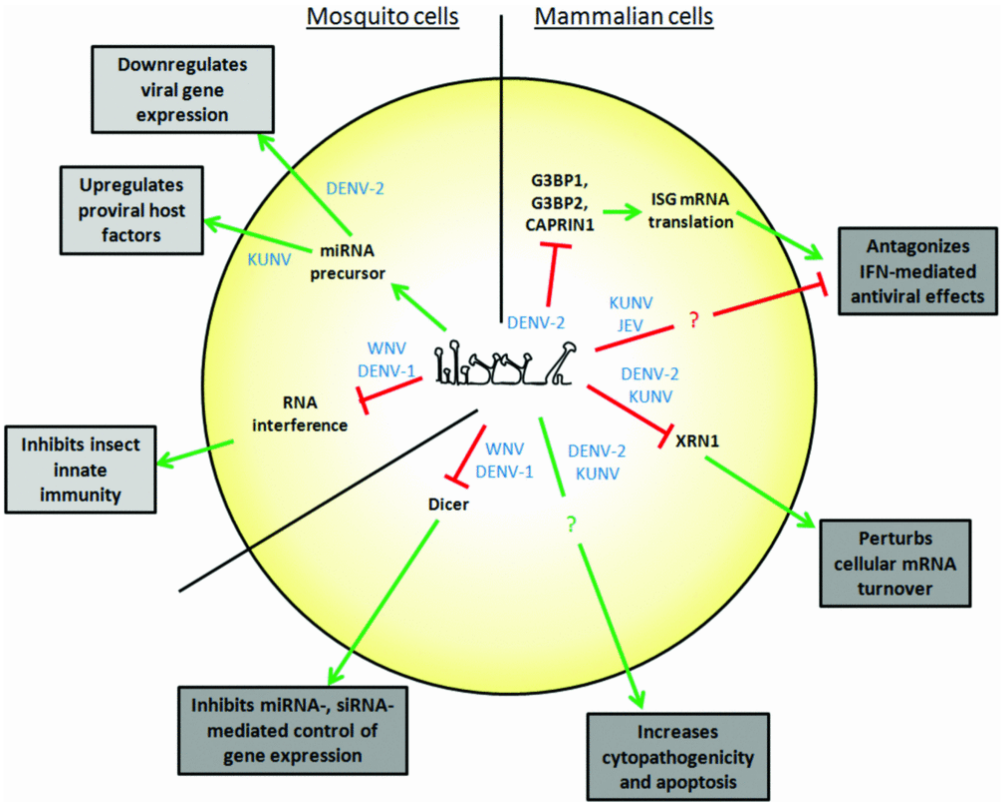

Bidet and Garcia-Blanco, 2014

Figure 1.13 Cellular functions of noncoding sfRNA Several cellular targets and characterized functions for the various sfRNAs (indicated in blue) have been summarized. RNA interference (RNAi) and interferon (IFN) pathways are insect and mammalian-specific host defense mechanisms

Functions of sfRNA that have been described include: regulation of RNAi pathway, modulation of interferon pathway and inhibition of RNA decay.

1.2.2.2.2.1 Inhibition of cellular RNA decay

The biological process of mRNA turnover occurs in cytoplasmic structures known as processing bodies (PBs). Given their canonical role in mRNA decay, PB machinery is hypothesized to have potent antiviral activity against viral RNA genomes. Antagonizing PB-associated functions is thus a strategy employed by many viruses to evade cellular defences (Lloyd, 2012). Likewise, flaviviral sfRNA has been shown to interact with XRN1, increasing the overall messenger RNA (mRNA) stability within the host cell (Moon et al., 2012). This is possible as XRN1 remains associated with sfRNA after stalling at the 3'UTR RNA structures. This results in an accumulation of uncapped RNA transcripts in infected cells. On the other hand, this accumulation of partial RNAs is not noticed in cells infected with a kunjin virus (KUNV) mutant that is unable to produce sfRNA (Moon et al., 2012). Although the reason behind this inhibition is not clearly elucidated as yet, it is suggested that disruption of mRNA homeostasis by preventing XRN1 function might impair cellular functions to benefit the virus.

1.2.2.2.2.2 Perturbing the RNAi pathway

The inhibition of gene expression by RNA molecules is known as RNA interference (RNAi). Typically, the target mRNA molecules get destroyed in this process. Two types of small RNA molecule, microRNA (miRNA) and small interfering RNA (siRNA) are central to RNA interference. Both RNAs can be produced by the same pathway after which their precursors are processed

by endonucleases such as Dicer before being loaded into the RNA-induced silencing complex (RISC). In flavivirus-infected cells, RNAi mediated silencing of genes is impaired and expression of DENV and WNV sfRNAs inhibit DICER cleavage of double stranded RNA by directly binding to and saturating the RNAse (Pijlman, 2014; Schnettler et al., 2012). Given that RNAi has direct and broad antiviral activity in arthropod cells, the suppression of RNAi pathway by sfRNA could be a host-specific evasion of innate immunity in mosquito cells (Bidet and Garcia-Blanco, 2014).

1.2.2.2.2.3 Interference with IFN-mediated innate immune responses

The antagonism of the innate immune response is one of the better characterized functions of sfRNA. sfRNA has been implicated in the evasion of IFN-α/β pathway in DENV (Bidet et al., 2014), KUNV (Schuessler et al., 2012) and JEV (Chang et al., 2013).

During JEV infection, sfRNA inhibited IFN production by interfering with the phosphorylation, activation and nuclear translocation of IRF3 (Chang et al., 2013). Without sfRNA production, KUNV mutants were inhibited in IFN-competent cell lines and mice. These mutants were especially sensitive to exogenous IFN suggesting that KUNV sfRNA likely impairs ISG expression or function (Schuessler et al., 2012). In both cases, however, the actual mechanism of action was not fully determined.

In DENV-infected cells, it was recently reported that sfRNA sequesters three multifunctional RNA binding proteins (G3BP1, G3BP2 and CAPRIN1)

required for translation of ISG mRNAs (Bidet et al., 2014). This led to inhibition of ISG expression and renders the infected cells unable to mount an efficient antiviral state. This is the first mechanism proposed at the molecular level for the interaction between sfRNA and RNA binding proteins to impede host immune response. What is remarkable is that this mechanism is not conserved between flaviviruses or even between DENV-2 and DENV-3. This finding proposes that specific mechanism of action of sfRNA for viral evasion of the IFN response may diverge widely between related viruses and even strains (Diamond, 2009; Schoggins et al., 2011; Umareddy et al., 2008). Thus, it appears likely that different sfRNAs may target various host factors to perturb multiple stages of the IFN pathway using a sfRNA as a common pan-flaviviral strategy to inhibit the host innate immune response (Figure 1.14).

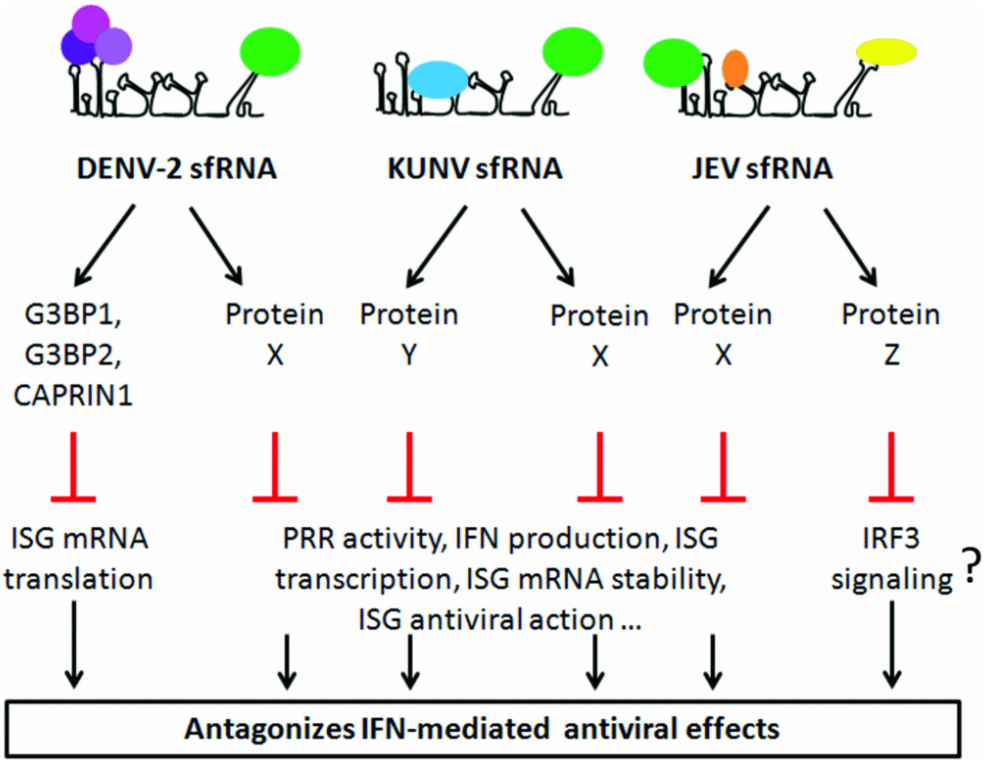

Bidet and Garcia-Blanco., 2014

Figure 1.14 Model depicting diverse strategies for sfRNA-mediated viral evasion of the IFN response Model proposes that rapidly evolving sequences in the sfRNA permit different viruses to sequestrate various types of host proteins (X, Y and Z). Binding to host proteins inhibits their activity, resulting in antagonism of the IFN response at different stages.

To summarize, DENV has many tactical approaches to inhibit the host's innate immune response which may impact the adaptive immune response and ultimately modulate the disease outcome.

1.3 Epidemiology

1.3.1 Dengue is an emerging disease

Over the last five decades, global dengue incidence has grown precipitously throughout the tropical and subtropical world, endangering an estimated 3 billion people – over 40% of the world's population (Figure 1.15) (Bhatt et al., 2013; Guzman et al., 2010; Simmons et al., 2012). Where only 9 countries had experienced severe dengue epidemics before 1970, the disease is now endemic in more than 100 countries in Africa, South-east Asia, Eastern Mediterranean, the Americas and Western Pacific (WHO, 2007)

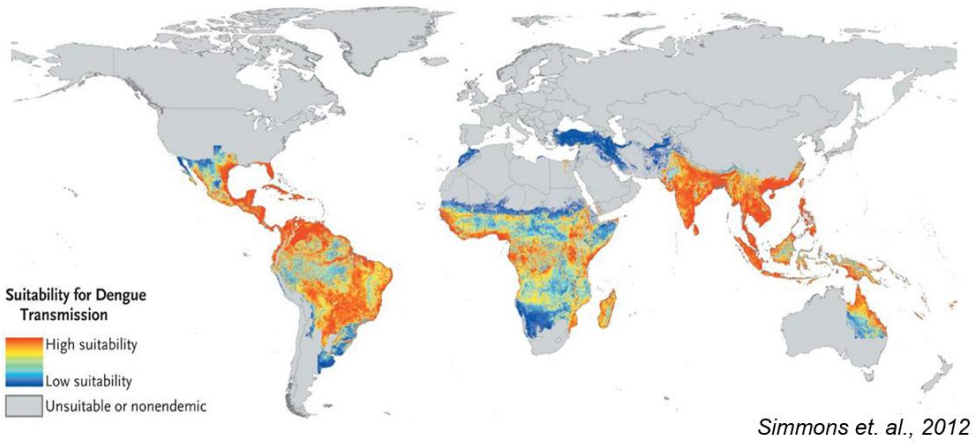

Figure 1.15 Global dengue risk Risk status was determined based on combined reports from the World Health Organization, the Centers for Disease Control and Prevention, Gideon online, ProMED, DengueMap, Eurosurveillance, and published literature.

This spread of dengue across the tropics and subtropics is mainly due to an increased geographical distribution of the virus and its mosquito vector from demographical change, unprecedented and uncontrolled urbanization, inadequate domestic water supplies, increased international travel and trade

(Gubler, 2001, 2004; Gubler and Meltzer, 1999; Rigau-Perez et al., 1998). This convergence of factors has resulted in an increase in the number of reported cases.

Based on World Health Organization reports, dengue cases have exceeded 1.2 million in 2008 and over 2.3 million in 2010 (Figure 1.16) (WHO, 2014). In 2013, 2.35 million cases were reported in Americas alone and this number continues in an upward trend. Furthermore, these reported cases are likely to underestimate the true burden of disease. A recent report using cartographic approaches estimated an intimidating figure of 390 million dengue infections each year (Figure 1.2)(Bhatt et al., 2013; WHO, 2014). Another recent report showed that India alone has an estimated 5.8 million dengue cases per year, a stark contrast to the reported 20, 500 cases after adjusting for under-reporting (Shepard et al., 2014).

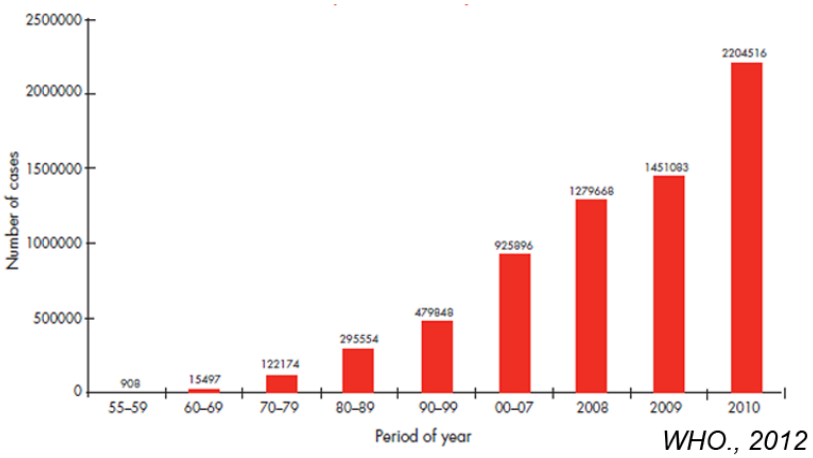

Figure 1.16 Average number of reported dengue cases Average numbers of dengue and severe dengue cases reported annually to WHO between 1955 to 2007. Number of cases reported in recent years: 2008-2010.

Besides increasing incidence of dengue cases in contrast with observations made 30 years ago, more places are also in recent years

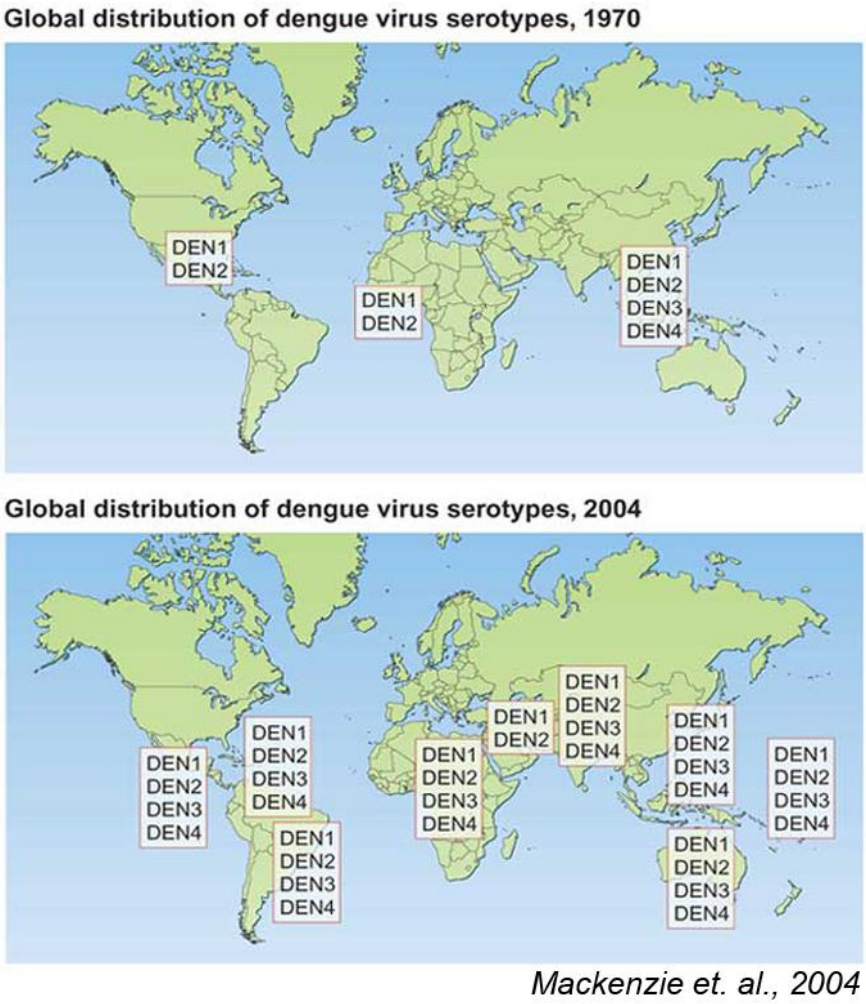

Figure 1.17 Change in distribution of dengue serotypes over the past 30 years

reporting the co-circulation of all four dengue virus serotypes (DENV-1-4) at any given time (Figure 1.17) (Mackenzie et al., 2004). Such endemicity for all four serotypes, or hyperendemicity, contributes to increased risk of secondary infection and the increased risk of emergence of new and perhaps fitter strains (Gubler and Trent, 1993). All these factors culminate in increased incidence of severe disease and epidemic dengue.

1.3.2 Problems caused by dengue as an emerging disease

The public health and economic impact of dengue is greatly underestimated because of limited surveillance data and gross under-reporting either due to the insensitivity of clinical diagnosis in regions without sufficient laboratory support. Despite this, severe dengue disease has now emerged as a major cause of hospitalizations and deaths globally. The number of severe cases reported between 1981 and 1995 was four times higher than that of the previous 30 years (Gubler, 1998b). Approximately 500,000 people with severe dengue require hospitalization every year, a considerable proportion of whom are children and about 2.5% of those affected die (Gubler, 2002).

Furthermore, dengue brings a costly burden with a 2009 estimate reporting that 700 000 disability-adjusted life years (DALYs) are lost to dengue globally each year (Hotez et al., 2009; Meltzer et al., 1998). The main burden of this mortality and morbidity lie with children in most dengue endemic countries, thus placing dengue among the most significant diseases of children worldwide (Guzman et al., 2002; Hammond et al., 2005)

Dengue also causes substantial economic loss. The economic cost for dengue is an average of US$41.5 million per year based on distribution of costs in Singapore from 2000-2009 (Carrasco et al., 2011). A review of all nations in Americas estimated an aggregate annual cost of US $2.1 billion for dengue, excluding costs pertaining to dengue prevention

(Shepard et al., 2011). Indirect or "productivity" losses amounted to 60% of this cost. Yet another study revealed an annual economic burden of US $950 million among 12 nations in South East Asia, with ~52% of these costs amounting from productivity losses (Shepard et al., 2013). Thus, the extensive impact of dengue has ranked it as the most important mosquito-borne viral disease in the world (WHO, 2014)

1.3.3 Interplay of host and viral factors in dengue epidemics

In the absence of a licensed vaccine, antiviral therapy or sustainable preventative measures, the geographic distribution of DENV has increased over the last 40 years causing frequent cyclical epidemics. Although the emergence of epidemic dengue is complex and multifactorial, including urbanization, globalization and lack of mosquito control, this section shall provide deeper insights into the complex dynamics between immunological determinants (namely, serotype switch) and viral genetics in the context of dengue epidemics.

1.3.3.1 Serotype switch linked to dengue epidemics

Herd immunity proposes that when the majority of a population are immune or less susceptible to a disease, such as dengue, the chains of infection are disrupted with less susceptible individuals getting infected. Since DENV infection is serotype-specific, this means that introduction of new serotypes into a population would lead to dengue epidemics. Furthermore, if a population has been previously exposed to one serotype of DENV, heterologous antibodies could enhance virus replication. This would lead to higher viremia in infected individuals that would increase virus transmission to mosquitoes and hence, expansion of epidemics.

Therefore, previously it was widely thought that a serotype switch was responsible for most dengue epidemics in endemic countries, because of

lowered herd immunity to the new serotype and the likelihood of enhanced dengue infection. This was evident in Cuba, where DENV-1 caused a nationwide epidemic of dengue fever in 1977 and introduction of DENV-2 in 1982 resulted in a massive epidemic of severe dengue disease (Kouri et al., 1989). Similarly in 2001-2002, upon introduction of DENV-3, there was another major epidemic in Cuba (Alvarez et al., 2006). In Martinique, four outbreaks occurred between 2001 and 2010, all of which were characterized by the predominance of a new serotype replacing a previous serotype: DENV-3 in 2001, DENV-4 in 2005, DENV-2 in 2007, DENV-1 and DENV-4 in 2010 (Thomas et al., 2014). In French Polynesia, after almost a decade of DENV-1 circulation, the introduction of DENV-4 resulted in an epidemic in 2009 (Cao-Lormeau et al., 2011). Likewise, in Iquitos, Peru, the introduction of DENV-3 in 2001 resulted in replacement of the co-circulating DENV-1 and DENV-2, subsequently causing an epidemic. Subsequently, DENV-3 was displaced by DENV-4 in 2008 resulting in another major outbreak (Stoddard et al., 2014).

A shift in dominant serotypes from DENV-2 to DENV-3 in 1987 and DENV-4 to DENV-3 in 1995 also resulted in severe outbreaks in Bangkok, Thailand (Nisalak et al., 2003). In Singapore, serotype switch also played a role in dengue epidemiology. A major outbreak in 2005 occurred when the predominant DENV-2 serotype was suddenly displaced by DENV-1 (Koh et al., 2008). Interestingly, despite the population having been exposed to DENV-2 previously which should have increased herd immunity to DENV-2,

another DENV-2 outbreak occurred in 2007. Upon further probing, it was discovered that a change in DENV-2 viral genotype accompanied this 2007 epidemic (Lee et al., 2010). Therefore, serotype switch alone cannot explain the resurgence of many epidemics and viral genetics play an undeniable role in the epidemic potential of DENVs.

1.3.3.2 Virus genetics linked to recent epidemics

Several studies have reported the association between the emergence of novel dengue genotypes and the onset of epidemics (Bennett et al., 2006; Kanakaratne et al., 2009; Liang et al., 2013; Messer et al., 2003; OhAinle et al., 2011; Steel et al., 2010; Vu et al., 2010). This is evident in Puerto Rico, a densely populated island in the Americas where the first recorded dengue epidemic occurred in 1915 (Brathwaite Dick et al., 2012). Dengue was first identified in 1969 and DENV-2 persisted for 8 years prior to 1994 (Figure 1.18) (Brathwaite Dick et al., 2012; McElroy et al., 2011).

In 1994 a novel DENV-2 genotype emerged in Puerto Rico and triggered an island-wide outbreak (Bennett et al., 2006). This outbreak was the largest Puerto Rican dengue epidemic on record in terms of hospitalizations and deaths at the time (Rigau-Perez et al., 2001). A total of 24,700 cases were detected with at least 23% of the patients showing hemorrhagic manifestations and 19% hospitalized. 40 deaths were reported. Up till the DENV-4 epidemic in 1998 and the 2007 DENV-3/DENV-2 epidemic, the 1994 epidemic produced the most hospitalizations, severe disease cases and deaths in Puerto Rico (Bennett et al., 2003; Tomashek et al., 2012). Disease severity also remained unchanged throughout the entire year. Lowered herd immunity could not be attributed as the cause of this outbreak since DENV-2 had been circulating in Puerto Rico prior to the

epidemic. Partial genome sequencing of the structural genes later revealed that three distinct DENV-2 lineages were circulating during this epidemic: the endemic lineage introduced to Puerto Rico in 1984 and two foreign lineages that appeared for the first time on the island in 1994 (Figure 1.19) (Bennett et al., 2006).

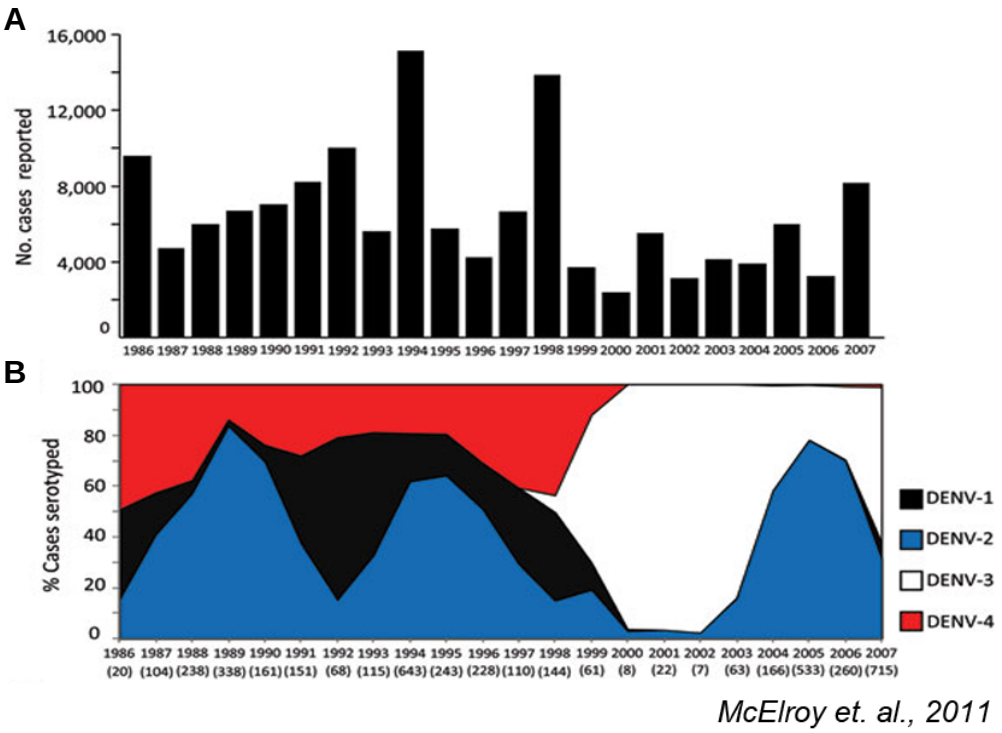

Figure 1.18 Historic Overview of dengue in Puerto Rico, 1986-2007 (A) Number of dengue cases per year, reported to Centers for Disease Control and Prevention's Dengue Branch. (B) Percentage of each serotype identified relative to the total positive serotype identifications. Numbers in parenthesis indicate numbers of DENV-2 per year.

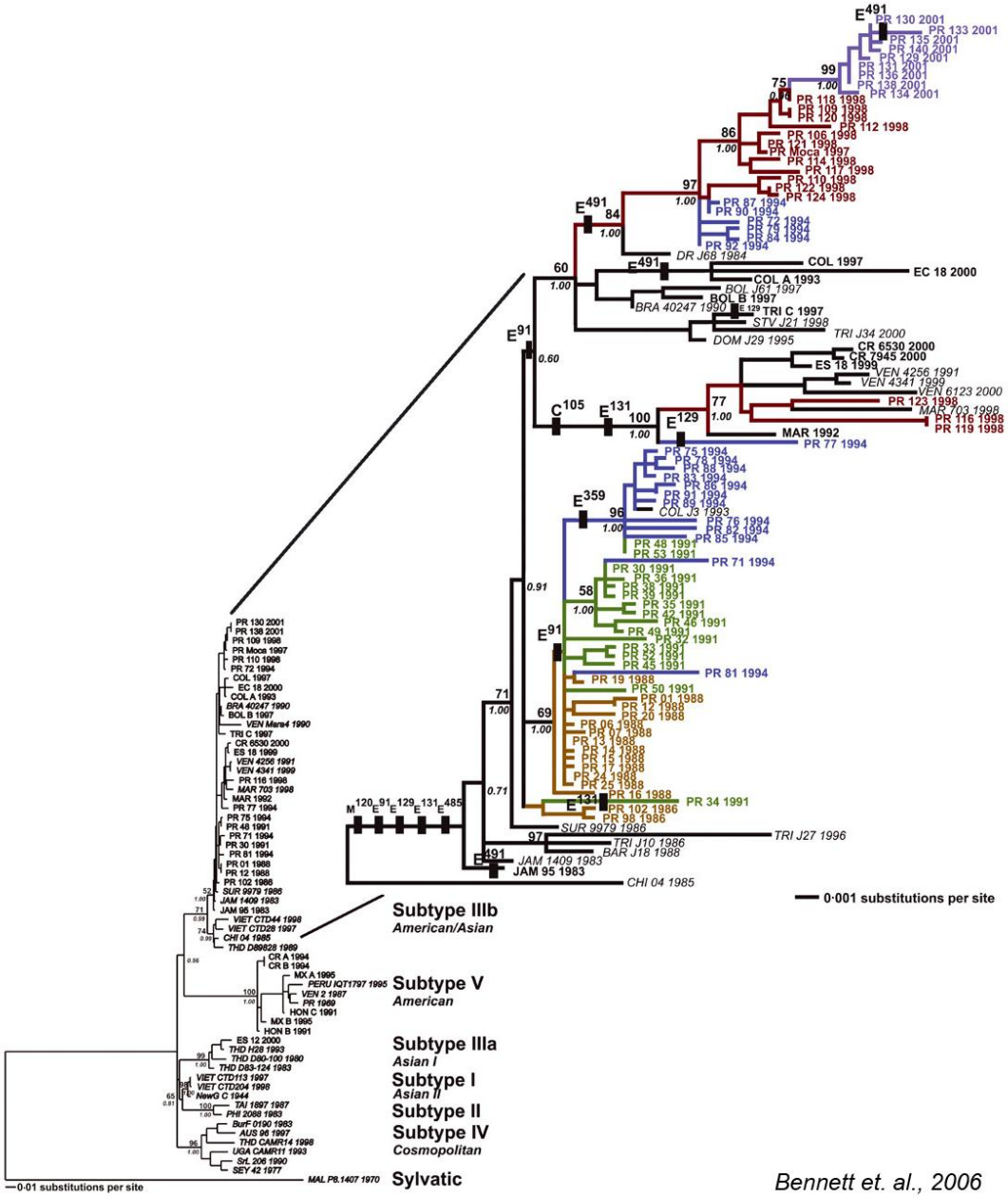

Figure 1.19 Maximum-likelihood (ML) phylogenetic tree of DENV-2 sequences in Puerto Rico and other countries. Analysis was based on published sequences of the structural genes (capsid, membrane and envelope). All samples are coded by location, number and year of isolation: Australia (AUS), Bolivia (BOL), Brazil (BRA), Burkino Faso (BurF), China (CHI), Colombia (COL), Costa Rica (CR), Ecuador (EC), El Salvador (ES), Honduras (HON), Jamaica (JAM), Malaysia (MAL, sylvatic), Martinique (MAR), Mexico (MEX), New Guinea (NewG C), Peru, Philippines (PHI), Puerto Rico, (PR), Seychelles (SEY), Sri Lanka (SrL), Surinam (SUR), Taiwan (TAI), Thailand (THD), Trinidad (TRI), Uganda (UGA), Venezuela (VEN), Vietnam (VIET), Barbados (BAR), Dominica (DOM), Dominican Republic (DR) and St Vincent (STV). Colour coding of branches shows the year of sample isolation for PR sequences with foreign isolates coloured black. Bootstrap-support values appear above and below nodes, respectively. Unambiguous amino acid changes in the structural genes are indicated along the major lineages, highlighted with black bars and labeled with amino acid positions within the genes.

One of these foreign DENV-2 lineages includes only 4 divergent isolates from 1994 to 1998, suggesting that it never became established in Puerto Rico. The other foreign lineage rapidly became dominant and persisted through 2001 (Bennett et al., 2006). The appearance of this dominant foreign lineage and the concomitant dengue epidemic of 1994 strongly suggest that this particular lineage possessed greater fitness than the endemic strain of DENV-2 that had been in circulation on the island. Similar introduction or evolution of new viral genotypes or subtypes resulting in epidemic dengue has been reported elsewhere.

In Sri Lanka, DENV-3 was responsible for the first dengue hemorrhagic fever outbreak in that country's history in 1989 despite the fact that this serotype had been in circulation since at least 1981. That outbreak was associated with a lineage change in the endemic genotype of DENV-3 (Messer et al., 2003). Abrupt increases in reported dengue cases in 1989 and 2000 were again observed in Sri Lanka, and this coincided with emergence of new clades of DENV-3 (Kanakaratne et al., 2009). Notably, DENV-3 isolates from mild and severe disease outbreaks fell into genetically distinct groups, thus suggesting a role for viral genetics in severe dengue disease.

In Nicaragua, a sudden increase in dengue disease severity was detected across DENV-2 epidemic seasons. This was found to coincide with a clade replacement event where the endemic Asian/American DENV-2 NI-1 was replaced by a new virus clade NI-2B. *In vitro* studies showed that NI-2B

viruses had increased fitness in human and mosquito cells, thus supporting the emergence of a fitter virus (Figure 1.14) (OhAinle et al., 2011).

In the Pacific islands, the American genotype DENV-2 was circulating since 1971, causing epidemics of varying intensity and clinical severity. However, upon reaching Tonga in 1973, near-silent transmission was observed for more than a year. Whole genome sequencing and phylogenetic analysis revealed that a clade change had occurred with the Tonga viruses being genetically distinct, thus coinciding with decreased disease severity, viremia levels and epidemic potential (Gubler et al., 1978; Steel et al., 2010)

Genotype replacement events in Vietnam, Thailand and Cambodia also occurred resulting in a complete replacement of the dominant Asian/American lineage viruses by Asian I viruses (Vu et al., 2010). *In vitro* studies showed little difference in infectivity of mosquitoes but significantly higher plasma viremia levels were observed in patients infected with Asian I lineage viruses. The latter could have resulted in greater likelihood of mosquito infection upon taking blood meal from dengue patients. In Canton, China, DENV-3 was introduced in 2009 after almost 30 years since its previous circulation (Liang et al., 2013). However, a larger outbreak only occurred in 2010. Epidemiological and phylogenetic analyses showed that the outbreak in 2010 was caused by a different strain of DENV-3.

Collectively, the abovementioned epidemiological studies reveal the association between DENV strains and epidemic emergence. Despite these

associations, however, little is known about the underlying mechanisms behind the genetic determinants of viral fitness in epidemiological settings.

1.4 What is the molecular basis for dengue epidemics - Gaps in knowledge

The literature review has elaborated on the contribution of viral factors to severe dengue pathogenesis and increased epidemic potential, otherwise referred to as epidemiological fitness throughout this text. Indeed, epidemiological fitness is a term coined in this study to indicate the ability of a virus to propagate itself in a natural human-mosquito-human transmission. Epidemiological fitness thus encompasses several factors, including virus replication rate and the ability to evade host immune responses. For instance, a virus that replicates rapidly *in vitro* may not necessarily be epidemiologically fitter as it is unable to suppress host immune responses.

Although molecular studies have shown that genetic differences in DENV can result in increased replication, viremia and hence more efficient transmission to mosquitoes, there remains a lack of knowledge into how these genetic differences can mechanistically result in epidemics at a molecular level. On the other hand, despite the strong association between emergence of new viral phylogenetic clades and epidemic dengue reported in several locations globally, epidemiological studies are unable to provide mechanistic explanations for how genetic differences alter epidemiological fitness of DENV. Combining epidemiologic studies with molecular investigations could thus be highly informative not only on the virus origin but also as a predictor of its epidemic potential.

This thesis thus attempts to bridge these gaps in knowledge by studying DENV-2 isolates from the 1994 Puerto Rican epidemic. The main aims are:-

(1) To define the regions of the DENV-2 genome that could contribute towards greater epidemiological fitness.

(2) To determine the molecular mechanism that contributes to epidemiological fitness.

CHAPTER 2:

Materials and Methods.

2.1 Cells

HuH-7, C6/36, Vero and BHK-21 cells were purchased from the American Type Culture Collection (ATCC, USA) and cultured according to ATCC recommendations.

Harvesting and culture of primary monocytes was carried out in collaboration with Eugenia Ong and approved by the National University of Singapore Institutional Review Board (NUS IRB reference code 12-160). Venous blood was collected from the principal investigator in BD sodium heparin vacutainers (Biomed Diagnostics, Singapore). Then the blood was diluted with 2 volumes of 0.5% bovine serum albumin (BSA, Sigma-Aldrich, USA) in phosphate buffered solution (PBS, 1st Base, Singapore) (0.5% PBS/BSA). Diluted blood was layered carefully onto Ficoll-hypaque (GE healthcare, Singapore) and centrifuged at 750g, without brakes. After centrifugation, interphase cells that contain the peripheral blood mononuclear cells (PBMC) were aspirated and transferred to a clean tube, after which the PMBC were washed thrice with 0.5% PBS/BSA and resuspended in growth medium (RPMI-1640 supplemented with 10% fetal bovine serum, 100U/ml penicillin and 100µg/ml streptomycin). Cells were then counted and seeded onto T25 tissue culture flasks (NUNC, Bio Laboratories, Singapore) at $1x10^7$ cells per flask. They were incubated at 37°C, 5% CO_2 for 2.5 hours to allow the monocytes to adhere to the flask surface. After this incubation, adhered cells were washed 5 times with PBS to

remove the non-adherent cells, and replenished with fresh growth medium. This was followed by an overnight incubation at 37°C, 5% CO_2 to allow the PBMC to recover before use in experiments.

2.2 Viruses

The DENV-2 infected patient sera used in this study were gifts from the Dengue Branch of the Centers for Disease Control and Prevention, Puerto Rico. These patient sera were obtained during the 1994 DENV-2 epidemic in Puerto Rico. Low-passage stocks of virus isolates were generated by inoculating acute patient sera onto C6/36 cells as previously described (Christenbury et al., 2010). These virus stocks were propagated in the C6/36 cell line and harvested 7 days post-infection following filtration. All viral isolates included in this study were passaged less than 5 times. Viruses were confirmed to be DENV-2 by an immunofluorescence assay, aliquoted and stored at −80 °C until use.

2.3 Plaque assay.

BHK-21 cells were seeded in 24-well plates (NUNC, Bio Laboratories, Singapore) overnight. The next day, serial dilutions (10-fold) of the virus were added to the confluent cells and incubated for 1 hour at 37°C. Following incubation, the media was aspirated and replaced with 0.8% methyl-cellulose in maintenance medium (RPMI-1640, 2% FCS, 25mM HEPES, penicillin and streptomycin). Then, the cells were incubated at 37˚C for 5 days and fixed with 20% formaldehyde at room temperature for 20 min.

After fixing, cells were washed with water, and 1ml of 1% crystal violet was added for 20 min. The plates were washed, dried and the plaque forming units per ml (pfu/ml) calculated.

2.4 Infections

HuH-7 cells were seeded onto 24-well plates at a dilution of $2x10^5$ cells per well overnight. When they reached ~80% confluency the next day, they were counted for an estimate of cell numbers. Viruses were then diluted in maintenance medium (1xDMEM, 2% FCS).accordingly to achieve a suitable multiplicity of infection (MOI), after which they were added onto the cells and incubated for 1 hour at 37°C. After the incubation, cells were washed with 1xPBS and maintenance medium was added. Infected cells were incubated at 37°C and subsequently harvested at various time-points. All HuH-7 infections were performed at a MOI of 1 for 24 hours unless otherwise indicated. After infection, the supernatant was harvested for plaque assay while RNA was extracted from infected cells for quantitative real-time PCR (qRT-PCR). Infection of Vero cells was performed exactly as described above.

For primary monocytes, infection was performed at MOI 10 with an enhancing concentration of humanized 3H5 monoclonal antibody (0.391µg/ml) to permit efficient uptake of the viruses, as previously described (Chan et al., 2014). Infectivity was measured using qRT-PCR on RNA from infected cells at 24 hpi and plaque assay on supernatant harvested at 72 hpi.

2.5 Sequence and structure analysis

The complete coding and non-coding regions of the clinical isolates were sequenced previously (Christenbury et al., 2010). The maximum likelihood phylogenetic tree was constructed using MEGA6 (Tamura et al., 2013) with the GTR+Γ4 model of nucleotide substitution from an alignment of 158 open reading frame DENV-2 sequences from Puerto Rico and neighboring countries. Neighbor-joining trees with a maximum likelihood optimized nucleotide model were generated using PAUP for full genomes of the 39 Puerto Rican isolates and 154 Nicaraguan isolates (Swofford, 1993). Statistical support for the topology of all the trees was determined by 1000 bootstrap replications. Individual gene trees were generated with the same method described above. Topological congruence of the gene trees with the genome tree was determined by the Shimodaira-Hasegawa and the Kashino-Hasegawa likelihood based tests (Kishino and Hasegawa, 1989; Shimodaira and Hasegawa, 1999). To construct the secondary structures of the 3'UTR, the chemical probing model proposed by Chapman et al, 2014 was used (Chapman et al., 2014a). Since the substitutions in the Nicaraguan clade replacement event were found to be a covariation of a base pairing, the UNAFold webserver was used to estimate the impact of this covariation on the molecule's free energy (Markham and Zuker, 2005).

2.6 Quantification of RNA

Total RNA from infected cells was extracted using Trizol (Invitrogen, Life Technologies, USA) or the RNeasy kit (Qiagen, Germany) as per manufacturer's protocols. Superscript III reverse transcriptase and random hexamers (Invitrogen, Life Technologies, USA) were used in the reverse transcription reactions to generate cDNA according to manufacturer's protocol. Quantitative real-time PCR (qRT-PCR) was performed on 2µl of cDNA using the iQ™ SYBR Green Supermix Kit (Bio-Rad, USA) according to the manufacturer's instructions. All PCR reactions were set up in triplicates and normalized against GAPDH mRNA levels (GAPDH primers: GAPDH-F/GAPDH-R).

Quantification of gRNA and sfRNA levels was performed as previously described (Bidet et al., 2014). Briefly, one primer (QG-For) anneals upstream of the stop codon, recognizing on the gRNA while the second primer (QGSF-For) anneals on the 3'UTR, downstream from the start of sfRNA, thus amplifying both gRNA and sfRNA. The reverse primer (QGSF-Rev) which anneals downstream of the dumbbell 2 structure is kept consistent in both instances, leading to PCR products of lengths 309bp and 184bp respectively. Reactions were carried out in the Roche Lightcycler® 480 (Roche Diagnostics, USA) machine with the following conditions: 95°C for 5 min, followed by 45 cycles of 95°C for 10 sec, 55°C for 5 sec and 72°C for 10 sec. For every reaction, the molar amount of template, n(G) and n(GSF) was calculated using a standard curve generated from serial dilutions of in-vitro

transcribed, full length pDENrep-FH (DENV-2 replicon) RNA. gRNA levels corresponded to the n(G) molar amounts while sfRNA was calculated by subtracting n(GSF)-n(G). Ratios of sfRNA:gRNA were determined by dividing the levels of sfRNA with gRNA. Quantification of intracellular viral RNA levels was carried out as detailed above, using a different primer set (LYL-F/ LYL-R) as previously published (Lai et al., 2007). This pair of primers bind within the 3'UTR, amplifying both gRNA and sfRNA. Primer sequences are shown in the table below (Table 2.1).

Primers used to detect the IFN-β and NFκB expression levels were obtained from OriGene. Cycling conditions for the quantification of immune genes: 95°C for 5 min, followed by 45 cycles of 95°C for 5 sec, 53°C for 10 sec and 72°C for 10 sec. Each reaction was accompanied by a matching reaction quantifying GAPDH mRNA levels for normalization. Results were expressed as fold change in target gene over untreated control cells, normalized to the GAPDH mRNA using this formula: Fold change = $2^{-d(dct)}$.

Table 2.1 List of primers used for qRT-PCR

Primer Name	Primer Sequence (5'-3')
QG-For	CCATGAAAAGATTCAGAAG
QGSF-For	GTGAGCCCCGTCCAAGG
QGSF-Rev	GCTGCGATTTGTAAGGG
GAPDH-F	GAGTCAACGGATTTGGTCGT
GAPDH-R	TTGATTTTGGAGGGATCTCG
LYL-F	TTGAGTAAACYRTGCTGCCTGTAGCTC
LYL-R	GAGACAGCAGGATCTCTGGTCTYTC

2.7 Northern hybridization

HuH-7 cells were infected with MOI 10 of DENV-2 and RNA harvested 24 hpi using Trizol (Invitrogen, Life Technologies, USA). Uninfected cells were used as control. Northern hybridizations were then performed as previously described (Pijlman et al., 2008) with slight modifications. Briefly, 10μg of purified RNA was denatured in a formamide buffer and run on a 1% formaldehyde-agarose gel at 80V for ~ 105 min. After that, the gel was soaked in autoclaved water thrice for 15 min each, denatured in 50mM NaOH for 20 min, neutralized in 100mM Tris-HCL (ph 7.0-7.5) for 20 min and finally soaked in 10x SSC for 15 min. Transfer of the RNA from the gel onto the Hybond-N^+ membrane (Amersham, GE Healthcare Lifesciences, USA) was then carried out overnight with 20x SSC buffer. Following the overnight transfer, the membrane was rinsed in 10x SSC after which RNA on the membrane was crosslinked using the CL-1000 UV crosslinker (UVP, USA).

Radioactive RNA probes were next prepared using the MAXIscript® T7 kit (Ambion, Life Technologies, USA), as per manufacturer's instructions. PCR products were first generated from uninfected HuH-7 cells using beta-actin primers (NB_ACTIN_F: 5'-CTAGAAGCTTTAATACGACTCACTATAGGGTGACCCATGCCCACCATCAC-3' and NB_ACTIN_R: 5'-CTAGGCTAGCATAGAGCACAGAGCCTCGCCTTT-3') and from a vector containing an antisense DENV-2 3'UTR sequence using the following primers (AW013: 5'-

ATAAAGCTTTAATACGACTCACTATAGGGAGAACCTGTTGATTCAACAGCAC-3’ and AW014: 5’-GGTCGGTCGTCTTCTCCCGCTAGCATAAAGAAGAGGAAGAGGCAGG-3’). The PfuUltra II HS fusion polymerase (Agilent Technologies, USA) was used for PCR reactions. Then, 1µg of purified 3’UTR and beta-actin PCR products were in-vitro transcribed with 5µl α^{32}P dUTP. Reactions were stopped with 1µl 0.5M EDTA and labeled RNA probes were purified with mini Quick Spin RNA columns (Roche Life Science, USA). Incorporation was measured with a Geiger counter. Denaturation of the labeled probes was carried out at 95°C for 5 min followed by snap cooling on ice. Probes were then centrifuged briefly before addition to the membrane.

Overnight hybridization of probes to the membrane was performed in ULTRAhyb® Ultrasensitive Hybridization (Ambion, Life Technologies, USA) at 43°C. After hybridization, the following washes were done in the respective order: 6xSSC/0.1% SDS buffer at room temperature for 15 min (3 times); 6xSSC/0.1% SDS buffer at 43°C for 15 min (1 time); 0.1xSSC/0.1% SDS buffer at room temperature for 15 min. The background of the membrane was consistently checked with a Geiger counter between washes to ensure that radioactivity is not too high. Finally, the membrane was wrapped in cling film, exposed on a phosphorscreen for about 3 hours up to overnight (depending on signal strength) and signals were quantified using a Typhoon phosphorimager (Amersham, GE Healthcare Lifesciences, USA).

Intensity of the bands was calculated using ImageJ software (National Institutes of Health, USA).

2.8 siRNAs

The siRNAs used for knockdown experiments were obtained from Singapore Applied Biologics (SABio, Singapore). 100nM siRNA was transfected into HuH-7 cells seeded onto 24-well plates using DharmaFect2 (Dharmacon, GE Healthcare Lifesciences, USA) according to manufacturer's instructions 48 hours prior to infection. AllStars negative control siRNA (Qiagen, USA) was used as the control siRNA (siC). The siRNAs for IRF3 knockdown target three different sequences in IRF3 RNA (IRF3-01: 5'-GCAAAGAAGGGUUGCGUUU-3'; IRF3-03: 5'-AUGCACAGCAGGAGGAUUU-3' and IRF3-04: 5'-GGGAAGAGUGGGAGUUCGA-3'). Knockdown efficiency was determined by Western blot using anti-IRF3 antibody (1:3000) (Cell Signaling Technology, USA).

2.9 Western blot

Cells were trypsinized, washed twice in 1xPBS and resuspended in lysis buffer (50µl lysis buffer for up to $2x10^5$ cells) containing 1% NP-40, 150mM NaCl, and 50mM Tris, pH 8.0 in the presence of protease and phosphatase inhibitors (Sigma-Aldrich, USA). After centrifugation, the cell lysates were exposed to 1x loading buffer and separated by SDS-PAGE. After transfer to polyvinylidene fluoride (PVDF) (Merck Millipore, USA), IRF3 and GAPDH

proteins were detected with anti-rabbit IRF3 antibody (1:3000) (Cell Signaling Technology, USA) and anti-mouse GAPDH antibody (1:3000) (Abcam, UK) respectively. Addition of appropriate HRP-conjugated antibodies (Dako, Agilent Technologies, USA) followed and bands were visualized using enhanced chemiluminescence (ECL) (Amersham, GE Healthcare Lifesciences, USA) for development.

2.10 Constructs

The DENV-2 reporter replicon system (pDENrep-FH) has been described previously and was a gift from Eva Harris (Holden et al., 2006). This replicon has the backbone of the *Thai 16681* DENV-2 strain (U87411.1) and contains *Renilla luciferase* and a T7 promoter region. Point mutations were made to create the other replicons (pDENrep-FH/PR1, pDENrep-FH/PR2B/28nt, pDENrep-FH/PR2B/117nt and pDENrep-FH/PR2B) using the Quikchange site-directed mutagenesis kit (Stratagene, Agilent Technologies, USA) as per manufacturer's instructions. A *Firefly luciferase* containing construct pTNT-Ffluc was used as the normalization control.

2.11 *In vitro* transcription

All DENV replicon DNA templates were generated by *XbaI* digestion of the corresponding plasmids, followed by phenol-chloroform extraction and ethanol precipitation. The T7 RiboMax large-scale RNA production system (Promega, USA) and $m^7G(5')ppp(5')A$ RNA Cap Structure Analog (New England Biolabs, USA) were used to generate capped RNA by *in vitro*

transcription with the modifications to the manufacturer's protocol as previously detailed (Friebe and Harris, 2010). Briefly, a 20µl mastermix was set up as follows: 5x buffer (4µl), rGTP (1.5µl) rCTP (1.5µl), rUTP (1.5µl), rATP (0.3µl), A cap (6µl), T7 enzyme (2µl), RNAsin Ribonuclease inhibitor (1µl) (Promega, USA), 1µg linearized DNA and RNAse-free water. After 30min incubation at 37°C, another 0.72µl of rATP was added to each reaction. Reactions were then left to incubate overnight at 37°C. After in-vitro transcription, each reaction is incubated with 1 µl RNase-Free DNase at 37°C for 15min. RNA is then purified using the RNeasy kit (Qiagen, Germany) as per manufacturer's protocols before electroporation.

2.12 Electroporation and dual-luciferase assay

Briefly, HuH-7 cells were trypsinized and washed thrice with cold, sterile PBS after which they were counted and resuspended to 1×10^7 cells/ml in cold Opti-MEM (Invitrogen, Life Technologies, USA). 800µl of the cell suspension was aliquoted into each 4mm electroporation cuvette (Bio-Rad, USA) followed by addition of 10µg of purified replicon RNA and 1 µg of pTNT-Ffluc. After one pulse at 950µF and 250V with a Gene Pulser II system (Bio-Rad, USA), cells were incubated at room temperature for 10 min. Cells were gently transferred from each cuvette to 11.2ml of pre-warmed media and 500 µl of this final mixture was aliquoted into each well (sufficient for a 24-well plate). Cells were harvested at various time-points using the passive lysis buffer (Promega, USA) and luciferase activity was measured using the

Dual Luciferase Reporter Assay system (Promega, USA) according to manufacturer's instructions.

2.13 sfRNA transfections

DENV-2 3′UTR templates were PCR amplified from PR-2B viral cDNA to add a T7 promoter immediately upstream of the DENV-2 stop codon and *in vitro* transcribed using the Megascript T7 transcription kit (Life technologies, USA). A size-matched control RNA was similarly prepared from the pGEM-T vector (Promega, USA). Primers used for the amplification of DENV-2 3'UTR templates are T7 D2 3UTR For (5'-TAATACGACTCACTATAGGGAAGAGATTCAGA-3') and D2 3UTR Rev (5'AGA ACC TGT TGA TTC AAC AGC ACC3'). For the amplification of the size-matched control RNA, pGEM Non For (5'-CTAGGGATCCTAATACGACTCACTATAGGGCGAATT-3') and pGEM Non Rev (5'-CTAGGGATCCGTTCTTTCCTGCGTTATCCCCTGA-3') were used.

The RNAs were decapped by a 45 min tobacco acid pyrophosphatase (Epicentre, Illumina, USA) treatment at 37°C, purified using the RNeasy kit (Qiagen, Germany) and subjected to heat denaturation followed by cooling to form secondary structures. All RNAs were quantified spectrophotometrically and agarose gel electrophoresis was used to verify their integrity before use. 500ng of the RNAs was either co-electroporated with pDENrep-FH or transfected into HuH-7 cells at 90% confluency pre-seeded on 24-well plates along with polyinosinic-polycytidylic acid (PolyIC) (1μg/μl per well) to

stimulate the RIG-I pathway using Lipofectamine RNAiMax (Life Technologies, USA) as per manufacturer's instructions.

2.14 RNA-protein interactions

2.14.1 SILAC-qMS

Viral RNA was extracted from virus supernatants of PR-1 and PR-2B viruses utilizing the QIAamp viral RNA mini kit (Qiagen, Germany). Then, cDNA was made with the Superscript III reverse transcriptase and random hexamers (Invitrogen, Life Technologies, USA). Short DENV-2 PCR products comprising of the proximal end of the 3'UTR (SL-II to SL-IV) were next prepared from the viral cDNA using AW005-PR-FOR (5' CGG GTA TGT GCG TCT GGA TCC TAT RGG AAG AGG AAG AGG CMG G 3') and AW135R (5' TTG TTG CTG CGA TTT GTA AGG G 3'). Similarly, a size-matched control PCR product was constructed from a plasmid containing the DENV-2 NS2A open reading frame as reported before (Ward et al., 2011). Tobramycin aptamers were then incorporated into the partial UTRs including the control and the Megascript T7 transcription kit (Life technologies, USA) was utilized to produce the RNAs.

Meanwhile, stable isotope labeling by amino acids in cell culture (SILAC) was carried out to obtain labeled (i.e. light, medium, heavy) HuH-7 cell lysates (Mann, 2006; Ong et al., 2002). The prepared RNAs were bound to a tobramycin matrix, incubated with SILAC-labeled cell lysates, washed and

eluted using excess tobramycin (Ward et al., 2011; Ward et al., 2014). Eluates were finally analyzed by quantitative mass spectrometry (qMS) at the Quantitative Proteomics group, Institute of Molecular and Cell Biology, Singapore. In order to identify the proteins involved in innate immunity, the list of proteins from the MS data was loaded into GO term finder. 32 out of 1199 proteins were represented in the GO term "innate response process"(Boyle et al., 2004).

2.14.2 RNA-immunoprecipitations

Viral infections were performed at MOI 5 on HuH-7 cells pre-seeded onto T175 cell culture flasks. At 24 hpi, RNA-immunoprecipitations (RIP) were carried out using the MAGNA-RIP kit (Merck Millipore, USA) following manufacturer's recommendations. Briefly, infected cells were lysed with the RIP lysis buffer (Merck Millipore, USA). In the meantime, 5µg of the anti-TRIM25 (BD Biosciences, USA) or anti-MAVS (Abcam, UK) were incubated with the magnetic beads (Merck Millipore, USA) at room temperature for 30 min to form beads-antibody complexes alongside with the respective isotype control antibodies (Abcam, UK).

After washing, the beads-antibody complexes were resuspended in RIP immunoprecipitation buffer (Merck Millipore, USA) and cell lysates were added to these complexes. After resuspending, 50µl each of the final mixture was removed for subsequent qRT-PCR and western blot analysis. This was labeled as “Input”. The mixture was then incubated overnight at 4°C. The

next morning, 50µl of the mixture (labeled "Sup") was removed for western blot analysis. The remaining bead suspension was washed at least six times, pelleted and resuspended into a total volume of 500µl. From this final mixture, described as "Pellet", 250µl was resuspended in RLT buffer (RNeasy kit, QIAGEN, Germany) for qRT-PCR and the remaining 250µl stored for western blot analysis. The levels of RNA in RIP were determined by qRT-PCR and normalized to GAPDH mRNA levels, control mouse IgG (TRIM25) and rabbit IgG (MAVS) RIP levels following this formula: **Fold enrichment = 2^{-ddCt} where $ddCT = ((CT_{RNA,IP} - CT_{GAPDH,IP}) - (CT_{RNA,controlIP} - CT_{GAPDH,controlIP}))$**

2.15 Co-immunoprecipitation and immunoblot analysis

Transfected or infected HuH-7 cells were trypsinized, washed twice in 1xPBS and resuspended in lysis buffer (50µl lysis buffer for up to $2x10^5$ cells) containing 0.1% NP-40, 150mM NaCl, and 50mM Tris, pH 8.0 in the presence of protease and phosphatase inhibitors (Sigma-Aldrich, USA). Cells were left on ice to allow lysis for at least 1 hour, after which they were spun down at maximum speed in the pre-cooled centrifuge for 10 min. Cell lysate was removed without disturbing the pelleted debris and separated into tubes for the subsequent immunoprecipitations.

5ug of anti-mouse TRIM25 (BD Biosciences, USA) or anti-rabbit RIG-I (Alexis, Enzo Life Sciences, USA) antibody was incubated with the cell lysates overnight at 4°C. Each antibody was paired with its respective isotype control antibodies (Abcam, UK). Protein A agarose beads (Thermo Scientific,

USA) were washed with immunoprecipitation buffer (25mM Tris, 150mM NaCl, pH 7.2) and incubated with lysate for 2.5 hours at 4°C. After washing, proteins were eluted with SDS-PAGE loading buffer and respective proteins were detected. Primary antibodies used were: anti-TRIM25 (1:5000) (BD Biosciences, USA), anti-MAVS (1:1000) (Abcam, UK), anti-ubiquitin (1:1000) (P4D1, Santa Cruz Biotechnology, USA) and anti-RIG-I (1:1000) (Alexis, Enzo Life Sciences, USA). Appropriate HRP-conjugated antibodies (Dako, Agilent Technologies, USA) were used as secondary antibodies and bands were visualized using ECL (Amersham, GE Healthcare Lifesciences, USA) for chemiluminescence development.

2.16 Statistical analysis

All results are presented as mean ± SD of at least 3 independent experiments, unless otherwise indicated. Data were analyzed using two-tailed unpaired Student's t-test or ANOVA and considered significant if $p<0.05$ (*$p<0.05$; **$p<0.01$; ***$p<0.001$; ****$p<0.0001$). All calculations were done using GraphPad Prism v5.0 (GraphPad Software Inc, USA).

CHAPTER 3:

RESULTS

SECTION 3.1:

Subgenomic flavivirus RNA is a critical determinant of the epidemiological fitness of Dengue-2.

3.1.1 Comparative analysis of the 1994 Puerto Rican DENV-2 isolates

To gain insights into how genetic variation of DENV could modulate the outcomes in an epidemic, we examined a DENV serotype 2 (DENV-2) clade replacement event in Puerto Rico that coincided with an island-wide epidemic in 1994 (Bennett et al., 2006; Rigau-Perez et al., 2001). This epidemic was the largest on record, with the highest reported numbers of hospitalization (2004), severe dengue cases (139) and deaths (40) in Puerto Rico until 1998 (Bennett et al., 2006; McElroy et al., 2011). Using complete coding sequences of clinical isolates obtained during the epidemic and other DENV-2 GenBank sequences from Puerto Rico and neighbouring countries, we built a maximum likelihood phylogenetic tree (Figure 3.1). The maximum likelihood phylogenetic tree is a statistically established simple model that supposes the least evolutionary change to explain the observed data. Thus, this method searches for the tree with the highest probability to interpret the 1994 clade replacement event. Results showed that three distinct clades (PR-1, PR-2A and PR-2B) within the American/Asian genotype were circulating in Puerto Rico in 1994, which is concordant with previous analysis using partial genome sequences (Figure. 3.1) (Bennett et al., 2006). Clade PR-1 was regularly isolated from clinical cases from 1986 to 1995. It is thus referred to as “endemic” throughout this study since it has been prevalent in Puerto Rico prior to the 1994 epidemic. The second clade PR-2 contains viruses isolated beginning in 1994 and can be subdivided into PR-2A, which persisted at low levels till 1998 and PR-2B. The PR-2B viruses arose in 1994 at the onset of

the epidemic, replacing the PR-1 clade to become the dominant DENV-2 clade in Puerto Rico after 1994 and persisted until 2007.

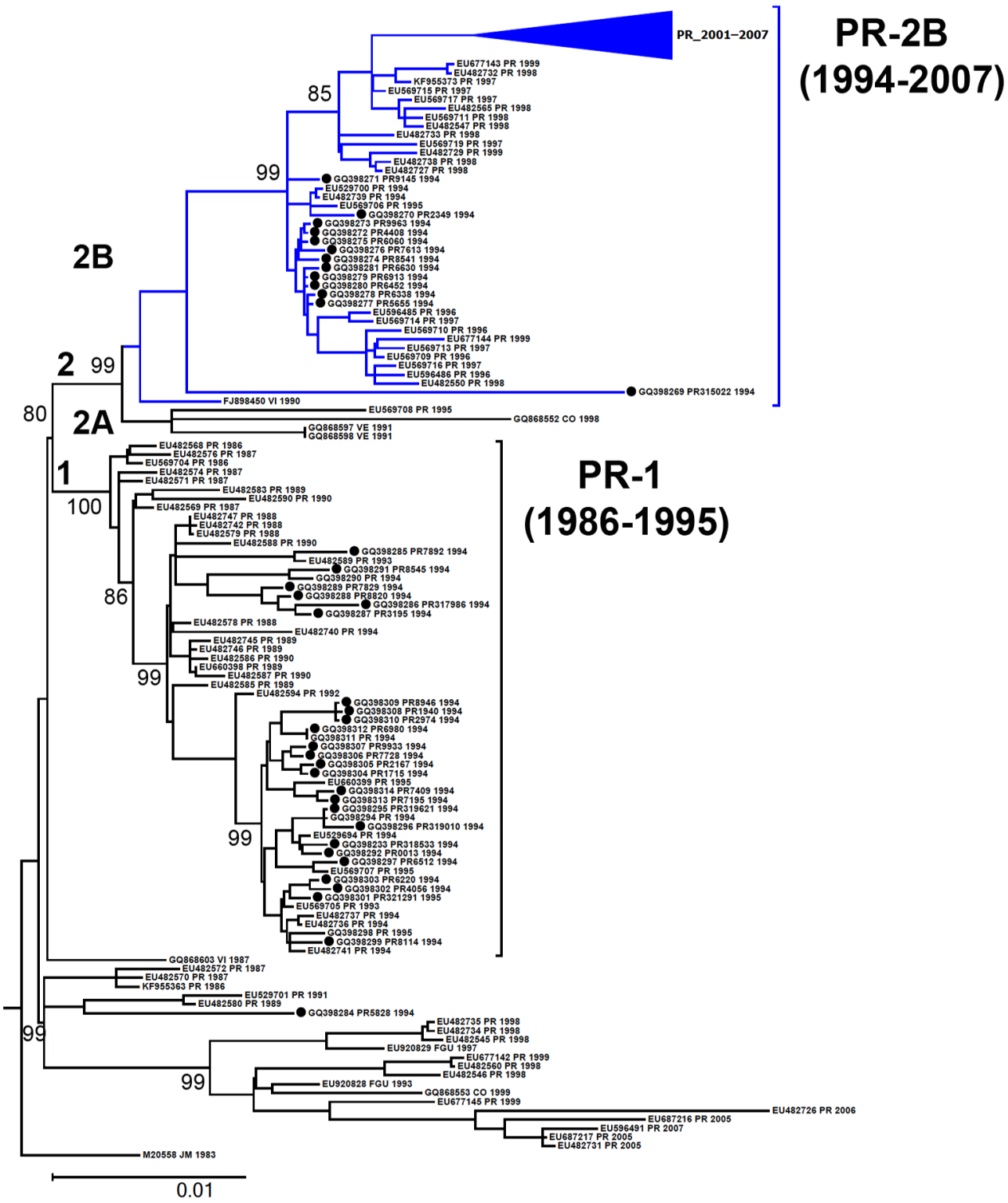

Figure 3.1 Whole genome phylogenetic tree of DENV-2 clinical isolates from Puerto Rico and neighboring countries Black dots indicate viruses used in this study. *Data from Esteban Finol.*

In order to assess the parts of the DENV genome in which the nucleotide substitutions could be responsible for the separation of the Puerto Rican isolates into two clades, the Shimodaira-Hasegawa (SH) test was performed (Buckley et al., 2001). The SH test is a widely used method that corrects for the fact that the parameters for the substitution process and the branch lengths in a maximum likelihood tree are estimated. Hence, it is a completely unbiased comparison of tree topology of maximum likelihood trees. Using this method, the topology of the full genome phylogenetic tree was compared with that of each tree constructed from different regions of the DENV genome.

This analysis identified variations in NS1, NS3, NS5 and the 3'UTR as potentially critical to how the viruses segregated into PR-1 versus PR-2B clades (Figure 3.2). The SH test on the other regions of the genome showed statistically significant differences compared to the whole genome tree indicating that sequence differences in these parts of the genome are unlikely to account for the segregation of these isolates into the observed clades (Figure 3.3).

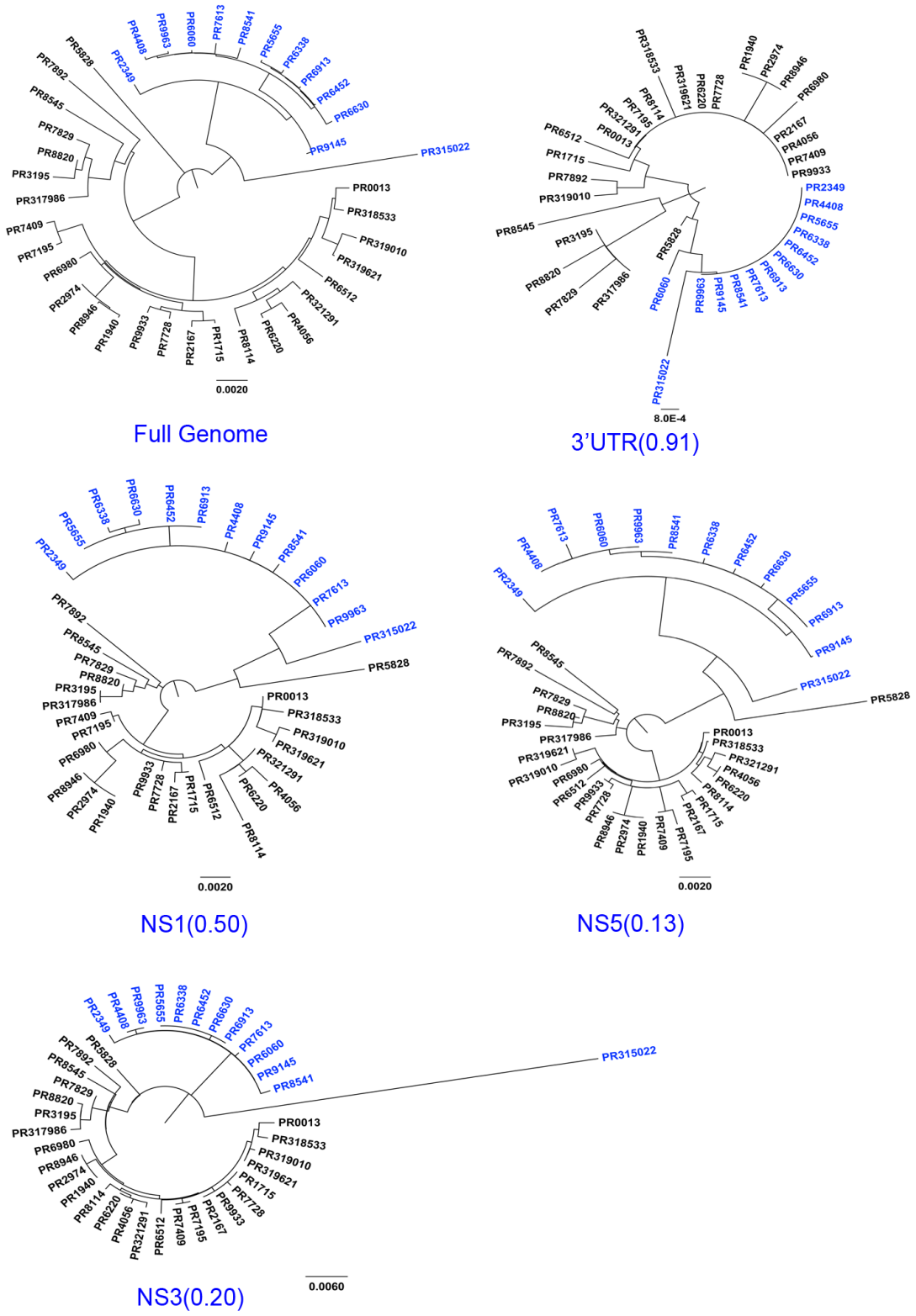

Figure 3.2 Phylogenetic trees of the whole genome, 3'UTR, NS1, NS3 and NS5 regions of Puerto Rican clinical isolates used in this study Isolates from PR-1 lineage are marked in black while isolates from the PR-2B lineage are in blue. The p-values generated by the SH test are shown below each tree in brackets. This test statistic is the score difference between the Maximum Likelihood tree (full genome phylogenetic tree) and every other tree compared. Comparison with NS1, NS3, NS5 regions and the 3'UTR yield p-values that are not significant, indicating that they are good explanations of the dataset, which separates the isolates into two lineages. *Data from Justin Bahl.*

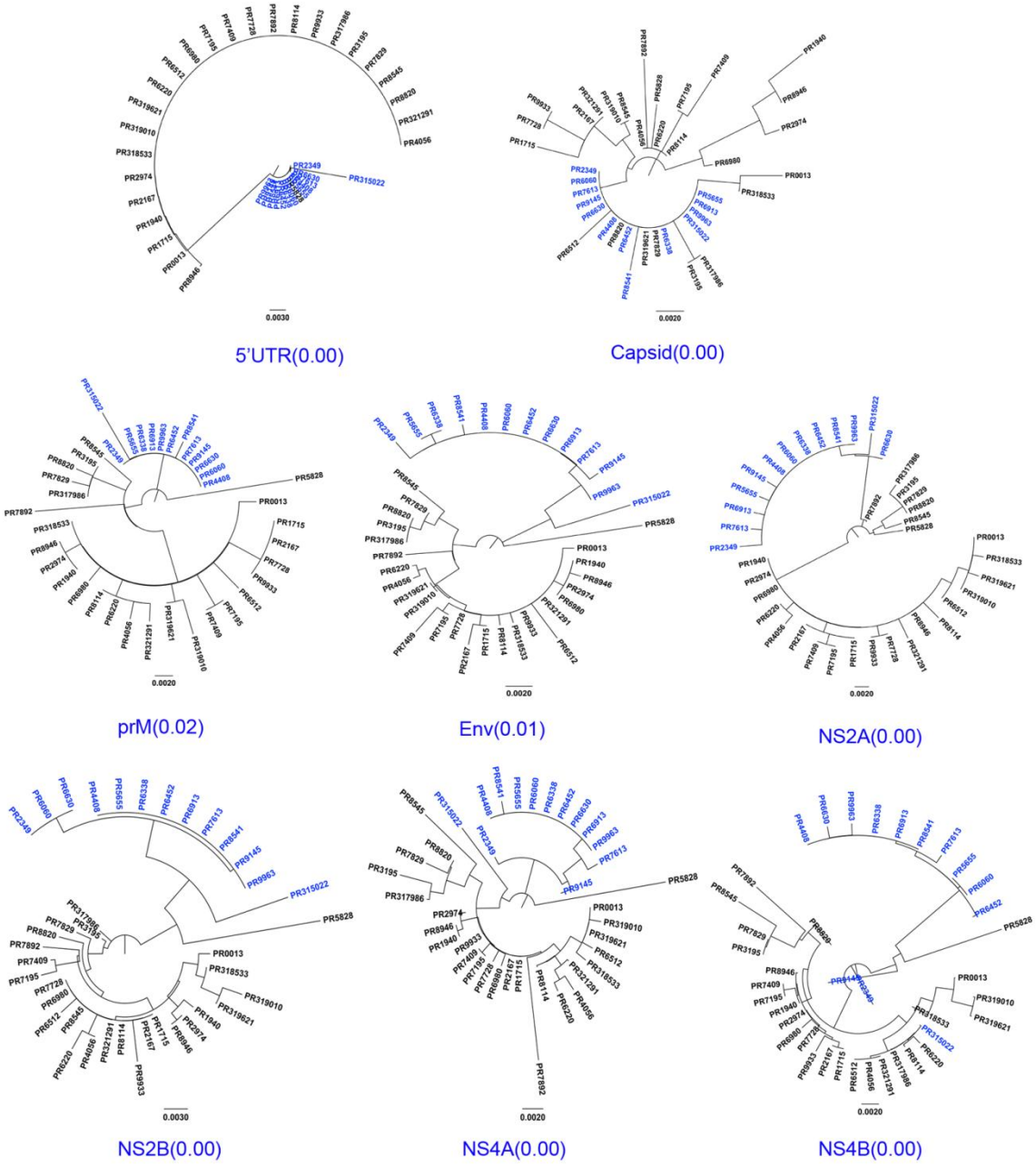

Figure 3.3 Phylogenetic trees of the other genetic regions of Puerto Rican clinical isolates used in this study Isolates belonging to the PR-1 lineage are marked in black color while the isolates from the PR-2B lineage are highlighted in blue. The p-values generated by the SH test are shown below each tree in brackets. This test statistic is the score difference between the Maximum Likelihood tree (full genome phylogenetic tree) and every other tree compared. From the SH test scores, these regions are significantly different from the whole genome tree (Figure 3.2) indicating that they are not likely to lead to the segregation of the isolates into PR-1 and PR-2B. *Data from Justin Bahl.*

To complement the SH test findings, we also aligned the complete genome sequences and identified both amino acid and nucleotide substitutions occurring in at least 25 % of the isolates from each clade (Figures 3.2 and 3.3). Variant residues identified were omitted from analysis to reduce noise resulting from stochastic effects. Using these criteria, we observed a total of 17 non-synonymous amino acid changes throughout the DENV-2 genome of PR-2B isolates as compared to PR-1 as well as 2 nucleotide differences in the 5'UTR and 3 nucleotide differences in the variable region of the 3'UTR (Table 3.1).

The results from Table 3.1 were then combined with the data from the SH test to identify the substitutions that were critical in the PR-1 and PR-2B segregation. These were in NS1, NS3, NS5 and 3'UTR (Table 3.1). There were 2 amino acid changes in NS1 and NS3 while NS5 had a total of 6 amino acid substitutions. Within the 3'UTR, all PR-2B isolates had guanine and adenine at positions 10301 and 10331, respectively (Table 3.1). Twelve out of thirteen PR-2B isolates had cytosine at position 10389 (Table 3.1). In contrast, all PR-1 lineage viruses had adenine and guanine at positions 10301 and 10331, respectively, while 92.3% of viruses studied had thymine at position10389 (Table 3.1).

Collectively, these findings suggest that genetic differences in NS1, NS3, NS5 regions and the 3'UTR may have conferred greater epidemiological fitness to the dominant PR-2B viruses compared to endemic PR-1.

Table 3.1 Amino acid and nucleotide substitutions present in at least 25%of the PR-2B viruses.

Amino acid substitutions		Endemic	Dominant Foreign
Gene	**position**	**aa (%)**	**aa (%)**
E	91	**V** (100)	**I** (100)
	491	**A** (100)	**V** (100)
NS1	10	**S** (100)	**N** (100)
	164	**T** (68)	**S** (92.3)
NS2A	72	**I** (76)	**V** (100)
NS2B	8	**I** (92)	**V** (100)
NS3	31	**L** (100)	**F** (84.6)
	418	**R** (100)	**K** (92.3)
NS4A	36	**A** (100)	**V** (76.9)
NS4B	19	**A** (80)	**I** (76.9)
	175	**I** (100)	**V** (76.9)
NS5	269	**S** (100)	**N** (92.3)
	375	**K** (100)	**R** (100)
	435	**I** (100)	**V** (100)
	514	**R** (100)	**K** (92.3)
	596	**R** (100)	**K** (100)
	891	**R** (100)	**K** (92.3)
Nucleotide substitutions		**Endemic**	**Dominant Foreign**
UTR	**position**	**nt (%)**	**nt (%)**
5'	40	**U** (100)	**G** (100)
	48	**A** (100)	**U** (100)
3'	10301	**A** (100)	**G** (100)
	10331	**G** (100)	**A** (100)
	10389	**U** (76)	**C** (92.3)

%: Percentages of viruses over total number of isolates in each clade bearing the substitutions. Regions identified by the SH test to be responsible for the segregation of PR-1 and PR-2B into two separate clades are highlighted in blue. Substitutions in these regions are likely to be significant for our study.

3.1.2 Viral isolates from the PR-2B clade produce less viral RNA and infectious particles at 24 hours p.i. but higher relative amounts of sfRNA

Besides interacting with the viral RNA genome to form the replication complex, DENV NS1, NS3 and NS5 are known to downregulate the innate immune response (Ye et al., 2013). More recently, the 3'UTR of the DENV and other flaviviral genomes have also been shown to play a critical role in regulating the interferon response through the production of subgenomic flavivirus RNA (sfRNA) (Bidet et al., 2014; Schuessler et al., 2012). Pseudoknot structures in the 3'UTR are essential in sfRNA production as they prevent complete degradation of DENV RNA by the cellular XRN1 (Chapman et al., 2014b).

To determine if the substitutions in PR-2B viruses might affect the structure and pseudoknot formation in the 3'UTR, we next constructed the 3'UTR structure for the PR-1 viruses using a newly proposed model (Chapman et al., 2014a). Structural analysis showed that the first A-to-G substitution preceded stemloop (SL)-II and was positioned on a linear stretch of RNA (Figure 3.4). The other two 3'UTR substitutions found in PR-2B isolates mapped to SL-II and SL-IV respectively (Figure 3.4). Remarkably, the G-to-A substitution at position 10331 was on the exact site where pseudoknot pk1 is predicted to form while the third substitution was on a side loop of SL-IV (Figure 3.4). Since two of the 3'UTR substitutions found in PR-2B isolates map to stemloops where pseudoknots are likely to form, we

tested for a possible role for sfRNA in modulating fitness in our viruses. (Chapman et al., 2014a; Funk et al., 2010; Silva et al., 2010).

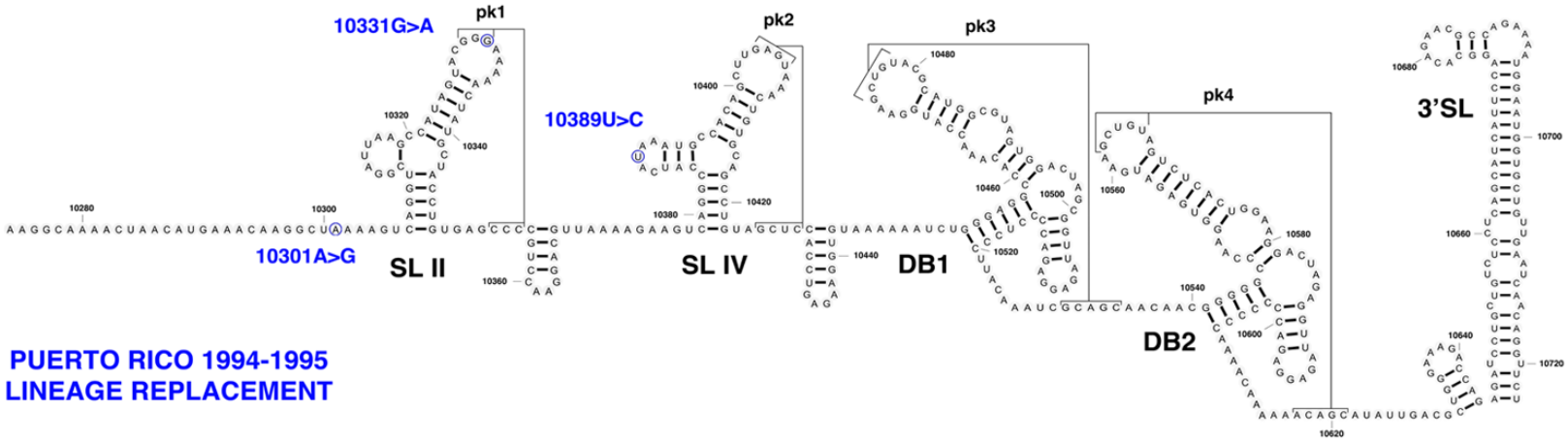

Figure 3.4 Structure of the Puerto Rican PR-1 DENV-2 3'UTR The 3 substitutions present in the structure of PR-2B viruses are indicated in blue. Annotations are as follows: SL, stemloop; pk, pseudoknot; DB, dumbbell. *Data from Esteban Finol.*

To measure viral fitness *in vitro*, we performed DENV infection assays in human hepatoma (HuH-7) cells. Cells were infected with each isolate for 24 hours at a multiplicity of infection (MOI) of 0.1. After which, the culture supernatants were titrated by plaque assay and intracellular RNA levels were measured by quantitative RT-PCR (qRT-PCR), using a previously described method (Bidet et al., 2014).

We expected PR-2B isolates to replicate more efficiently than PR-1 viruses that they replaced in Puerto Rico. However, plaque assays performed on BHK-21 cells with culture supernatants at 24 hours post-infection (hpi) showed that the PR-1 viruses produced more viral progenies than the PR-2B viruses (Figure 3.5A). Likewise, DENV genomic RNA (gRNA) levels were significantly higher in cells infected with PR-1 compared to PR-2B viruses, a trend consistent with plaque titers (Figure. 3.5B). The degree of difference in sfRNA levels between PR-1 and PR-2B viruses was smaller although statistically significant (Figure 3.5C), resulting in PR-2B viruses having much higher sfRNA:gRNA ratios compared to PR-1 viruses (Figure 3.5D). Collectively, these findings suggest that PR-2B viruses produce at least 100 fold more sfRNA relative to gRNA during replication.

To validate the qRT-PCR findings, we used another published method to measure intracellular viral RNA levels (Lai et al., 2007). Results showed that the differences in the DENV genome copies between PR-1 and PR2B viruses diminished to below statistically significant levels (Figure 3.5E). This

was interesting and confirmed our findings that PR-2B viruses produce more sfRNA:gRNA as compared to PR-1, as this qPCR assay targeted the 3'UTR region of the DENV genome.

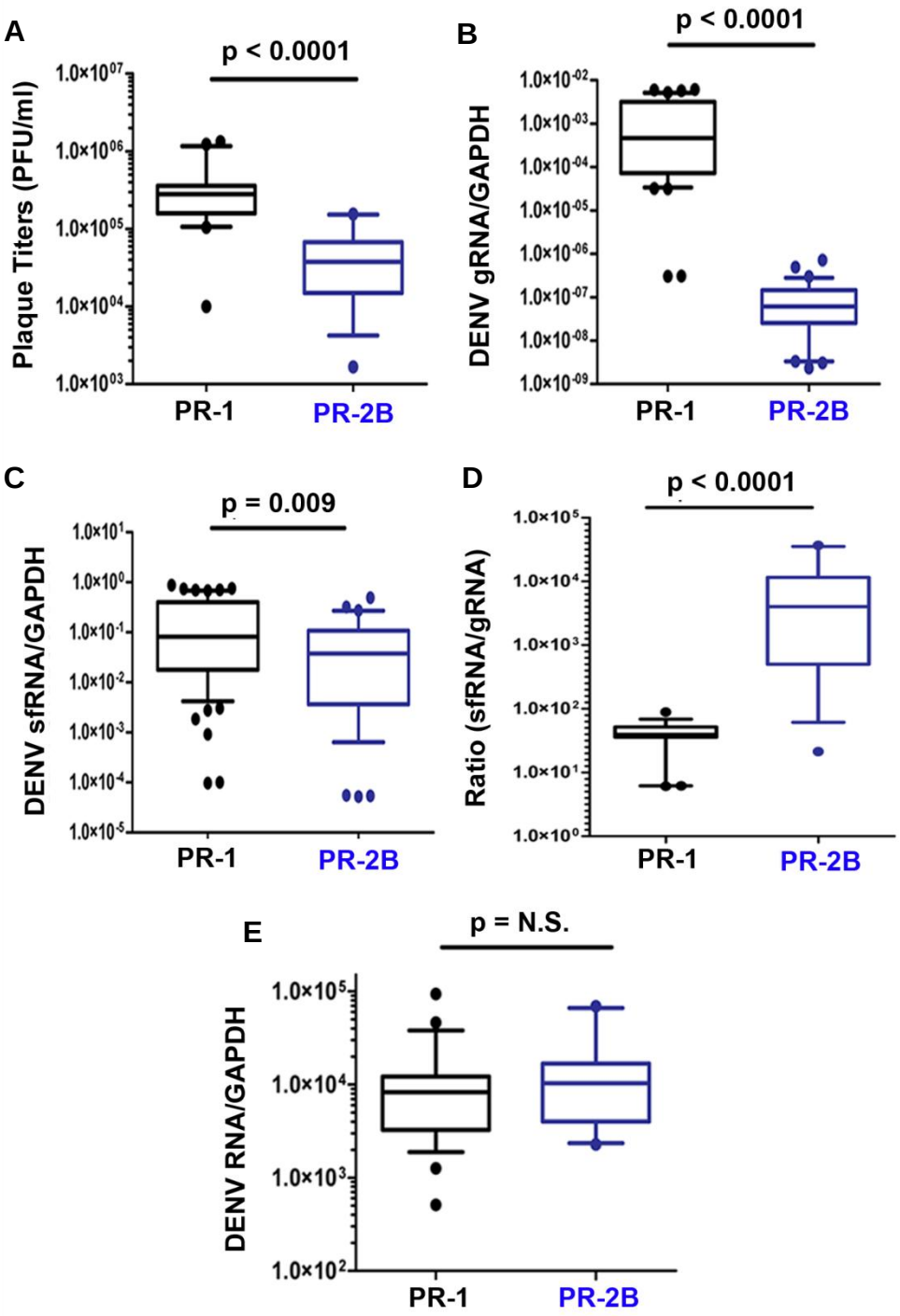

Figure 3.5 DENV infection assays in human hepatoma (HuH-7) cells Black boxes indicate the PR-1 viruses and blue boxes indicate the PR-2B isolates. (A) Plaque titers of PR-1 and PR-2B DENV-2 viruses at 24 hpi in HuH-7 cells infected at an MOI of 0.1. (B) PR-1 and PR-2B DENV-2 genomic RNA (gRNA) in infected HuH-7 cells (MOI = 0.1), 24 hpi. (C) PR-1 and PR-2B DENV-2 sfRNA in infected HuH-7 cells (MOI = 0.1), 24 hpi. (D) Ratio of sfRNA:gRNA in HuH-7 cells infected with PR-1 and PR-2B viruses at MOI 0.1, 24 hpi.(E) Quantification of DENV RNA in infected cells (MOI O.1, 24 hpi) using a different set of primers targeting the 3'UTR.

To further confirm that PR-2B isolates are indeed producing more sfRNA to gRNA, northern blot was performed on two isolates, one from each clade. Infection was carried out on HuH-7 cells at MOI 10 in triplicates and RNA was purified using Trizol reagent, before being subjected to northern hybridization. Quantification of the band intensity using ImageJ software yielded lower sfRNA:gRNA ratios which could be due to multiple reasons: Differences in assay type, MOI of infection, cell quantity, probe (radioactive probe versus Sybr green in qRT-PCR) etc. However, results attained were similar to qRT-PCR with the PR-2B virus producing a higher sfRNA:gRNA ratio as compared to the PR-1 virus (Figure 3.6). Collectively, these findings suggest that PR-2B viruses produce more sfRNA relative to gRNA during replication.

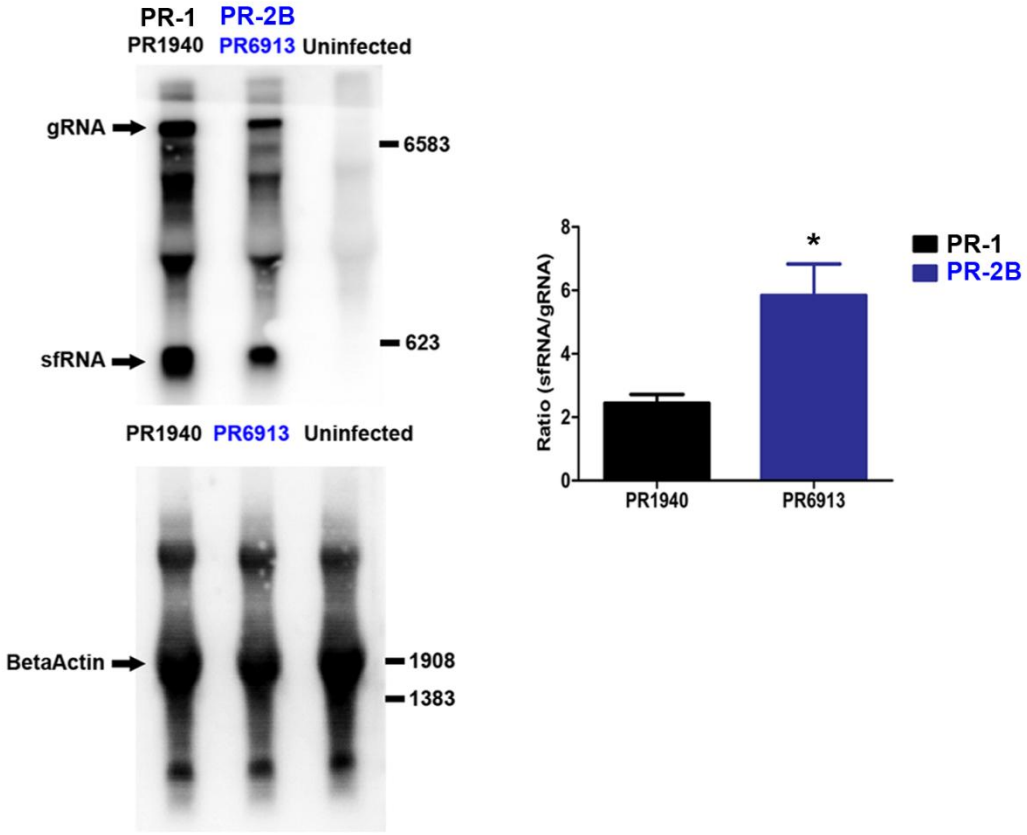

Figure 3.6 Northern blot showing gRNA and sfRNA amounts HuH-7 cells were infected with one clinical isolate from each clade (MOI 10) at 24 hpi. Beta-actin was used as the background control. Experiments were repeated thrice and graph depicts quantification of sfRNA:gRNA ratios from 3 separate gels using ImageJ software.

3.1.3 Increased sfRNA:gRNA in Nicaraguan DENV-2

Increased production of sfRNA relative to gRNA in an epidemic clade of viruses is not unique to the PR-2B viruses from Puerto Rico. Another DENV-2 clade replacement event was previously reported in Nicaragua that resulted in increased disease severity and hospitalization (OhAinle et al., 2011).

We applied the SH test to the full genome of these clinical isolates and similarly identified variations in NS1, NS5 and the 3'UTR that differentiate the viruses into clades NI-1 (endemic) and NI-2B (epidemic) (Figure 3.7). Comparison of the full genome tree with other regions of the genome resulted in p-values that were significant, confirming that they are not likely to have caused the NI-1 and NI-2B segregation seen in the full genome phylogenetic tree (Figure 3.8).

Upon structural analysis of the 3'UTR, the first substitution was located before the start of SL-II, thus not likely to induce any conformational change in 3'UTR structure. In this case, the other two 3'UTR substitutions occur in SL-IV and predict that clade NI-2B SL-IV would be energetically more stable (Figure 3.9). The minimal free energy required for the SL-IV folding in NI-2B isolates is 1.5 kcal/mol less than NI-1.

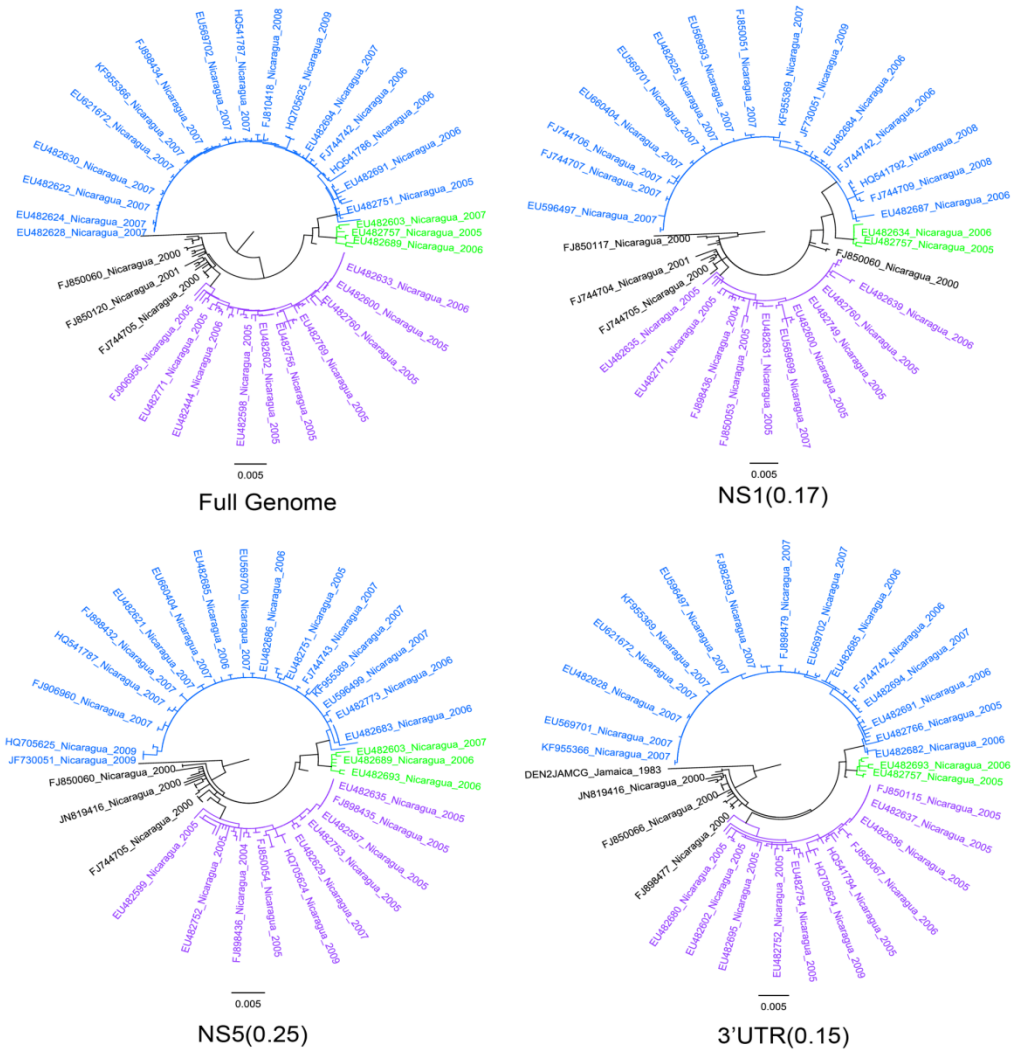

Figure 3.7 Phylogenetic trees of the whole genome, 3'UTR, NS1 and NS5 regions of Nicaraguan DENV-2 isolates Major Nicaraguan clades are highlighted (black: Nicaraguan isolates from 2000-2001; purple: NI-1; green: NI-2A; blue: NI-2B). NI-1 was the endemic clade while NI-2B was the epidemic clade that rapidly came into dominance replacing NI-1. NI-2A, similar to PR-2A, appeared to be an intermediate clade with very few viral isolates belonging to it. The p-values generated by the SH test are shown below each tree in brackets. This test statistic is the score difference between the Maximum Likelihood tree (full genome phylogenetic tree) and every other tree compared. Comparison with NS1, NS5 regions and the 3'UTR yield p-values that are not significant, indicating that they are good explanations of the dataset, which separates the viruses into NI-1 and NI-2B clades. *Data from Esteban Finol.*

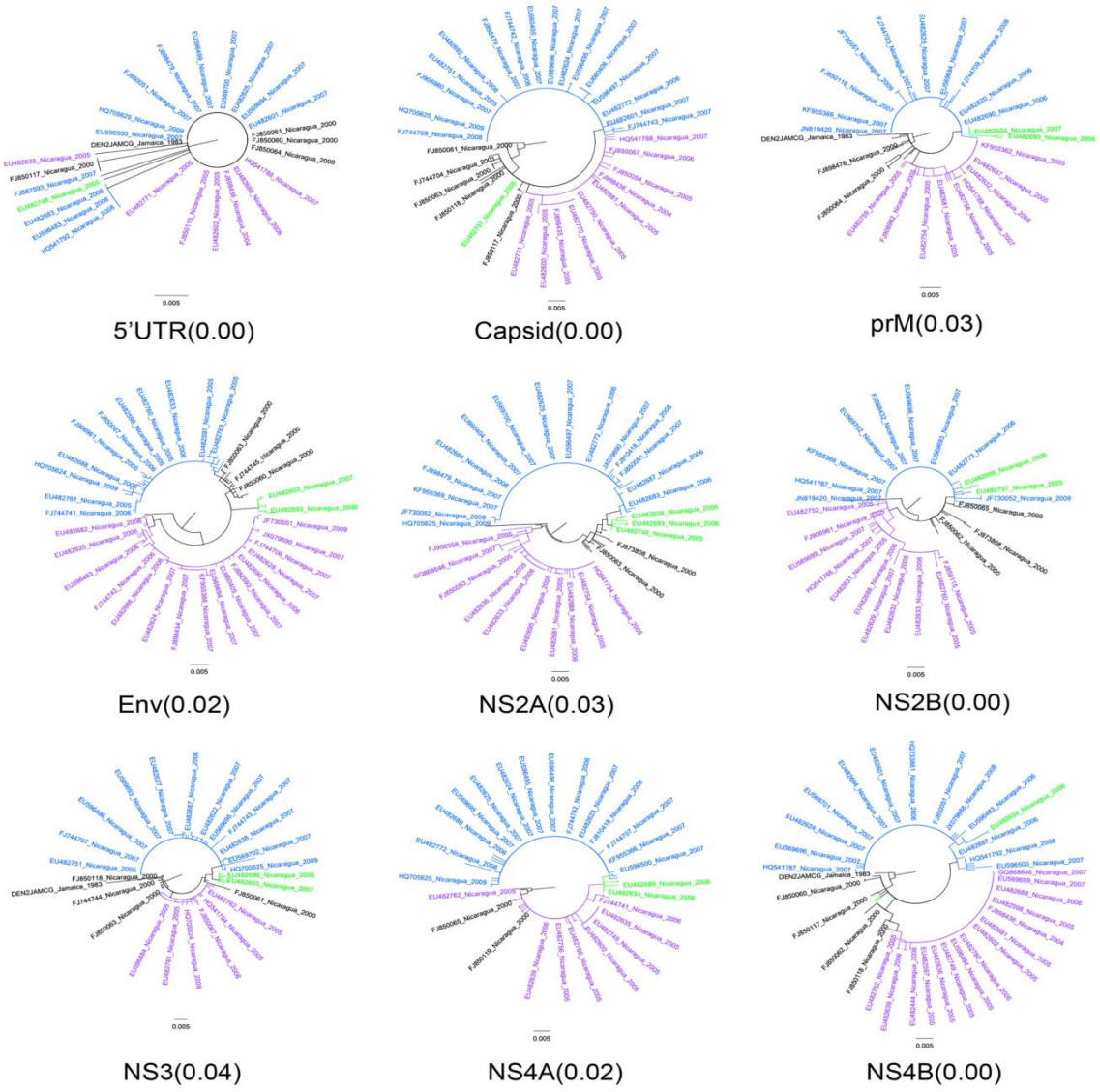

Figure 3.8 Phylogenetic trees of the other genetic regions of Nicaraguan DENV-2 isolates Major Nicaraguan clades are highlighted (black: Nicaraguan isolates from 2000-2001; purple: NI-1; green: NI-2A; blue: NI-2B). The p-values generated by the SH test are shown below each tree in brackets. This test statistic is the score difference between the Maximum Likelihood tree (full genome phylogenetic tree) and every other tree compared. Comparison with 5'UTR, Capsid, prM (premembrane), Env (envelope), NS2A, NS2B, NS3, NS4A, and NS4B regions yield p-values that are significant, indicating that they are different from the full genome tree that separates the viruses into NI-1 and NI-2B clades. *Data from Esteban Finol.*

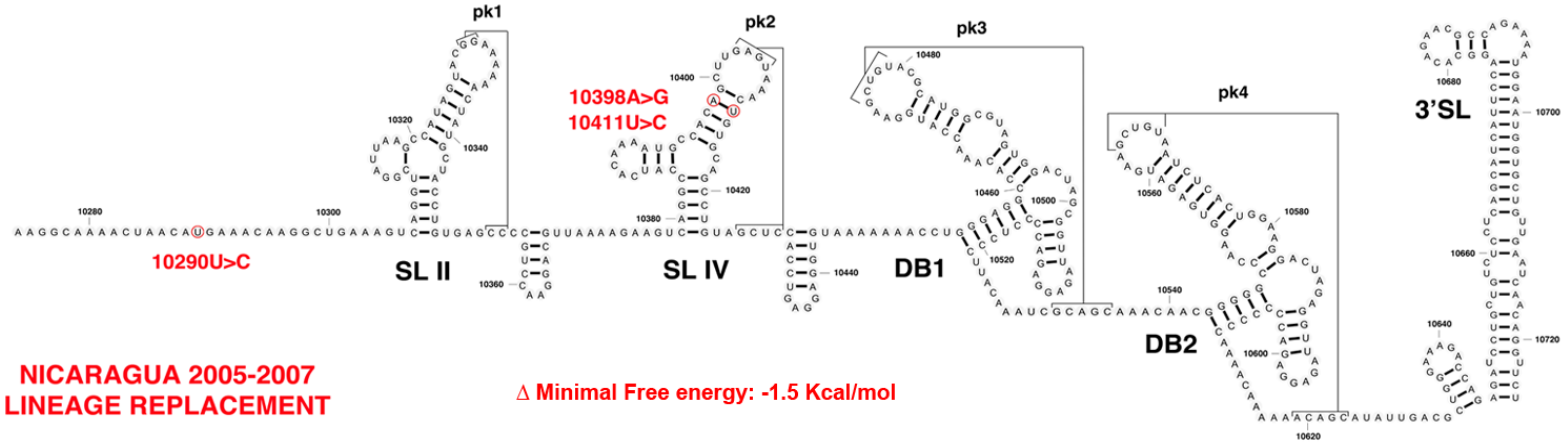

Figure 3.9 Structure of the Nicaraguan DENV-2 NI-1 3'UTR Substitutions observed in the NI-2B clade are shown in red. Minimal free energy for the SL-IV folding in NI-2B clade is shown. Annotations are as follows: SL, stemloop; pk, pseudoknot; DB, dumbbell. *Data from Esteban Finol.*

Analysis of the sfRNA:gRNA ratios indicated that 3 out of the 4 NI-2B viruses had a 3-4 fold higher sfRNA:gRNA ratio compared to the endemic NI-1 viruses that they replaced in 2005-07 (Figure 3.10). Collectively, these data suggest that the increased production of sfRNA relative to gRNA levels may contribute to the fitness of DENV-2 in distinct epidemiological settings.

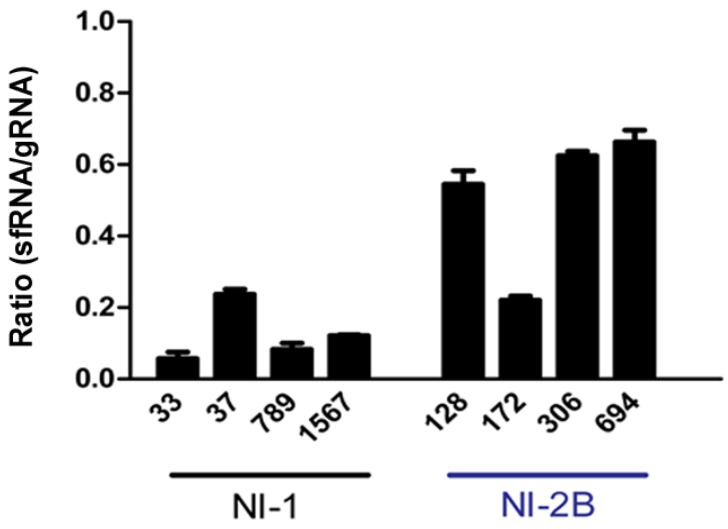

Figure 3.10 Quantification of sfRNA:gRNA ratios in HuH-7 cells at 48 hpi with clinical isolates from Nicaragua NI-1, DENV-2 Asian-American genotype present in Managua, Nicaragua, through 2005. NI-2B: Clade that replaced NI-1, 2006-8. *Data from Chunling Wang*

SECTION 3.2:

PR-2B DENV-2 replication is associated with reduced expression of IFN-β relative to PR-1 DENV-2.

3.2.1 sfRNA suppresses type I interferon expression for greater replication rates in the later stages of infection

The greater production of sfRNA relative to gRNA may confer selective advantage to PR-2B, leading to greater epidemiological fitness, by subverting the host innate immune responses through mechanisms that have yet to be fully defined (Bidet et al., 2014; Schuessler et al., 2012). Thus, we next compared the replication kinetics of selected PR-1 and PR-2B viruses at 24 and 96 hpi and their effect on interferon expression. While the plaque titers of PR-2B isolates were significantly lower at 24 hpi, they grew at a faster rate than PR-1 viruses between 24 and 96 hpi such that no difference in viral titers was observed at 96 hpi (Figure 3.11). Interestingly, expression of interferon-beta (IFN-β) was significantly lower in HuH-7 cells infected with PR-2B compared with PR-1 DENV isolates throughout the course of infection (Figure 3.12), suggesting that the higher sfRNA:gRNA ratio downregulated or even suppressed IFN-β response.

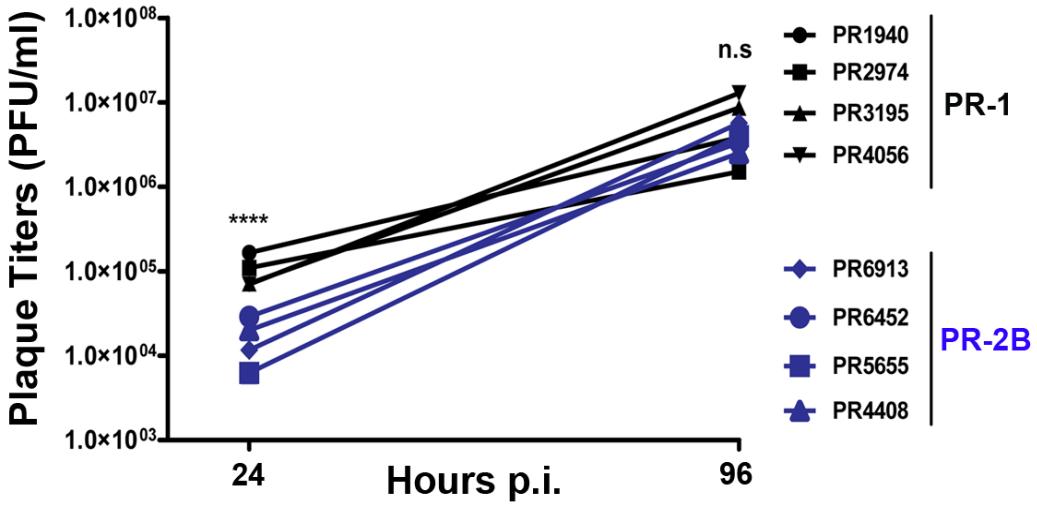

Figure 3.11 Plaque titers following infection of HuH-7 cells with selected viruses from each clade at 24 and 96 hpi Lines in black depict the PR-1 viruses and the blue lines depict the PR-2B viruses.

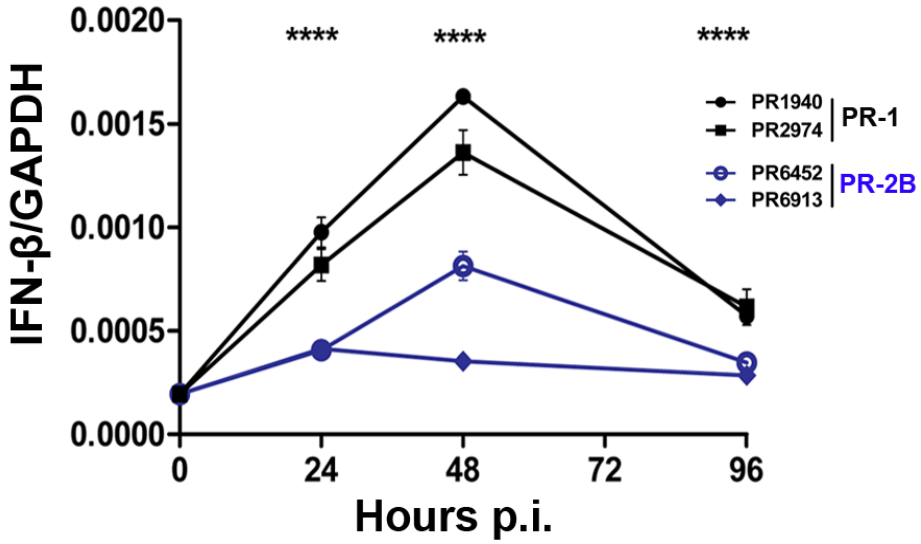

Figure 3.12 Expression levels of IFN-β in infected HuH-7 cells at various time-points p.i. Quantitative real-time PCR was used to detect expression levels of IFN-β, normalized to GAPDH. Black lines depict PR-1 isolates and blue lines indicate PR-2B viruses.

The trends observed in infection of HuH-7 cells were replicated in primary monocytes, which are target cells for DENV in humans. Infection with PR-2B isolates, using antibody-enhanced condition that is associated with greater risk of severe dengue, produced less gRNA (Figure 3.13A) and greater sfRNA:gRNA ratios (Figure 3.13B) compared to PR-1 viruses at 24 hpi. Likewise, at 72 hpi, the plaque titers of PR-1 and PR-2B isolates were similar suggesting that PR-2B viruses caught up with PR-1 despite significantly lower gRNA levels at 24 hpi (Figure 3.13C).

Similar to infection in HuH-7 cells, IFN-β expression in primary monocytes was reduced following infection with PR-2B as compared to PR-1 viruses at 24 hpi (Figure 3.13D)

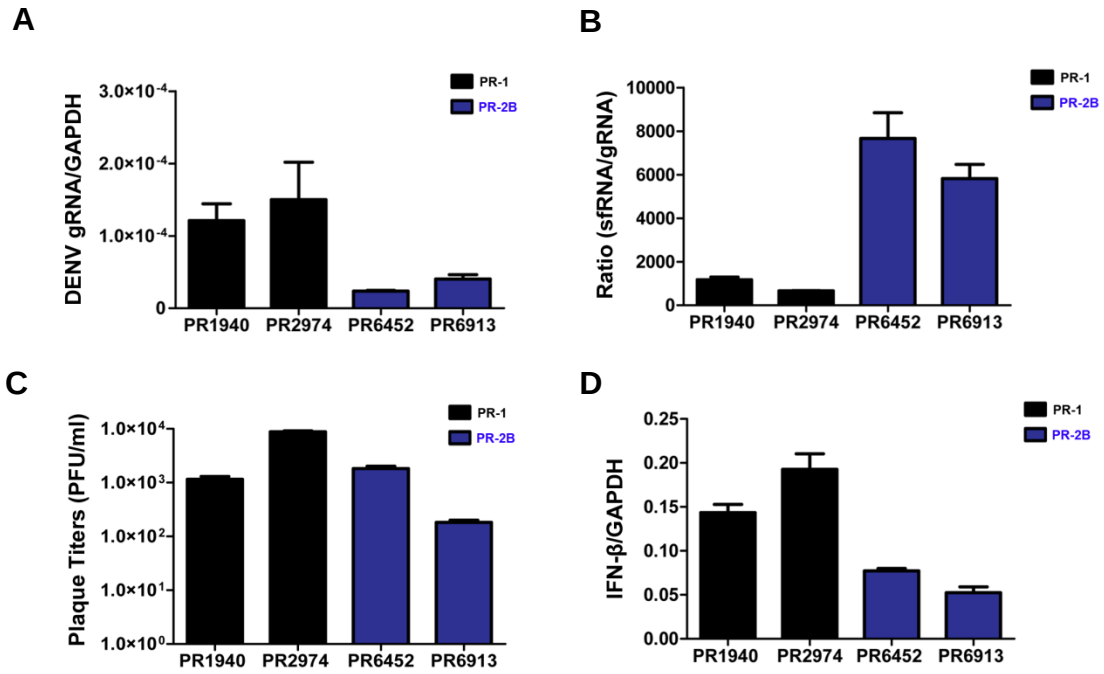

Figure 3.13 Infection assays with selected viruses in primary monocytes (A) Quantification of DENV-2 gRNA at 24 hpi. Infection was carried out with selected PR-1 and PR-2B DENV-2 viruses opsonized with enhancing concentrations of humanized 3H5 monoclonal antibodies (B) Quantification of sfRNA:gRNA ratios in primary monocytes, 24 hpi. (C) Plaque titers from supernatant of infected primary monocytes at 72 hpi. (D) IFN-β expression in primary monocytes at 24 hpi. *Data obtained in collaboration with Eugenia Ong.*

3.2.2 Replication of PR-1 viruses is rescued more significantly in IFN-β deficient systems as compared to PR-2B

The reduced IFN-β expression in both HuH-7 and primary monocytes when infected with PR-2B compared to PR-1 viruses suggests that the higher sfRNA levels produced by PR-2B viruses downregulated the signaling that leads to type-I IFN expression. To test that possibility, we knocked down the expression of IRF3, which activates the transcription of IFN-β in response to viral infection. Indeed, silencing of IRF3 resulted in significantly increased replication of PR-1 but not PR-2B viruses (Figure 3.14A), suggesting that sfRNA from PR-2B acted upstream of IRF3 to downregulate IFN expression.

To test this possibility further, infection assays were performed on African green monkey (Vero) cells. Both the IFN-α (Diaz et al., 1988) and IFN-β (Mosca and Pitha, 1986) genes are deleted in Vero cells, making them type-I interferon deficient. As such, infection of Vero cells would likely lead to a significant increase in replication for PR-1 viruses as compared to PR-2B since PR-2B viruses already have a mechanism that is able to downregulate interferon expression efficiently.

As expected, an increase in plaque titers was noted for all viruses as they can replicate more efficiently in the absence of interferon. However, PR-1 DENV-2 produced significantly higher plaque titers at 96 hpi in IFN-deficient Vero cells as compared to PR-2B viruses (Figure 3.14B). These findings collectively suggest that PR-2B produce higher

sfRNA:gRNA ratios to suppress type-I IFN expression during replication more effectively than PR-1 viruses.

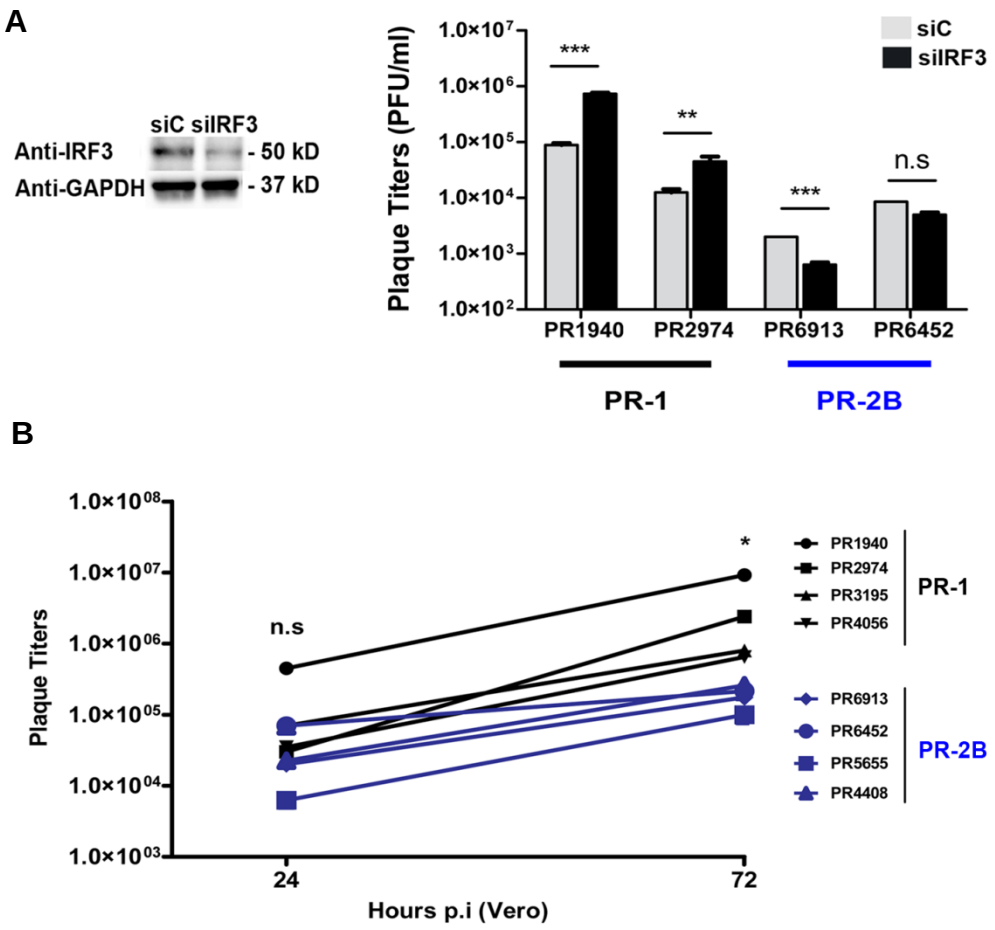

Figure 3.14 Infection of IFN-deficient systems by PR-1 and PR-2B viruses (A) IRF3 knockdown. Plaque titers of supernatant quantified at 24 hpi with selected viruses from each clade. Western blot was performed with antibodies against GAPDH and IRF3, respectively, to confirm knockdown. Sizes of respective proteins are as indicated. (B) Infection of Vero cells with selected isolates from both lineages. Plaque titers obtained from supernatant at 24 and 72 hpi are shown. Black lines: PR-1; Blue lines:PR-2B.

SECTION 3.3:

Subgenomic flavivirus RNA attenuates Type I interferon antiviral response for increased replication.

3.3.1 Residues in the 3'UTR affect sfRNA levels and DENV replication

Given the observed association between increased sfRNA:gRNA ratios and reduced IFN-β expression, we examined if the three nucleotide substitutions in the 3'UTR could functionally account for the increased sfRNA:gRNA ratios. To eliminate the possible contributions of the variations in NS1, NS3 and NS5, we performed mutagenesis studies using a previously characterized DENV-2 replicon reporter, pDENrep-FH (Holden et al., 2006) This reporter was originally derived from the DENV-2 Thai 16681 viral isolate and has the structural genes replaced with *Renilla luciferase*.

The nucleotides at the 3 positions of interest were substituted to match either the PR-1 or PR-2B viruses (Figure 3.15). At 72 hours post-electroporation, replicons with residues found in the PR-2B clade (i.e. pDENrep-FH/PR2B/28nt, pDENrep-FH/PR2B/117nt and pDENrep-FH/PR2B) produced less gRNA but higher ratios of sfRNA:gRNA compared to pDENrep-FH/PR1 which bears the PR-1 residues (Figure 3.15A). Likewise, replicons with PR-2B residues also showed reduced replication rate as indicated by the luciferase activity (Figure 3.15B). These findings indicate that substitutions in these 3 nucleotide positions can account for the observed differences in sfRNA:gRNA ratios in PR-1 and PR-2B viruses. They also suggest that DENV-2 is particularly sensitive to variations in this genomic location and that alterations in the sequence can directly influence the amount of gRNA and sfRNA produced by a particular virus.

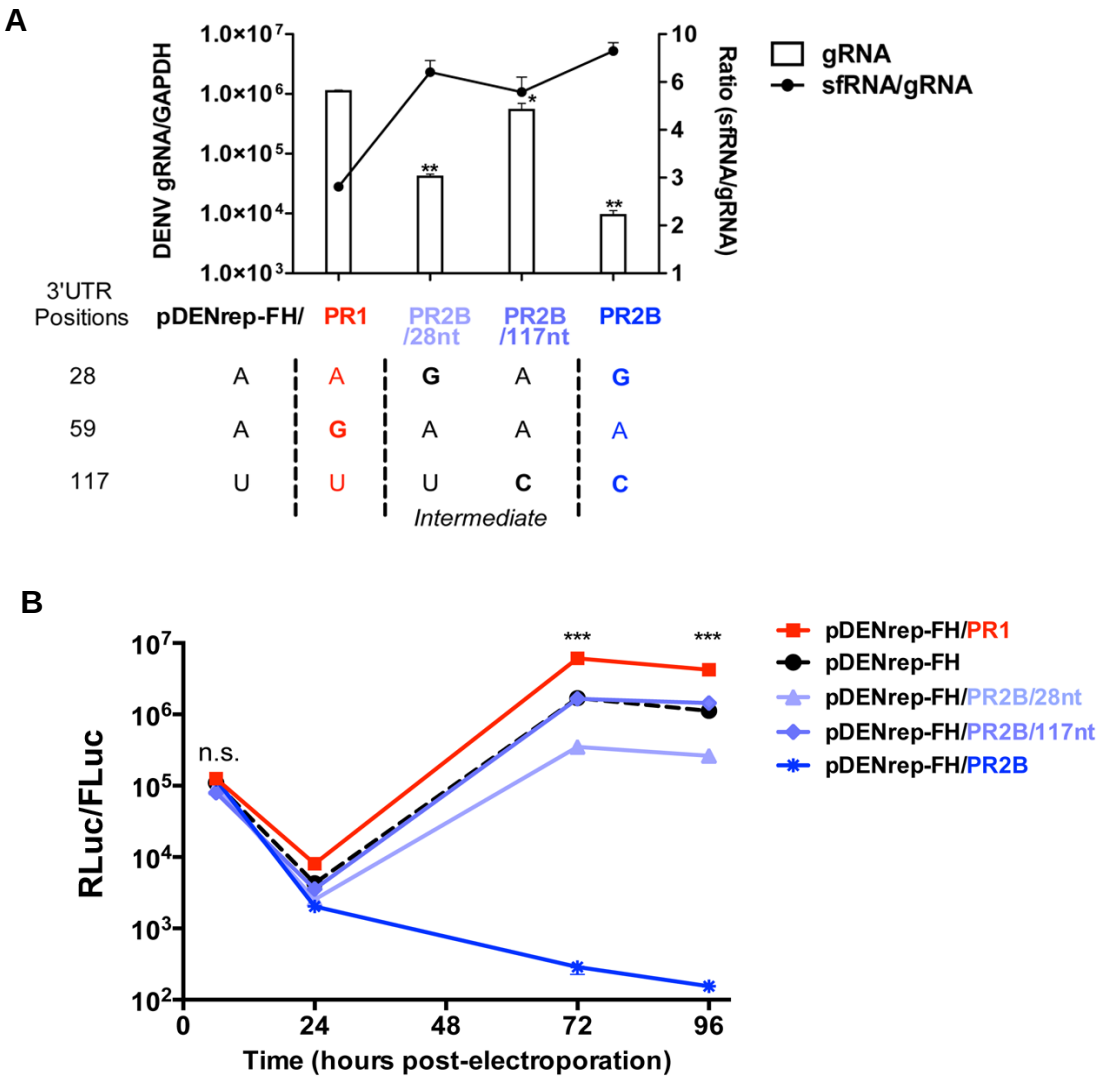

Figure 3.15 Electroporation of HuH-7 cells with mutants bearing relevant residues (A) Quantification of gRNA levels and sfRNA:gRNA ratios in HuH-7 cells, 72 hours post-electroporation with replicons bearing nucleotide residues representative of PR-1 or PR-2B DENV-2. Bars show the gRNA levels (left axis); while lines show sfRNA:gRNA ratios (right axis). (B) Luciferase reporter activity for the original replicon (pDENrep-FH) and mutated replicons at various time-points post-electroporation. Determination of firefly luciferase (FLuc) levels served as internal normalization controls. Black lines: PR-1; Blue lines: PR-2B.

3.3.2 Subgenomic flavivirus RNA downregulates IFN-β gene expression

To test whether sfRNA plays a functional role in modulating IFN-β expression, we co-transfected *in vitro*-transcribed PR-2B sfRNA or a size-matched RNA control with pDENrep-FH into HuH-7 cells. As compared to NFκB expression where no difference was seen, IFN-β expression was significantly reduced with sfRNA co-transfection at 72 hours post-electroporation (Figure 3.16A). Correspondingly, pDENrep-FH replication was significantly increased with sfRNA co-transfection compared to co-transfection with control RNA (Figure 3.16B).

To investigate if sfRNA is able to downregulate IFN expression upon stimulation of the RIG-I signaling pathway, we co-transfected sfRNA or size-matched control RNA with polyinosinic-polycytidylic acid (polyIC). PolyIC, a ligand of RIG-I, is able to induce interferon response after transfection into cells, thus simulating infection with a RNA virus. Transfection efficiency was first tested and qRT-PCR confirmed that there was no difference in levels of sfRNA or CtrlRNA when transfected with polyIC (Figure 3.17A). Experimental data confirmed that transfection with polyIC induced expression of IFN-β in HuH-7 cells (Figure 3.17B). Upon co-transfection with sfRNA, a significantly reduced IFN-β expression was observed but no such reduction was seen in the presence of CtrlRNA (Figure 3.17B). Taken collectively, these data indicate that sfRNA attenuates type-I interferon expression to promote increased DENV replication.

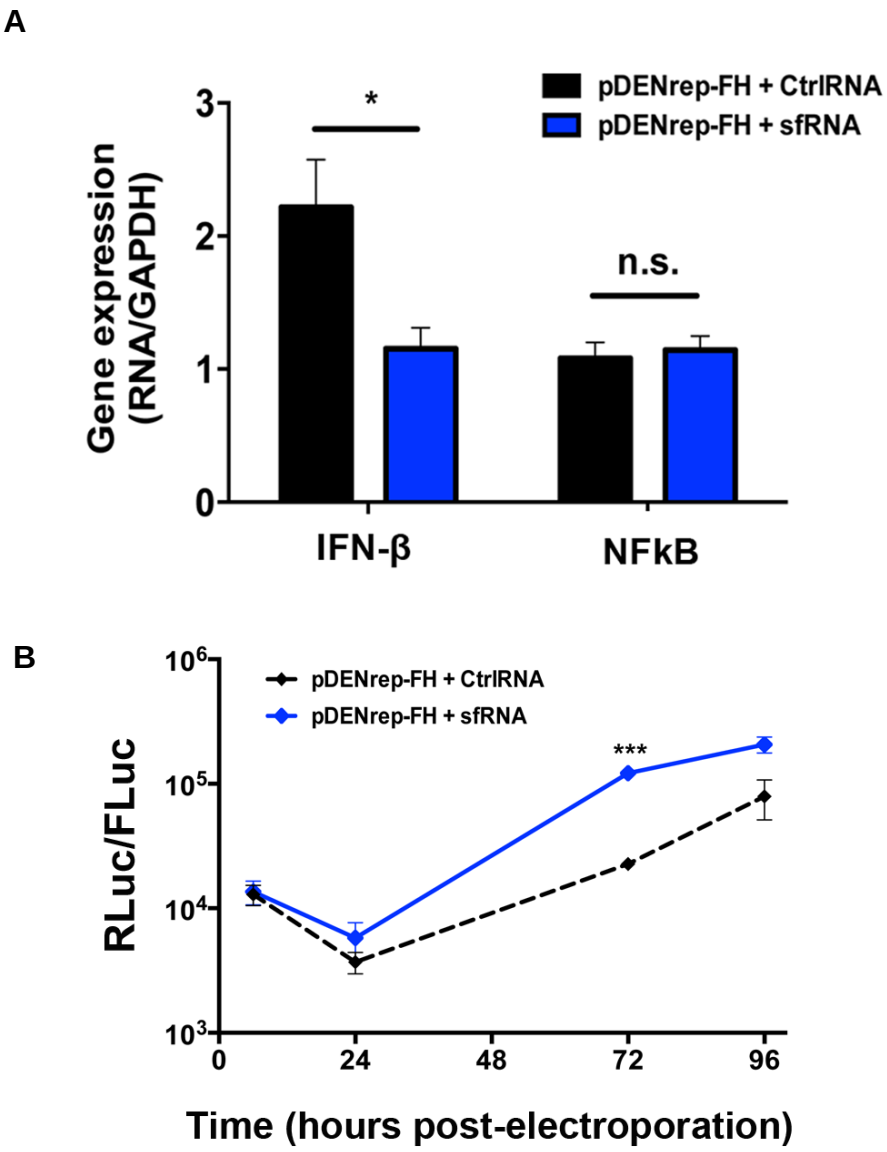

Figure 3.16 Electroporation of sfRNA with DENV-2 replicon (A) Quantification of IFN-β and NFkB expression using qRT-PCR at 72 hours post-electroporation with either pDENrep-FH + sfRNA or pDENrep-FH + CtrlRNA. (B) Luciferase reporter activity (RLuc) for pDENrep-FH + sfRNA and pDENrep-FH + CtrlRNA at various time-points post-electroporation. Determination of firefly luciferase levels (FLuc) served as internal normalization controls.

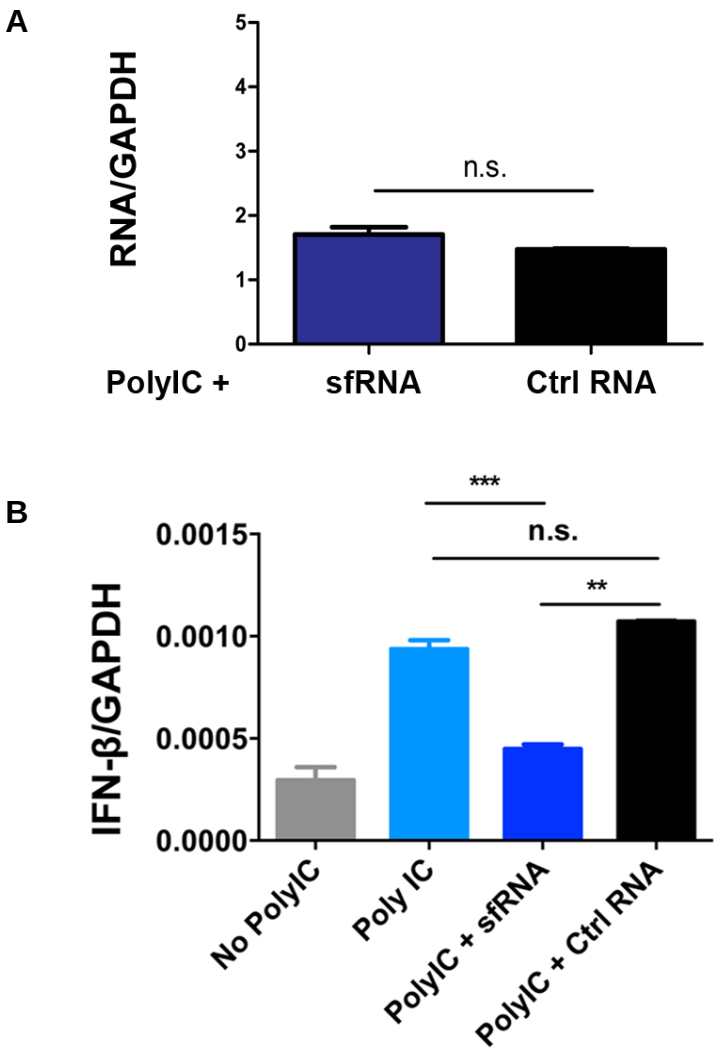

Figure 3.17 Co-transfection of sfRNA and PolyIC into HuH-7 cells (A) Validation of transfection efficiency upon transfection with sfRNA or size matched RNA control (Ctrl RNA) using qRT-PCR, 24 hours post-transfection with polyIC. Results show that there is no significant difference in transfection efficiency between the two RNAs (B) Quantification of IFN-β expression in HuH-7 cells transfected with PolyIC and sfRNA or CtrlRNA using qRT-PCR at 24 hours post-transfection. Annotations as depicted: No PolyIC (with transfection reagent but no PolyIC), PolyIC (only PolyIC), Poly IC + sfRNA (with *in vitro*-transcribed sfRNA and PolyIC), PolyIC + Ctrl RNA (with size-matched control RNA and PolyIC).

SECTION 3.4:

Subgenomic flavivirus RNA binds TRIM25 to inhibit TRIM25 de-ubiquitylation.

3.4.1 Mass spectrometry identified TRIM25 as a RNA-binding protein that binds better to PR-2B sfRNA than PR-1 sfRNA

The suppression of IFN-β expression is likely to be due to specific sfRNA-protein interactions. We thus used stable isotope labeling by amino acids in cell culture followed by quantitative mass spectrometry (SILAC-qMS) to identify host proteins that bind preferentially to the proximal end of the 3'UTR (SL-II to SL-IV) of PR-1 or PR-2B viruses (Ward et al., 2014). Briefly, a tobramycin RNA aptamer was incorporated into RNAs containing the partial 3'UTRs (PR-1 or PR-2B) or a size-matched control cloned from the DENV-2 NS2A open reading frame (Ctrl) (Ward et al., 2011). RNA was bound to a tobramycin matrix, incubated with SILAC-labeled cell lysates, washed and eluted using excess tobramycin. Eluates were then sent to the Quantitative Proteomics Laboratory, Institute of Molecular and Cellular Biology, Singapore for qMS analysis, thus allowing a direct comparison of proteins bound to the PR-1 3'UTR, PR-2B 3'UTR or control RNA.

A total of 1199 proteins were detected, a majority of which were non-specific background binders that were pulled down with both control RNA and the 3'UTRs. To further analyse these results, the student t-test was performed on three replicate experiments to prioritize candidate binding partners. This was followed by multiple sampling correction using the Benjamini-Hochberg method (FDR). Upon analysis, 198 proteins were found to be enriched (at least 1.5 fold change) with DENV 3'UTR compared to control RNA indicating that they are interacting partners of

DENV 3'UTR (Appendix, Figure 3.18). Both volcano plots depict the specific interactome of PR-1 (Figure 3.18A) and PR-2B (Figure 3.18B) RNAs as compared to control RNA, thus only the significantly enriched proteins (with positive log2 fold change and p-value < 0.05) are important. Of note, in comparison to PR-1, more interacting partners of PR-2B were evident based on the filtering criteria (Figure 3.18).

Notably, several of these proteins are known intermediates in the signaling pathway regulating type-I IFN expression (Figure 3.18C). Of these, the tripartite motif containing 25 (TRIM25) and mitochondrial antiviral signaling (MAVS) proteins were striking (Figure 3.18). Both proteins were significantly enriched in the presence of PR-2B 3'UTR as compared to PR-1. In addition, both TRIM25 and MAVS function directly upstream and downstream respectively of the viral RNA sensor, RIG-I, to regulate type I IFN expression, and are directly involved in host antiviral response (Gack et al., 2009; Gack et al., 2007; Seth et al., 2005).

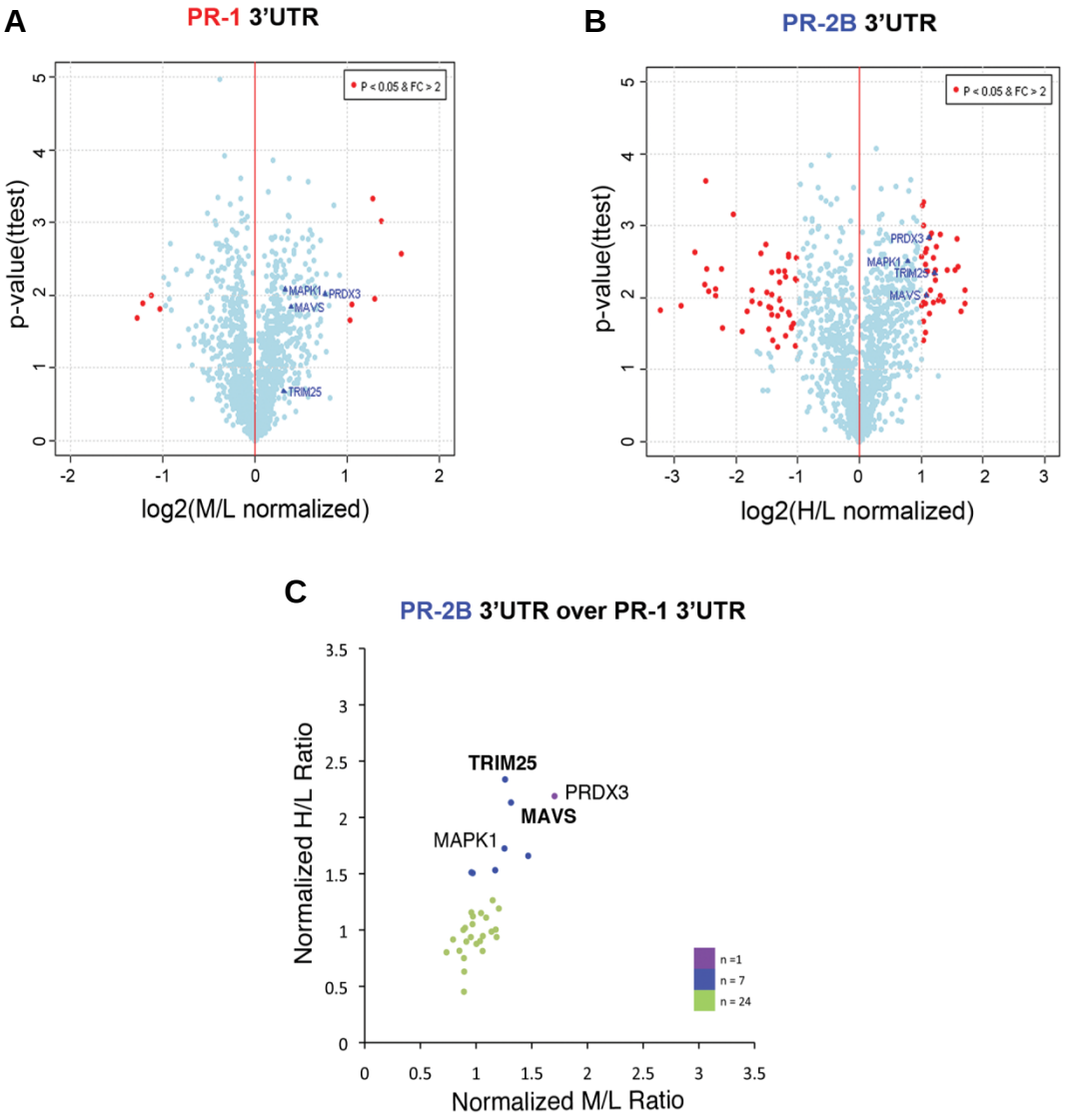

Figure 3.18 Plots derived from mass spectrometry showing the distribution of select RNA binding proteins Volcano plots displaying proteins enriched with partial 3'UTRs (sequence ranging from the start of SL-II to the end of SL-IV) of PR-1 (A) or PR-2B (B) clades as compared to control RNA. Red dots represent significantly enriched proteins (with positive log2 fold changes). The 4 labeled proteins (TRIM25, MAVS, Mitogen-Activated Protein Kinase 1 - MAPK1, Peroxiredoxin 3 - PRDX3) were highlighted from our data to be involved in IFN-β signaling. Annotations as depicted: M/L (PR-1 3'UTR divided by control), H/L (PR-2B 3'UTR divided by control). (C) Dot plot highlighting the 32 proteins selected by the GO term finder to be involved in type I interferon response. Annotations as depicted: M/L (PR-1 3'UTR divided by control), H/L (PR-2B 3'UTR divided by control). Green dots show proteins with H/L and M/L ratios lower than 1.5 (i.e. not significantly enriched). Purple dots show proteins with H/L and M/L ratios higher than 1.5 (i.e. significantly enriched in presence of both 3'UTRs) and the blue dots show proteins with H/L ratio higher than 1.5 but M/L ratio lower than 1.5 (i.e. significantly enriched with PR-2B 3'UTR as compared to PR-1 3'UTR). *Data from Jayantha Gunaratne*

To validate our SILAC-qMS findings for both TRIM25 and MAVS, we first immunoprecipitated TRIM25 or MAVS from cells infected with PR-2B virus or PR-1 virus and quantified the sfRNA and gRNA bound to either of these proteins. Significantly higher levels of sfRNA compared to gRNA were detected with TRIM25 immunoprecipitation as compared to immunoprecipitation using isotype IgG controls, with the difference being more pronounced when PR-2B DENV was used (Figure 3.19). On the other hand immunoprecipitation of MAVS from either DENV-2 infection did not enrich for either sfRNA or gRNA (Figure 3.20). This led us to focus on the interaction of DENV sfRNA with TRIM25.

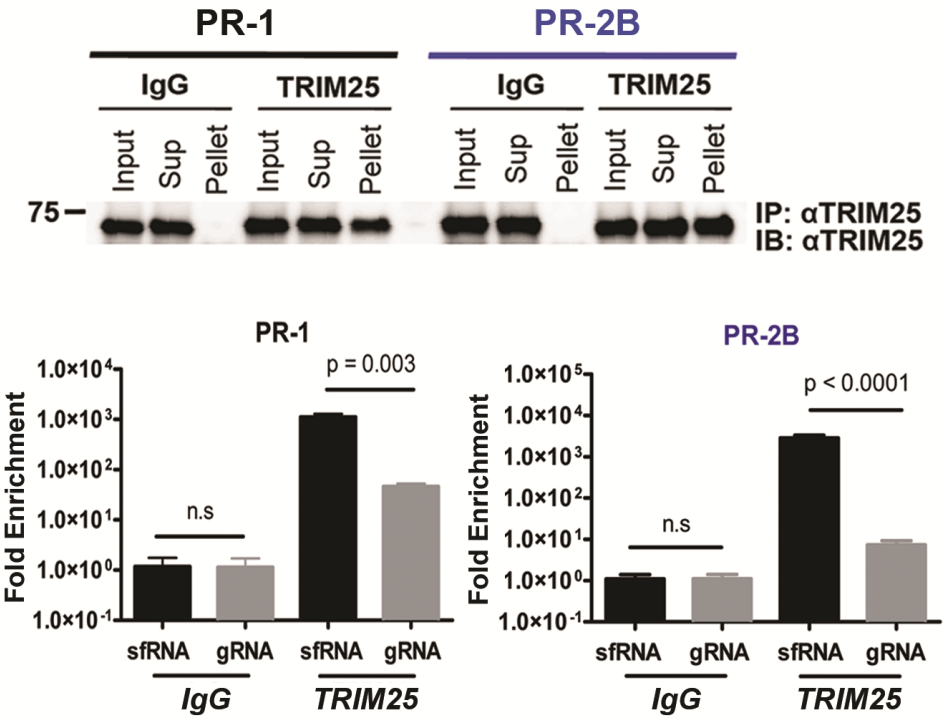

Figure 3.19 Validation of TRIM25 binding by RNA-immunoprecipitation (RIP) RIP was performed on HuH-7 cells 24 hpi with 2 viruses, one from each clade (MOI 5). Infected cells were subjected to TRIM25 or anti-mouse IgG control pull-down followed by immunoblotting with TRIM25 to confirm efficacy of pull-down. Input: Cell lysate before RIP; Sup: Supernatant following incubation of antibody-coated beads with cell lysate; Pellet: Final product after washing. The two bar charts show qRT-PCR results measuring fold enrichment of sfRNA and gRNA upon pull-down with TRIM25.

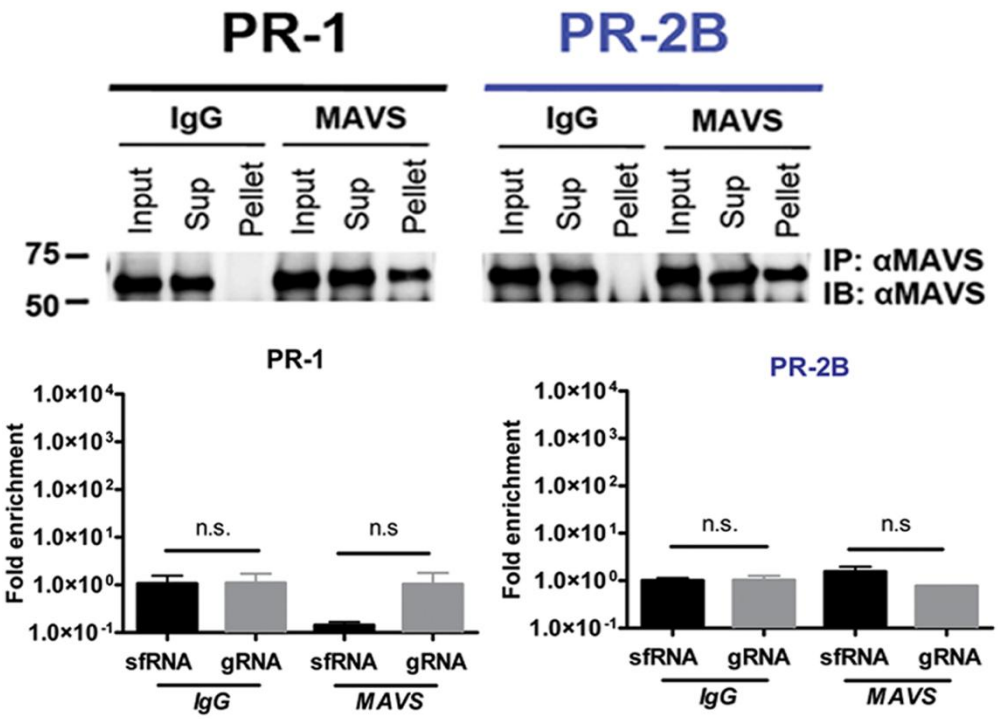

Figure 3.20 RNA-immunoprecipitation of MAVS RIP was performed as described above but pull-down was performed with MAVS or anti-rabbit IgG control. Input: Cell lysate before RIP; Sup: Supernatant following incubation of antibody-coated beads with cell lysate; Pellet: Final product after washing. The two bar charts show qRT-PCR results measuring fold enrichment of sfRNA and gRNA upon pull-down with MAVS.

3.4.2 PR-2B 3'UTR binds to TRIM25 more stably than PR-1, preventing its de-ubiquitylation

TRIM25 is an E3 ligase that polyubiquitylates RIG-I for sustained and amplified signal transduction (Gack et al., 2007). TRIM25 is stabilized via de-ubiquitylation by the ubiquitin-specific peptidase 15 (USP15) (Pauli et al., 2014). To examine if sfRNA interferes with these processes, we immunoprecipitated TRIM25 from DENV-2 infected cell lysates and probed for ubiquitin. Results showed a band identical in size to TRIM25 (about 71kDa) in lysates infected with either PR-1 or PR-2B virus (Figure 3.21). This suggests the possibility that sfRNA interferes with the de-ubiquitylation of TRIM25 to reduce sustained RIG-I signaling.

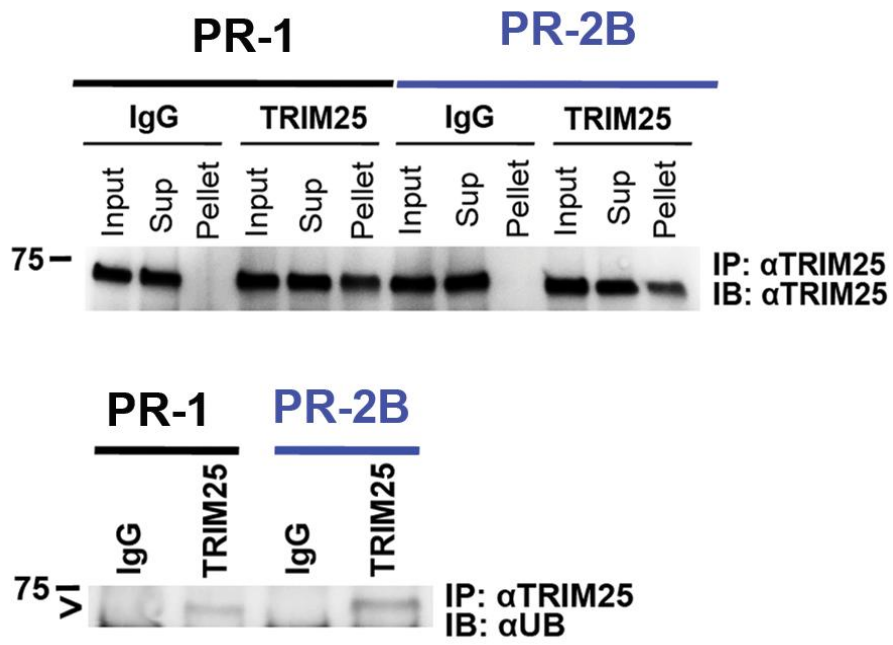

Figure 3.21 Immunoprecipitation of TRIM25 upon viral infection Lysates from HuH-7 cells infected with 2 viruses, one from each clade (MOI 5). Infected cells were subjected to TRIM25 or anti-mouse IgG control pull-down followed by immunoblotting with TRIM25 and ubiquitin (UB). Input: Cell lysate before RIP; Sup: Supernatant following incubation of antibody-coated beads with cell lysate; Pellet: Final product after washing. Arrow indicates ubiquitylated bands.

To confirm this possibility, we transfected HuH-7 cells with sfRNA or size-matched control RNA and immunoprecipitated RIG-I from the cell lysates. We next immunoblotted for TRIM25 and ubiquitin. Results showed that sfRNA did not prevent TRIM25 from binding RIG-I (Figure 3.22). However, TRIM25 co-immunoprecipitated with RIG-I remained ubiquitylated as indicated by a specific band identical in size to TRIM25 on the anti-ubiquitin immunoblot upon transfection of PR-2B but not PR-1 sfRNA (Figure 3.22). This finding indicates that PR-2B sfRNA interferes with the de-ubiquitylation and hence activation of the enzymatic function of TRIM25 to prevent amplified and sustained RIG-I signaling for type-I IFN induction.

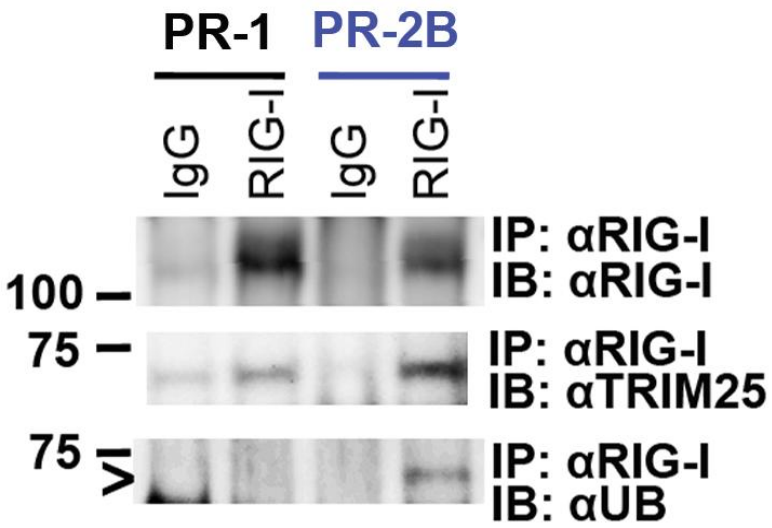

Figure 3.22 Immunoprecipitation of RIG-I after transfection of cells with sfRNA HuH-7 cell lysates, after transfection with PR-1 sfRNA, PR-2B sfRNA or size-matched RNA control were subjected to RIG-I pull-down followed by immunoblotting with RIG-I, TRIM25 and UB. Arrow indicates ubiquitylated bands.

CHAPTER 4:

DISCUSSION

4.1 Summary of findings

The global and intense transmission of dengue virus (DENV) has led to increasing genetic diversity of this virus, some of which appear to be associated with epidemic dengue. However, the underlying mechanism of viral fitness in a natural epidemiological setting remains poorly defined. Here we conducted *in vitro* studies using low passage clinical isolates to identify a determinant of fitness in a foreign dominant DENV-2 PR-2B clade, which emerged during the 1994 epidemic and replaced the endemic DENV-2 PR-1 clade in Puerto Rico. The PR-2B DENV-2 produced increased levels of sfRNA during replication to bind and inhibit de-ubiquitylation of TRIM25, which is needed to activate its E3 ligase activity. The E3 ligase activity is critical for sustained and amplified RIG-I signaling. Without which, type-I interferon expression becomes attenuated. Our findings demonstrate a unique viral RNA-host protein interaction to evade the innate immune response for epidemiological fitness.

Until this study, the epidemic potential of dengue has mainly been attributed to two factors: host resistance due to a lowered herd immunity and viral genetics. The former explanation has been widely studied and reviewed elsewhere (Alvarez et al., 2006; Halstead et al., 2010; Halstead and O'Rourke, 1977; Kouri et al., 1989; Vaughn et al., 2000) although the mechanisms remain to be fully understood. The latter explanation is now backed by several epidemiological observations (Lee et al., 2012b; Messer et al., 2003; OhAinle et al., 2011; Steel et al., 2010; Vu et al., 2010)

although none of these studies provided a mechanistic explanation for how viral genomic variations gave rise to epidemiologically fitter virus.

Indeed, viral genetics plays an important role in the epidemiological fitness of many viruses. Genomic analysis of the Ebola viruses isolated in the 2014 outbreak, which is largest outbreak to date, showed a rapid accumulation of genetic variation in the viruses that could have resulted in increased transmission (Gire et al., 2014). During the 2009 influenza A outbreak, the H1NI virus was shown to have significant pandemic potential based on its high transmissibility (Glinsky, 2010). Clinical, epidemiological and genomic analysis further confirmed that the increased disease severity was associated with novel mutations in hemagglutinin gene of the virus (Glinsky, 2010).

That genomic factors can give rise to epidemiologically fitter virus suggests that viral surveillance programs could incorporate viral genome sequence data into its activities. Indeed, this suggestion has been made previously (Ooi and Gubler, 2009; Ooi, 2007). Genomic surveillance of DENV could aid early warning of impending epidemics to trigger earlier responses. Without which, most public health responses to epidemics are often “too little too late” (Gubler, 2001, 2011). However, not all genetic changes can result in dengue epidemics. Successful genomic surveillance must thus depend on a mechanistic understanding of which sequence variations are functionally important and how these give rise to epidemiologically fitter virus. Elucidating the underlying mechanisms behind genetic variations that occur in the constantly evolving DENV

could thus be useful for predicting epidemic emergence. This was the motivation of this thesis.

The following discussion will first highlight the novel mechanism by which sfRNA modulates interferon expression through TRIM25 de-ubiquitylation. Finally, the role of 3'UTR in flaviviral pathogenesis and other DENV epidemics where sfRNA might have contributed to the increased epidemiological fitness will be discussed.

4.2 sfRNA-mediated de-ubiquitylation of TRIM25 leads to increased DENV epidemiological fitness

To our knowledge, this is the first report that provides a mechanism for increased DENV fitness and its epidemic potential. This is also the first finding that reports TRIM25 as an RNA binding protein.

TRIM25 belongs to the tripartite motif (TRIM) protein family which is involved in various cellular processes such as antiviral defence and cell proliferation (Nisole et al., 2005). TRIM25 consists of a RING domain at the N-terminus followed by a B-box domain, a coiled-coil domain and a SPRY domain at the C-terminus (Nisole et al., 2005). The RING domain is a specialized zinc finger of 40-60 residues and appears to be mainly involved in protein-protein interactions. Interestingly the RING domains in most TRIM proteins, including TRIM25, have E3 ubiquitin (UB) ligase activity (Joazeiro and Weissman, 2000).

E3 ubiquitin ligases are proteins that are primarily responsible for granting specificity to ubiquitin conjugation (Joazeiro and Weissman, 2000). They recruit the E2 ubiquitin-conjugating enzyme, recognize the specific substrate and assist or directly catalyze the ubiquitin transfer from E2 to the protein substrate. Ubiquitylation is a potent targeting signal for protein degradation and as such, E3 ubiquitin ligases are of profound importance in cell biology and regulate diverse cellular processes such as cell trafficking and DNA repair. Indeed the E3 ligase activity of TRIM25 is required to elicit host antiviral innate immunity in mammalian cells (Gack et al., 2007).

In 2007, Gack et al showed that the SPRY domain of TRIM25 interacts with the caspase recruitment (CARD) domain at the N-terminus to deliver Lys63-linked UB moiety to RIG-I (Gack et al., 2007). This induces robust ubiquitylation of RIG-I which results in a marked increase in its downstream signaling activity. Both RIG-I and MDA5 are cytosolic receptors for viral RNA. Upon viral RNA recognition, RIG-I interacts with a mitochondrial protein, MAVS to trigger downstream signal transduction.

Briefly, activation of MAVS results its massive polymerization that recruits several TRAF proteins (Liu et al., 2013). The TRAF proteins then promote ubiquitylation that recruits NFκB essential modulator (NEMO) protein to the MAVS signaling complex which in turn, triggers the cytosolic kinases, IκB kinase (IKK) and TBK-1 (Liu et al., 2013). IKK and TBK-1 activate the transcription factors NFκB and IRF3 respectively, leading to the MAVS-mediated induction of Type I interferon (Liu et al., 2013). Hence, through its interaction with RIG-I which stimulates downstream MAVS signaling, TRIM25 is critical for IFN-β production and antiviral activity after an RNA virus infection (Gack et al., 2007).

More recently, the ubiquitin specific protease 15 (USP15) has been identified as a critical regulator of TRIM25 and RIG-I mediated antiviral immune response (Pauli et al., 2014). Since the Lys48-linked ubiquitylation of TRIM25 stimulates its proteosomal degradation, USP15 de-ubiquitylates TRIM25. De-ubiquitylation of TRIM25 is therefore essential in preventing its degradation, leading to its stabilization which

ultimately promotes the RIG-I signaling pathway and leads to IFN-β production.

That TRIM25 is the target of sfRNA is highly interesting as influenza virus also targets this important amplifier of RIG-I signaling (Gack et al., 2009). In the latter case, however, TRIM25 inhibition is mediated by protein-protein interaction through the influenza-encoded NS1 protein. Namely, a newly identified domain in the influenza NS1 protein interacts with the coiled-coil domain of TRIM25 blocking its multimerization and RIG-I CARD ubiquitylation. Our findings reveal that subgenomic flavivirus RNA (sfRNA), a highly structured non coding RNA generated by members of the *Flavivirus* genus, interacts with TRIM25. Not only does this finding emphasize the vital role of TRIM25 in modulating viral infections, but it shows that reducing sustained and amplified IFN expression could be important to many viruses, as IFN renders uninfected cells resistant to viral infection.

Based on our findings, we propose a model to explain the 1994 dengue outbreak in Puerto Rico that coincided with the emergence of PR-2B viruses (Figure 4.1). The initial results showing lower replication of PR-2B viruses were unexpected and seemed incongruent to us initially, given the epidemiological outcome. Subsequent investigations revealed that these viruses "sacrifice" their gRNA for sfRNA to evade the innate immune response to achieve greater replication efficiency at the later stages of infection. The higher sfRNA:gRNA ratios could represent a "double whammy": greater levels of sfRNA result in increased inhibition

of TRIM25 while reduced gRNA result in lower stimulation of RIG-I/MDA5 RNA sensors. Reduced IFN response in the early stages of infection would ensure availability of susceptible cells for spread of the virus in a human host to reach viremia levels sufficient to infect mosquito vectors for further transmission. This is probably why the PR-2B viruses had a higher epidemic potential when they emerged in 1994.

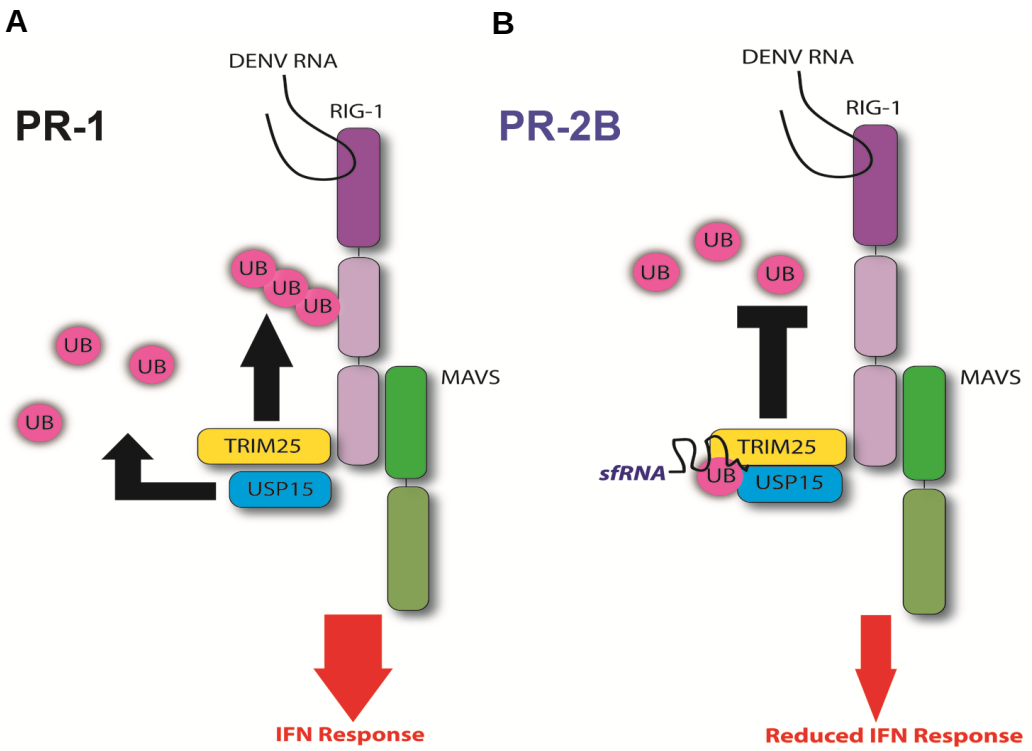

Figure 4.1 Proposed model depicting how sfRNA inhibits RIG-I signaling for amplified and sustained type I interferon response (A) Upon recognition of viral RNA, RIG-I recruits MAVS and starts a downstream signaling cascade that leads to IFN production. However, RIG-I needs to be ubiquitylated by TRIM25 before it can facilitate IFN production and TRIM25 has to be de-ubitquitylated by USP15 before it can ubiquitylate RIG-I. (B) When PR-2B viruses infect cells, the increased amounts of sfRNA:gRNA produced and the 3'UTR substitutions in the sfRNA cause a more stable interaction of sfRNA with TRIM25. This prevents TRIM25 from de-ubiquitylation. TRIM25 is thus unable to ubiquitylate RIG-I, resulting in a reduced IFN response. PR-2B viruses are then able to replicate more efficiently over time and the infection can spread more easily as cells cannot attain an antiviral state. This likely leads to increased viremia in infected individuals causing higher epidemic transmission.

4.3 Role of 3' noncoding RNA – Key to DENV pathogenesis?

The 3' noncoding region, although deemed essential for replication and translation, has been largely ignored in flavivirus pathogenesis until recently when Khromykh's laboratory and colleagues delved into the study of sfRNA (Alvarez et al., 2005; Friebe and Harris, 2010; Pijlman et al., 2008). Interestingly, findings indicate that sfRNA represents a pan-flaviviral strategy employed to antagonize the host innate immune response. Indeed, sfRNA likely contributes to viral pathogenesis by acting on various pathways (Bidet and Garcia-Blanco, 2014; Roby et al., 2014).

Consistent with our present study, Schuessler et al. had reported that sfRNA contributes to viral evasion of the type I interferon response upon infection with another flavivirus, West Nile virus (Schuessler et al., 2012). However, in their study, the mechanism by which sfRNA acts to down-regulate the type I interferon response was not determined. Another study had recently reported on the downregulation of interferon through profound inhibition of ISG translation by dengue sfRNA (Bidet et al., 2014). Thus, sfRNA might target IFN through multiple mechanisms, highlighting the importance of IFN as a potent antiviral during DENV infection.

One interesting question that arises is: Is the phenotype observed due to the amounts of sfRNA produced by the PR-2B viruses or differences in sfRNA sequence?

4.3.1 Amount of sfRNA produced

Initial experiments indicated that the amounts of sfRNA:gRNA in infected cells played an undeniably important role in downregulating IFN (Figure 3.5). Production of sfRNA is determined by the pseudoknot formation in the 3'UTR (Chapman et al., 2014a; Chapman et al., 2014b). There are 3 nucleotide substitutions present on the 3'UTR of the PR-2B viruses (Figure 3.4): One was on the linear RNA before SL-II; the second substitution was in fact, on the site of the predicted pseudoknot formation and the last substitution was on the side loop of SL-IV. Based on the proximity of these residues to the site of pseudoknot formation on the 3'UTR of the PR-2B viruses, it is possible that these residues may affect the pseudoknot strength or folding. If the pseudoknot is stronger, it will prevent complete degradation of the gRNA resulting in increased amounts of sfRNA. Likewise, if the folding is affected, the structures formed in the 3'UTR might be less or more stable leading to less or more sfRNA formation respectively.

Interestingly, the third substitution resided on SL-IV of the PR-2B 3'UTR structure. That substitutions on SL-IV were also observed in Nicaraguan DENV-2 NI-2B clade of viruses (Figure 3.9) strengthens the likelihood that nucleotide sequences in this region also influence viral fitness through their ability to affect sfRNA levels. Similar observations have also been made for the related West Nile virus where it was shown that when the SL-II structure on 3'UTR is deleted, the secondary structures SL-IV and dumbbell 1 (DB1) downstream of SL-II were able to

prevent further degradation of gRNA leading to production of sfRNAs (Funk et al., 2010). Thus, we deem it likely that SL-IV of DENV-2 might be involved in some molecular interactions which might be modulating sfRNA levels although detailed structural studies are required to confirm this.

4.3.2 Sequence of sfRNA produced

A second possibility is that the sequence of the sfRNA may determine its interaction with target proteins and consequently its effect on host immune pathways. This was suggested by the mass spectrometry results that showed an increased enrichment of TRIM25 with PR-2B 3'UTR as compared to PR-1 (Figure 3.20). Thus, PR-2B sfRNA binds to TRIM25 more stably than PR-1, indicating that the sequence of sfRNA produced by PR-2B plays a significant role in its modulation of the IFN response. Sequence variations in 3'UTR could lead to differential binding to other host RNA-binding proteins apart from TRIM25 which would then modify various pathways in cells (Refer to Appendix).

Indeed, sequence variations in the 3'UTR can directly lead to modifications to either the secondary structures (Chapman et al., 2014b) or binding affinities of individual residues. Such modifications can alter long-range viral RNA-RNA, viral RNA-viral protein and viral RNA-host RNA-binding protein interactions that regulate critical steps in DENV lifecycle. For instance, the nucleotide substitution on position 10389 of PR-2B is located on the side loop of SL-IV (Figure 3.4), where free

hydroxyl groups could potentially form hydrogen bonds with amino acids of interacting proteins.

To conclude, it appears that both the amounts and sequences of sfRNA play a central role in its role during DENV infection although further testing is required to establish this idea. Collectively, our results demonstrate that the 3'UTR is important in flavivirus infections and cannot be ignored in interplay of viral genetics, pathogenesis and epidemiological fitness.

4.4 Experimental limitations and alternative explanations

Although this work addressed the question of epidemiological fitness of DENV-2 viruses as adequately as possible *in vitro*, it is regardless an *in vitro* system and not ideal. As these isolates were collected through passive virologic surveillance, no clinical data was collected systematically, which meant that we could not determine if sequence changes were associated with disease outcome as well. Likewise, the lack of an immunocompetent animal model that mimics systemic DENV infection in humans, meant that there was no ideal *in vivo* system that could be used to study if the pathogenesis processes were also different with isolates from each of these clades. The closest that we came to an "*in vivo*" system was the use of primary human monocytes isolated fresh from peripheral blood; monocytes are primary targets of DENV infection. However, while the findings from primary monocytes does shed light on the intracellular mechanisms that operate during

infection, it does not provide any indication on how the intercellular response may operate to cause disease.

With regards to experimental setup, we utilized the DENV-2 replicon to study replication. However, it is to be noted that this DENV-2 replicon has a Thai 16681 DENV-2 backbone and is not of the same sequence as the Puerto Rican viruses. Although it could be used to study individual point mutations in the 3'UTR, it would have been better to either use a replicon with the same sequence as the PR viruses or construct infectious clones based on the PR-1 and PR-2B viruses. Furthermore, the main drawback of the replicon system is that only one round of replication could be studied as the replicon does not contain the structural genes that allow packaging, release and re-infection of cells. Hence we could not correlate the later timepoints of viral infection with the results from the replicon assay. On the other hand, with infectious clones, one could even swap the 3'UTRs and perform experiments to better correlate with the viral infection assay.

The study of dengue epidemiological fitness would also benefit from understanding the how these viruses behave in the mosquito vector. This is a limitation of this study. It would be interesting to determine if sfRNA:gRNA levels play similar immunomodulatory roles in mosquitoes.

4.5 Future directions

4.5.1 Role of 3'UTR in DENV epidemiological fitness – Further investigation warranted

The substitutions on 3'UTR leading to increased epidemiological fitness is unlikely to be unique to the 1994 DENV2 outbreak in Puerto Rico. Although the mechanism behind the increased sfRNA levels (Figure 3.10) in the Nicaraguan isolates might be different from our findings, the fact that 3'UTR suggests that this region of the genome is important for epidemiological fitness. Besides the 1994 dengue outbreak in Puerto Rico, which is the focus of this thesis, there are other epidemiological studies that reported clade changes in DENV (Bennett et al., 2006; Messer et al., 2003; OhAinle et al., 2011; Steel et al., 2010; Vu et al., 2010). In future, it would be riveting to perform similar experiments with viruses from these outbreaks to check if substitutions in the 3'UTR might have affected the viral epidemiological fitness (Bennett et al., 2006; Messer et al., 2003; OhAinle et al., 2011; Steel et al., 2010; Vu et al., 2010).

Historically, many DENV phylogenetic analyses conducted have largely excluded the non-coding 3'UTR sequences (Weaver and Vasilakis, 2009). Our findings indicate that DENV genome sequence must include the 3'UTR as it could determine the epidemic potential of DENV. Determination of the conserved and dynamic regions of the 3'UTR during virus evolution could be equally useful in future predictions of DENV epidemic emergence.

4.5.2 Deeper insights on the contribution of sfRNA to viral pathogenesis

What we found with regards to the mechanism behind sfRNA-mediated de-ubiquitylation of TRIM25 is but the tip of the iceberg. In future, it would be critical to shed light on the following aspects: What determines the specificity of TRIM25 binding? Which domain of TRIM25 does sfRNA bind? Which structures or residues on sfRNA are involved in this interaction? Does USP15 play an active role in the sfRNA-TRIM25 interaction? Is MAVS involved in this binding?

Apart from the interaction with TRIM25, other RNA-binding proteins could also interact with sfRNA that determines the phenotype of the virus. These proteins may be involved in alternative sfRNA-mediated proviral interactions which could affect various immune pathways or cellular processes. Alternatively, the different sfRNAs from the other DENV serotypes and flaviviruses may contribute in various ways to virus-host interactions upon infection. Studying the interactome of sfRNA could thus shed light on important determinants of DENV pathogenesis.

Elucidating the fine details behind these interactions will be crucial in the future consideration of vaccine design. Upon understanding how sfRNA contributes to DENV pathogenesis, appropriate alterations could be made to various residues in the 3'UTR to attenuate a vaccine sufficiently while enhancing its efficacy in individuals.

4.6 Conclusion

In conclusion, our study demonstrates a novel mechanism of sfRNA-mediated IFN downregulation through the de-ubiquitylation of an E3 ligase, TRIM25. The higher sfRNA:gRNA ratios produced in the early phase of PR-2B infection could represent a "one-two punch" against the host response: greater levels of sfRNA inhibit TRIM25, while reduced gRNA results in lower stimulation of RIG-I/MDA5 RNA sensors. Reducing IFN responses in the early stages of infection would ensure that the virus is able to spread to neighbouring cells more effectively allowing them to reach viremia levels sufficient to infect mosquito vectors for further transmission. Meanwhile, the PR-2B isolates are also likely to result in greater disease pathogenesis because of the higher viremia and sfRNA levels in infected cells. Thus, the more efficient transmission of PR-2B viruses as well as the greater dengue pathogenesis upon PR-2B infection might have contributed to the DENV-2 epidemic in Puerto Rico when this clade emerged in 1994.

This study also demonstrates that by combining epidemiologic studies with molecular investigations, viral phylogenetic information could be informative not only on the virus origin but also potentially as a predictor of its epidemiological fitness.

References

Aguirre, S., Maestre, A.M., Pagni, S., Patel, J.R., Savage, T., Gutman, D., Maringer, K., Bernal-Rubio, D., Shabman, R.S., Simon, V.*, et al.* (2012). DENV inhibits type I IFN production in infected cells by cleaving human STING. PLOS Pathog *8*, e1002934.

Alvarez, D.E., Ezcurra, A.L.D., Fucito, S., and Gamarnik, A.V. (2005). Role of RNA structures present at the 3 ' UTR of dengue virus on translation, RNA synthesis, and viral replication. Virology *339*, 200-212.

Alvarez, M., Rodriguez-Roche, R., Bernardo, L., Vazquez, S., Morier, L., Gonzalez, D., Castro, O., Kouri, G., Halstead, S.B., and Guzman, M.G. (2006). Dengue hemorrhagic fever caused by sequential dengue 1-3 virus infections over a long time interval: Havana epidemic, 2001-2002. Am J Trop Med Hyg *75*, 1113-1117.

Ashour, J., Laurent-Rolle, M., Shi, P.Y., and Garcia-Sastre, A. (2009). NS5 of dengue virus mediates STAT2 binding and degradation. J Virol *83*, 5408-5418.

Barnes, W.J.S., and Rosen, L. (1974). Fatal hemorrhagic disease and shock associated with primary dengue Infection on a Pacific Island. Am J Trop Med Hyg *23*, 495-506.

Bennett, S.N., Holmes, E.C., Chirivella, M., Rodriguez, D.M., Beltran, M., Vorndam, V., Gubler, D.J., and McMillan, W.O. (2003). Selection-driven evolution of emergent dengue virus. Mol Biol Evol *20*, 1650-1658.

Bennett, S.N., Holmes, E.C., Chirivella, M., Rodriguez, D.M., Beltran, M., Vorndam, V., Gubler, D.J., and McMillan, W.O. (2006). Molecular evolution of dengue 2 virus in Puerto Rico: positive selection in the viral envelope accompanies clade reintroduction. J Gen Virol *87*, 885-893.

Bhatt, S., Gething, P.W., Brady, O.J., Messina, J.P., Farlow, A.W., Moyes, C.L., Drake, J.M., Brownstein, J.S., Hoen, A.G., Sankoh, O.*, et al.* (2013). The global distribution and burden of dengue. Nature *496*, 504-507.

Bidet, K., Dadlani, D., and Garcia-Blanco, M.A. (2014). G3BP1, G3BP2 and CAPRIN1 are required for translation of interferon stimulated mRNAs and are targeted by a dengue virus non-coding RNA. PLOS Pathog *10*, e1004242.

Bidet, K., and Garcia-Blanco, M.A. (2014). Flaviviral RNAs: weapons and targets in the war between virus and host. Biochem J *462*, 215-230.

Boyle, E.I., Weng, S., Gollub, J., Jin, H., Botstein, D., Cherry, J.M., and Sherlock, G. (2004). GO::TermFinder--open source software for accessing Gene Ontology information and finding significantly enriched Gene Ontology terms associated with a list of genes. Bioinformatics *20*, 3710-3715.

Brathwaite Dick, O., San Martin, J.L., Montoya, R.H., del Diego, J., Zambrano, B., and Dayan, G.H. (2012). The history of dengue outbreaks in the Americas. Am J Trop Med Hyg *87*, 584-593.

Brault, A.C., Kinney, R.M., Maharaj, P.D., Green, E.N.G., Reisen, W.K., and Huang, C.Y.H. (2011). Replication of the primary dog kidney-53 dengue 2 virus vaccine candidate in Aedes aegypti is modulated by a mutation in the 5 ' untranslated region and amino acid substitutions in nonstructural proteins 1 and 3. Vector-Borne Zoonot *11*, 683-689.

Buckley, T.R., Simon, C., Shimodaira, H., and Chambers, G.K. (2001). Evaluating hypotheses on the origin and evolution of the New Zealand alpine cicadas (Maoricicada) using multiple-comparison tests of tree topology. Mol Biol Evol *18*, 223-234.

Cao-Lormeau, V.M., Roche, C., Aubry, M., Teissier, A., Lastere, S., Daudens, E., Mallet, H.P., Musso, D., and Aaskov, J. (2011). Recent emergence of dengue virus serotype 4 in French Polynesia results from multiple introductions from other South Pacific Islands. PLOS one *6*, e29555.

Capeding, M.R., Tran, N.H., Hadinegoro, S.R., Ismail, H.I., Chotpitayasunondh, T., Chua, M.N., Luong, C.Q., Rusmil, K., Wirawan, D.N., Nallusamy, R.*, et al.* (2014). Clinical efficacy and safety of a novel tetravalent dengue vaccine in healthy children in Asia: a phase 3, randomised, observer-masked, placebo-controlled trial. Lancet *384*, 1358-1365.

Carrasco, L.R., Lee, L.K., Lee, V.J., Ooi, E.E., Shepard, D.S., Thein, T.L., Gan, V., Cook, A.R., Lye, D., Ng, L.C.*, et al.* (2011). Economic impact of dengue illness and the cost-effectiveness of future vaccination programs in Singapore. PLOS Negl Trop Dis *5*, e1426.

Chan, K.R., Ong, E.Z., Tan, H.C., Zhang, S.L.X., Zhang, Q., Tang, K.F., Kaliaperumal, N., Lim, A.P.C., Hibberd, M.L., Chan, S.H.*, et al.* (2014). Leukocyte immunoglobulin-like receptor B1 is critical for antibody-dependent dengue. Proc Natl Acad Sci U S A *111*, 2722-2727.

Chan, K.R., Zhang, S.L., Tan, H.C., Chan, Y.K., Chow, A., Lim, A.P., Vasudevan, S.G., Hanson, B.J., and Ooi, E.E. (2011). Ligation of Fc gamma receptor IIB inhibits antibody-dependent enhancement of dengue virus infection. Proc Natl Acad Sci U S A *108*, 12479-12484.

Chan, Y.K., Huang, I.C., and Farzan, M. (2012). IFITM proteins restrict antibody-dependent enhancement of dengue virus infection. PLOS one *7*, e34508.

Chang, R.Y., Hsu, T.W., Chen, Y.L., Liu, S.F., Tsai, Y.J., Lin, Y.T., Chen, Y.S., and Fan, Y.H. (2013). Japanese encephalitis virus non-coding RNA inhibits activation of interferon by blocking nuclear translocation of interferon regulatory factor 3. Vet Microbiol *166*, 11-21.

Chapman, E.G., Costantino, D.A., Rabe, J.L., Moon, S.L., Wilusz, J., Nix, J.C., and Kieft, J.S. (2014a). The structural basis of pathogenic subgenomic flavivirus RNA (sfRNA) production. Science *344*, 307-310.

Chapman, E.G., Moon, S.L., Wilusz, J., and Kieft, J.S. (2014b). RNA structures that resist degradation by Xrn1 produce a pathogenic Dengue virus RNA. Elife *3* e01892.

Chareonsirisuthigul, T., Kalayanarooj, S., and Ubol, S. (2007). Dengue virus (DENV) antibody-dependent enhancement of infection upregulates the production of anti-inflammatory cytokines, but suppresses anti-DENV free radical and pro-inflammatory cytokine production, in THP-1 cells. J Gen Virol *88*, 365-375.

Charlier, N., Leyssen, P., De Clercq, E., and Neyts, J. (2004). Rodent models for the study of therapy against flavivirus infections. Antivir Res *63*, 67-77.

Chawla, T., Chan, K.R., Zhang, S.L., Tan, H.C., Lim, A.P., Hanson, B.J., and Ooi, E.E. (2013). Dengue virus neutralization in cells expressing Fc gamma receptors. PLOS one *8*, e65231.

Chen, H.L., Lin, S.R., Liu, H.F., King, C.C., Hsieh, S.C., and Wang, W.K. (2008a). Evolution of dengue virus type 2 during two consecutive outbreaks with an increase in severity in southern Taiwan in 2001-2002. Am J Trop Med Hyg *79*, 495-505.

Chen, S.T., Lin, Y.L., Huang, M.T., Wu, M.F., Cheng, S.C., Lei, H.Y., Lee, C.K., Chiou, T.W., Wong, C.H., and Hsieh, S.L. (2008b). CLEC5A is critical for dengue-virus-induced lethal disease. Nature *453*, 672-676.

Chen, Y., Maguire, T., Hileman, R.E., Fromm, J.R., Esko, J.D., Linhardt, R.J., and Marks, R.M. (1997). Dengue virus infectivity depends on envelope protein binding to target cell heparan sulfate. Nat Med *3*, 866-871.

Chen, Y.C., Wang, S.Y., and King, C.C. (1999). Bacterial lipopolysaccharide inhibits dengue virus infection of primary human monocytes/macrophages by blockade of virus entry via a CD14-dependent mechanism. J Virol *73*, 2650-2657.

Christenbury, J.G., Aw, P.P., Ong, S.H., Schreiber, M.J., Chow, A., Gubler, D.J., Vasudevan, S.G., Ooi, E.E., and Hibberd, M.L. (2010). A method for full genome sequencing of all four serotypes of the dengue virus. J Virol Methods *169*, 202-206.

Cologna, R., Armstrong, P.M., and Rico-Hesse, R. (2005). Selection for virulent dengue viruses occurs in humans and mosquitoes. J Virol *79*, 853-859.

Gubler, D.J., Kuno, G., and Markoff L. (2007). Flaviviruses. In Fields Virology, D.M. Knipe, and P.M. Howley, ed. (Lippincott-Raven), pp. 1154-1252.

da Costa, V.G., Marques-Silva, A.C., Floriano, V.G., and Moreli, M.L. (2014). Safety, immunogenicity and efficacy of a recombinant tetravalent dengue vaccine: a meta-analysis of randomized trials. Vaccine *32*, 4885-4892.

Daffis, S., Szretter, K.J., Schriewer, J., Li, J., Youn, S., Errett, J., Lin, T.Y., Schneller, S., Zust, R., Dong, H.*, et al.* (2010). 2'-O methylation of the viral mRNA cap evades host restriction by IFIT family members. Nature *468*, 452-456.

Darnell, J.E., Kerr, I.M., and Stark, G.R. (1994). Jak-STAT pathways and transcriptional activation in response to IFNs and other extracellular signaling proteins. Science *264*, 1415-1421.

Dayan, G.H., Garbes, P., Noriega, F., Izoton de Sadovsky, A.D., Rodrigues, P.M., Giuberti, C., and Dietze, R. (2013a). Immunogenicity and safety of a recombinant tetravalent dengue vaccine in children and adolescents ages 9-16 years in Brazil. Am J Trop Med Hyg *89*, 1058-1065.

Dayan, G.H., Thakur, M., Boaz, M., and Johnson, C. (2013b). Safety and immunogenicity of three tetravalent dengue vaccine formulations in healthy adults in the USA. Vaccine *31*, 5047-5054.

de Alwis, R., Beltramello, M., Messer, W.B., Sukupolvi-Petty, S., Wahala, W.M., Kraus, A., Olivarez, N.P., Pham, Q., Brien, J.D., Tsai, W.Y.*, et al.* (2011). In-depth analysis of the antibody response of individuals exposed to primary dengue virus infection. PLOS Negl Trop Dis *5*, e1188.

Devignot, S., Sapet, C., Duong, V., Bergon, A., Rihet, P., Ong, S., Lorn, P.T., Chroeung, N., Ngeav, S., Tolou, H.J.*, et al.* (2010). Genome-wide expression profiling deciphers host responses altered during dengue shock syndrome and reveals the role of innate immunity in severe dengue. PLOS one *5*, e11671.

Dhodapkar, K.M., Banerjee, D., Connolly, J., Kukreja, A., Matayeva, E., Veri, M.C., Ravetch, J.V., Steinman, R.M., and Dhodapkar, M.V. (2007). Selective blockade of the inhibitory Fcgamma receptor (FcgammaRIIB) in human dendritic cells and monocytes induces a type I interferon response program. J Exp Med *204*, 1359-1369.

Diallo, M., Ba, Y., Sall, A.A., Diop, O.M., Ndione, J.A., Mondo, M., Girault, L., and Mathiot, C. (2003). Amplification of the sylvatic cycle of dengue virus type 2, Senegal, 1999-2000: entomologic findings and epidemiologic considerations. Emerg Infect Dis *9*, 362-367.

Diamond, M.S. (2009). Mechanisms of evasion of the type I interferon antiviral response by flaviviruses. J Interf Cytok Res *29*, 521-530.

Diamond, M.S., Roberts, T.G., Edgil, D., Lu, B., Ernst, J., and Harris, E. (2000). Modulation of Dengue virus infection in human cells by alpha, beta, and gamma interferons. J Virol *74*, 4957-4966.

Diaz, M.O., Ziemin, S., Le Beau, M.M., Pitha, P., Smith, S.D., Chilcote, R.R., and Rowley, J.D. (1988). Homozygous deletion of the alpha- and beta 1-interferon genes in human leukemia and derived cell lines. Proc Natl Acad Sci U S A *85*, 5259-5263.

Dong, H., Chang, D.C., Hua, M.H., Lim, S.P., Chionh, Y.H., Hia, F., Lee, Y.H., Kukkaro, P., Lok, S.M., Dedon, P.C.*, et al.* (2012). 2'-O methylation of internal adenosine by flavivirus NS5 methyltransferase. Plos Pathog *8*, e1002642.

Durbin, A.P., Kirkpatrick, B.D., Pierce, K.K., Elwood, D., Larsson, C.J., Lindow, J.C., Tibery, C., Sabundayo, B.P., Shaffer, D., Talaat, K.R.*, et al.* (2013). A single dose of any of four different live attenuated tetravalent dengue vaccines is safe and immunogenic in flavivirus-naive adults: a randomized, double-blind clinical trial. J Infect Dis *207*, 957-965.

Eisen, L., Beaty, B.J., Morrison, A.C., and Scott, T.W. (2009). ProactiveVector control strategies and improved monitoring and evaluation practices for dengue prevention. J Med Entomol *46*, 1245-1255.

Fan, Y.H., Nadar, M., Chen, C.C., Weng, C.C., Lin, Y.T., and Chang, R.Y. (2011). Small noncoding RNA modulates Japanese encephalitis virus replication and translation in trans. Virol J *8*, 492.

Fernandez-Garcia, M.D., Mazzon, M., Jacobs, M., and Amara, A. (2009). Pathogenesis of flavivirus infections: using and abusing the host cell. Cell Host Microbe *5*, 318-328.

Friebe, P., and Harris, E. (2010). Interplay of RNA elements in the dengue virus 5' and 3' ends required for viral RNA replication. J Virol *84*, 6103-6118.

Funk, A., Truong, K., Nagasaki, T., Torres, S., Floden, N., Balmori Melian, E., Edmonds, J., Dong, H., Shi, P.Y., and Khromykh, A.A. (2010). RNA structures required for production of subgenomic flavivirus RNA. J Virol *84*, 11407-11417.

Gack, M.U., Albrecht, R.A., Urano, T., Inn, K.S., Huang, I.C., Carnero, E., Farzan, M., Inoue, S., Jung, J.U., and Garcia-Sastre, A. (2009). Influenza A virus NS1 targets the ubiquitin ligase TRIM25 to evade recognition by the host viral RNA sensor RIG-I. Cell Host Microbe *5*, 439-449.

Gack, M.U., Shin, Y.C., Joo, C.H., Urano, T., Liang, C., Sun, L., Takeuchi, O., Akira, S., Chen, Z., Inoue, S*., et al.* (2007). TRIM25 RING-finger E3 ubiquitin ligase is essential for RIG-I-mediated antiviral activity. Nature *446*, 916-920.

Gire, S.K., Goba, A., Andersen, K.G., Sealfon, R.S., Park, D.J., Kanneh, L., Jalloh, S., Momoh, M., Fullah, M., Dudas, G*., et al.* (2014). Genomic surveillance elucidates Ebola virus origin and transmission during the 2014 outbreak. Science *345*, 1369-1372.

Glinsky, G.V. (2010). Genomic analysis of pandemic (H1N1) 2009 reveals association of increasing disease severity with emergence of novel hemagglutinin mutations. Cell Cycle *9*, 958-970.

Goh, K.T. (1995). Changing epidemiology of dengue in Singapore. Lancet *346*, 1098.

Graham, R.R., Juffrie, M., Tan, R., Hayes, C.G., Laksono, I., Ma'roef, C., Erlin, Sutaryo, Porter, K.R., and Halstead, S.B. (1999). A prospective seroepidemiologic study on dengue in children four to nine years of age in Yogyakarta, Indonesia I. studies in 1995-1996. Am J Trop Med Hyg *61*, 412-419.

Grant, D., Tan, G.K., Qing, M., Ng, J.K.W., Yip, A., Zou, G., Xie, X.P., Yuan, Z.M., Schreiber, M.J., Schul, W*., et al.* (2011). A single amino acid in nonstructural protein NS4B confers virulence to dengue virus in AG129 mice through enhancement of viral RNA synthesis. J Virol *85*, 7775-7787.

Green, A.M., Beatty, P.R., Hadjilaou, A., and Harris, E. (2014). Innate immunity to dengue virus infection and subversion of antiviral responses. J Mol Biol *426*, 1148-1160.

Gubler, D.J. (1989). Aedes aegypti and Aedes aegypti-borne disease control in the 1990s: top down or bottom up. Charles Franklin Craig Lecture. Am J Trop Med Hyg *40*, 571-578.

Gubler, D.J. (1998a). Dengue and dengue hemorrhagic fever. Clin Microbiol Rev *11*, 480-496.

Gubler, D.J. (1998b). Resurgent vector-borne diseases as a global health problem. Emerg Infect Dis *4*, 442-450.

Gubler, D.J. (2001). Epidemic dengue/dengue haemorrhagic fever as a public health problem in the 21st century. Symp Soc Gen Microbi *60*, 247-267.

Gubler, D.J. (2002). The global emergence/resurgence of arboviral diseases as public health problems. Arch Med Res *33*, 330-342.

Gubler, D.J. (2004). The changing epidemiology of yellow fever and dengue, 1900 to 2003: full circle? Comp Immunol Microb *27*, 319-330.

Gubler, D.J. (2011). Dengue, Urbanization and Globalization: The Unholy Trinity of the 21(st) Century. Trop Med Health *39*, 3-11.

Gubler, D.J., and Clark, G.G. (1994). Community-based integrated control of Aedes aegypti: a brief overview of current programs. Am J Trop Med Hyg *50*, 50-60.

Gubler, D.J., and Meltzer, M. (1999). Impact of dengue/dengue hemorrhagic fever on the developing world. Adv Virus Res *53*, 35-70.

Gubler, D.J., Reed, D., Rosen, L., and Hitchcock, J.R., Jr. (1978). Epidemiologic, clinical, and virologic observations on dengue in the Kingdom of Tonga. Am J Trop Med Hyg *27*, 581-589.

Gubler, D.J., and Trent, D.W. (1993). Emergence of epidemic dengue/dengue hemorrhagic fever as a public health problem in the Americas. Infect Agent Dis *2*, 383-393.

Guirakhoo, F., Arroyo, J., Pugachev, K.V., Miller, C., Zhang, Z.X., Weltzin, R., Georgakopoulos, K., Catalan, J., Ocran, S., Soike, K.*, et al.* (2001). Construction, safety, and immunogenicity in nonhuman primates of a chimeric yellow fever-dengue virus tetravalent vaccine. J Virol *75*, 7290-7304.

Guy, B., Guirakhoo, F., Barban, V., Higgs, S., Monath, T.P., and Lang, J. (2010). Preclinical and clinical development of YFV 17D-based chimeric vaccines against dengue, West Nile and Japanese encephalitis viruses. Vaccine *28*, 632-649.

Guy, B., Nougarede, N., Begue, S., Sanchez, V., Souag, N., Carre, M., Chambonneau, L., Morrisson, D.N., Shaw, D., Qiao, M.*, et al.* (2008). Cell-mediated immunity induced by chimeric tetravalent dengue vaccine in naive or flavivirus-primed subjects. Vaccine *26*, 5712-5721.

Guzman, M.G., Halstead, S.B., Artsob, H., Buchy, P., Farrar, J., Gubler, D.J., Hunsperger, E., Kroeger, A., Margolis, H.S., Martinez, E., *et al.* (2010). Dengue: a continuing global threat. Nat Rev Microbiol *8*, S7-16.

Guzman, M.G., and Harris, E. (2014). Dengue. Lancet *14*, 60572-60579.
Guzman, M.G., and Kouri, G. (2002). Dengue: an update. Lancet Infect Dis *2*, 33-42.

Guzman, M.G., Kouri, G., Bravo, J., Valdes, L., Vazquez, S., and Halstead, S.B. (2002). Effect of age on outcome of secondary dengue 2 infections. Int J Infect Dis *6*, 118-124.

Guzman, M.G., Kouri, G., and Halstead, S.B. (2000). Do escape mutants explain rapid increases in dengue case-fatality rates within epidemics? Lancet *355*, 1902-1903.

Guzman, M.G., and Vazquez, S. (2010). The complexity of antibody-dependent enhancement of dengue virus infection. Viruses *2*, 2649-2662.

Halstead, S.B. (1974). Etiologies of the experimental dengues of Siler and Simmons. Am J Trop Med Hyg *23*, 974-982.

Halstead, S.B. (2007). Dengue. Lancet *370*, 1644-1652.

Halstead, S.B. (2008). Dengue virus-mosquito interactions. Annu Rev Entomol *53*, 273-291.

Halstead, S.B., Mahalingam, S., Marovich, M.A., Ubol, S., and Mosser, D.M. (2010). Intrinsic antibody-dependent enhancement of microbial infection in macrophages: disease regulation by immune complexes. Lancet Infect Dis *10*, 712-722.

Halstead, S.B., Nimmannitya, S., and Cohen, S.N. (1970). Observations related to pathogenesis of dengue hemorrhagic fever. IV. Relation of disease severity to antibody response and virus recovered. Yale J Biol Med *42*, 311-328.

Halstead, S.B., and O'Rourke, E.J. (1977). Antibody-enhanced dengue virus infection in primate leukocytes. Nature *265*, 739-741.

Hammond, S.N., Balmaseda, A., Perez, L., Tellez, Y., Saborio, S.I., Mercado, J.C., Videa, E., Rodriguez, Y., Perez, M.A., Cuadra, R., *et al.* (2005). Differences in dengue severity in infants, children, and adults in a 3-year hospital-based study in Nicaragua. Am J Trop Med Hyg *73*, 1063-1070.

Hanley, K.A., Manlucu, L.R., Manipon, G.G., Hanson, C.T., Whitehead, S.S., Murphy, B.R., and Blaney, J.E. (2004). Introduction of mutations into the non-structural genes or 3 ' untranslated region of an attenuated dengue virus type 4 vaccine candidate further decreases replication in rhesus monkeys while retaining protective immunity. Vaccine *22*, 3440-3448.

Holden, K.L., Stein, D.A., Pierson, T.C., Ahmed, A.A., Clyde, K., Iversen, P.L., and Harris, E. (2006). Inhibition of dengue virus translation and RNA synthesis by a morpholino oligomer targeted to the top of the terminal 3' stem-loop structure. Virology *344*, 439-452.

Holmes, E.C., and Burch, S.S. (2000). The causes and consequences of genetic variation in dengue virus. Trends Microbiol *8*, 74-77.

Hotez, P.J., Fenwick, A., Savioli, L., and Molyneux, D.H. (2009). Rescuing the bottom billion through control of neglected tropical diseases. Lancet *373*, 1570-1575.

Jiang, D., Weidner, J.M., Qing, M., Pan, X.B., Guo, H., Xu, C., Zhang, X., Birk, A., Chang, J., Shi, P.Y.*, et al.* (2010). Identification of five interferon-induced cellular proteins that inhibit west nile virus and dengue virus infections. J Virol *84*, 8332-8341.

Joazeiro, C.A., and Weissman, A.M. (2000). RING finger proteins: mediators of ubiquitin ligase activity. Cell *102*, 549-552.

Johnson, A.J., and Roehrig, J.T. (1999). New mouse model for dengue virus vaccine testing. J Virol *73*, 783-786.

Kanakaratne, N., Wahala, W.M., Messer, W.B., Tissera, H.A., Shahani, A., Abeysinghe, N., de-Silva, A.M., and Gunasekera, M. (2009). Severe dengue epidemics in Sri Lanka, 2003-2006. Emerg Infect Dis *15*, 192-199.

Kawano, H., Rostapshov, V., Rosen, L., and Lai, C.J. (1993). Genetic determinants of dengue type 4 virus neurovirulence for mice. J Virol *67*, 6567-6575.

Kelly, E.P., Polo, S., Sun, W., and Falgout, B. (2011). Evolution of attenuating mutations in dengue-2 strain S16803 PDK50 vaccine and comparison of growth kinetics with parent virus. Virus Genes *43*, 18-26.

Kishino, H., and Hasegawa, M. (1989). Evaluation of the maximum likelihood estimate of the evolutionary tree topologies from DNA sequence data, and the branching order in hominoidea. J Mol Evol *29*, 170-179.

Kliks, S.C., Nimmanitya, S., Nisalak, A., and Burke, D.S. (1988). Evidence that maternal dengue antibodies are important in the development of dengue hemorrhagic fever in infants. Am J Trop Med Hyg *38*, 411-419.

Koh, B.K., Ng, L.C., Kita, Y., Tang, C.S., Ang, L.W., Wong, K.Y., James, L., and Goh, K.T. (2008). The 2005 dengue epidemic in Singapore: epidemiology, prevention and control. Ann Acad Med Singap *37*, 538-545.

Kouri, G.P., Guzman, M.G., and Bravo, J.R. (1987). Why dengue haemorrhagic fever in Cuba? 2. An integral analysis. Trans R Soc Trop Med Hyg *81*, 821-823.

Kouri, G.P., Guzman, M.G., Bravo, J.R., and Triana, C. (1989). Dengue haemorrhagic fever/dengue shock syndrome: lessons from the Cuban epidemic, 1981. Bull World Health Organ *67*, 375-380.

Kuhn, R.J., Zhang, W., Rossmann, M.G., Pletnev, S.V., Corver, J., Lenches, E., Jones, C.T., Mukhopadhyay, S., Chipman, P.R., Strauss, E.G.*, et al.* (2002). Structure of dengue virus: implications for flavivirus organization, maturation, and fusion. Cell *108*, 717-725.

Lai, Y.L., Chung, Y.K., Tan, H.C., Yap, H.F., Yap, G., Ooi, E.E., and Ng, L.C. (2007). Cost-effective real-time reverse transcriptase PCR (RT-PCR) to screen for Dengue virus followed by rapid single-tube multiplex RT-PCR for serotyping of the virus. J Clin Microbiol *45*, 935-941.

Lambrechts, L., Scott, T.W., and Gubler, D.J. (2010). Consequences of the expanding global distribution of Aedes albopictus for dengue virus transmission. PLOS Negl Trop Dis *4*, e646.

Lee, K.G., Xu, S., Kang, Z.H., Huo, J., Huang, M., Liu, D., Takeuchi, O., Akira, S., and Lam, K.P. (2012a). Bruton's tyrosine kinase phosphorylates Toll-like receptor 3 to initiate antiviral response. Proc Natl Acad Sci U S A *109*, 5791-5796.

Lee, K.S., Lai, Y.L., Lo, S., Barkham, T., Aw, P., Ooi, P.L., Tai, J.C., Hibberd, M., Johansson, P., Khoo, S.P.*, et al.* (2010). Dengue virus surveillance for early warning, Singapore. Emerg Infect Dis *16*, 847-849.

Lee, K.S., Lo, S., Tan, S.S., Chua, R., Tan, L.K., Xu, H., and Ng, L.C. (2012b). Dengue virus surveillance in Singapore reveals high viral diversity through multiple introductions and in situ evolution. Infect Genet Evol *12*, 77-85.

Leitmeyer, K.C., Vaughn, D.W., Watts, D.M., Salas, R., de Chacon, I.V., Ramos, C., and Rico-Hesse, R. (1999). Dengue virus structural differences that correlate with pathogenesis. J Virol *73*, 4738-4747.

Li, L., Lok, S.M., Yu, I.M., Zhang, Y., Kuhn, R.J., Chen, J., and Rossmann, M.G. (2008). The flavivirus precursor membrane-envelope protein complex: structure and maturation. Science *319*, 1830-1834.

Liang, H., Luo, L., Yang, Z., Di, B., Bai, Z., He, P., Jing, Q., and Zheng, X. (2013). Re-emergence of dengue virus type 3 in Canton, China, 2009-2010, associated with multiple introductions through different geographical routes. PLOS one *8*, e55353.

Libraty, D.H., Acosta, L.P., Tallo, V., Segubre-Mercado, E., Bautista, A., Potts, J.A., Jarman, R.G., Yoon, I.K., Gibbons, R.V., Brion, J.D.*, et al.* (2009). A prospective nested case-control study of Dengue in infants: rethinking and refining the antibody-dependent enhancement dengue hemorrhagic fever model. PLOS Med *6*, e1000171.

Libraty, D.H., Endy, T.P., Houng, H.S., Green, S., Kalayanarooj, S., Suntayakorn, S., Chansiriwongs, W., Vaughn, D.W., Nisalak, A., Ennis, F.A.*, et al.* (2002). Differing influences of virus burden and immune activation on disease severity in secondary dengue-3 virus infections. J Infect Dis *185*, 1213-1221.

Lin, K.C., Chang, H.L., and Chang, R.Y. (2004). Accumulation of a 3'-terminal genome fragment in Japanese encephalitis virus-infected mammalian and mosquito cells. J Virol *78*, 5133-5138.

Lindenbach, B.D., Thiel, H.J., and Rice, C.M. (2007). Flaviviridae: The Viruses and Their Replication. In Fields Virology, D.M. Knipe, and P.M. Howley, ed. (Lippincott-Raven), pp. 1102-1152.

Liu, R., Yue, L., Li, X., Yu, X., Zhao, H., Jiang, Z., Qin, E., and Qin, C. (2010). Identification and characterization of small sub-genomic RNAs in dengue 1-4 virus-infected cell cultures and tissues. Biochem Bioph Res Co *391*, 1099-1103.

Liu, S., Chen, J., Cai, X., Wu, J., Chen, X., Wu, Y.T., Sun, L., and Chen, Z.J. (2013). MAVS recruits multiple ubiquitin E3 ligases to activate antiviral signaling cascades. Elife *2*, e00785.

Liu, Y., Liu, H.B., Zou, J., Zhang, B., and Yuan, Z.M. (2014). Dengue virus subgenomic RNA induces apoptosis through the Bcl-2-mediated PI3k/Akt signaling pathway. Virology *448*, 15-25.

Lloyd, R.E. (2012). How do viruses interact with stress-associated RNA granules? PLOS Pathog *8*, e1002741.

Loo, Y.M., Fornek, J., Crochet, N., Bajwa, G., Perwitasari, O., Martinez-Sobrido, L., Akira, S., Gill, M.A., Garcia-Sastre, A., Katze, M.G.*, et al.* (2008). Distinct RIG-I and MDA5 signaling by RNA viruses in innate immunity. J Virol *82*, 335-345.

Lye, D.C., Lee, V.J., Sun, Y., and Leo, Y.S. (2009). Lack of efficacy of prophylactic platelet transfusion for severe thrombocytopenia in adults with acute uncomplicated dengue infection. Clin Infect Dis *48*, 1262-1265.

Mackenzie, J.S., Gubler, D.J., and Petersen, L.R. (2004). Emerging flaviviruses: the spread and resurgence of Japanese encephalitis, West Nile and dengue viruses. Nat Med *10*, S98-109.

Mann, M. (2006). Functional and quantitative proteomics using SILAC. Nat Rev Mol Cell Bio *7*, 952-958.
Markham, N.R., and Zuker, M. (2005). DINAMelt web server for nucleic acid melting prediction. Nucleic Acids Res *33*, W577-581.

Mazzon, M., Jones, M., Davidson, A., Chain, B., and Jacobs, M. (2009). Dengue virus NS5 inhibits interferon-alpha signaling by blocking signal transducer and activator of transcription 2 phosphorylation. J Infect Dis *200*, 1261-1270.

McElroy, K.L., Santiago, G.A., Lennon, N.J., Birren, B.W., Henn, M.R., and Munoz-Jordan, J.L. (2011). Endurance, refuge, and reemergence of dengue virus type 2, Puerto Rico, 1986-2007. Emerg Infect Dis *17*, 64-71.

Meltzer, M.I., Rigau-Perez, J.G., Clark, G.G., Reiter, P., and Gubler, D.J. (1998). Using disability-adjusted life years to assess the economic impact of dengue in Puerto Rico: 1984-1994. Am J Trop Med Hyg *59*, 265-271.

Messer, W.B., Gubler, D.J., Harris, E., Sivananthan, K., and de Silva, A.M. (2003). Emergence and global spread of a dengue serotype 3, subtype III virus. Emerg Infect Dis *9*, 800-809.

Miller, J.L., Dewet, B.J.M., Martinez-Pomares, L., Radcliffe, C.M., Dwek, R.A., Rudd, P.M., and Gordon, S. (2008). The mannose receptor mediates dengue virus infection of macrophages. PLOS Pathog *4*, e17.

Monath, T.P. (1994). Dengue: the risk to developed and developing countries. Proc Natl Acad Sci U S A *91*, 2395-2400.

Moon, S.L., Anderson, J.R., Kumagai, Y., Wilusz, C.J., Akira, S., Khromykh, A.A., and Wilusz, J. (2012). A noncoding RNA produced by arthropod-borne flaviviruses inhibits the cellular exoribonuclease XRN1 and alters host mRNA stability. RNA *18*, 2029-2040.

Morrison, J., Aguirre, S., and Fernandez-Sesma, A. (2012). Innate immunity evasion by dengue virus. Viruses *4*, 397-413.

Mosca, J.D., and Pitha, P.M. (1986). Transcriptional and posttranscriptional regulation of exogenous human beta interferon gene in simian cells defective in interferon synthesis. Mol Cell Biol *6*, 2279-2283.

Mukhopadhyay, S., Kuhn, R.J., and Rossmann, M.G. (2005). A structural perspective of the flavivirus life cycle. Nat Rev Microbiol *3*, 13-22.

Mullard, A. (2014). Sanofi's dengue vaccine rounds final corner. Nat Rev Drug Discov *13*, 801-802.

Munoz-Jordan, J.L., Laurent-Rolle, M., Ashour, J., Martinez-Sobrido, L., Ashok, M., Lipkin, W.I., and Garcia-Sastre, A. (2005). Inhibition of alpha/beta interferon signaling by the NS4B protein of flaviviruses. J Virol *79*, 8004-8013.

Munoz-Jordan, J.L., Sanchez-Burgos, G.G., Laurent-Rolle, M., and Garcia-Sastre, A. (2003). Inhibition of interferon signaling by dengue virus. Proc Natl Acad Sci U S A *100*, 14333-14338.

Nasirudeen, A.M., Wong, H.H., Thien, P., Xu, S., Lam, K.P., and Liu, D.X. (2011). RIG-I, MDA5 and TLR3 synergistically play an important role in restriction of dengue virus infection. PLOS Negl Trop Dis *5*, e926.

Nisalak, A., Endy, T.P., Nimmannitya, S., Kalayanarooj, S., Thisayakorn, U., Scott, R.M., Burke, D.S., Hoke, C.H., Innis, B.L., and Vaughn, D.W. (2003). Serotype-specific dengue virus circulation and dengue disease in Bangkok, Thailand from 1973 to 1999. Am J Trop Med Hyg *68*, 191-202.

Nisole, S., Stoye, J.P., and Saib, A. (2005). TRIM family proteins: retroviral restriction and antiviral defence. Nat Rev Microbiol *3*, 799-808.

OhAinle, M., Balmaseda, A., Macalalad, A.R., Tellez, Y., Zody, M.C., Saborio, S., Nunez, A., Lennon, N.J., Birren, B.W., Gordon, A.*, et al.* (2011). Dynamics of dengue disease severity determined by the interplay between viral genetics and serotype-specific immunity. Science Transl Med *3*, 114ra128.

Ong, S.E., Blagoev, B., Kratchmarova, I., Kristensen, D.B., Steen, H., Pandey, A., and Mann, M. (2002). Stable isotope labeling by amino acids in cell culture, SILAC, as a simple and accurate approach to expression proteomics. Mol Cell Proteomics *1*, 376-386.

Ooi, E.E., Goh, K.T., and Gubler, D.J. (2006). Dengue prevention and 35 years of vector control in Singapore. Emerg Infect Dis *12*, 887-893.

Ooi, E.E., and Gubler, D.J. (2009). Dengue in Southeast Asia: epidemiological characteristics and strategic challenges in disease prevention. Cad Saude Publica *25*, S115-124.

Ooi, E.E., Gubler, D.J., Nam, V.S., 2007. (2007). Dengue research needs related to surveillance and emergency response. Report of the Scientific Working Group Meeting on Dengue, 2006 World Health Organization, Geneva, 124-133.

Ooi, E.E., Hart, T.J., Tan, H.C., and Chan, S.H. (2001). Dengue seroepidemiology in Singapore. Lancet *357*, 685-686.

Osorio, J.E., Huang, C.Y.H., Kinney, R.M., and Stinchcomb, D.T. (2011). Development of DENVax: A chimeric dengue-2 PDK-53-based tetravalent vaccine for protection against dengue fever. Vaccine *29*, 7251-7260.

Pastorino, B., Nougairede, A., Wurtz, N., Gould, E., and de Lamballerie, X. (2010). Role of host cell factors in flavivirus infection: Implications for pathogenesis and development of antiviral drugs. Antivir Res *87*, 281-294.

Pauli, E.K., Chan, Y.K., Davis, M.E., Gableske, S., Wang, M.K., Feister, K.F., and Gack, M.U. (2014). The ubiquitin-specific protease USP15 promotes RIG-I-mediated antiviral signaling by deubiquitylating TRIM25. Sci Signal *7*, ra3.

Pijlman, G.P. (2014). Flavivirus RNAi suppression: decoding non-coding RNA. Curr Opin Virol *7*, 55-60.

Pijlman, G.P., Funk, A., Kondratieva, N., Leung, J., Torres, S., van der Aa, L., Liu, W.J., Palmenberg, A.C., Shi, P.Y., Hall, R.A*., et al.* (2008). A highly structured, nuclease-resistant, noncoding RNA produced by flaviviruses is required for pathogenicity. Cell Host Microbe *4*, 579-591.

Platanias, L.C. (2005). Mechanisms of type-I- and type-II-interferon-mediated signalling. Nat Rev Immunol *5*, 375-386.

Platt, K.B., Linthicum, K.J., Myint, K.S., Innis, B.L., Lerdthusnee, K., and Vaughn, D.W. (1997). Impact of dengue virus infection on feeding behavior of Aedes aegypti. Am J Trop Med Hyg *57*, 119-125.

Rico-Hesse, R. (1990). Molecular evolution and distribution of dengue viruses type 1 and 2 in nature. Virology *174*, 479-493.

Rico-Hesse, R., Harrison, L.M., Salas, R.A., Tovar, D., Nisalak, A., Ramos, C., Boshell, J., de Mesa, M.T., Nogueira, R.M., and da Rosa, A.T. (1997). Origins of dengue type 2 viruses associated with increased pathogenicity in the Americas. Virology *230*, 244-251.

Rigau-Perez, J.G., Clark, G.G., Gubler, D.J., Reiter, P., Sanders, R.J., and Vorndam, A.V. (1998). Dengue and dengue haemorrhagic fever. Lancet *352*, 971-977.

Rigau-Perez, J.G., Vorndam, A.V., and Clark, G.G. (2001). The dengue and dengue hemorrhagic fever epidemic in Puerto Rico, 1994-1995. Am J Trop Med Hyg *64*, 67-74.

Roby, J.A., Pijlman, G.P., Wilusz, J., and Khromykh, A.A. (2014). Noncoding subgenomic flavivirus RNA: multiple functions in West Nile virus pathogenesis and modulation of host responses. Viruses *6*, 404-427.

Rodriguez-Madoz, J.R., Belicha-Villanueva, A., Bernal-Rubio, D., Ashour, J., Ayllon, J., and Fernandez-Sesma, A. (2010). Inhibition of the type I interferon response in human dendritic cells by dengue virus infection requires a catalytically active NS2B3 complex. J Virol *84*, 9760-9774.

Rodriguez-Roche, R., Alvarez, M., Gritsun, T., Halstead, S., Kouri, G., Gould, E.A., and Guzman, M.G. (2005). Virus evolution during a severe dengue epidemic in Cuba, 1997. Virology *334*, 154-159.

Rosen, L. (1977). The Emperor's New Clothes revisited, or reflections on the pathogenesis of dengue hemorrhagic fever. Am J Trop Med Hyg *26*, 337-343.

Rosen, L., Rozeboom, L.E., Sweet, B.H., and Sabin, A.B. (1954). The transmission of dengue by Aedes polynesiensis Marks. Am J Trop Med Hyg *3*, 878-882.

Sabchareon, A., Wallace, D., Sirivichayakul, C., Limkittikul, K., Chanthavanich, P., Suvannadabba, S., Jiwariyavej, V., Dulyachai, W., Pengsaa, K., Wartel, T.A.*, et al.* (2012). Protective efficacy of the recombinant, live-attenuated, CYD tetravalent dengue vaccine in Thai schoolchildren: a randomised, controlled phase 2b trial. Lancet *380*, 1559-1567.

Sabin, A.B. (1952). Research on dengue during World War II. Am J Trop Med Hyg *1*, 30-50.

Saeedi, B.J., and Geiss, B.J. (2013). Regulation of flavivirus RNA synthesis and capping. RNA *4*, 723-735.

Sanchez, I.J., and Ruiz, B.H. (1996). A single nucleotide change in the E protein gene of dengue virus 2 Mexican strain affects neurovirulence in mice. J Gen Virol *77*, 2541-2545.

Sangkawibha, N., Rojanasuphot, S., Ahandrik, S., Viriyapongse, S., Jatanasen, S., Salitul, V., Phanthumachinda, B., and Halstead, S.B. (1984). Risk factors in dengue shock syndrome: a prospective epidemiologic study in Rayong, Thailand. I. The 1980 outbreak. Am J Epidemiol *120*, 653-669.

Sariol, C.A., Martinez, M.I., Rivera, F., Rodriguez, I.V., Pantoja, P., Abel, K., Arana, T., Giavedoni, L., Hodara, V., White, L.J.*, et al.* (2011). Decreased dengue replication and an increased anti-viral humoral response with the use of combined Toll-like receptor 3 and 7/8 agonists in macaques. PLOS one *6*, e19323.

Scherbik, S.V., Paranjape, J.M., Stockman, B.M., Silverman, R.H., and Brinton, M.A. (2006). RNase L plays a role in the antiviral response to West Nile virus. J Virol *80*, 2987-2999.

Schliessmann, D.J. (1967). Aedes aegypti eradication program of the United States--progress report 1965. Am J Public Health N *57*, 460-465.

Schnettler, E., Sterken, M.G., Leung, J.Y., Metz, S.W., Geertsema, C., Goldbach, R.W., Vlak, J.M., Kohl, A., Khromykh, A.A., and Pijlman, G.P. (2012). Noncoding flavivirus RNA displays RNA interference suppressor activity in insect and Mammalian cells. J Virol *86*, 13486-13500.

Schoggins, J.W., Wilson, S.J., Panis, M., Murphy, M.Y., Jones, C.T., Bieniasz, P., and Rice, C.M. (2011). A diverse range of gene products are effectors of the type I interferon antiviral response. Nature *472*, 481-485.

Schreiber, M.J., Holmes, E.C., Ong, S.H., Soh, H.S., Liu, W., Tanner, L., Aw, P.P., Tan, H.C., Ng, L.C., Leo, Y.S.*, et al.* (2009). Genomic epidemiology of a dengue virus epidemic in urban Singapore. J Virol *83*, 4163-4173.

Schuessler, A., Funk, A., Lazear, H.M., Cooper, D.A., Torres, S., Daffis, S., Jha, B.K., Kumagai, Y., Takeuchi, O., Hertzog, P.*, et al.* (2012). West Nile virus noncoding subgenomic RNA contributes to viral evasion of the type I interferon-mediated antiviral response. J Virol *86*, 5708-5718.

Seth, R.B., Sun, L., Ea, C.K., and Chen, Z.J. (2005). Identification and characterization of MAVS, a mitochondrial antiviral signaling protein that activates NF-kappaB and IRF 3. Cell *122*, 669-682.

Shepard, D.S., Coudeville, L., Halasa, Y.A., Zambrano, B., and Dayan, G.H. (2011). Economic impact of dengue illness in the Americas. Am J Trop Med Hyg *84*, 200-207.

Shepard, D.S., Halasa, Y.A., Tyagi, B.K., Adhish, S.V., Nandan, D., Karthiga, K.S., Chellaswamy, V., Gaba, M., and Arora, N.K. (2014). Economic and disease burden of dengue Illness in India. Am J Trop Med Hyg *91*, 1235-1242.

Shepard, D.S., Undurraga, E.A., and Halasa, Y.A. (2013). Economic and disease burden of dengue in Southeast Asia. PLOS Negl Trop Dis *7*, e2055.

Shimodaira, H., and Hasegawa, M. (1999). Multiple comparisons of log-likelihoods with applications to phylogenetic inference. Mol Biol Evol *16*, 1114-1116.

Silva, P.A.G.C., Pereira, C.F., Dalebout, T.J., Spaan, W.J.M., and Bredenbeek, P.J. (2010). An RNA pseudoknot is required for production of yellow fever virus subgenomic RNA by the host nuclease XRN1. J Virol *84*, 11395-11406.

Simmons, C.P., Chau, T.N., Thuy, T.T., Tuan, N.M., Hoang, D.M., Thien, N.T., Lien le, B., Quy, N.T., Hieu, N.T., Hien, T.T*., et al.* (2007). Maternal antibody and viral factors in the pathogenesis of dengue virus in infants. J Infect Dis *196*, 416-424.

Simmons, C.P., Farrar, J.J., Nguyen v, V., and Wills, B. (2012). Dengue. New Engl J Med *366*, 1423-1432.

Sirigulpanit, W., Kinney, R.M., and Leardkamolkarn, V. (2007). Substitution or deletion mutations between nt 54 and 70 in the 5' non-coding region of dengue type 2 virus produce variable effects on virus viability. J Gen Virol *88*, 1748-1752.

Snow, G.E., Haaland, B., Ooi, E.E., and Gubler, D.J. (2014). Research on Dengue during World War II Revisited. Am J Trop Med Hyg *91*, 1203-1217.

St John, A.L., Abraham, S.N., and Gubler, D.J. (2013). Barriers to preclinical investigations of anti-dengue immunity and dengue pathogenesis. Nat Rev Microbiol *11*, 420-426.

Steel, A., Gubler, D.J., and Bennett, S.N. (2010). Natural attenuation of dengue virus type-2 after a series of island outbreaks: a retrospective phylogenetic study of events in the South Pacific three decades ago. Virology *405*, 505-512.

Stoddard, S.T., Wearing, H.J., Reiner, R.C., Jr., Morrison, A.C., Astete, H., Vilcarromero, S., Alvarez, C., Ramal-Asayag, C., Sihuincha, M., Rocha, C*., et al.* (2014). Long-term and seasonal dynamics of dengue in Iquitos, Peru. PLOS Negl Trop Dis *8*, e3003.

Streatfield, R., Bielby, G., and Sinclair, D. (1993). A primary dengue 2 epidemic with spontaneous haemorrhagic manifestations. Lancet *342*, 560-561.

Swofford, D.L. (1993). Paup - a computer program for phylogenetic inference using maximum parsimony. J Gen Physiol *102*, A9-A9.

Tamura, K., Stecher, G., Peterson, D., Filipski, A., and Kumar, S. (2013). MEGA6: Molecular Evolutionary Genetics Analysis version 6.0. Mol Biol Evol *30*, 2725-2729.

Tassaneetrithep, B., Burgess, T.H., Granelli-Piperno, A., Trumpfherer, C., Finke, J., Sun, W., Eller, M.A., Pattanapanyasat, K., Sarasombath, S., Birx, D.L.*, et al.* (2003). DC-SIGN (CD209) mediates dengue virus infection of human dendritic cells. J Exp Med *197*, 823-829.

Thein, S., Aung, M.M., Shwe, T.N., Aye, M., Zaw, A., Aye, K., Aye, K.M., and Aaskov, J. (1997). Risk factors in dengue shock syndrome. Am J Trop Med Hyg *56*, 566-572.

Thomas, L., Najioullah, F., Besnier, F., Valentino, R., Cesaire, J.R., and Cabie, A. (2014). Clinical presentation of dengue by serotype and year of epidemic in Martinique. Am J Trop Med Hyg *91*, 138-145.

Thomas, S.J. (2014). Preventing Dengue - Is the Possibility Now a Reality? New Engl J Med. Published online December 9, 2014. http://www.nejm.org/doi/pdf/10.1056/NEJMe1413146

Thomas, S.J., and Endy, T.P. (2011). Critical issues in dengue vaccine development. Curr Opin Infect Dis *24*, 442-450.

Tomashek, K.M., Gregory, C.J., Rivera Sanchez, A., Bartek, M.A., Garcia Rivera, E.J., Hunsperger, E., Munoz-Jordan, J.L., and Sun, W. (2012). Dengue deaths in Puerto Rico: lessons learned from the 2007 epidemic. PLOS Negl Trop Dis *6*, e1614.

Tsai, Y.T., Chang, S.Y., Lee, C.N., and Kao, C.L. (2009). Human TLR3 recognizes dengue virus and modulates viral replication in vitro. Cell Microbiol *11*, 604-615.

Umareddy, I., Tang, K.F., Vasudevan, S.G., Devi, S., Hibberd, M.L., and Gu, F. (2008). Dengue virus regulates type I interferon signalling in a strain-dependent manner in human cell lines. J Gen Virol *89*, 3052-3062.

Urosevic, N., van Maanen, M., Mansfield, J.P., Mackenzie, J.S., and Shellam, G.R. (1997). Molecular characterization of virus-specific RNA produced in the brains of flavivirus-susceptible and -resistant mice after challenge with Murray Valley encephalitis virus. J Gen Virol *78*, 23-29.

Valle, J.R.D., Chavez-Salinas, S., Medina, F., and del Angel, R.M. (2005). Heat shock protein 90 and heat shock protein 70 are components of dengue virus receptor complex in human cells. J Virol *79*, 4557-4567.

van der Schaar, H.M., Rust, M.J., Chen, C., van der Ende-Metselaar, H., Wilschut, J., Zhuang, X., and Smit, J.M. (2008). Dissecting the cell entry pathway of dengue virus by single-particle tracking in living cells. PLOS Pathog *4*, e1000244.

van der Schaar, H.M., Wilschut, J.C., and Smit, J.M. (2009). Role of antibodies in controlling dengue virus infection. Immunobiology *214*, 613-629.

Vasilakis, N., Cardosa, J., Diallo, M., Sall, A.A., Holmes, E.C., Hanley, K.A., Weaver, S.C., Mota, J., and Rico-Hesse, R. (2010). Sylvatic dengue viruses share the pathogenic potential of urban/endemic dengue viruses. J Virol *84*, 3726-3727.

Vasilakis, N., Tesh, R.B., and Weaver, S.C. (2008). Sylvatic dengue virus type 2 activity in humans, Nigeria, 1966. Emerg Infect Dis *14*, 502-504.

Vaughn, D.W., Green, S., Kalayanarooj, S., Innis, B.L., Nimmannitya, S., Suntayakorn, S., Endy, T.P., Raengsakulrach, B., Rothman, A.L., Ennis, F.A., *et al.* (2000). Dengue viremia titer, antibody response pattern, and virus serotype correlate with disease severity. J Infect Dis *181*, 2-9.

Vaughn, D.W., Green, S., Kalayanarooj, S., Innis, B.L., Nimmannitya, S., Suntayakorn, S., Rothman, A.L., Ennis, F.A., and Nisalak, A. (1997). Dengue in the early febrile phase: viremia and antibody responses. J Infect Dis *176*, 322-330.

Velazquez, L., Fellous, M., Stark, G.R., and Pellegrini, S. (1992). A protein tyrosine kinase in the interferon-alpha/beta signaling pathway. Cell *70*, 313-322.

Villar, L., Dayan, G.H., Arredondo-Garcia, J.L., Rivera, D.M., Cunha, R., Deseda, C., Reynales, H., Costa, M.S., Morales-Ramirez, J.O., Carrasquilla, G., *et al.* (2014). Efficacy of a tetravalent dengue vaccine in children in Latin America. New Engl J Med. Published online November 3, 2014. http://www.nejm.org/doi/full/10.1056/NEJMoa1411037

Vu, T.T., Holmes, E.C., Duong, V., Nguyen, T.Q., Tran, T.H., Quail, M., Churcher, C., Parkhill, J., Cardosa, J., Farrar, J., *et al.* (2010). Emergence of the Asian 1 genotype of dengue virus serotype 2 in viet nam: in vivo fitness advantage and lineage replacement in South-East Asia. PLOS Negl Trop Dis *4*, e757.

Wang, W.K., Chao, D.Y., Kao, C.L., Wu, H.C., Liu, Y.C., Li, C.M., Lin, S.C., Ho, S.T., Huang, J.H., and King, C.C. (2003). High levels of plasma dengue viral load during defervescence in patients with dengue hemorrhagic fever: implications for pathogenesis. Virology *305*, 330-338.

Ward, A.M., Bidet, K., Yinglin, A., Ler, S.G., Hogue, K., Blackstock, W., Gunaratne, J., and Garcia-Blanco, M.A. (2011). Quantitative mass spectrometry of DENV-2 RNA-interacting proteins reveals that the DEAD-box RNA helicase DDX6 binds the DB1 and DB2 3' UTR structures. RNA Biol *8*, 1173-1186.

Ward, A.M., Gunaratne, J., and Garcia-Blanco, M.A. (2014). Identification of dengue RNA binding proteins using RNA chromatography and quantitative mass spectrometry. Methods Mol Biol *1138*, 253-270.

Watts, D.M., Porter, K.R., Putvatana, P., Vasquez, B., Calampa, C., Hayes, C.G., and Halstead, S.B. (1999). Failure of secondary infection with American genotype dengue 2 to cause dengue haemorrhagic fever. Lancet *354*, 1431-1434.

Weaver, S.C., and Vasilakis, N. (2009). Molecular evolution of dengue viruses: contributions of phylogenetics to understanding the history and epidemiology of the preeminent arboviral disease. Infect Genet Evol *9*, 523-540.

Webster, D.P., Farrar, J., and Rowland-Jones, S. (2009). Progress towards a dengue vaccine. Lancet Infect Dis *9*, 678-687.

Whitehead, S.S., Blaney, J.E., Durbin, A.P., and Murphy, B.R. (2007). Prospects for a dengue virus vaccine. Nat Rev Microbiol *5*, 518-528.

Whitehead, S.S., Hanley, K.A., Blaney, J.E., Gilmore, L.E., Elkins, W.R., and Murphy, B.R. (2003). Substitution of the structural genes of dengue virus type 4 with those of type 2 results in chimeric vaccine candidates which are attenuated for mosquitoes, mice, and rhesus monkeys. Vaccine *21*, 4307-4316.

WHO 2014. Dengue and Severe dengue. World Health Organization, Geneva. http://www.who.int/mediacentre/factsheets/fs117/en/

WHO 2007. Global Alert and Response (GAR) - Impact of Dengue. World Health Organization, Geneva. http://www.who.int/csr/disease/dengue/impact/en/

WHO 2009. Dengue: Guidelines for diagnosis, treatment, prevention and control. World Health Organization, Geneva. http://whqlibdoc.who.int/publications/2009/9789241547871_eng.pdf?ua=1

WHO 2012. Handbook for clinical management of dengue. World Health Organization, Geneva. http://apps.who.int/iris/bitstream/10665/76887/1/9789241504713_eng.pdf

Wills, B.A., Nguyen, M.D., Ha, T.L., Dong, T.H., Tran, T.N., Le, T.T., Tran, V.D., Nguyen, T.H., Nguyen, V.C., Stepniewska, K.*, et al.* (2005). Comparison of three fluid solutions for resuscitation in dengue shock syndrome. New Engl J Med *353*, 877-889.

Wilson, J.R., de Sessions, P.F., Leon, M.A., and Scholle, F. (2008). West Nile virus nonstructural protein 1 inhibits TLR3 signal transduction. J Virol *82*, 8262-8271.

Wolfe, N.D., Kilbourn, A.M., Karesh, W.B., Rahman, H.A., Bosi, E.J., Cropp, B.C., Andau, M., Spielman, A., and Gubler, D.J. (2001). Sylvatic transmission of arboviruses among Bornean orangutans. Am J Trop Med Hyg *64*, 310-316.

Wright, W.F., and Pritt, B.S. (2012). Update: The diagnosis and management of dengue virus infection in North America. Diagn Microbiol Infect Dis *73*, 215-220.

Yauch, L.E., Zellweger, R.M., Kotturi, M.F., Qutubuddin, A., Sidney, J., Peters, B., Prestwood, T.R., Sette, A., and Shresta, S. (2009). A protective role for dengue virus-specific CD8+ T cells. J Immunol *182*, 4865-4873.

Ye, J., Zhu, B., Fu, Z.F., Chen, H., and Cao, S. (2013). Immune evasion strategies of flaviviruses. Vaccine *31*, 461-471.

Yew, Y.W., Ye, T., Ang, L.W., Ng, L.C., Yap, G., James, L., Chew, S.K., and Goh, K.T. (2009). Seroepidemiology of dengue virus infection among adults in Singapore. Ann Acad Med Singap *38*, 667-675.
Yu, C.Y., Chang, T.H., Liang, J.J., Chiang, R.L., Lee, Y.L., Liao, C.L., and Lin, Y.L. (2012). Dengue virus targets the adaptor protein MITA to subvert host innate immunity. PLOS Pathog *8*, e1002780.

Zhang, Y., Zhang, W., Ogata, S., Clements, D., Strauss, J.H., Baker, T.S., Kuhn, R.J., and Rossmann, M.G. (2004). Conformational changes of the flavivirus E glycoprotein. Structure *12*, 1607-1618.

Zompi, S., Montoya, M., Pohl, M.O., Balmaseda, A., and Harris, E. (2012). Dominant cross-reactive B cell response during secondary acute dengue virus infection in humans. PLOS Negl Trop Dis *6*, e1568.

APPENDIX

1. Cell culture medium

1.1 Fetal bovine serum (FBS)

Heat-inactivate at 56°C for 30mins

Aliquot into 50ml Falcon tubes.

Store at -20°C till further use.

1.2 C6/36 growth medium, 500ml

5ml of Penicillin/Streptomycin (100x liquid, Gibco)

40ml FBS

Top up to 500ml with Leibovitz's L-15 medium (Gibco) and filter-sterilize

1.3 C6/36 maintenance medium, 500ml

5ml of Penicillin/Streptomycin (100X liquid, Gibco)

10ml FBS

Top up to 500ml with Leibovitz's L-15 medium (Gibco) and filter-sterilize

1.4 HuH-7 growth medium, 500ml

Add 40ml FBS.

Top up to 500ml with Dulbecco's modified eagle's medium, DMEM (High glucose, Sodium pyruvate) (Gibco) and filter-sterilize

1.5 HuH-7 growth medium, 500ml

Add 10ml FBS.

Top up to 500ml with Dulbecco's modified eagle's medium, DMEM (High glucose, Sodium pyruvate) (Gibco) and filter-sterilize

1.6 BHK-21 growth medium, 500ml

5ml of L-glutamine (200nM, Gibco)

5ml of sodium pyruvate (100mM, Gibco)

5ml of Penicillin/Streptomycin (100X liquid, Gibco)

50ml FBS

Top up to 500ml with RPMI-1640 (Gibco) and filter-sterilize

1.7 BHK-21 maintenance medium, 500ml

5ml of L-glutamine (200nM, Gibco)

5ml of sodium pyruvate (100mM, Gibco)

5ml of Penicillin/Streptomycin (100X liquid, Gibco)

10ml FBS

Top up to 500ml with RPMI-1640 (Gibco) and filter-sterilize

1.8 Vero growth medium, 500ml

5ml of sodium pyruvate (100mM, Gibco)

5ml of Non-essential amino acids (10mM, Gibco)

50ml FBS

Top up to 500ml with Medium-199 (Gibco) and filter-sterilize

1.5 Vero maintenance medium, 500ml

5ml of sodium pyruvate (100mM, Gibco)

5ml of Non-essential amino acids (10mM, Gibco)

10ml FBS

Top up to 500ml with Medium-199 (Gibco) and filter-sterilize

2. Plaque assay

2.1 0.8% methycellulose overlay

(A) 2 x RPMI

Dissolve RPMI-1640 powder (Gibco) in 500ml deionized water

10ml sodium bicarbonate (7.5%, Gibco)

5ml sodium pyruvate (100mM, Gibco)

20ml FBS

Filter-sterilize

(B) 1.6% carboxy-methyl cellulose (CMC)

Dissolve 8g of CMC (Calbiochem) in deionized water

Autoclave-sterilize at 121°C, 20min

Add 1 part of 2X RPMI (A) to 1 part of 1.6% CMC (B) in 50ml Falcon tubes.

Shake vigorously to mix. Store at 4°C.

2.2 0.5% crystal violet in 25% formaldehyde

5g crystal violet (Sigma)

676ml 37% Formaldehyde

Top up to 1L with 1XPBS

3. Northern Hybridization

3.1 10x MOPS buffer

200 mM MOPS (Sigma)

10mM sodium acetate

10mM EDTA

Ensure that the pH is 7.0 and store in a dark bottle.

3.2 1% formaldehyde-agarose gel

(A) Solution A

1.5g agarose

100ml DEPC-water

Microwave until agarose is completely dissolved and incubate in a 55°C waterbath for 15min.

(B) Solution B

15ml 10x MOPS buffer

24.3ml formaldehyde

10.7ml DEPC-water

Mix (B) with (A) and pour the mixture into a gel cast.

3.3 Formamide buffer

10ml formamide

3.5ml formaldehyde

2ml 10x MOPS buffer

3.4 Electrophoresis buffer

100ml 10x MOPS buffer

80ml formaldehyde

820ml DEPC-water

4. Western blot

4.1 Lysis buffer for western blot

4.383g sodium chloride

5ml Nonidet-P40 buffer

3.03g Tris

Dissolve in 500ml with milli-Q water

Adjust to pH 8.0

Protease and phosphastase inhibitors (Sigma) added fresh at 1:100

4.2 Lysis buffer for co-immunoprecipitation

4.383g sodium chloride

0.5ml Nonidet-P40 buffer

3.03g Tris

Dissolve in 500ml with milli-Q water

Adjust to pH 8.0

Protease and phosphatase inhibitors (Sigma) added fresh at 1:100

4.3 Immunoprecipitation buffer

1.51g Tris

4.383g sodium chloride

Dissolve in 500ml with milli-Q water

Adjust to pH 7.2

4.4 10x SDS running buffer

288g glycine

60.4g Tris base

20g SDS

Dissolve in 2 liters with de-ionized water

To use, dilute 1 in 10 to use at 1x SDS running buffer

4.5 Transfer buffer

3g Tris

14.4g glycine

200ml methanol

Top up to 1 liter with de-ionized water

5. SILAC

5.1 LIGHT media, K0R0

500µl K0 (Sigma, L8662)

500µL R0 (Sigma, A8094)

50ml dialyzed FBS (Thermo, Research Instruments, Singapore)

5ml of Penicillin/Streptomycin (100x liquid, Gibco)

SILAC-DMEM (Thermo, Research Instruments, Singapore)

Filter sterilize before use

5.2 MEDIUM media, K4R6

500µl K4 (Cambridge Isotope Laboratories, DLM-2640)

500µL R6 (Cambridge Isotope Laboratories, CLM-2247)

50ml dialyzed FBS (Thermo, Research Instruments, Singapore)

5ml of Penicillin/Streptomycin (100x liquid, Gibco)

SILAC-DMEM (Thermo, Research Instruments, Singapore)

Filter sterilize before use

5.3 HEAVY media, K8R10

500µl K8 (Cambridge Isotope Laboratories, CNLM-291)

500µL R10 (Cambridge Isotope Laboratories, CNLM-539)

50ml dialyzed FBS (Thermo, Research Instruments, Singapore)

5ml of Penicillin/Streptomycin (100x liquid, Gibco)

SILAC-DMEM (Thermo, Research Instruments, Singapore)

Filter sterilize before use

Mass spectrometry results. List of RNA binding proteins identified after pull-down with DENV-2 3'UTR (SL-II to SL-IV section) as compared to control RNA. Gene names are indicated. L2, L4 and L6 are normalized readings from three separate experiments. Annotations as depicted: M/L (PR-1 3'UTR divided by control), H/L (PR-2B 3'UTR divided by control). H/M (PR 2B 3'UTR divided by PR-1 3'UTR)

Gene names	Ratio M/L L2	Ratio M/L L4	Ratio M/L L6	Log (M/L) mean	Pvalue (ttest)	Ratio H/L L2	Ratio H/L L4	Ratio H/L L6	Log (H/L) mean	Pvalue (ttest)	Ratio H/M L2	Ratio H/M L4	Ratio H/M L6	Log (H/M) mean	Pvalue (ttest)
CAPRIN1	0.765	0.766	0.764	-0.387	0.000	1.396	1.229	0.636	0.041	0.917	1.154	1.093	1.004	0.113	0.193
PRKRA	0.802	0.795	0.799	-0.325	0.000	1.017	0.950	1.054	0.009	0.860	1.239	1.161	1.236	0.277	0.012
SHMT2	1.145	1.141	1.139	0.191	0.000	1.408	1.497	1.687	0.610	0.015	1.287	1.292	1.333	0.383	0.002
RPS11	0.896	0.897	0.892	-0.159	0.000	0.950	0.950	0.983	-0.057	0.072	1.060	0.996	1.021	0.036	0.303
HARS	1.287	1.303	1.287	0.370	0.000	1.234	1.246	1.298	0.333	0.004	0.980	0.893	0.990	-0.069	0.285
PDLIM1	1.503	1.473	1.503	0.578	0.000	1.870	1.656	1.847	0.839	0.004	1.108	1.120	1.141	0.167	0.006
RARS	1.108	1.100	1.104	0.143	0.000	1.437	1.396	1.467	0.519	0.002	1.228	1.274	1.302	0.342	0.005
AP3S1	0.758	0.762	0.747	-0.404	0.000	0.765	0.753	0.787	-0.381	0.002	0.845	0.927	0.897	-0.170	0.050
RPL28	0.897	0.893	0.900	-0.157	0.000	1.119	0.965	1.081	0.074	0.370	1.249	1.066	1.101	0.184	0.119

RBMS1	2.404	2.505	2.345	1.273	0.000	0.947	1.043	0.974	-0.018	0.702	0.288	0.414	0.390	-1.475	0.012
OTUD6B	0.832	0.821	0.832	-0.271	0.001	0.992	0.837	0.862	-0.160	0.168	1.019	1.073	1.017	0.051	0.179
PRMT1	1.772	1.859	1.794	0.854	0.001	2.011	2.159	2.023	1.045	0.001	1.039	1.118	1.069	0.104	0.079
RPL3	0.902	0.906	0.898	-0.149	0.001	1.184	1.208	1.472	0.358	0.070	1.371	1.385	1.379	0.463	0.000
RDX	0.707	0.684	0.700	-0.521	0.001	0.648	0.585	0.651	-0.674	0.006	0.892	0.888	0.932	-0.146	0.023
GLDC	1.279	1.306	1.277	0.364	0.001	1.510	1.375	1.468	0.536	0.006	1.082	1.067	1.148	0.136	0.053
ESYT1	1.277	1.294	1.310	0.371	0.001	0.785	1.221	0.734	-0.169	0.540	0.578	0.670	0.519	-0.772	0.019
ABCE1	0.943	0.946	0.941	-0.084	0.001	1.223	1.201	1.122	0.240	0.024	1.297	1.259	1.144	0.301	0.031
EIF3E	0.924	0.925	0.931	-0.110	0.001	0.856	0.904	0.892	-0.178	0.018	0.930	0.948	0.939	-0.091	0.007
UFM1	0.732	0.755	0.742	-0.429	0.001	0.439	0.412	0.358	-1.317	0.004	0.507	0.494	0.484	-1.015	0.000
DDX6	2.711	2.453	2.608	1.372	0.001	2.394	2.398	2.642	1.308	0.001	0.913	0.917	0.990	-0.090	0.139
RPS23	0.901	0.910	0.908	-0.141	0.001	0.883	0.894	0.903	-0.162	0.003	0.999	0.976	0.917	-0.054	0.282
HDLBP	0.746	0.758	0.734	-0.423	0.001	0.753	0.712	0.678	-0.487	0.008	0.917	0.970	0.953	-0.080	0.079

HSPA5	0.942	0.943	0.948	-0.083	0.001	0.706	0.712	0.663	-0.529	0.004	0.701	0.792	0.717	-0.442	0.015
WARS	1.491	1.560	1.493	0.599	0.001	1.264	1.173	1.290	0.312	0.017	0.852	0.763	0.869	-0.275	0.043
RPL6	0.841	0.852	0.834	-0.247	0.001	1.280	1.089	1.220	0.255	0.066	1.638	1.239	1.429	0.512	0.048
YTHDF1	0.842	0.859	0.847	-0.236	0.001	0.822	0.899	0.879	-0.208	0.033	1.015	0.991	0.958	-0.018	0.536
MYO1E	1.269	1.306	1.274	0.359	0.001	1.532	1.439	1.707	0.637	0.013	1.427	1.695	1.387	0.582	0.023
RPS4X	0.877	0.875	0.862	-0.199	0.001	1.157	1.132	1.069	0.162	0.041	1.332	1.221	1.180	0.313	0.026
HNRPDL	1.568	1.564	1.491	0.624	0.001	1.363	1.582	1.600	0.596	0.015	0.961	1.034	1.043	0.017	0.691
RPL18	0.861	0.870	0.877	-0.202	0.001	1.177	1.086	1.045	0.139	0.111	1.395	1.214	1.159	0.324	0.056
SNRPA	1.147	1.166	1.168	0.214	0.002	1.620	1.982	1.966	0.886	0.011	1.333	1.446	1.594	0.540	0.019
DNM2	1.141	1.122	1.127	0.176	0.002	0.615	0.523	0.520	-0.860	0.008	0.508	0.508	0.540	-0.948	0.001
RBX1	1.436	1.390	1.459	0.514	0.002	0.803	0.838	0.851	-0.268	0.009	0.582	0.608	0.560	-0.778	0.002
HNRNPU	1.234	1.200	1.222	0.285	0.002	1.002	1.146	1.196	0.153	0.186	0.890	0.920	0.849	-0.175	0.035
S100P	1.489	1.529	1.445	0.573	0.002	0.804	1.011	0.979	-0.110	0.399	0.510	0.631	0.532	-0.848	0.012

IST1	1.127	1.132	1.147	0.183	0.002	1.103	0.962	0.830	-0.062	0.655	1.053	0.943	0.862	-0.075	0.462
HMGB1	1.251	1.294	1.284	0.352	0.002	1.897	1.618	1.759	0.811	0.007	1.382	1.360	1.217	0.398	0.020
SSBP1	1.701	1.628	1.586	0.712	0.002	0.819	0.930	0.961	-0.151	0.165	0.463	0.545	0.532	-0.966	0.006
ADRBK1	0.815	0.812	0.792	-0.310	0.002	0.944	0.893	0.914	-0.125	0.032	1.121	1.030	1.105	0.117	0.089
SND1	0.777	0.770	0.747	-0.387	0.002	1.030	0.965	0.982	-0.012	0.712	1.258	1.252	1.270	0.333	0.000
VASP	0.512	0.520	0.561	-0.914	0.002	0.166	0.272	0.174	-2.332	0.009	0.236	0.329	0.276	-1.849	0.006
NUDT21	0.731	0.742	0.764	-0.424	0.002	1.289	1.209	1.206	0.303	0.010	1.610	1.580	1.412	0.615	0.009
ARSB	1.338	1.400	1.351	0.446	0.002	1.033	1.011	1.008	0.025	0.166	0.732	0.742	0.704	-0.462	0.003
LRRC47	0.813	0.830	0.803	-0.295	0.002	0.517	0.458	0.504	-1.023	0.003	0.617	0.609	0.652	-0.677	0.002
PTMS	0.789	0.766	0.794	-0.353	0.002	0.139	0.236	0.189	-2.444	0.008	0.184	0.273	0.194	-2.228	0.006
GSDMD	1.496	1.530	1.602	0.625	0.002	1.993	2.207	2.218	1.095	0.002	1.270	1.329	1.304	0.379	0.002
MAGEB1	0.810	0.806	0.831	-0.294	0.002	0.950	0.961	0.774	-0.167	0.242	1.241	1.445	1.066	0.312	0.133
DNAJB1	0.818	0.836	0.842	-0.265	0.002	0.972	1.039	1.045	0.026	0.514	1.166	1.149	1.155	0.210	0.001

UBL5	0.928	0.938	0.929	-0.103	0.002	0.899	0.869	0.903	-0.168	0.011	0.883	0.937	0.921	-0.131	0.036
SRSF3	0.777	0.781	0.750	-0.379	0.002	0.715	0.728	0.732	-0.464	0.000	0.840	0.895	0.876	-0.201	0.018
KARS	1.229	1.277	1.251	0.324	0.002	1.368	1.314	1.421	0.451	0.005	1.026	1.093	1.059	0.083	0.089
SERPINH 1	1.382	1.316	1.334	0.426	0.002	1.512	1.555	1.325	0.547	0.017	0.996	1.006	0.964	-0.017	0.466
MAP1A	0.825	0.819	0.797	-0.298	0.002	0.507	0.527	0.441	-1.029	0.006	0.634	0.681	0.706	-0.571	0.006
YTHDF3	0.869	0.867	0.886	-0.194	0.002	0.861	0.937	0.724	-0.258	0.142	0.932	1.087	0.792	-0.106	0.506
PRMT3	1.442	1.512	1.543	0.583	0.002	1.016	1.421	0.971	0.163	0.447	0.980	0.912	0.895	-0.108	0.113
FARSA	1.150	1.126	1.130	0.183	0.002	1.240	1.151	1.219	0.266	0.015	1.116	0.981	1.029	0.058	0.400
SPTBN2	1.358	1.298	1.357	0.419	0.003	1.626	1.467	1.494	0.611	0.006	1.428	1.233	1.144	0.337	0.070
GSTK1	1.171	1.160	1.193	0.232	0.003	0.947	0.920	0.966	-0.083	0.056	0.739	0.786	0.773	-0.385	0.005
RBMS2	3.069	3.282	2.701	1.589	0.003	1.085	1.142	1.147	0.169	0.022	0.251	0.336	0.358	-1.684	0.009
EIF3K	0.945	0.954	0.947	-0.076	0.003	0.760	0.875	0.847	-0.276	0.046	0.731	0.867	0.833	-0.308	0.054

CCT6A	1.067	1.073	1.081	0.102	0.003	1.293	1.367	1.344	0.416	0.003	1.211	1.218	1.185	0.269	0.002
TPT1	0.677	0.625	0.647	-0.622	0.003	0.576	0.587	0.576	-0.787	0.000	0.810	1.000	0.844	-0.183	0.188
HNRNPR; HNRPR	0.874	0.883	0.895	-0.178	0.003	0.883	0.804	1.007	-0.161	0.229	0.909	0.952	1.251	0.038	0.814
HSD17B4	0.650	0.672	0.701	-0.570	0.003	0.772	0.528	0.787	-0.547	0.101	0.931	0.781	0.752	-0.290	0.093
YTHDF2	0.841	0.830	0.858	-0.246	0.003	0.786	0.968	0.775	-0.254	0.134	0.960	1.138	0.981	0.033	0.710
EEF1A1;EEF1A1P5	0.896	0.910	0.912	-0.142	0.003	0.880	0.877	0.998	-0.126	0.176	1.011	0.988	1.123	0.055	0.433
A1CF	0.806	0.810	0.836	-0.291	0.003	0.931	0.996	1.032	-0.021	0.673	1.151	1.155	1.158	0.207	0.000
SNX5	1.485	1.578	1.620	0.641	0.003	1.809	1.943	1.992	0.936	0.002	1.085	1.111	1.180	0.169	0.042
GLT25D1	1.254	1.297	1.318	0.367	0.003	2.020	1.810	1.731	0.887	0.006	1.523	1.398	1.318	0.496	0.015
EPB41L2	1.232	1.189	1.228	0.282	0.003	1.337	1.386	1.346	0.439	0.001	1.009	1.019	0.942	-0.016	0.699
NHP2L1	0.699	0.746	0.730	-0.465	0.003	1.196	1.021	1.270	0.211	0.154	1.441	1.236	1.550	0.488	0.037

LDHA	1.155	1.165	1.191	0.226	0.003	0.925	1.003	1.011	-0.031	0.533	0.802	0.829	0.799	-0.305	0.003
RPL21	0.875	0.894	0.894	-0.172	0.004	1.044	0.961	1.000	0.002	0.964	1.195	1.083	1.015	0.131	0.195
IGF2BP2	0.913	0.924	0.929	-0.117	0.004	0.821	0.831	0.771	-0.309	0.012	0.794	0.837	0.800	-0.304	0.006
SYNCRIP	0.799	0.830	0.827	-0.289	0.004	0.856	0.831	0.959	-0.184	0.100	1.102	1.041	1.101	0.112	0.054
LMO7	1.458	1.520	1.404	0.546	0.004	1.787	1.701	1.915	0.847	0.003	1.143	1.282	1.252	0.292	0.029
AP2S1	1.163	1.203	1.175	0.239	0.004	1.388	1.303	1.811	0.570	0.059	1.134	0.977	1.246	0.155	0.270
MCM3	1.121	1.096	1.108	0.148	0.004	1.422	1.465	0.662	0.155	0.720	1.071	1.237	0.570	-0.135	0.732
EEF1G	1.223	1.229	1.276	0.313	0.004	1.065	1.344	0.977	0.161	0.362	0.791	0.948	0.772	-0.263	0.106
EEF1E1	1.145	1.166	1.183	0.220	0.004	1.168	1.250	1.308	0.311	0.023	0.934	0.984	1.078	-0.005	0.946
RPL32	0.888	0.862	0.873	-0.194	0.004	1.220	1.185	1.245	0.283	0.005	1.303	1.277	1.202	0.333	0.011
BRK1	1.162	1.201	1.167	0.234	0.004	0.984	0.981	1.047	0.005	0.884	0.893	0.882	0.810	-0.216	0.040
AP3D1	0.757	0.790	0.797	-0.356	0.004	0.878	0.785	1.122	-0.124	0.501	1.055	0.974	1.234	0.114	0.372
STAT2	0.773	0.815	0.793	-0.334	0.004	0.898	0.994	0.855	-0.130	0.180	1.133	1.205	1.065	0.180	0.073

ARPC1A	1.425	1.557	1.534	0.589	0.004	1.383	1.608	1.326	0.520	0.025	0.939	0.944	0.933	-0.091	0.003
PPP1R14A	0.567	0.583	0.512	-0.854	0.004	0.179	0.168	0.184	-2.496	0.000	0.229	0.266	0.343	-1.861	0.008
HDAC6	0.748	0.784	0.736	-0.404	0.005	0.415	0.504	0.349	-1.259	0.014	0.670	0.743	0.400	-0.776	0.106
BCCIP	1.272	1.257	1.210	0.318	0.005	1.249	1.091	1.186	0.231	0.056	0.781	1.061	0.929	-0.126	0.429
RPL19	0.876	0.900	0.894	-0.168	0.005	1.453	0.894	1.145	0.191	0.444	1.627	1.113	1.279	0.404	0.128
HIST1H3A	0.662	0.593	0.610	-0.687	0.005	0.897	0.815	1.144	-0.086	0.614	1.178	1.284	1.850	0.495	0.132
PSMA3	1.161	1.192	1.150	0.223	0.005	0.924	1.019	1.059	-0.001	0.983	0.735	0.811	0.821	-0.344	0.021
GLUL	0.729	0.740	0.687	-0.477	0.005	0.905	0.901	0.841	-0.182	0.034	1.271	1.206	1.169	0.280	0.015
RPL18A	0.873	0.854	0.883	-0.201	0.005	1.172	1.090	1.039	0.136	0.114	1.241	1.185	1.167	0.260	0.010
DHX9	0.890	0.871	0.896	-0.175	0.005	0.999	1.012	0.993	0.002	0.842	1.065	1.158	1.118	0.154	0.048
EIF5	0.989	0.986	0.986	-0.019	0.005	0.660	0.705	0.809	-0.470	0.032	0.707	0.755	0.891	-0.358	0.069
HNRNPM	1.283	1.216	1.270	0.329	0.005	1.803	1.941	2.221	0.986	0.008	1.264	1.398	1.547	0.483	0.029

EIF4B	0.624	0.560	0.625	-0.732	0.005	0.156	0.063	0.125	-3.226	0.015	0.152	0.077	0.125	-3.135	0.008
MCM6	1.601	1.710	1.830	0.775	0.005	1.115	1.229	1.838	0.444	0.182	0.709	0.632	0.640	-0.601	0.008
EPB41L5	1.642	1.652	1.489	0.672	0.005	1.399	1.617	1.523	0.595	0.010	0.844	1.154	1.080	0.025	0.874
TMEM189 ;UBE2V2; UBE2V1	1.141	1.156	1.119	0.187	0.005	0.897	1.074	0.986	-0.025	0.773	0.884	1.209	1.071	0.065	0.672
LSM12	1.722	2.005	1.947	0.916	0.005	0.621	0.760	0.757	-0.495	0.036	0.350	0.455	0.342	-1.400	0.009
SWAP70	0.882	0.864	0.850	-0.209	0.005	0.957	0.972	1.131	0.024	0.780	1.069	1.031	1.621	0.279	0.314
TUFM	0.699	0.740	0.678	-0.503	0.005	0.507	0.526	0.518	-0.952	0.000	0.718	0.761	0.735	-0.439	0.003
PSMB1	1.126	1.165	1.154	0.199	0.005	0.881	1.166	1.021	0.023	0.863	0.776	0.996	0.755	-0.259	0.179
TUBB4B	1.089	1.079	1.103	0.125	0.005	1.140	1.136	1.054	0.150	0.055	0.935	0.989	0.933	-0.071	0.122
RNASET2	1.312	1.422	1.385	0.456	0.006	1.159	1.117	1.200	0.212	0.019	0.771	0.771	0.749	-0.389	0.001
GATM	1.188	1.217	1.163	0.250	0.006	1.133	1.076	1.063	0.125	0.047	0.898	0.924	0.849	-0.169	0.043

AKR1C1;AKR1C2	1.417	1.416	1.317	0.467	0.006	1.388	1.515	1.239	0.461	0.032	0.994	0.987	0.911	-0.054	0.310
AHNAK	0.545	0.515	0.458	-0.986	0.006	0.143	0.088	0.193	-2.897	0.013	0.224	0.167	0.350	-2.085	0.022
POLR1C	1.336	1.426	1.453	0.490	0.006	1.508	1.708	1.927	0.771	0.017	1.180	1.392	1.200	0.326	0.050
MSN	1.215	1.208	1.269	0.299	0.006	0.843	0.840	0.877	-0.229	0.008	0.636	0.660	0.690	-0.596	0.003
NUMB;NUMBL	1.177	1.204	1.153	0.236	0.006	1.119	1.066	1.295	0.209	0.131	1.012	1.145	0.965	0.054	0.540
EFTUD2	0.887	0.910	0.888	-0.160	0.006	1.488	1.607	1.487	0.610	0.004	1.608	1.755	1.632	0.735	0.003
SPTAN1	1.326	1.362	1.440	0.460	0.006	1.699	1.773	1.494	0.723	0.010	1.219	1.375	1.073	0.282	0.112
KIAA1033	0.745	0.777	0.719	-0.422	0.006	0.904	0.957	0.895	-0.123	0.056	1.236	1.326	1.182	0.318	0.022
PFKM	1.376	1.439	1.321	0.462	0.006	2.147	1.957	2.201	1.070	0.002	1.504	1.385	1.566	0.569	0.008
ADAT3	1.573	1.439	1.605	0.620	0.006	1.297	1.709	2.257	0.774	0.079	0.815	1.287	1.256	0.132	0.600
PROSC	0.789	0.756	0.732	-0.398	0.006	0.712	0.767	0.733	-0.440	0.005	0.914	0.956	1.007	-0.062	0.264

EIF2AK2	0.728	0.749	0.786	-0.407	0.006	0.682	0.741	0.830	-0.418	0.037	0.906	0.928	1.059	-0.056	0.510
EHHADH	0.812	0.761	0.775	-0.354	0.006	1.004	0.896	0.918	-0.092	0.204	1.171	1.241	1.107	0.229	0.041
CORO1C	1.400	1.534	1.550	0.578	0.006	1.168	1.333	1.282	0.333	0.028	0.889	0.800	0.852	-0.241	0.032
SUPT4H1	1.394	1.345	1.284	0.423	0.007	1.095	1.325	1.257	0.289	0.072	0.781	0.912	0.824	-0.256	0.060
TUBB4A	1.156	1.190	1.142	0.217	0.007	1.235	0.929	1.139	0.129	0.402	0.951	0.722	1.023	-0.170	0.382
CLIC1	0.894	0.894	0.917	-0.149	0.007	2.177	2.553	3.084	1.366	0.011	2.615	2.844	2.829	1.465	0.001
ASCC3	0.568	0.530	0.471	-0.939	0.007	0.509	0.299	0.311	-1.468	0.027	1.022	0.598	0.671	-0.429	0.210
NCL	1.148	1.145	1.110	0.181	0.007	1.040	1.168	1.038	0.112	0.187	0.824	0.905	0.851	-0.219	0.031
NARS	0.889	0.881	0.856	-0.193	0.007	0.856	0.830	0.864	-0.234	0.005	0.960	0.937	1.003	-0.049	0.227
RPS15A	0.925	0.901	0.905	-0.135	0.007	0.959	1.017	1.008	-0.008	0.780	1.028	1.078	1.036	0.066	0.090
TRA2B	0.804	0.745	0.778	-0.367	0.007	1.788	1.676	1.887	0.833	0.003	1.977	2.136	2.032	1.034	0.001
SRGAP1; SRGAP2	1.528	1.366	1.464	0.537	0.008	1.832	1.477	1.798	0.761	0.017	0.715	1.052	0.973	-0.150	0.471

ACACA	1.688	1.534	1.479	0.646	0.008	1.408	1.139	1.187	0.310	0.080	0.929	0.748	0.851	-0.252	0.108
FOCAD	0.836	0.793	0.835	-0.284	0.008	0.695	0.605	0.826	-0.508	0.059	0.914	0.844	1.067	-0.094	0.445
RPS27	0.879	0.872	0.843	-0.210	0.008	1.028	0.973	0.868	-0.068	0.444	1.132	0.996	0.981	0.049	0.535
IGF2R	1.162	1.128	1.119	0.184	0.008	0.926	0.823	0.759	-0.263	0.087	0.816	0.826	0.688	-0.369	0.049
TARS	1.260	1.184	1.227	0.291	0.008	1.187	1.208	1.297	0.298	0.017	0.904	1.028	1.036	-0.019	0.798
TPRKB	1.126	1.164	1.175	0.208	0.008	0.949	1.038	1.123	0.048	0.562	0.812	0.773	0.879	-0.286	0.034
FERMT2	1.134	1.157	1.188	0.213	0.008	1.233	1.331	1.472	0.424	0.029	1.169	1.225	1.285	0.294	0.018
RPS6	0.884	0.883	0.851	-0.197	0.008	0.999	1.018	1.046	0.030	0.255	1.121	1.127	1.169	0.188	0.010
EIF1	0.861	0.814	0.830	-0.261	0.008	0.813	0.803	0.774	-0.328	0.004	0.830	0.917	0.912	-0.176	0.063
RPS27A;UBC;UBB;UBA52	0.872	0.851	0.828	-0.234	0.008	0.937	0.865	0.645	-0.312	0.197	0.974	1.010	0.903	-0.057	0.354
RPL15	0.869	0.880	0.841	-0.212	0.008	1.235	1.123	1.093	0.200	0.065	1.412	1.190	1.188	0.332	0.057

MAPK1	1.203	1.278	1.283	0.327	0.008	1.630	1.733	1.810	0.785	0.003	1.348	1.274	1.367	0.410	0.006
ACOX3	1.427	1.447	1.604	0.575	0.008	1.946	1.662	1.596	0.789	0.012	1.274	1.166	1.091	0.233	0.070
MCM4	1.576	1.727	1.488	0.673	0.009	1.263	1.270	1.281	0.346	0.000	0.755	0.757	0.796	-0.379	0.004
RPL31	0.913	0.882	0.901	-0.154	0.009	1.094	1.097	1.000	0.087	0.184	1.136	1.149	1.125	0.185	0.002
STRAP	0.723	0.685	0.761	-0.469	0.009	0.331	0.372	0.417	-1.428	0.004	0.486	0.528	0.511	-0.978	0.001
NXT2;NXT1	1.133	1.108	1.153	0.178	0.009	1.197	0.987	1.179	0.159	0.217	0.941	0.905	0.954	-0.100	0.049
DARS;DKFZp781B11202	1.093	1.119	1.087	0.137	0.009	1.188	1.234	1.330	0.321	0.021	1.108	1.086	1.195	0.175	0.053
MOV10	0.913	0.907	0.884	-0.149	0.009	1.009	1.016	1.031	0.027	0.107	1.040	1.113	1.131	0.130	0.073
COMMD3	1.286	1.257	1.198	0.318	0.009	1.076	1.053	1.072	0.093	0.010	0.715	0.771	0.765	-0.415	0.007
DYNC1LI1	1.282	1.385	1.411	0.442	0.009	2.741	2.705	4.207	1.654	0.016	1.971	2.077	2.823	1.177	0.018
PPA2	1.294	1.397	1.283	0.404	0.009	0.849	1.805	1.250	0.313	0.425	0.637	1.205	0.866	-0.196	0.536

SNX2	1.412	1.573	1.615	0.614	0.009	1.706	1.534	1.538	0.669	0.006	1.168	1.031	0.949	0.064	0.539
EIF3I	0.940	0.930	0.917	-0.106	0.009	0.816	0.867	0.812	-0.267	0.012	0.879	0.876	0.868	-0.194	0.001
RPL9	0.920	0.918	0.894	-0.135	0.009	1.138	1.095	1.121	0.160	0.010	1.189	1.103	1.141	0.194	0.026
RPS16	0.919	0.908	0.889	-0.143	0.009	1.070	1.056	1.039	0.077	0.023	1.160	1.132	1.106	0.179	0.012
HIST1H1D;HIST1H1E;HIST1H1C	0.831	0.877	0.855	-0.228	0.010	1.457	1.348	1.358	0.472	0.006	1.512	1.435	1.334	0.511	0.010
RPS7	0.890	0.921	0.897	-0.148	0.010	0.912	0.914	0.906	-0.135	0.001	0.994	0.926	0.936	-0.072	0.151
PRDX3	1.659	1.575	1.879	0.765	0.010	2.174	2.083	2.310	1.129	0.001	1.249	1.284	1.132	0.287	0.035
S100A11	1.876	1.731	1.559	0.780	0.010	2.753	3.119	3.143	1.585	0.002	1.623	1.680	1.942	0.802	0.010
HIST1H4A	0.535	0.433	0.416	-1.125	0.010	0.882	0.907	0.919	-0.148	0.013	1.664	1.883	2.597	1.008	0.034
RPL8	0.908	0.888	0.871	-0.170	0.010	1.293	1.346	1.248	0.373	0.007	1.361	1.406	1.373	0.464	0.001
TARDBP	0.653	0.739	0.705	-0.518	0.010	0.961	0.868	2.831	0.413	0.528	1.278	1.251	3.617	0.844	0.237

HNRNPA3	1.138	1.189	1.199	0.233	0.010	1.904	2.150	1.978	1.006	0.003	1.467	1.568	1.361	0.549	0.011
CLINT1	1.343	1.455	1.309	0.451	0.010	1.191	1.111	1.095	0.178	0.041	0.819	0.775	0.729	-0.371	0.017
CORO1B	1.186	1.160	1.126	0.210	0.010	0.758	0.700	0.684	-0.487	0.008	0.689	0.524	0.465	-0.858	0.036
PCBD1	1.504	1.733	1.507	0.658	0.010	1.019	1.219	1.199	0.192	0.146	0.668	0.698	0.747	-0.507	0.008
PDCD4	0.779	0.830	0.766	-0.338	0.011	0.792	0.679	0.769	-0.425	0.025	1.045	0.828	0.900	-0.120	0.346
GRWD1	0.809	0.757	0.818	-0.332	0.011	0.581	0.538	0.621	-0.789	0.006	0.708	0.702	0.784	-0.454	0.012
HSPB1	0.669	0.753	0.677	-0.518	0.011	0.396	0.432	0.292	-1.440	0.014	0.528	0.627	0.494	-0.871	0.014
TRMT1	0.907	0.871	0.875	-0.178	0.011	0.832	0.719	0.958	-0.268	0.155	0.865	0.869	0.968	-0.153	0.102
TMA16	1.276	1.240	1.357	0.367	0.011	1.212	1.065	0.947	0.096	0.447	0.849	0.784	0.642	-0.409	0.077
AP3B1	0.797	0.785	0.845	-0.307	0.011	0.940	0.875	1.005	-0.091	0.253	1.182	1.125	1.217	0.231	0.020
WASF2	1.164	1.209	1.142	0.228	0.011	1.577	1.709	1.308	0.606	0.034	1.258	1.274	1.024	0.238	0.145
UBE2O	0.587	0.532	0.464	-0.928	0.011	0.149	0.227	0.230	-2.336	0.008	0.273	0.462	0.496	-1.332	0.039
CALR	1.140	1.146	1.100	0.174	0.011	0.355	0.579	0.564	-1.037	0.046	0.324	0.603	0.514	-1.104	0.054

FN1	0.829	0.767	0.770	-0.344	0.011	0.655	0.601	0.572	-0.717	0.006	0.801	0.808	0.766	-0.337	0.005
KPNA2	0.901	0.877	0.859	-0.186	0.011	0.532	0.545	0.564	-0.870	0.001	0.599	0.621	0.641	-0.689	0.002
TFAM	2.132	2.947	2.352	1.295	0.011	1.325	1.587	1.168	0.432	0.078	0.553	0.471	0.484	-0.995	0.005
RPS5	0.884	0.915	0.880	-0.164	0.011	1.043	1.016	1.031	0.043	0.058	1.159	1.060	1.084	0.138	0.072
HNRNPK	0.857	0.861	0.814	-0.245	0.011	0.657	0.871	0.421	-0.685	0.154	0.738	0.961	0.585	-0.424	0.177
DYNLL1	1.166	1.232	1.250	0.282	0.011	0.966	1.086	1.044	0.044	0.471	0.761	0.873	0.792	-0.309	0.034
DRG1	1.240	1.161	1.188	0.258	0.012	1.088	1.069	1.088	0.113	0.005	0.929	0.878	0.908	-0.145	0.026
CSDE1	0.828	0.828	0.772	-0.306	0.012	1.098	1.080	0.692	-0.095	0.706	1.226	1.279	0.939	0.186	0.313
SORD	0.867	0.905	0.896	-0.169	0.012	0.863	0.923	0.826	-0.202	0.050	1.024	0.972	0.888	-0.059	0.429
RPL13	0.911	0.885	0.917	-0.145	0.012	1.017	1.008	0.918	-0.030	0.597	1.095	1.104	0.937	0.060	0.516
CDC37	1.186	1.145	1.222	0.243	0.012	0.865	1.018	0.929	-0.096	0.291	0.729	0.817	0.659	-0.450	0.038
ERI3;PRN PIP	0.627	0.645	0.728	-0.588	0.012	0.539	0.590	0.640	-0.766	0.009	0.740	0.866	0.852	-0.291	0.056

SLC9A3R1	0.822	0.805	0.864	-0.269	0.013	0.548	0.611	0.500	-0.860	0.009	0.690	0.721	0.582	-0.596	0.024
RPL36AL	0.936	0.938	0.914	-0.106	0.013	0.829	0.815	0.700	-0.360	0.043	0.826	0.825	0.818	-0.281	0.000
EIF4E	0.873	0.816	0.836	-0.249	0.013	0.804	0.816	0.998	-0.204	0.181	0.963	1.034	1.043	0.018	0.677
SF3B1	0.854	0.862	0.898	-0.199	0.013	1.823	1.988	1.863	0.918	0.002	2.086	2.182	2.027	1.068	0.001
RRBP1	1.140	1.195	1.134	0.209	0.013	1.108	1.108	1.080	0.136	0.008	0.917	0.941	0.853	-0.148	0.075
EIF3A	0.840	0.890	0.863	-0.211	0.013	0.917	0.954	0.893	-0.119	0.051	0.978	1.035	1.027	0.019	0.545
PABPC1	0.380	0.399	0.520	-1.221	0.013	0.296	0.356	0.413	-1.507	0.008	0.739	0.831	0.879	-0.297	0.056
PAPOLA; PAPOLB	0.857	0.869	0.815	-0.240	0.013	0.882	1.030	1.230	0.053	0.738	0.849	0.799	1.157	-0.116	0.555
MCM7	1.821	2.428	2.002	1.049	0.013	1.110	1.343	1.098	0.237	0.129	0.686	0.586	0.544	-0.731	0.018
RPS28	0.941	0.946	0.923	-0.095	0.014	0.995	0.921	0.887	-0.099	0.180	0.965	0.982	0.984	-0.034	0.063
CNOT1	1.982	1.714	1.580	0.808	0.014	1.701	1.601	2.392	0.901	0.038	0.883	0.983	1.208	0.023	0.880

AP3M1	0.808	0.829	0.757	-0.326	0.014	0.870	0.827	0.706	-0.326	0.070	1.222	1.114	0.981	0.139	0.269
PFKL	1.149	1.234	1.188	0.251	0.014	1.628	1.474	1.536	0.627	0.004	1.231	1.244	1.242	0.309	0.000
PABPC4	0.457	0.488	0.596	-0.971	0.014	0.402	0.420	0.482	-1.207	0.004	0.789	0.853	0.841	-0.273	0.016
XRCC6	1.186	1.177	1.264	0.273	0.014	0.793	0.832	0.927	-0.236	0.071	0.681	0.717	0.736	-0.492	0.004
ATIC	0.823	0.806	0.868	-0.266	0.014	0.857	0.841	0.744	-0.299	0.043	0.966	1.145	0.894	-0.005	0.965
DHX30	0.880	0.910	0.866	-0.176	0.014	1.284	1.148	1.096	0.231	0.077	1.349	1.234	1.257	0.355	0.012
COMMD7	1.791	1.604	1.469	0.693	0.014	1.576	1.091	1.210	0.352	0.156	0.752	0.702	0.799	-0.415	0.016
RPS29	0.928	0.953	0.936	-0.091	0.014	0.997	0.946	1.092	0.014	0.835	1.049	1.011	1.043	0.048	0.103
DDX1	1.051	1.079	1.072	0.094	0.014	1.210	1.162	1.155	0.233	0.008	1.059	1.047	1.051	0.074	0.005
SNX1	1.266	1.337	1.433	0.426	0.014	1.685	1.567	1.784	0.745	0.005	1.231	1.027	1.219	0.208	0.134
MAVS	1.245	1.301	1.395	0.392	0.015	1.907	2.051	2.439	1.085	0.009	1.419	1.746	1.662	0.681	0.017
FAU	0.826	0.884	0.842	-0.234	0.015	0.787	0.816	0.875	-0.277	0.026	0.847	0.890	1.052	-0.112	0.359
ITIH2	0.702	0.773	0.671	-0.486	0.015	0.605	0.667	0.647	-0.646	0.004	0.842	0.952	0.922	-0.145	0.110

SERF2	0.838	0.882	0.823	-0.239	0.015	0.134	0.182	0.158	-2.673	0.002	0.165	0.229	0.210	-2.329	0.004
HMGB3	1.140	1.215	1.219	0.252	0.015	1.478	1.262	1.214	0.393	0.045	1.201	1.041	0.861	0.036	0.821
PSMB5	1.212	1.246	1.151	0.266	0.015	0.944	1.118	1.081	0.063	0.488	0.734	0.913	0.846	-0.273	0.098
MAP4	0.784	0.696	0.692	-0.468	0.015	0.230	0.261	0.240	-2.037	0.001	0.289	0.293	0.259	-1.837	0.001
EEF1D	1.323	1.416	1.252	0.410	0.015	1.095	1.135	1.145	0.170	0.013	0.770	0.896	0.830	-0.268	0.051
NAP1L1	1.290	1.178	1.252	0.309	0.015	1.021	1.100	1.118	0.109	0.114	0.736	0.862	0.809	-0.321	0.040
LARS2	1.755	1.595	1.435	0.669	0.015	1.810	1.583	1.450	0.685	0.018	1.025	1.193	1.001	0.097	0.345
MCM2	1.430	1.728	1.519	0.636	0.016	1.286	1.646	1.330	0.498	0.047	0.905	0.820	0.944	-0.171	0.105
HIST2H3A;H3F3A;HIST3H3;H3F3C	0.584	0.458	0.435	-1.034	0.016	0.810	0.821	0.844	-0.278	0.004	1.421	1.786	1.229	0.547	0.073
MSI2	1.221	1.138	1.170	0.234	0.016	1.235	1.329	1.321	0.372	0.008	0.939	1.338	0.911	0.065	0.751
RPS3A	0.904	0.916	0.875	-0.155	0.016	1.196	1.107	1.099	0.180	0.044	1.340	1.261	1.247	0.358	0.008

EIF4G1	0.752	0.810	0.828	-0.330	0.016	0.257	0.201	0.186	-2.234	0.004	0.337	0.253	0.223	-1.907	0.008
EPS8L3	0.895	0.840	0.854	-0.213	0.016	0.869	0.832	0.899	-0.208	0.024	0.927	0.876	0.892	-0.155	0.023
MYH10	0.478	0.514	0.624	-0.902	0.016	0.515	0.478	0.368	-1.155	0.016	0.924	0.918	0.567	-0.352	0.270
YBX1	0.904	0.869	0.910	-0.161	0.016	0.884	0.876	0.944	-0.151	0.047	0.980	1.073	1.033	0.039	0.408
FKBP2	1.047	1.075	1.065	0.087	0.016	0.918	0.994	0.971	-0.058	0.232	0.851	0.822	0.853	-0.249	0.005
CTPS2	1.137	1.207	1.221	0.248	0.016	1.311	1.241	1.317	0.366	0.006	1.003	1.003	1.132	0.062	0.397
PARG	0.655	0.761	0.725	-0.489	0.016	0.681	0.839	1.040	-0.250	0.292	0.919	1.210	1.368	0.202	0.356
RPL24	0.922	0.885	0.916	-0.140	0.016	0.900	0.856	0.855	-0.200	0.015	0.926	0.914	0.976	-0.092	0.085
ECH1	1.118	1.185	1.132	0.195	0.017	1.151	1.221	1.051	0.188	0.096	1.025	1.107	1.027	0.074	0.181
NCAPD2	0.680	0.781	0.693	-0.481	0.017	0.272	0.407	0.566	-1.332	0.049	0.452	0.582	0.607	-0.882	0.022
DR1	0.835	0.849	0.892	-0.221	0.017	0.447	0.483	0.420	-1.153	0.003	0.494	0.559	0.404	-1.055	0.016
TUBB	1.077	1.104	1.125	0.140	0.017	0.959	1.113	1.084	0.070	0.401	0.869	0.885	0.820	-0.221	0.022
TPP2	1.100	1.119	1.159	0.171	0.017	1.455	1.266	1.378	0.448	0.017	1.185	1.181	1.150	0.229	0.004

FTL	1.400	1.460	1.268	0.458	0.017	0.882	0.949	1.183	-0.005	0.973	0.537	0.649	0.947	-0.533	0.157
RPS9	0.875	0.878	0.918	-0.169	0.017	1.065	1.035	1.009	0.051	0.152	1.198	1.083	1.067	0.156	0.097
FGG	0.832	0.886	0.829	-0.237	0.017	0.937	1.278	1.057	0.113	0.478	0.997	1.253	1.125	0.164	0.228
TCP1	1.018	1.022	1.028	0.033	0.017	1.277	1.302	1.277	0.362	0.001	1.200	1.235	1.227	0.288	0.002
EEF1B2	1.229	1.382	1.283	0.375	0.017	1.017	1.407	1.218	0.267	0.187	0.856	0.999	0.855	-0.151	0.181
C20orf27	0.862	0.793	0.841	-0.266	0.017	0.558	0.517	0.686	-0.779	0.024	0.643	0.660	0.837	-0.498	0.055
RPL23A	1.180	1.192	1.117	0.217	0.018	1.197	1.203	1.131	0.235	0.015	0.904	0.990	1.009	-0.049	0.420
COMMD1	1.415	1.498	1.283	0.481	0.018	1.170	1.080	1.953	0.434	0.246	0.740	0.636	0.910	-0.408	0.113
XRCC5	1.127	1.171	1.213	0.226	0.018	0.769	0.867	0.557	-0.477	0.129	0.598	0.714	0.483	-0.759	0.043
HNRNPH3	1.337	1.582	1.566	0.576	0.018	1.201	1.374	1.578	0.460	0.056	0.812	0.972	0.898	-0.165	0.159
GOLGA3	0.836	0.849	0.895	-0.218	0.018	1.793	1.838	1.547	0.783	0.010	1.880	2.236	1.515	0.890	0.032
MTHFD1	0.823	0.879	0.815	-0.254	0.018	0.891	0.834	0.608	-0.382	0.154	0.968	0.905	0.741	-0.207	0.216
AIMP1	1.162	1.240	1.153	0.244	0.018	1.127	1.153	1.103	0.173	0.011	0.971	0.999	0.985	-0.022	0.196

RPS3	0.868	0.896	0.837	-0.207	0.018	1.201	1.119	1.110	0.192	0.033	1.390	1.273	1.284	0.395	0.010
COMMD9	1.547	1.322	1.374	0.497	0.018	1.148	1.149	1.330	0.270	0.062	0.723	0.793	0.863	-0.338	0.045
UPF1	1.075	1.125	1.098	0.136	0.018	1.210	1.210	1.204	0.273	0.000	1.038	1.081	1.069	0.087	0.037
ABHD10	1.434	1.432	1.257	0.456	0.019	1.554	1.402	1.573	0.592	0.008	1.051	1.067	0.929	0.019	0.790
NAP1L4b; NAP1L4	1.317	1.196	1.213	0.311	0.019	0.862	1.087	0.883	-0.091	0.483	0.725	0.869	0.808	-0.324	0.050
EZR	1.022	1.035	1.036	0.044	0.019	0.832	0.772	0.843	-0.295	0.018	0.790	0.767	0.824	-0.334	0.008
GNB2L1	0.875	0.889	0.831	-0.210	0.019	1.118	1.091	1.071	0.129	0.019	1.279	1.186	1.308	0.330	0.016
LAGE3	1.376	1.236	1.243	0.360	0.019	1.151	1.293	1.533	0.396	0.081	0.777	1.161	1.177	0.029	0.898
ARHGAP18	1.279	1.498	1.441	0.489	0.019	1.647	1.916	1.727	0.816	0.006	1.286	1.150	1.157	0.258	0.039
DDB1	0.901	0.899	0.936	-0.133	0.019	0.907	0.972	1.015	-0.053	0.375	0.963	1.209	1.083	0.112	0.360
PKM2	0.841	0.852	0.900	-0.211	0.019	0.785	0.980	0.812	-0.226	0.152	0.945	1.171	0.916	0.006	0.961

SPTBN1	1.285	1.235	1.404	0.385	0.020	1.651	1.575	1.631	0.695	0.001	1.403	1.259	1.176	0.351	0.042
PPHLN1	1.471	1.324	1.595	0.545	0.020	0.935	0.683	1.260	-0.105	0.722	0.609	0.511	0.822	-0.655	0.082
STXBP1	1.382	1.218	1.358	0.397	0.020	1.144	1.059	1.131	0.151	0.049	0.732	0.864	0.817	-0.317	0.046
DHX36	0.863	0.899	0.837	-0.208	0.020	0.936	0.850	0.875	-0.174	0.051	1.024	0.997	1.029	0.023	0.241
RPP25L	1.077	1.051	1.087	0.100	0.020	0.794	0.959	0.968	-0.146	0.257	0.717	0.848	0.855	-0.315	0.063
COMMD4	1.397	1.285	1.226	0.379	0.020	1.125	1.386	1.080	0.251	0.153	0.819	0.956	0.850	-0.196	0.100
EEA1	1.173	1.180	1.278	0.274	0.020	1.153	1.144	0.870	0.066	0.668	1.040	0.994	0.910	-0.030	0.651
RPL5	0.895	0.924	0.876	-0.155	0.020	1.395	1.390	1.722	0.580	0.030	1.571	1.481	1.658	0.649	0.005
PAIP1	0.338	0.394	0.525	-1.280	0.021	0.163	0.169	0.355	-2.225	0.026	0.485	0.477	0.578	-0.968	0.008
PDAP1	0.796	0.721	0.680	-0.453	0.021	0.341	0.318	0.485	-1.416	0.017	0.756	0.521	0.688	-0.627	0.060
ABI1	1.139	1.231	1.157	0.232	0.021	1.295	1.385	1.232	0.381	0.016	0.969	1.027	0.935	-0.035	0.476
MAPRE1	1.181	1.304	1.204	0.297	0.021	1.423	1.408	1.561	0.548	0.007	0.921	1.132	1.067	0.051	0.622
STXBP3	1.460	1.880	1.614	0.716	0.021	2.092	2.364	2.621	1.232	0.006	1.351	1.453	1.665	0.570	0.023

RPS25	0.857	0.911	0.863	-0.190	0.021	1.086	1.039	1.388	0.216	0.239	1.335	1.124	1.170	0.271	0.069
METAP2	0.748	0.834	0.739	-0.373	0.021	1.155	0.895	0.751	-0.122	0.569	1.500	1.007	0.978	0.188	0.444
FKBP3	0.760	0.821	0.846	-0.307	0.021	0.717	0.826	1.034	-0.236	0.265	1.101	0.981	1.235	0.138	0.285
PSMB3	1.142	1.141	1.224	0.225	0.022	0.852	1.052	0.975	-0.065	0.541	0.840	0.895	0.773	-0.261	0.051
ADSL	0.909	0.877	0.923	-0.148	0.022	0.964	0.912	0.853	-0.139	0.114	1.004	1.138	0.894	0.010	0.927
S100A6	2.183	2.346	1.653	1.027	0.022	2.173	2.904	2.236	1.273	0.011	1.014	1.184	1.132	0.147	0.157
LRRC40	0.876	0.924	0.907	-0.148	0.022	0.865	0.740	0.822	-0.309	0.043	0.911	0.860	0.850	-0.195	0.024
RPL13A	0.872	0.910	0.917	-0.153	0.022	1.154	1.055	1.156	0.164	0.064	1.346	1.155	1.268	0.326	0.037
VARS	1.371	1.212	1.371	0.396	0.022	1.565	1.863	2.029	0.855	0.016	1.049	1.480	1.438	0.386	0.136
DIP2B	0.804	0.798	0.712	-0.377	0.022	1.088	1.063	1.052	0.094	0.022	1.291	1.325	1.301	0.385	0.001
HNRNPL	1.282	1.156	1.237	0.291	0.022	1.698	1.769	1.526	0.732	0.007	1.259	1.382	1.085	0.306	0.095
CSNK2A2	1.092	1.072	1.124	0.132	0.022	0.804	0.983	0.942	-0.142	0.250	0.758	0.918	0.846	-0.255	0.086
SMG1	0.871	0.831	0.790	-0.269	0.022	0.919	0.857	0.706	-0.282	0.132	1.020	1.159	0.956	0.059	0.548

TJP1	1.196	1.355	1.258	0.343	0.022	1.339	1.402	1.217	0.397	0.022	1.162	1.008	0.980	0.066	0.475
SET	1.347	1.194	1.335	0.368	0.022	0.724	0.934	1.044	-0.168	0.395	0.517	0.759	0.697	-0.624	0.065
CUL4A	1.118	1.141	1.079	0.154	0.023	1.063	1.029	0.921	0.003	0.962	0.939	1.015	1.011	-0.018	0.671
ARRB1	0.820	0.748	0.836	-0.321	0.023	0.970	1.039	0.994	0.001	0.976	1.207	1.286	0.992	0.208	0.207
MRPS25	0.758	0.620	0.647	-0.573	0.023	0.989	0.926	0.846	-0.123	0.202	1.208	1.259	1.170	0.277	0.012
VPS35	1.095	1.150	1.171	0.186	0.023	1.225	1.312	1.236	0.330	0.009	1.075	1.119	1.064	0.119	0.033
ACTN4;ACTN1;ACTN2	1.787	1.749	1.407	0.712	0.023	0.845	1.154	0.921	-0.052	0.736	0.469	0.727	0.732	-0.668	0.088
EIF3B	0.918	0.926	0.882	-0.138	0.024	0.920	0.958	0.901	-0.111	0.050	0.939	1.048	0.964	-0.025	0.651
AHSA1	1.164	1.124	1.224	0.226	0.024	2.471	2.545	3.027	1.417	0.004	2.094	2.422	2.239	1.168	0.003
LIN7C;LIN7A	1.253	1.201	1.137	0.258	0.024	0.834	0.870	0.846	-0.235	0.006	0.574	0.683	0.499	-0.784	0.027
RPS18	0.932	0.923	0.889	-0.129	0.024	1.086	1.043	1.083	0.098	0.035	1.115	1.103	1.102	0.146	0.001

PLD3	1.353	1.246	1.192	0.335	0.024	1.043	1.245	1.180	0.205	0.113	0.917	0.963	0.866	-0.129	0.100
TIMM13	1.099	1.060	1.109	0.123	0.025	1.043	1.014	0.937	-0.004	0.933	0.842	0.907	0.798	-0.238	0.047
DDX3X;DDX3Y	0.921	0.945	0.904	-0.115	0.025	0.642	0.649	0.661	-0.620	0.000	0.679	0.659	0.666	-0.583	0.000
CNOT10	1.468	1.511	1.872	0.685	0.025	2.017	1.790	1.690	0.870	0.007	0.989	0.991	0.758	-0.142	0.382
RPL4	0.802	0.871	0.870	-0.240	0.026	1.238	1.028	1.135	0.176	0.150	1.454	1.231	1.228	0.378	0.043
CAPN1	0.725	0.820	0.814	-0.350	0.026	0.587	0.590	0.629	-0.734	0.002	0.714	0.720	0.752	-0.457	0.003
CBS	1.161	1.244	1.311	0.307	0.026	0.922	1.350	1.361	0.253	0.305	0.808	0.916	0.875	-0.209	0.058
APOB	0.764	0.861	0.784	-0.318	0.026	0.644	0.876	0.766	-0.404	0.088	0.888	0.990	0.941	-0.091	0.183
SPR	0.614	0.740	0.581	-0.641	0.026	0.732	0.722	0.647	-0.516	0.012	1.031	0.972	1.128	0.059	0.446
KPNA3	0.888	0.805	0.827	-0.253	0.026	0.490	0.571	0.534	-0.915	0.005	0.579	0.640	0.599	-0.724	0.003
RPS15	0.893	0.892	0.834	-0.197	0.026	1.065	1.060	1.048	0.081	0.007	1.115	1.106	1.154	0.170	0.012
EDF1	0.773	0.865	0.781	-0.312	0.026	1.086	0.902	1.030	0.005	0.959	1.325	0.949	1.088	0.150	0.394

MATR3	0.826	0.877	0.788	-0.269	0.026	1.907	1.802	1.829	0.884	0.001	2.200	2.073	2.119	1.091	0.001
AP2B1	1.140	1.267	1.202	0.265	0.026	1.662	1.641	1.415	0.649	0.013	1.439	1.467	1.231	0.459	0.029
POP7	1.296	1.197	1.162	0.283	0.026	1.016	1.022	1.122	0.073	0.255	0.709	0.807	0.799	-0.377	0.024
CCDC53	0.751	0.854	0.782	-0.332	0.026	0.637	0.742	0.475	-0.718	0.062	0.879	0.939	0.770	-0.218	0.123
RPS10	0.943	0.899	0.922	-0.118	0.027	0.998	0.994	1.045	0.017	0.533	1.042	1.060	1.067	0.079	0.016
PCNA	1.319	1.167	1.297	0.332	0.027	0.686	0.711	0.784	-0.462	0.015	0.494	0.616	0.594	-0.823	0.014
ABCF1	0.746	0.727	0.614	-0.529	0.027	0.209	0.195	0.133	-2.511	0.007	0.284	0.267	0.271	-1.866	0.000
FAM129B	1.121	1.211	1.228	0.246	0.027	1.108	1.050	1.413	0.239	0.211	0.829	0.852	0.931	-0.201	0.057
HDGF	1.404	1.407	1.726	0.590	0.027	2.659	2.838	3.358	1.554	0.004	1.501	1.565	1.576	0.629	0.001
HNRNPA0	0.921	0.865	0.903	-0.158	0.027	0.829	0.906	0.794	-0.248	0.047	0.816	1.030	0.727	-0.237	0.250
NMT1	0.861	0.897	0.821	-0.219	0.027	0.808	0.708	0.613	-0.504	0.049	0.960	0.716	0.778	-0.301	0.139
PRDX2	1.057	1.101	1.105	0.121	0.027	0.813	0.964	0.916	-0.159	0.161	0.742	0.831	0.720	-0.390	0.025
HSD17B1	1.227	1.118	1.201	0.240	0.027	0.665	0.750	0.771	-0.460	0.020	0.526	0.642	0.592	-0.774	0.012

0															
DHX15	1.270	1.160	1.315	0.318	0.028	1.248	1.281	1.323	0.360	0.005	0.952	1.066	1.010	0.011	0.831
KIAA0196	0.764	0.799	0.676	-0.425	0.028	0.946	0.983	0.837	-0.120	0.227	1.162	1.209	1.124	0.220	0.018
RPL7A	0.897	0.900	0.841	-0.186	0.028	1.210	1.606	1.710	0.577	0.064	1.114	1.320	1.431	0.358	0.079
BIN1	1.366	1.698	1.414	0.571	0.028	0.945	1.015	1.462	0.163	0.492	0.694	0.784	0.944	-0.320	0.131
GCLM	1.246	1.311	1.476	0.423	0.028	2.272	2.312	1.660	1.041	0.022	1.644	1.153	1.142	0.372	0.165
PSMA2	1.098	1.155	1.191	0.198	0.028	0.908	1.110	1.009	0.008	0.932	0.824	0.895	0.773	-0.270	0.048
CTSL1	0.873	0.928	0.879	-0.163	0.029	0.615	0.689	0.587	-0.668	0.010	0.642	0.661	0.730	-0.564	0.010
DNAJA1	0.842	0.883	0.910	-0.189	0.029	1.392	1.191	1.178	0.322	0.054	1.284	1.234	1.368	0.372	0.013
ARPC5L	1.078	1.132	1.151	0.164	0.029	0.929	1.033	1.023	-0.009	0.872	0.888	0.935	0.928	-0.126	0.032
SEC23B	1.105	1.150	1.080	0.152	0.029	1.083	1.126	1.100	0.141	0.013	1.071	0.936	0.959	-0.019	0.779
ANP32E	1.229	1.124	1.238	0.258	0.029	0.646	0.745	0.898	-0.404	0.099	0.505	0.656	0.720	-0.689	0.046
UGGT1	1.348	1.592	1.314	0.499	0.029	0.844	0.927	1.145	-0.053	0.725	0.693	0.684	0.905	-0.407	0.090

PTGR1	0.883	0.853	0.798	-0.245	0.029	1.042	1.188	0.988	0.097	0.347	1.271	1.334	1.283	0.374	0.003
CHMP4B	1.249	1.157	1.315	0.308	0.029	1.829	1.604	1.753	0.787	0.005	1.295	1.371	1.310	0.406	0.004
SEPSECS	0.632	0.688	0.513	-0.722	0.029	0.564	0.601	0.589	-0.775	0.001	0.906	0.938	1.045	-0.057	0.454
UTRN	1.299	1.183	1.373	0.359	0.029	0.277	3.329	0.340	-0.557	0.676	0.224	2.895	0.366	-0.691	0.603
RBM14	1.275	1.230	1.439	0.392	0.029	1.483	1.616	1.648	0.661	0.005	0.992	1.187	1.049	0.102	0.314
KHDRBS1	0.733	0.813	0.677	-0.437	0.030	0.447	0.575	0.519	-0.969	0.012	0.631	0.768	0.681	-0.532	0.023
LRRC59	1.170	1.342	1.318	0.350	0.030	1.305	1.451	1.859	0.605	0.057	0.967	1.052	1.241	0.112	0.401
CS	1.140	1.284	1.251	0.291	0.030	1.037	1.209	1.164	0.182	0.112	1.140	0.952	1.048	0.062	0.496
NPM1	1.204	1.126	1.255	0.255	0.030	0.720	0.931	0.961	-0.212	0.250	0.483	0.802	0.688	-0.636	0.099
RPS13	0.897	0.935	0.878	-0.147	0.031	1.036	1.041	1.037	0.054	0.001	1.084	1.059	1.067	0.097	0.011
SRP72	0.801	0.873	0.876	-0.236	0.031	0.543	0.550	0.638	-0.797	0.009	0.655	0.600	0.667	-0.644	0.005
XPOT	1.165	1.096	1.193	0.202	0.031	0.723	0.855	1.103	-0.185	0.407	0.831	0.804	1.031	-0.179	0.251
KTN1	1.422	1.238	1.515	0.471	0.032	2.079	2.262	1.949	1.066	0.003	1.588	1.884	1.346	0.670	0.041

PSMD13	1.083	1.091	1.149	0.147	0.032	1.179	1.351	1.217	0.319	0.033	1.145	1.182	1.083	0.184	0.038
HNRPLL	1.193	1.408	1.302	0.377	0.032	1.414	1.872	1.382	0.624	0.047	0.947	1.328	1.212	0.202	0.299
PELO	0.786	0.884	0.827	-0.267	0.032	0.792	0.822	0.832	-0.295	0.005	0.924	1.088	0.963	-0.016	0.844
DNAJB4	1.222	1.122	1.132	0.212	0.032	1.846	1.691	1.916	0.860	0.004	1.402	1.481	1.497	0.546	0.003
SNTB1	1.287	1.634	1.567	0.573	0.032	0.999	1.106	1.111	0.098	0.188	0.699	0.640	0.678	-0.574	0.004
GMPS	1.166	1.188	1.092	0.199	0.033	1.013	1.087	1.078	0.082	0.124	0.857	0.966	0.989	-0.096	0.273
EIF5B	0.784	0.882	0.837	-0.263	0.033	0.792	0.807	0.837	-0.301	0.006	0.821	0.890	0.965	-0.168	0.130
HSDL2	1.054	1.100	1.108	0.121	0.034	1.497	1.171	1.151	0.337	0.110	1.378	1.074	0.902	0.139	0.517
TIMM8B	1.073	1.104	1.147	0.147	0.034	0.894	0.875	0.913	-0.162	0.012	0.765	0.784	0.711	-0.410	0.010
OLA1	1.076	1.054	1.038	0.078	0.034	0.863	0.911	0.996	-0.118	0.191	0.787	0.850	0.891	-0.249	0.042
DYNLRB1 ;DYNLRB 2	0.899	0.939	0.940	-0.112	0.034	0.928	0.929	0.802	-0.178	0.127	0.919	0.975	0.844	-0.134	0.156

HNRNPC	1.195	1.119	1.252	0.248	0.034	1.474	1.498	1.801	0.664	0.019	1.200	1.168	1.720	0.423	0.143
PLOD2	1.019	1.038	1.026	0.039	0.034	0.866	0.736	0.705	-0.384	0.051	0.793	0.722	0.708	-0.435	0.013
MDK	0.848	0.771	0.718	-0.363	0.035	0.662	0.559	0.596	-0.727	0.009	0.765	0.796	0.752	-0.375	0.004
DDX19B	0.616	0.651	0.786	-0.555	0.035	0.719	0.824	0.905	-0.300	0.090	1.166	1.203	1.129	0.221	0.014
EIF4G1	0.800	0.890	0.799	-0.271	0.035	0.637	0.720	0.675	-0.564	0.008	0.741	0.761	0.789	-0.390	0.004
COPG1	1.067	1.131	1.086	0.130	0.035	0.753	0.800	0.723	-0.400	0.011	0.681	0.712	0.661	-0.547	0.003
TRMT5	1.545	1.240	1.466	0.497	0.035	0.689	0.923	0.993	-0.221	0.304	0.498	0.779	0.649	-0.663	0.071
RPL17	0.875	0.935	0.883	-0.156	0.035	1.021	0.907	0.991	-0.041	0.508	1.010	0.956	1.172	0.060	0.568
RPLP0;RPLP0P6	0.893	0.932	0.866	-0.158	0.036	1.130	1.145	1.087	0.164	0.018	1.207	1.231	1.222	0.287	0.001
XPO1	1.080	1.064	1.039	0.085	0.036	1.963	0.916	0.717	0.122	0.806	1.508	0.849	0.746	-0.022	0.951
NT5C2	1.388	1.770	1.392	0.591	0.037	1.391	1.566	1.270	0.489	0.031	0.998	0.949	0.898	-0.078	0.217
FIG4	1.372	1.672	1.922	0.713	0.037	1.745	1.798	1.773	0.825	0.000	1.124	1.231	0.949	0.131	0.355

HSPG2	0.812	0.719	0.652	-0.465	0.037	1.216	0.916	0.801	-0.055	0.786	1.582	1.062	1.465	0.433	0.133
RPS8	0.906	0.911	0.846	-0.172	0.037	1.094	1.016	0.987	0.044	0.423	1.207	1.089	1.056	0.157	0.114
EWSR1	1.222	1.508	1.472	0.480	0.038	0.935	1.100	1.028	0.026	0.735	0.720	0.769	0.632	-0.504	0.026
EIF4A2	0.831	0.874	0.914	-0.197	0.038	0.637	0.687	0.716	-0.558	0.008	0.891	0.831	0.853	-0.221	0.017
PLOD1	1.065	1.034	1.039	0.065	0.038	1.494	1.330	1.472	0.516	0.010	1.301	1.320	1.179	0.339	0.022
ETF1	1.079	1.168	1.162	0.184	0.038	1.290	1.340	1.349	0.407	0.003	1.169	1.087	1.107	0.164	0.035
OAS3	0.566	0.761	0.589	-0.659	0.039	0.707	0.840	0.690	-0.429	0.041	1.428	1.398	1.290	0.455	0.009
DFNA5	0.731	0.736	0.579	-0.561	0.039	2.596	2.104	2.831	1.317	0.009	2.733	2.898	5.326	1.799	0.028
MACF1	1.230	1.523	1.335	0.441	0.039	1.002	0.902	0.827	-0.140	0.223	0.819	0.650	0.643	-0.516	0.046
ILF3	0.912	0.958	0.924	-0.103	0.039	0.761	0.752	0.806	-0.372	0.007	0.832	0.822	0.890	-0.239	0.021
TARBP2	0.765	0.693	0.839	-0.389	0.040	0.630	0.900	0.737	-0.420	0.106	0.625	1.340	0.894	-0.139	0.704
MRTO4	1.156	1.190	1.084	0.192	0.040	1.113	1.134	1.090	0.153	0.011	0.973	0.988	0.912	-0.063	0.213
RPL12	0.904	0.903	0.952	-0.121	0.040	1.126	1.166	1.226	0.229	0.023	1.181	1.204	1.225	0.267	0.003

KPNB1	1.357	1.429	1.181	0.398	0.040	1.070	1.275	1.057	0.176	0.180	0.804	0.856	1.085	-0.141	0.397
ANP32B	1.190	1.085	1.164	0.195	0.040	0.807	0.971	1.043	-0.098	0.470	0.679	0.914	0.836	-0.316	0.131
PACS1	1.120	1.115	1.056	0.133	0.040	0.674	0.769	0.645	-0.527	0.020	0.505	0.548	0.556	-0.900	0.002
METTL16	1.176	1.098	1.093	0.165	0.040	1.917	1.974	1.848	0.935	0.001	1.608	1.816	1.548	0.725	0.009
RPS24	0.875	0.906	0.818	-0.209	0.041	0.941	0.940	0.938	-0.090	0.000	1.034	0.982	0.996	0.005	0.844
ATPIF1	1.080	1.062	1.036	0.083	0.041	1.197	1.231	1.215	0.280	0.002	1.187	1.099	1.152	0.196	0.026
RPS19	0.930	0.908	0.864	-0.152	0.041	1.053	1.038	1.005	0.045	0.150	1.079	1.052	1.130	0.120	0.059
PDE12	0.886	0.859	0.932	-0.165	0.041	0.321	0.362	0.445	-1.425	0.009	0.377	0.420	0.458	-1.262	0.004
EIF4A1	0.983	0.976	0.989	-0.026	0.041	0.998	0.989	0.963	-0.024	0.264	0.984	0.949	0.981	-0.042	0.132
G3BP2	1.398	1.173	1.396	0.399	0.042	0.746	0.766	0.931	-0.304	0.095	0.535	0.588	0.637	-0.773	0.009
TATDN1	1.029	1.040	1.018	0.041	0.042	0.838	0.912	0.880	-0.191	0.033	0.792	0.784	0.886	-0.287	0.037
SMC4	0.980	0.956	0.967	-0.047	0.042	0.994	1.155	1.120	0.121	0.208	1.097	1.107	1.140	0.156	0.012
CKAP5	0.612	0.800	0.646	-0.554	0.042	0.273	0.414	0.315	-1.605	0.012	0.521	0.504	0.517	-0.961	0.000

SRP14	0.919	0.958	0.910	-0.106	0.042	1.089	0.907	0.905	-0.053	0.608	1.467	0.880	1.020	0.133	0.606
MITD1	0.717	0.861	0.756	-0.367	0.043	0.750	0.836	0.862	-0.296	0.040	0.972	0.973	0.925	-0.064	0.118
ACAD11	0.663	0.597	0.792	-0.558	0.043	0.473	0.438	0.620	-0.987	0.023	0.749	0.739	0.752	-0.421	0.000
NHP2	0.835	0.796	0.695	-0.371	0.043	1.171	1.186	1.281	0.277	0.021	1.359	1.390	1.522	0.508	0.010
DDX19A	0.791	0.614	0.725	-0.502	0.043	0.937	0.835	0.992	-0.122	0.235	1.092	1.470	1.277	0.345	0.109
SLIRP	1.365	1.159	1.374	0.374	0.043	1.339	1.595	1.751	0.634	0.031	1.125	1.372	1.149	0.275	0.093
FLNB	1.244	1.209	1.103	0.243	0.043	1.125	1.053	1.126	0.138	0.050	0.961	0.866	1.034	-0.072	0.433
RPL26	0.840	0.837	0.921	-0.210	0.043	1.042	1.033	0.990	0.030	0.315	1.228	1.100	1.049	0.167	0.130
PPP1CA; PPP1CC	1.088	1.051	1.044	0.085	0.043	0.817	0.971	0.905	-0.159	0.157	0.763	0.707	0.853	-0.373	0.042
MAP2	0.699	0.753	0.562	-0.585	0.044	0.173	0.151	0.220	-2.479	0.004	0.259	0.180	0.400	-1.915	0.029
EIF3EIP;EIF3L	0.932	0.922	0.871	-0.140	0.044	0.893	0.911	0.901	-0.150	0.003	0.975	0.965	1.008	-0.026	0.312

AP2A1	1.085	1.196	1.136	0.187	0.044	1.730	1.545	1.021	0.482	0.172	1.481	1.216	0.792	0.171	0.587
RPL38	0.941	0.945	0.897	-0.109	0.045	0.788	0.732	0.609	-0.503	0.045	0.838	0.793	0.632	-0.418	0.079
AARS	1.476	1.197	1.474	0.460	0.045	0.678	0.781	0.903	-0.355	0.097	0.437	0.657	0.605	-0.842	0.043
MVD	0.609	0.784	0.739	-0.501	0.045	0.693	1.116	0.967	-0.140	0.563	1.213	1.323	1.431	0.400	0.028
TLN2	0.763	0.879	0.749	-0.331	0.045	0.368	0.320	0.307	-1.596	0.002	0.785	0.555	0.439	-0.796	0.082
TSR1	0.801	0.861	0.723	-0.335	0.045	0.705	0.661	0.588	-0.622	0.015	0.796	0.953	0.809	-0.235	0.105
OSBP	1.063	1.091	1.140	0.134	0.045	1.398	1.395	1.513	0.520	0.005	1.128	1.085	1.138	0.159	0.018
RPS12	0.921	0.958	0.906	-0.108	0.045	1.064	1.047	1.031	0.067	0.037	1.061	1.043	1.102	0.095	0.055
PUS1	1.154	1.066	1.145	0.165	0.045	0.965	1.139	0.981	0.036	0.685	0.848	1.045	0.895	-0.112	0.342
CNOT7	1.607	1.877	1.322	0.665	0.045	1.629	2.019	1.400	0.734	0.041	1.032	1.085	1.167	0.128	0.130
AP1M1	1.166	1.421	1.325	0.378	0.046	1.395	1.551	1.361	0.520	0.012	1.176	1.122	0.998	0.132	0.202
PSMB4	1.081	1.183	1.188	0.201	0.046	0.841	1.184	0.958	-0.023	0.889	0.765	0.971	0.709	-0.308	0.152
CDV3	0.575	0.776	0.567	-0.661	0.046	0.176	0.391	0.284	-1.893	0.030	0.325	0.467	0.473	-1.266	0.019

SARS	1.316	1.139	1.346	0.337	0.047	0.746	0.899	1.020	-0.182	0.299	0.574	0.807	0.741	-0.514	0.074
RPL22	1.060	1.094	1.043	0.091	0.047	1.087	1.174	1.175	0.195	0.035	1.096	1.070	1.129	0.135	0.026
NSUN2	1.132	1.077	1.062	0.124	0.047	0.584	0.579	0.608	-0.761	0.001	0.512	0.617	0.546	-0.846	0.009
RBM47	0.686	0.814	0.823	-0.374	0.047	0.853	0.911	0.984	-0.129	0.163	1.328	1.066	1.174	0.245	0.117
HUWE1	0.863	0.792	0.717	-0.343	0.047	0.348	0.332	0.232	-1.740	0.011	0.366	0.427	0.325	-1.434	0.006
TUBB2A	1.184	1.091	1.228	0.222	0.048	1.108	0.922	1.065	0.040	0.666	0.754	0.786	0.823	-0.346	0.011
ECI2	1.226	1.592	1.566	0.537	0.048	0.999	1.336	1.191	0.223	0.210	0.760	0.850	1.000	-0.210	0.208
MAP1S	0.894	0.857	0.935	-0.161	0.048	0.573	0.532	0.571	-0.841	0.002	0.462	0.540	0.668	-0.861	0.031
GAR1	0.793	0.903	0.852	-0.237	0.048	1.220	1.336	1.176	0.313	0.029	1.420	1.446	1.386	0.503	0.001
TTC37	0.775	0.878	0.736	-0.332	0.048	0.635	0.946	0.849	-0.323	0.200	0.876	1.060	1.226	0.062	0.700
CSDA	0.692	0.591	0.795	-0.540	0.048	0.444	0.541	0.675	-0.874	0.037	0.618	0.826	0.916	-0.366	0.165
SEC24C	1.059	1.059	1.026	0.067	0.049	1.080	1.216	1.084	0.170	0.094	1.010	1.074	1.054	0.064	0.134
SERBP1	0.715	0.865	0.724	-0.387	0.049	0.411	0.436	0.595	-1.076	0.023	0.443	0.539	0.655	-0.893	0.032

RPL36	0.841	0.920	0.904	-0.172	0.049	1.146	1.031	1.034	0.096	0.196	1.252	1.167	1.087	0.222	0.064
SRSF7	0.837	0.904	0.789	-0.248	0.049	1.086	1.069	0.910	0.026	0.776	1.288	1.234	1.052	0.247	0.109
ENAH	1.069	1.171	1.133	0.168	0.049	1.055	1.050	0.793	-0.062	0.692	0.968	0.901	0.934	-0.099	0.080
GRB10	0.931	0.847	0.852	-0.191	0.049	0.839	0.762	0.835	-0.302	0.022	0.892	0.946	0.972	-0.096	0.119
NOB1	0.809	0.821	0.679	-0.383	0.050	0.589	0.572	0.604	-0.765	0.001	0.654	0.705	0.721	-0.529	0.006
SNRPD3	0.968	0.926	0.930	-0.088	0.050	1.377	1.355	1.628	0.534	0.024	1.295	1.416	1.550	0.502	0.022
EIF2A	0.876	0.746	0.830	-0.294	0.050	0.778	0.655	0.877	-0.387	0.086	0.918	0.782	1.025	-0.148	0.322
ANP32A	1.233	1.125	1.323	0.292	0.050	0.661	0.826	0.915	-0.333	0.137	0.521	0.737	0.670	-0.653	0.048
S100A13	0.903	0.883	0.950	-0.133	0.050	0.759	0.868	0.782	-0.319	0.033	0.769	0.967	0.824	-0.236	0.137
SRPK1	0.537	0.729	0.465	-0.820	0.051	1.050	1.376	0.849	0.098	0.674	1.279	1.691	1.919	0.684	0.058
SRC;YES 1;FYN	1.420	1.509	1.185	0.448	0.051	1.582	1.869	1.727	0.784	0.008	1.257	1.274	1.256	0.336	0.000
PPP1R12	1.432	1.187	1.231	0.355	0.051	1.120	1.036	1.054	0.097	0.105	0.840	0.859	0.820	-0.252	0.006

A															
TRIM4	0.802	0.907	0.795	-0.263	0.051	0.827	0.872	0.876	-0.221	0.014	1.102	1.052	1.010	0.076	0.171
TRA2A	0.749	0.874	0.722	-0.360	0.051	1.773	1.959	1.909	0.910	0.002	2.370	2.204	2.297	1.195	0.001
DLD	1.096	1.239	1.237	0.250	0.051	1.332	1.404	1.278	0.419	0.009	1.325	1.164	1.035	0.225	0.161
SUPT5H	1.119	1.141	1.264	0.230	0.051	1.152	1.050	1.386	0.248	0.170	0.980	0.951	1.078	0.002	0.976
FLNA	1.055	1.022	1.049	0.060	0.052	1.253	1.188	1.198	0.278	0.007	1.285	1.104	1.191	0.252	0.058
PDIA6	1.066	1.156	1.169	0.176	0.052	0.654	0.810	0.657	-0.508	0.038	0.616	0.648	0.585	-0.700	0.004
RTCD1	0.878	0.862	0.942	-0.163	0.052	0.901	0.909	1.022	-0.085	0.283	1.055	0.991	1.115	0.074	0.272
DDX39B;BAT1	1.107	1.140	1.054	0.137	0.053	1.558	1.604	1.476	0.628	0.003	1.339	1.365	1.398	0.451	0.002
PRKCI	1.115	1.049	1.070	0.108	0.053	0.730	0.645	0.868	-0.430	0.075	0.670	0.602	0.642	-0.650	0.005
ATP6V1E1	1.685	1.328	1.287	0.509	0.053	1.002	1.116	1.084	0.093	0.184	0.630	0.879	0.767	-0.412	0.098

GAS2	0.687	0.648	0.841	-0.473	0.054	1.839	1.742	1.723	0.821	0.001	2.368	2.611	1.991	1.207	0.009
PCBP2	0.934	0.865	0.923	-0.142	0.054	0.973	0.912	0.924	-0.095	0.079	0.936	0.950	0.855	-0.132	0.109
DNM1L	1.152	1.177	1.066	0.177	0.054	1.601	1.604	1.420	0.622	0.009	1.191	1.202	1.114	0.224	0.023
PFDN2	1.084	1.187	1.099	0.166	0.055	0.967	1.075	1.162	0.091	0.358	0.972	0.988	0.929	-0.055	0.174
CCDC58	1.284	1.162	1.117	0.245	0.055	1.011	1.020	0.972	0.001	0.957	0.771	0.896	0.948	-0.203	0.149
ESYT2	1.611	1.207	1.523	0.522	0.055	1.636	1.488	1.935	0.745	0.021	0.950	0.994	0.939	-0.058	0.146
PSME4	0.925	0.835	0.896	-0.177	0.056	0.875	0.860	0.968	-0.152	0.103	1.048	1.042	1.111	0.093	0.086
MAGOH	0.945	0.978	0.948	-0.063	0.056	1.037	1.142	0.944	0.053	0.570	1.039	1.091	0.937	0.029	0.701
HNRNPH1	1.131	1.054	1.080	0.121	0.056	1.377	1.482	1.579	0.563	0.010	1.124	1.349	1.305	0.328	0.056
AP1S1	1.120	1.226	1.329	0.289	0.056	1.178	1.440	1.491	0.446	0.052	1.016	1.141	1.014	0.077	0.302
EIF3D	0.973	0.931	0.944	-0.076	0.056	0.909	0.909	0.930	-0.126	0.007	0.916	0.994	0.967	-0.062	0.217
IFIT5	0.625	0.781	0.798	-0.454	0.057	0.794	0.816	0.796	-0.318	0.002	1.236	1.251	0.996	0.208	0.191
LARP1	0.912	0.862	0.798	-0.225	0.057	0.632	0.781	0.606	-0.580	0.036	0.721	0.882	0.711	-0.381	0.063

FARSB	1.088	1.083	1.179	0.158	0.058	1.303	1.194	1.289	0.335	0.014	1.121	1.059	1.088	0.123	0.036
CBR1	0.849	0.916	0.797	-0.230	0.058	0.961	0.900	0.995	-0.072	0.229	1.047	0.965	1.193	0.090	0.419
UFD1L	1.117	1.251	1.118	0.215	0.058	1.592	1.554	1.004	0.437	0.180	1.589	1.420	0.915	0.349	0.287
TRIO	0.813	0.671	0.581	-0.553	0.059	0.567	0.282	0.218	-1.614	0.059	0.838	0.428	0.451	-0.876	0.107
POLR2L	1.167	1.073	1.207	0.199	0.060	1.197	1.235	1.361	0.336	0.027	0.904	1.057	1.176	0.056	0.662
GRSF1	2.135	1.331	1.753	0.772	0.060	1.396	1.148	0.900	0.176	0.437	0.669	0.840	0.526	-0.586	0.095
TIMM9	1.242	1.767	1.497	0.572	0.060	1.106	1.181	1.030	0.143	0.129	0.922	0.599	0.727	-0.439	0.135
ACLY	1.331	1.295	1.112	0.313	0.061	1.068	0.791	0.514	-0.401	0.320	0.679	0.688	0.423	-0.780	0.077
EMG1	0.919	0.931	0.969	-0.090	0.061	1.388	1.388	1.284	0.436	0.007	1.445	1.666	1.285	0.543	0.037
ARHGEF10L	0.771	0.691	0.869	-0.370	0.061	0.725	0.660	0.710	-0.519	0.006	0.845	0.798	0.791	-0.302	0.010
RPL11	0.823	0.913	0.905	-0.186	0.061	0.983	0.961	0.943	-0.056	0.082	0.998	1.006	1.004	0.004	0.338
ACOX1	0.959	0.973	0.934	-0.067	0.062	1.018	1.061	0.975	0.025	0.555	1.085	1.051	0.946	0.037	0.604

GARS	1.249	1.088	1.248	0.254	0.062	0.790	0.870	1.053	-0.156	0.330	0.634	0.830	0.840	-0.393	0.098
HMGB2	1.078	1.139	1.216	0.193	0.062	0.951	0.937	1.141	0.008	0.939	0.832	0.836	0.860	-0.247	0.004
RPL7	0.849	0.922	0.926	-0.155	0.063	1.357	1.159	1.242	0.322	0.039	1.551	1.330	1.364	0.497	0.018
RPL10A	0.837	0.932	0.895	-0.172	0.063	1.302	1.262	1.200	0.326	0.011	1.542	1.257	1.256	0.428	0.049
RPL35A	0.927	0.973	0.930	-0.084	0.064	1.170	1.091	1.088	0.158	0.044	1.203	1.116	1.075	0.177	0.066
CSTB	1.115	1.043	1.069	0.105	0.065	0.799	0.817	0.812	-0.305	0.001	0.645	0.721	0.712	-0.532	0.009
RBMX;RBMXL2;RBMXL1	1.232	1.077	1.172	0.213	0.065	0.601	0.640	0.694	-0.635	0.009	0.480	0.509	0.559	-0.958	0.004
HNRNPA2B1	1.104	1.038	1.066	0.096	0.065	1.315	1.407	1.491	0.488	0.011	1.082	1.332	1.277	0.293	0.085
PSMB6	1.127	1.189	1.065	0.171	0.065	0.930	1.093	1.012	0.014	0.857	0.821	0.927	0.922	-0.170	0.096
TRMT6	1.131	1.044	1.117	0.133	0.065	1.211	1.359	1.171	0.316	0.040	0.987	0.990	0.939	-0.042	0.236
RPL27A	0.899	0.881	0.957	-0.133	0.065	1.038	1.022	1.023	0.039	0.033	1.204	1.117	1.022	0.153	0.154

ALYREF	0.913	0.912	0.824	-0.181	0.066	0.444	0.254	0.472	-1.409	0.038	0.432	0.276	0.532	-1.326	0.042
WDR11	0.857	0.885	0.748	-0.273	0.067	0.963	0.590	0.457	-0.648	0.177	1.163	0.753	0.609	-0.302	0.386
NIPSNAP 3A;NIPSN AP3B	1.212	1.755	1.582	0.583	0.067	1.560	1.231	1.957	0.637	0.081	1.264	0.668	1.159	-0.010	0.975
ORF1	0.915	0.860	0.787	-0.231	0.068	0.836	0.855	0.815	-0.260	0.006	0.974	0.961	0.988	-0.038	0.083
PHGDH	1.087	1.035	1.106	0.105	0.068	0.952	1.205	1.021	0.076	0.529	0.940	0.988	0.924	-0.074	0.125
SKA2	1.390	1.124	1.250	0.322	0.068	1.000	1.166	0.863	0.003	0.984	0.727	0.875	0.618	-0.449	0.090
PAPSS2	1.207	1.686	1.407	0.506	0.068	1.156	0.854	1.349	0.137	0.552	0.934	0.668	0.919	-0.268	0.232
SURF2	0.750	0.650	0.858	-0.419	0.069	0.812	0.834	0.805	-0.292	0.003	1.014	1.212	1.104	0.147	0.188
RPSA;RP SAP58	0.943	0.930	0.870	-0.130	0.069	1.220	1.101	1.195	0.227	0.038	1.290	1.243	1.332	0.365	0.006
SKIV2L	0.901	0.821	0.744	-0.287	0.070	1.290	1.195	1.397	0.369	0.030	1.396	1.491	1.646	0.592	0.013
GDI2;GDI	0.851	0.784	0.656	-0.397	0.070	0.705	0.742	0.889	-0.369	0.068	1.181	0.836	1.008	-0.003	0.987

1															
TJP2	1.462	1.142	1.289	0.369	0.070	0.875	0.762	0.847	-0.275	0.045	0.511	0.750	0.606	-0.702	0.048
PET112	1.362	1.107	1.285	0.318	0.070	0.820	0.874	1.041	-0.141	0.305	0.691	0.767	0.775	-0.428	0.015
PRPF8	0.942	0.864	0.833	-0.187	0.071	0.804	0.782	0.676	-0.412	0.034	0.912	0.920	0.828	-0.176	0.069
C11orf48	0.816	0.921	0.778	-0.258	0.071	0.902	0.939	0.875	-0.144	0.039	1.076	1.042	1.021	0.065	0.100
OSBPL2	1.234	1.653	1.901	0.652	0.071	1.604	1.778	1.672	0.751	0.003	1.068	1.272	1.014	0.154	0.261
PDIA5	0.840	0.944	0.880	-0.173	0.072	1.123	1.012	1.101	0.108	0.143	1.291	1.148	1.147	0.255	0.046
EIF4G2	1.145	1.142	1.046	0.151	0.072	1.031	1.063	1.061	0.073	0.036	0.931	1.013	1.003	-0.026	0.565
RBM8A	0.732	0.891	0.833	-0.294	0.072	0.370	0.777	0.974	-0.613	0.283	0.478	0.769	0.668	-0.675	0.080
ZC3H15	1.483	1.218	1.179	0.363	0.072	0.798	0.668	0.737	-0.449	0.026	0.506	0.564	0.565	-0.878	0.004
FUS	1.062	1.163	1.207	0.192	0.073	1.588	1.749	1.822	0.780	0.006	1.494	1.395	1.252	0.461	0.025
RRM1	0.902	0.941	0.963	-0.097	0.073	1.055	1.057	1.008	0.056	0.130	1.059	1.131	1.129	0.145	0.043
RPS26;RP	0.815	0.892	0.925	-0.191	0.073	0.800	0.866	0.886	-0.235	0.035	1.039	0.948	1.230	0.092	0.490

S26P11															
ACADVL	1.193	1.172	1.445	0.338	0.073	2.274	2.298	2.562	1.247	0.002	1.833	2.014	1.599	0.854	0.013
SNAPIN	1.128	1.220	1.074	0.188	0.073	0.875	1.112	1.050	0.010	0.931	0.752	0.904	0.831	-0.275	0.070
PRDX1	1.025	1.082	1.075	0.085	0.074	0.897	0.989	0.953	-0.081	0.188	0.853	0.875	0.794	-0.251	0.027
TKT	0.875	0.958	0.902	-0.134	0.074	1.080	1.064	0.962	0.048	0.453	1.185	1.147	1.061	0.176	0.065
EIF2D	0.867	0.690	0.635	-0.466	0.074	0.435	0.392	0.592	-1.102	0.025	0.579	0.559	0.874	-0.608	0.099
UBR4	0.929	0.921	0.841	-0.159	0.074	0.707	0.799	0.604	-0.517	0.048	0.771	0.813	0.658	-0.426	0.043
TP53RK	1.223	1.066	1.169	0.203	0.074	1.191	1.153	1.363	0.301	0.055	0.973	1.006	1.099	0.035	0.571
PDIA4	1.102	1.031	1.094	0.105	0.075	0.954	0.976	1.088	0.006	0.927	0.809	0.970	0.984	-0.124	0.306
S100A16	1.139	1.091	1.044	0.125	0.075	0.939	1.091	0.953	-0.011	0.884	0.893	0.884	0.789	-0.228	0.058
CASK	1.157	1.076	1.060	0.133	0.076	0.873	0.767	0.767	-0.320	0.035	0.674	0.813	0.680	-0.475	0.032
EIF3C;EIF 3CL	0.915	0.905	0.810	-0.192	0.076	0.873	0.871	0.694	-0.308	0.107	0.906	0.960	0.772	-0.192	0.178

APEX1	0.904	0.968	0.934	-0.097	0.076	0.862	0.831	0.840	-0.244	0.004	0.831	0.930	0.905	-0.172	0.073
EIF4H	0.881	0.693	0.807	-0.340	0.078	0.327	0.312	0.457	-1.473	0.014	0.293	0.349	0.450	-1.479	0.014
RPS2	0.949	0.907	0.856	-0.147	0.078	1.205	1.093	1.092	0.175	0.066	1.328	1.234	1.279	0.356	0.007
PPIF	1.106	1.341	1.398	0.351	0.078	1.448	1.197	1.238	0.367	0.049	1.012	1.030	0.718	-0.139	0.498
SCYL1	1.081	1.295	1.245	0.267	0.078	1.412	1.590	1.463	0.572	0.008	1.331	1.045	1.249	0.265	0.126
PUS10	1.175	1.653	1.690	0.571	0.078	1.882	1.805	2.008	0.923	0.002	1.176	1.174	1.379	0.310	0.057
ACOT13	1.128	1.222	1.070	0.187	0.078	0.935	1.117	0.964	0.003	0.971	0.792	0.840	0.836	-0.283	0.009
SNRNP200	0.948	0.873	0.837	-0.177	0.079	1.304	1.121	1.108	0.232	0.092	1.501	1.281	1.340	0.455	0.022
CUL1	0.901	0.912	0.799	-0.202	0.080	1.079	0.905	0.952	-0.035	0.687	0.985	1.125	1.001	0.050	0.498
PSMA5	1.093	1.160	1.051	0.137	0.080	0.971	1.193	1.002	0.071	0.521	0.783	0.998	0.838	-0.203	0.191
FASN	1.247	1.067	1.202	0.226	0.080	0.796	0.764	0.854	-0.315	0.022	0.675	0.643	0.744	-0.543	0.013
GTF2I	1.193	1.055	1.133	0.170	0.080	1.361	1.205	1.764	0.511	0.088	1.232	1.158	1.207	0.261	0.010

NUDT16	1.119	1.045	1.161	0.147	0.081	0.837	0.878	1.047	-0.126	0.328	0.724	0.777	0.606	-0.518	0.040
TSEN34	1.349	1.486	1.123	0.390	0.081	1.368	1.777	0.988	0.422	0.227	0.899	1.213	0.952	0.018	0.902
TXNRD1	0.919	0.909	0.813	-0.186	0.081	0.694	0.697	0.680	-0.535	0.000	0.663	0.759	0.839	-0.414	0.052
	1.224	1.349	1.095	0.285	0.082	1.497	1.357	1.466	0.525	0.007	1.194	1.078	1.237	0.224	0.064
H6PD	1.350	1.185	1.107	0.275	0.082	1.377	1.057	1.601	0.407	0.146	1.119	0.903	1.415	0.172	0.455
RPS14	0.928	0.955	0.875	-0.122	0.083	1.025	1.030	1.017	0.034	0.025	1.048	1.048	1.026	0.057	0.029
PSMG1	1.812	1.195	1.481	0.560	0.084	0.986	1.172	3.488	0.670	0.361	0.679	1.239	1.261	0.029	0.931
PHAX	1.112	1.200	1.379	0.293	0.084	1.512	1.868	2.027	0.839	0.022	1.368	1.443	1.351	0.472	0.004
DTYMK	1.274	1.083	1.335	0.294	0.084	0.919	1.010	0.870	-0.103	0.243	0.797	0.844	0.640	-0.405	0.079
EIF3S3;EIF3H	0.960	0.937	0.887	-0.108	0.085	0.846	0.904	0.889	-0.186	0.023	0.949	0.960	0.938	-0.075	0.015
FAM120A	0.914	0.789	0.893	-0.212	0.085	1.015	0.856	0.878	-0.131	0.230	1.000	0.742	0.889	-0.201	0.251
RBM3	1.072	1.031	1.029	0.062	0.086	0.857	0.829	0.948	-0.190	0.082	0.738	0.798	0.788	-0.369	0.009

BLVRB	1.009	1.032	1.029	0.033	0.086	0.945	0.907	1.009	-0.070	0.256	0.884	0.908	0.958	-0.127	0.066
RPS17;RPS17L	0.885	0.953	0.842	-0.165	0.086	1.021	1.014	0.979	0.006	0.773	1.070	1.051	1.110	0.107	0.045
DECR2	0.761	0.894	0.890	-0.241	0.087	0.816	0.910	0.897	-0.195	0.058	0.878	0.996	0.706	-0.232	0.251
P4HB	1.221	1.131	1.062	0.184	0.087	0.940	1.022	0.900	-0.070	0.324	0.777	0.911	0.830	-0.256	0.062
RPL27	0.885	0.965	0.925	-0.113	0.087	1.228	1.095	1.168	0.217	0.045	1.230	1.175	1.181	0.257	0.007
PGK1	0.710	0.781	0.910	-0.329	0.087	0.760	0.941	0.824	-0.255	0.105	0.975	1.115	0.896	-0.012	0.906
GCN1L1	0.905	0.910	0.792	-0.206	0.087	0.433	0.466	0.341	-1.286	0.011	0.526	0.520	0.473	-0.984	0.002
URGCP	1.112	1.454	1.485	0.421	0.088	2.108	2.376	2.428	1.202	0.003	1.718	1.456	1.544	0.650	0.011
PPIH	1.279	1.133	1.089	0.219	0.088	0.982	0.764	0.641	-0.352	0.187	0.570	0.681	0.570	-0.725	0.014
PC	1.183	1.223	1.055	0.203	0.088	1.335	1.356	1.465	0.469	0.008	1.055	1.008	0.996	0.027	0.394
AP1G1	1.093	1.142	1.300	0.233	0.090	1.516	1.380	1.706	0.612	0.020	1.305	1.237	1.114	0.282	0.052
CMC1	0.882	0.842	0.955	-0.165	0.090	0.674	0.647	0.763	-0.529	0.018	0.741	0.816	0.805	-0.346	0.015

WIBG	0.638	0.803	0.473	-0.681	0.091	0.397	0.446	0.180	-1.656	0.056	0.500	0.591	0.496	-0.924	0.008
TSN	1.216	1.197	1.051	0.204	0.092	0.480	0.391	0.443	-1.196	0.005	0.343	0.318	0.364	-1.551	0.001
DYNLT1	1.047	1.016	1.063	0.059	0.093	0.980	0.953	1.045	-0.012	0.792	0.897	0.968	0.945	-0.095	0.099
EIF3F	0.950	0.965	0.901	-0.092	0.093	0.915	0.935	0.888	-0.132	0.026	0.953	0.954	0.985	-0.053	0.076
RPS27L	0.905	0.848	0.731	-0.278	0.093	0.946	1.085	0.832	-0.075	0.565	0.875	1.013	1.205	0.031	0.835
METTL1	1.380	1.731	1.173	0.496	0.093	2.108	2.229	1.604	0.971	0.022	1.317	1.312	1.288	0.384	0.001
TUBG1;TUBG2	0.978	0.961	0.929	-0.065	0.093	0.945	1.009	0.916	-0.065	0.254	1.012	0.937	0.884	-0.085	0.273
CDK1	1.270	1.184	1.064	0.226	0.093	1.060	0.964	0.914	-0.033	0.654	0.883	0.972	0.908	-0.120	0.101
H2AFZ;H2AFV	1.229	1.092	1.382	0.297	0.094	0.961	0.897	1.317	0.061	0.754	0.653	0.782	0.689	-0.502	0.023
RPL30	0.848	0.951	0.914	-0.147	0.094	1.131	1.110	1.124	0.166	0.002	1.136	1.079	1.094	0.141	0.024
PATL1	0.967	0.874	0.906	-0.128	0.094	0.657	0.620	0.681	-0.617	0.004	0.659	0.646	0.707	-0.577	0.005

RPS20	0.940	0.958	0.880	-0.112	0.094	1.059	1.063	1.008	0.061	0.132	1.095	1.097	1.077	0.124	0.005
LAP3	1.320	1.071	1.287	0.288	0.094	2.122	2.209	1.710	1.001	0.013	2.133	2.076	1.264	0.828	0.078
RFC2	1.351	1.122	1.562	0.415	0.096	1.279	1.155	1.351	0.332	0.038	1.065	0.885	0.929	-0.064	0.508
DUS2L	1.189	1.057	1.090	0.152	0.096	0.782	0.841	0.730	-0.353	0.027	0.615	0.857	0.686	-0.489	0.073
PDCD5	0.719	0.915	0.687	-0.383	0.097	0.647	0.792	0.702	-0.492	0.028	0.903	0.902	0.876	-0.162	0.008
EIF1AX;EIF1AY	0.948	0.930	0.855	-0.136	0.097	0.723	0.782	0.793	-0.387	0.011	0.751	0.800	0.820	-0.341	0.012
UBE2I	1.088	1.020	1.066	0.081	0.097	1.001	1.040	0.981	0.010	0.726	0.912	0.975	0.843	-0.138	0.150
STAT1	0.952	0.984	0.937	-0.063	0.098	1.204	1.203	1.062	0.207	0.075	1.186	1.268	1.096	0.241	0.058
FEN1	0.886	0.966	0.934	-0.107	0.098	0.721	0.828	0.763	-0.378	0.023	0.778	0.852	0.802	-0.304	0.016
CSNK2B	1.177	1.040	1.125	0.153	0.099	0.663	0.825	0.892	-0.345	0.115	0.560	0.784	0.753	-0.532	0.074
RPL37A	0.937	0.869	0.955	-0.121	0.099	1.058	1.124	1.393	0.242	0.182	1.128	1.176	1.783	0.414	0.189
TACO1	1.093	1.468	1.447	0.405	0.100	1.185	1.450	1.439	0.435	0.045	0.999	0.988	0.951	-0.031	0.291

MARS	0.969	0.940	0.895	-0.098	0.100	0.775	0.758	0.928	-0.292	0.087	0.977	0.927	0.937	-0.079	0.078
NARS2	0.949	0.801	0.793	-0.243	0.101	1.178	1.158	1.063	0.179	0.059	1.129	1.323	1.506	0.389	0.083
TYW3	1.041	1.065	1.138	0.112	0.101	1.199	1.161	1.090	0.201	0.038	1.052	0.910	0.786	-0.137	0.377
DUSP9	1.133	1.087	1.030	0.115	0.103	0.950	1.727	2.195	0.616	0.229	0.756	1.431	1.946	0.358	0.467
ETFB	1.060	1.064	1.169	0.132	0.104	0.723	0.673	0.710	-0.511	0.004	0.570	0.650	0.547	-0.768	0.009
GYG1	0.911	0.661	0.745	-0.385	0.104	0.626	0.485	0.551	-0.860	0.015	0.766	0.746	0.800	-0.376	0.006
TBC1D23	0.774	0.905	0.910	-0.217	0.105	0.832	0.915	0.931	-0.165	0.083	0.949	1.009	0.965	-0.037	0.291
SF3B5	1.021	1.107	1.096	0.103	0.107	1.347	1.470	1.310	0.458	0.012	1.204	1.197	1.204	0.265	0.000
STX5	1.140	1.028	1.134	0.137	0.107	1.500	1.532	1.059	0.427	0.132	1.348	1.656	0.726	0.232	0.583
HMMR	0.625	0.907	0.637	-0.490	0.107	0.372	0.268	0.272	-1.736	0.008	0.767	0.288	0.522	-1.039	0.127
SRSF10;FUSIP1	0.775	0.511	0.780	-0.565	0.107	1.244	0.931	1.303	0.198	0.323	1.571	1.843	1.512	0.710	0.015
YWHAZ	1.471	1.107	1.232	0.335	0.108	0.619	0.816	0.692	-0.506	0.049	0.461	0.640	0.471	-0.950	0.025

FAM115A	1.107	1.115	1.022	0.112	0.109	0.937	1.090	1.169	0.085	0.462	0.875	0.988	1.037	-0.052	0.548
CTSC	1.268	1.223	1.049	0.234	0.109	0.872	1.050	0.845	-0.123	0.333	0.669	0.846	0.710	-0.439	0.050
PAICS	0.854	0.964	0.908	-0.140	0.110	0.943	0.902	0.890	-0.134	0.033	1.097	0.987	0.949	0.013	0.852
ALDOC	0.898	0.979	0.922	-0.101	0.110	0.689	0.710	0.678	-0.531	0.001	0.769	0.762	0.771	-0.383	0.000
QARS	1.060	1.033	1.015	0.051	0.110	1.254	1.184	0.892	0.134	0.469	1.175	1.162	0.954	0.127	0.323
VPS29	1.039	1.218	1.200	0.201	0.110	1.062	1.189	1.080	0.149	0.100	0.903	0.968	0.832	-0.153	0.135
CTSB	0.959	0.938	0.869	-0.118	0.111	0.848	0.881	0.901	-0.191	0.017	0.848	0.820	1.052	-0.150	0.314
ILK	1.109	1.119	1.022	0.114	0.111	0.880	0.846	0.765	-0.271	0.047	0.764	0.742	0.763	-0.403	0.001
41889	1.319	1.062	1.192	0.246	0.112	1.392	1.340	1.308	0.429	0.004	1.039	1.195	1.123	0.159	0.112
BLOC1S1	1.094	1.365	1.155	0.262	0.112	1.015	1.320	1.133	0.201	0.209	0.837	0.896	0.944	-0.166	0.081
MAP1B	0.883	0.655	0.541	-0.559	0.113	0.327	0.334	0.204	-1.828	0.016	0.476	0.498	0.809	-0.794	0.083
RPS21	0.930	0.963	0.867	-0.122	0.113	0.999	0.978	0.872	-0.077	0.333	1.000	0.989	0.989	-0.010	0.184
RPLP1	0.819	0.817	0.962	-0.212	0.113	0.924	0.983	0.981	-0.056	0.196	1.029	1.094	0.912	0.012	0.887

PWP1	1.239	1.992	1.339	0.575	0.113	1.757	2.192	2.244	1.037	0.012	1.137	1.159	1.470	0.318	0.116
HSPA9	1.379	1.162	1.094	0.270	0.114	1.155	0.986	1.040	0.081	0.351	0.914	0.959	0.893	-0.118	0.061
ERP29	1.008	1.040	1.026	0.035	0.115	1.108	1.080	0.997	0.085	0.206	1.080	0.980	0.897	-0.025	0.778
ZC3HAV1	0.856	0.919	0.963	-0.133	0.115	0.770	0.958	0.963	-0.164	0.264	0.961	1.110	0.853	-0.046	0.718
EIF2S2	0.957	0.970	0.902	-0.086	0.115	0.847	0.702	0.717	-0.410	0.041	0.947	0.729	0.778	-0.299	0.119
FUBP3	1.607	1.527	1.089	0.472	0.116	0.801	0.900	0.640	-0.372	0.124	0.479	0.624	0.540	-0.877	0.015
CYFIP1	1.019	1.082	1.044	0.067	0.116	1.220	1.154	1.208	0.255	0.009	1.177	1.093	1.144	0.186	0.027
MAP2K1	1.371	1.281	1.059	0.298	0.116	1.441	1.220	1.301	0.398	0.030	0.861	0.975	1.256	0.025	0.888
DDX39A; DDX39	1.340	1.125	1.097	0.242	0.116	1.511	1.455	1.278	0.497	0.021	1.237	1.186	0.961	0.165	0.279
HSPA8	0.971	0.925	0.974	-0.064	0.117	0.884	0.839	0.831	-0.233	0.014	0.832	0.907	0.807	-0.238	0.042
C14orf166	1.017	1.077	1.044	0.064	0.117	0.977	0.945	1.000	-0.038	0.249	0.999	0.901	0.904	-0.099	0.179
CCT8	1.008	1.032	1.045	0.040	0.118	1.231	1.250	1.265	0.320	0.001	1.162	1.223	1.181	0.249	0.007

HSPE1	0.921	0.764	0.895	-0.222	0.118	0.930	1.079	1.168	0.076	0.514	1.054	1.322	1.288	0.281	0.112
KIAA0664	1.035	1.190	1.118	0.154	0.118	0.482	0.938	0.993	-0.385	0.369	0.493	0.806	0.864	-0.514	0.181
NMD3	0.717	0.636	0.922	-0.416	0.119	1.157	1.097	1.398	0.275	0.122	1.516	1.806	1.463	0.667	0.019
CDC42BPB	0.666	0.566	0.902	-0.519	0.119	0.821	0.334	0.715	-0.784	0.192	0.779	0.672	0.706	-0.479	0.017
IDH2	1.166	1.244	1.683	0.429	0.119	1.248	1.135	1.258	0.278	0.028	1.059	1.061	0.740	-0.089	0.660
MRPL11	1.043	1.050	1.137	0.105	0.120	0.752	0.865	0.870	-0.274	0.058	0.730	0.804	0.780	-0.376	0.012
PPM1G	1.168	1.032	1.207	0.181	0.120	0.541	0.648	0.644	-0.716	0.014	0.440	0.678	0.535	-0.883	0.039
MTTP	1.090	1.142	1.026	0.118	0.121	1.218	1.156	1.260	0.276	0.017	0.999	1.106	1.188	0.131	0.213
CTU2	1.039	1.049	1.131	0.101	0.121	0.644	0.695	0.747	-0.527	0.013	0.547	0.616	0.614	-0.758	0.005
IGF2BP1	1.137	1.170	1.026	0.150	0.121	1.035	1.031	1.106	0.079	0.136	0.811	0.861	0.930	-0.208	0.069
SPATS2L	1.039	1.021	1.009	0.032	0.121	1.062	1.109	1.038	0.097	0.075	0.858	0.955	0.942	-0.125	0.125
CSNK2A1; hCG_2198	1.109	1.029	1.170	0.139	0.122	0.805	0.901	0.967	-0.171	0.157	0.708	0.873	0.817	-0.329	0.066

4															
CCT2	1.019	1.086	1.118	0.102	0.124	1.191	1.251	1.313	0.323	0.015	1.177	1.208	1.242	0.273	0.007
PLEC	1.356	1.078	1.153	0.251	0.125	1.776	1.330	1.001	0.414	0.225	1.256	1.126	0.925	0.129	0.423
PIN4	0.905	0.859	0.697	-0.294	0.125	0.626	0.638	0.620	-0.671	0.000	0.750	0.853	0.920	-0.255	0.097
NQO1	1.027	1.067	1.132	0.104	0.126	1.011	1.123	1.018	0.070	0.288	0.908	1.070	0.957	-0.036	0.661
QKI	1.102	1.638	1.889	0.590	0.127	2.532	3.620	3.854	1.714	0.012	1.565	1.602	1.699	0.697	0.003
BTF3	0.980	0.985	0.949	-0.042	0.128	0.956	1.038	1.032	0.011	0.796	0.981	0.962	0.943	-0.056	0.076
COPB2	1.030	1.061	1.014	0.049	0.128	1.359	1.416	1.372	0.467	0.001	1.234	1.322	1.268	0.350	0.007
CUL2	1.032	1.177	1.234	0.195	0.128	1.121	1.377	1.285	0.330	0.063	0.994	1.063	1.120	0.081	0.247
SKIV2L2	0.913	0.985	0.939	-0.081	0.128	2.033	1.513	1.361	0.688	0.058	1.898	1.814	1.470	0.780	0.021
NCAPG	0.811	0.971	0.835	-0.202	0.129	0.862	0.864	0.914	-0.185	0.021	1.006	0.729	0.969	-0.164	0.380
SKP1	0.969	0.821	0.797	-0.219	0.129	0.579	0.624	0.678	-0.677	0.009	0.600	0.727	0.747	-0.540	0.032
DHX29	0.972	0.877	0.830	-0.167	0.129	0.797	0.694	0.560	-0.564	0.062	0.828	0.825	0.654	-0.388	0.075

TRMT61A	1.181	1.080	1.407	0.281	0.129	1.028	1.261	1.516	0.325	0.182	0.808	1.258	1.032	0.023	0.914
WDR1	1.013	1.035	1.067	0.054	0.130	1.265	1.266	1.230	0.326	0.002	1.170	1.233	1.063	0.206	0.081
IGF2BP3	0.966	0.898	0.828	-0.159	0.131	1.043	0.839	0.825	-0.157	0.288	0.859	0.880	0.925	-0.172	0.032
ELAC2	1.113	1.114	1.014	0.110	0.133	1.022	1.083	0.923	0.010	0.894	0.865	0.956	0.849	-0.170	0.086
SFPQ	1.006	1.038	1.048	0.043	0.133	2.102	2.000	2.086	1.044	0.000	2.188	1.876	1.889	0.985	0.005
SAR1A;SAR1B	1.080	1.097	1.298	0.207	0.135	1.869	1.704	2.766	1.046	0.039	1.601	1.393	2.181	0.761	0.058
SRSF6	1.295	1.109	1.069	0.206	0.135	2.340	2.122	2.275	1.166	0.001	1.805	2.242	1.929	0.988	0.009
MARK3	0.954	0.824	0.923	-0.154	0.136	0.614	0.501	0.743	-0.710	0.050	0.632	0.676	0.838	-0.494	0.056
EIF1B	0.846	0.973	0.808	-0.196	0.136	0.794	0.846	0.838	-0.277	0.010	0.775	0.773	0.901	-0.296	0.056
RPF2;BXDC1	0.846	0.868	0.620	-0.379	0.136	1.470	1.593	1.499	0.604	0.003	1.599	1.738	2.135	0.856	0.020
GRN	1.031	1.211	1.272	0.222	0.137	0.699	0.853	0.794	-0.360	0.050	0.637	0.904	0.621	-0.495	0.105

TDRD7	0.603	0.633	0.941	-0.492	0.137	0.412	0.348	0.478	-1.289	0.010	0.582	0.561	0.562	-0.815	0.000
CPOX	1.100	1.242	1.051	0.174	0.137	0.629	0.598	0.936	-0.503	0.133	0.626	0.452	0.967	-0.623	0.189
PPID	0.761	0.952	0.864	-0.225	0.137	0.914	1.041	0.772	-0.148	0.357	1.151	1.260	0.858	0.105	0.595
EDC3	0.989	0.913	0.920	-0.089	0.137	0.738	0.785	0.702	-0.433	0.011	0.693	0.837	0.699	-0.434	0.040
CTPS	1.052	1.289	1.133	0.207	0.137	1.059	1.237	1.098	0.175	0.124	0.954	0.911	1.031	-0.053	0.416
ARPC4;ARPC4-TTLL3	1.017	1.144	1.114	0.124	0.137	1.005	1.102	1.068	0.081	0.176	0.949	0.951	0.853	-0.126	0.138
KDELC1	1.285	1.802	1.147	0.469	0.139	1.262	1.438	1.219	0.381	0.034	1.033	0.958	1.042	0.015	0.743
DNAJC21	0.904	0.875	0.984	-0.121	0.139	1.114	0.833	1.084	0.003	0.983	1.147	0.831	1.112	0.028	0.868
DHX57	0.668	0.945	0.615	-0.455	0.139	0.695	0.739	0.841	-0.403	0.038	0.991	0.833	1.518	0.108	0.715
TUBB6	1.053	1.367	1.194	0.260	0.139	0.912	1.442	1.218	0.226	0.362	0.826	1.064	0.846	-0.143	0.346
ACAA1	0.962	0.986	0.927	-0.062	0.140	0.775	0.749	0.675	-0.450	0.018	0.825	0.728	0.739	-0.391	0.021

SRPK2	0.963	0.766	0.720	-0.304	0.140	1.513	0.777	0.734	-0.071	0.852	1.631	0.966	0.923	0.180	0.564
EIF3M	0.934	0.971	0.865	-0.116	0.141	0.884	0.986	0.902	-0.116	0.138	1.003	0.917	1.033	-0.025	0.677
ZCCHC6	0.959	0.952	0.864	-0.114	0.141	0.714	1.310	0.880	-0.094	0.750	0.767	1.069	1.121	-0.040	0.837
EIF2S3;EIF2S3L	1.018	1.038	1.008	0.030	0.141	1.038	1.010	1.008	0.026	0.199	1.019	0.930	1.001	-0.025	0.594
SEC24A	1.095	1.172	1.025	0.132	0.142	0.987	0.957	0.871	-0.094	0.225	1.015	0.845	0.828	-0.165	0.221
PIN1	1.383	1.519	1.047	0.379	0.143	1.247	1.241	0.924	0.172	0.353	0.752	0.678	0.838	-0.409	0.044
YWHAQ	1.722	1.080	1.391	0.457	0.143	0.820	0.874	0.587	-0.417	0.144	0.477	0.740	0.375	-0.973	0.077
CCDC72	0.938	0.727	0.867	-0.252	0.146	0.439	0.355	0.437	-1.292	0.006	0.450	0.480	0.487	-1.083	0.001
POLR2H	1.194	1.123	1.600	0.367	0.146	1.462	1.618	1.788	0.693	0.014	1.138	1.331	1.040	0.219	0.170
HSP90B1	1.142	1.017	1.087	0.112	0.146	0.791	0.874	0.853	-0.254	0.028	0.661	0.857	0.752	-0.410	0.063
SPATA5L1	0.632	0.951	0.577	-0.509	0.148	1.090	0.968	0.925	-0.011	0.888	1.561	1.054	1.289	0.361	0.158

UPF2	0.730	0.872	0.939	-0.247	0.148	0.343	0.665	0.551	-0.998	0.072	0.498	0.755	0.534	-0.772	0.053
RPL36A	1.084	1.079	1.295	0.199	0.148	1.641	1.547	1.396	0.608	0.012	1.450	1.462	1.150	0.429	0.063
STXBP2	1.030	1.098	1.203	0.148	0.150	0.750	0.965	0.950	-0.180	0.266	0.625	0.727	0.818	-0.476	0.051
TIAL1	0.977	0.827	0.891	-0.159	0.151	0.952	1.076	0.865	-0.058	0.588	0.937	1.167	0.987	0.036	0.739
DEK	0.915	0.766	0.932	-0.204	0.152	1.691	1.993	1.769	0.859	0.007	2.002	2.347	1.827	1.034	0.010
CKS1B	1.201	1.323	1.031	0.237	0.152	0.853	0.839	0.723	-0.317	0.053	0.709	0.601	0.665	-0.606	0.013
SAMD4B	1.460	1.189	1.069	0.297	0.153	0.832	0.939	0.765	-0.248	0.101	0.562	0.823	0.774	-0.494	0.102
PSMA4	1.014	1.203	1.168	0.170	0.155	0.894	1.165	1.177	0.098	0.529	0.888	0.866	1.097	-0.082	0.530
ACSL4	0.956	0.960	0.997	-0.043	0.156	1.122	1.055	1.061	0.109	0.062	1.136	1.006	0.906	0.017	0.876
PPIC	0.959	0.934	0.993	-0.057	0.156	0.942	0.990	1.097	0.011	0.881	0.858	1.183	0.967	-0.009	0.953
QTRTD1	1.025	1.034	1.104	0.076	0.156	0.688	0.854	0.872	-0.321	0.099	0.622	0.761	0.810	-0.461	0.057
NCBP2	0.976	0.936	0.865	-0.114	0.157	0.929	0.932	0.905	-0.117	0.012	0.986	0.938	0.861	-0.109	0.195
PACSIN3	0.713	0.972	0.788	-0.291	0.157	0.508	0.760	0.863	-0.528	0.149	1.253	0.853	0.954	0.010	0.959

HSP90AB1;HSP90AB3P	1.108	1.015	1.053	0.081	0.157	0.730	0.951	0.760	-0.308	0.122	0.626	0.942	0.718	-0.413	0.140
THUMPD3	1.070	1.008	1.099	0.081	0.157	0.718	1.042	1.115	-0.087	0.703	0.733	1.079	0.747	-0.253	0.299
VCP	1.177	1.019	1.097	0.132	0.158	0.500	0.644	0.654	-0.749	0.027	0.406	0.652	0.570	-0.910	0.046
COMMD6	1.178	1.754	1.167	0.423	0.161	1.002	0.792	1.126	-0.055	0.749	0.820	0.642	0.993	-0.312	0.228
C22orf28	1.091	1.103	1.006	0.092	0.161	1.060	1.049	1.135	0.112	0.088	1.007	0.945	1.107	0.025	0.743
NCBP1	0.949	0.902	0.766	-0.203	0.161	1.143	1.194	0.598	-0.097	0.791	1.177	1.330	0.699	0.044	0.892
TPP1	0.974	0.986	0.933	-0.053	0.161	1.027	1.069	1.126	0.102	0.119	1.093	1.139	1.129	0.164	0.012
STIP1	0.991	0.852	0.844	-0.163	0.162	0.586	0.766	0.589	-0.640	0.038	0.593	0.802	0.679	-0.544	0.049
YWHAE	1.377	1.290	1.019	0.285	0.163	0.778	0.810	0.616	-0.456	0.066	0.529	0.568	0.590	-0.831	0.003
QTRT1	1.038	1.030	1.125	0.088	0.163	0.702	0.900	0.961	-0.240	0.223	0.664	0.740	0.850	-0.420	0.055
ENO1	1.618	1.573	1.025	0.461	0.163	1.152	1.515	0.990	0.263	0.281	0.868	0.875	0.859	-0.205	0.001

LYAR	1.045	1.152	1.355	0.236	0.164	2.011	2.098	1.990	1.023	0.001	2.090	1.569	1.527	0.775	0.033
NDUFAB1	1.552	1.557	1.022	0.435	0.164	0.901	1.272	0.396	-0.379	0.527	0.571	0.684	0.538	-0.750	0.019
IMPDH2	1.044	1.037	1.002	0.039	0.164	1.177	1.240	1.633	0.418	0.104	1.140	1.499	1.640	0.495	0.088
PARVA	0.966	0.763	0.872	-0.213	0.165	0.742	0.685	0.764	-0.455	0.011	0.797	0.967	0.767	-0.253	0.134
VAV2	0.816	0.987	0.870	-0.171	0.168	0.720	0.696	0.835	-0.419	0.035	0.876	0.815	0.898	-0.214	0.036
ALDOA	0.997	0.947	0.958	-0.048	0.168	0.827	0.822	0.840	-0.270	0.001	0.842	0.866	0.837	-0.237	0.004
SNRNP70	0.833	0.980	0.909	-0.143	0.169	1.702	1.845	1.991	0.881	0.005	1.897	1.927	2.106	0.982	0.002
MANF	1.025	1.006	1.051	0.039	0.170	0.961	0.972	1.008	-0.029	0.298	0.851	0.936	0.885	-0.168	0.052
KIAA1967	1.029	1.142	1.044	0.099	0.172	1.898	1.955	1.749	0.899	0.003	1.673	1.568	1.575	0.682	0.002
PACSIN2	1.084	1.318	1.069	0.204	0.172	1.266	1.309	1.259	0.354	0.002	1.063	0.954	1.213	0.099	0.426
SF3B14	0.912	0.942	0.754	-0.209	0.172	0.889	0.914	1.149	-0.033	0.804	0.921	1.004	1.768	0.237	0.506
LARS	0.998	0.947	0.947	-0.053	0.172	1.150	1.077	1.172	0.179	0.040	1.111	1.159	1.216	0.215	0.029
C12orf29	1.107	1.009	1.162	0.125	0.172	0.719	0.769	0.896	-0.337	0.070	0.717	0.842	0.709	-0.408	0.036

TSPAN10	0.942	0.879	0.984	-0.098	0.173	1.008	1.110	1.209	0.145	0.195	1.071	1.046	1.261	0.166	0.189
NAA20	1.118	1.003	1.129	0.113	0.173	1.063	0.943	1.145	0.066	0.504	0.884	0.947	0.899	-0.137	0.045
CPSF7	0.987	0.640	0.685	-0.403	0.174	0.772	0.972	1.042	-0.118	0.460	0.753	1.550	1.390	0.233	0.547
TLN1	0.963	0.934	0.821	-0.146	0.174	0.378	0.351	0.323	-1.515	0.002	0.424	0.366	0.409	-1.326	0.002
GPD1L	0.878	0.881	0.613	-0.359	0.175	1.224	1.001	0.903	0.048	0.743	1.239	1.115	1.466	0.339	0.099
USP16	0.706	0.949	0.867	-0.261	0.175	0.821	0.799	0.947	-0.229	0.095	1.156	0.982	1.092	0.103	0.274
RPLP2	0.868	0.951	0.974	-0.105	0.175	0.905	0.984	0.989	-0.061	0.281	0.911	0.954	0.934	-0.101	0.034
CHMP2B	1.249	1.232	1.004	0.209	0.176	1.058	1.124	0.759	-0.050	0.804	0.949	0.935	0.714	-0.219	0.242
DOCK7	1.035	1.446	1.211	0.286	0.176	1.235	1.390	1.426	0.431	0.021	1.131	0.999	1.056	0.085	0.241
SNRPE	0.890	0.930	0.993	-0.094	0.177	1.996	1.966	1.813	0.943	0.002	1.916	1.957	1.657	0.878	0.007
VPS13C	1.047	1.170	1.036	0.115	0.178	0.509	0.545	0.362	-1.106	0.026	0.536	0.509	0.380	-1.090	0.019
DIS3L2	0.978	0.799	0.895	-0.172	0.178	0.998	1.101	0.991	0.041	0.495	1.018	1.317	1.105	0.189	0.227
AMBP	0.690	0.705	0.998	-0.347	0.181	0.948	0.775	5.645	0.684	0.531	1.132	1.192	5.536	0.967	0.327

PLS1	1.025	1.157	1.053	0.107	0.182	1.082	0.897	0.963	-0.033	0.718	1.227	0.869	0.809	-0.071	0.740
CNPY2	1.000	0.877	0.867	-0.132	0.184	0.532	0.646	0.508	-0.839	0.016	0.543	0.788	0.579	-0.671	0.056
CEP78	0.916	0.722	0.929	-0.235	0.184	1.408	1.272	1.287	0.402	0.013	1.386	1.573	1.556	0.587	0.010
GRIPAP1	0.877	0.932	0.991	-0.101	0.185	1.355	1.402	1.318	0.441	0.003	1.312	1.334	1.193	0.354	0.020
KRT18	0.768	0.663	0.987	-0.330	0.187	0.578	0.810	0.358	-0.858	0.128	0.661	1.204	0.324	-0.651	0.356
GTF2B	1.030	1.118	1.026	0.080	0.187	1.062	1.306	1.075	0.192	0.186	1.115	1.259	0.982	0.154	0.275
PSMA7;PSMA8	1.000	1.119	1.145	0.119	0.188	1.015	1.127	1.033	0.080	0.230	1.006	1.046	0.846	-0.056	0.614
EIF6	0.985	0.873	0.943	-0.101	0.188	0.687	0.744	0.708	-0.489	0.005	0.742	0.815	0.683	-0.426	0.029
PDLIM5	0.932	0.987	0.863	-0.111	0.188	0.971	0.867	0.900	-0.133	0.108	0.989	0.917	0.874	-0.112	0.163
ANXA1	1.107	1.033	1.294	0.188	0.189	2.927	2.955	4.033	1.708	0.008	2.737	3.007	3.135	1.563	0.001
RPL10	1.001	0.955	0.954	-0.044	0.190	0.960	0.937	0.935	-0.083	0.021	0.963	0.944	0.903	-0.095	0.074
AP1B1	1.037	1.131	1.360	0.224	0.191	0.918	0.914	0.937	-0.116	0.009	0.818	0.898	0.654	-0.353	0.122

SARS2;FBXO17	1.096	1.019	1.026	0.065	0.191	0.960	1.010	1.000	-0.015	0.576	0.861	0.931	0.989	-0.111	0.195
ARHGEF2	1.320	1.242	0.999	0.237	0.191	2.458	1.426	1.053	0.628	0.221	1.479	1.251	0.973	0.282	0.249
AK3	0.731	0.939	0.916	-0.223	0.192	1.131	1.566	1.113	0.326	0.179	1.378	1.385	1.366	0.461	0.000
HADHA	1.260	1.054	1.707	0.393	0.192	1.393	1.456	1.308	0.469	0.009	1.135	1.189	0.859	0.071	0.676
USP39	0.913	0.995	0.953	-0.070	0.193	1.345	1.295	1.468	0.451	0.014	1.690	1.317	1.448	0.563	0.033
METAP1	1.112	1.042	1.013	0.077	0.194	1.173	1.020	0.911	0.042	0.731	0.972	0.811	1.049	-0.091	0.494
YARS	0.978	0.991	0.938	-0.046	0.195	0.860	0.830	0.878	-0.225	0.011	0.858	0.860	0.921	-0.186	0.031
PLOD3	1.006	1.102	1.050	0.073	0.195	1.268	1.296	1.028	0.252	0.142	1.151	1.117	0.983	0.112	0.248
CUL3	1.147	1.009	1.070	0.103	0.195	0.846	0.658	0.818	-0.378	0.080	0.684	0.624	0.822	-0.503	0.050
XPO5	1.251	1.043	1.065	0.158	0.196	0.756	0.612	0.446	-0.759	0.075	0.650	0.614	0.309	-1.006	0.100
PYGL	0.996	1.143	1.154	0.131	0.196	0.885	0.971	0.961	-0.092	0.162	1.039	0.890	0.866	-0.107	0.322
PSMB2	1.125	1.232	1.007	0.161	0.197	0.970	1.112	0.920	-0.004	0.965	0.821	0.917	0.749	-0.275	0.082

PSMD9	1.454	1.037	2.063	0.546	0.197	1.252	2.840	3.963	1.272	0.124	0.834	2.393	1.621	0.564	0.332
CFL1;CFL 2	1.158	1.125	1.770	0.402	0.198	1.241	2.201	1.715	0.743	0.090	1.153	1.728	0.927	0.295	0.379
EIF3G	0.934	0.961	0.795	-0.162	0.198	0.674	0.713	0.752	-0.490	0.009	0.792	0.689	0.800	-0.399	0.029
NACA	1.058	1.011	1.138	0.094	0.198	1.275	1.216	1.198	0.298	0.008	1.266	1.157	1.192	0.268	0.020
HIST1H1B	0.972	0.750	0.891	-0.208	0.199	1.363	1.467	1.527	0.537	0.008	1.434	1.825	1.801	0.745	0.022
KPNA6;K PNA5	1.106	0.998	1.149	0.114	0.200	0.538	0.617	0.560	-0.809	0.005	0.370	0.684	0.531	-0.966	0.064
C6orf130	1.000	0.926	0.891	-0.092	0.200	1.085	0.914	0.939	-0.034	0.702	1.038	1.045	1.070	0.072	0.032
CASP7	1.359	1.125	1.033	0.220	0.201	1.714	1.714	1.399	0.680	0.020	1.460	1.306	1.269	0.425	0.021
FLII	1.199	1.191	0.992	0.168	0.202	2.210	0.774	0.953	0.235	0.663	1.661	0.685	1.234	0.163	0.707
GOT2	1.080	1.320	1.050	0.194	0.203	1.168	1.496	1.150	0.335	0.112	0.904	1.059	0.961	-0.040	0.607
SNRPC	0.935	0.936	1.003	-0.063	0.204	1.615	1.627	1.754	0.735	0.003	1.541	1.662	1.786	0.731	0.007

PPIA	1.124	1.046	1.011	0.083	0.205	0.973	1.048	0.948	-0.016	0.749	0.834	0.922	0.861	-0.198	0.044
COPS2	1.047	1.002	1.024	0.034	0.205	0.451	1.133	1.021	-0.313	0.534	0.391	0.982	0.956	-0.482	0.385
PTGES3	1.173	0.992	1.172	0.149	0.205	0.654	0.792	0.759	-0.449	0.033	0.553	0.762	0.620	-0.646	0.041
RAB3IL1	0.776	0.736	1.013	-0.263	0.205	1.502	1.242	1.248	0.406	0.046	1.598	1.719	1.190	0.569	0.073
CALM2;CALM1	1.180	1.000	1.105	0.127	0.207	0.850	0.872	0.872	-0.210	0.003	0.696	0.816	0.730	-0.423	0.025
GSTCD	0.816	0.802	1.011	-0.198	0.207	0.255	0.320	0.628	-1.429	0.067	0.320	0.410	0.710	-1.141	0.078
EPB41	0.943	0.982	0.846	-0.118	0.208	1.166	1.221	1.151	0.237	0.012	1.222	1.386	1.354	0.399	0.019
NLE1	1.123	1.291	1.014	0.185	0.209	1.167	1.009	1.033	0.094	0.284	1.052	0.863	1.046	-0.025	0.818
TRIM25	0.979	1.409	1.393	0.314	0.210	2.080	2.436	2.497	1.220	0.005	2.057	1.950	1.709	0.926	0.007
ILF2	1.004	1.005	1.020	0.013	0.210	0.858	0.867	0.938	-0.173	0.051	0.843	0.871	0.889	-0.205	0.012
UBE2N;UBE2NL	0.917	0.982	0.798	-0.159	0.212	0.912	0.918	1.022	-0.075	0.292	0.929	0.906	1.100	-0.037	0.714

CTTN	0.972	0.921	0.780	-0.172	0.213	0.434	0.432	0.490	-1.148	0.003	0.448	0.512	0.559	-0.988	0.009
SCYL2	0.766	0.878	0.992	-0.194	0.213	1.060	1.237	0.794	0.019	0.928	1.324	1.294	0.724	0.103	0.751
ISG20	0.685	1.026	0.697	-0.343	0.213	0.778	1.017	0.645	-0.324	0.232	1.114	0.935	0.765	-0.109	0.558
SHC1	1.020	1.083	1.249	0.155	0.215	2.349	1.937	2.431	1.156	0.008	1.962	1.691	1.838	0.869	0.005
PURA	0.986	0.927	0.821	-0.139	0.215	1.012	0.983	0.947	-0.029	0.401	1.043	1.069	0.989	0.047	0.287
DDX5	0.933	1.003	0.897	-0.084	0.217	1.144	1.168	1.132	0.199	0.004	1.288	1.259	1.388	0.390	0.012
COASY	1.012	0.829	0.857	-0.158	0.217	0.736	1.001	0.904	-0.196	0.273	0.712	1.230	0.997	-0.065	0.804
GTF3C5	1.258	0.995	1.149	0.175	0.218	1.348	1.143	1.468	0.392	0.066	1.076	1.096	1.342	0.221	0.163
CTNNBL1	1.342	0.978	1.486	0.321	0.219	1.507	1.415	1.195	0.450	0.046	1.123	1.246	0.848	0.082	0.668
OSBPL8	1.266	1.151	0.995	0.179	0.219	1.264	1.401	1.066	0.306	0.117	0.945	1.011	1.186	0.060	0.599
AP2M1	1.054	1.016	1.174	0.110	0.221	1.537	1.375	1.419	0.528	0.008	1.378	1.281	1.163	0.346	0.040
AK2	0.730	0.888	0.979	-0.219	0.221	0.919	1.147	1.081	0.063	0.577	1.138	1.366	1.111	0.263	0.108
ATE1	1.303	0.999	1.651	0.368	0.221	0.582	0.595	0.854	-0.586	0.082	0.399	0.649	0.494	-0.988	0.040

KHSRP	0.948	0.978	0.997	-0.037	0.222	1.132	0.921	1.389	0.178	0.407	1.154	0.997	1.406	0.231	0.249
G6PD	0.996	1.306	1.162	0.198	0.222	1.085	1.167	1.139	0.176	0.029	1.025	0.956	0.861	-0.082	0.380
ANXA6	1.166	1.071	1.004	0.108	0.225	0.519	0.561	0.511	-0.917	0.002	0.394	0.496	0.509	-1.110	0.011
ARF6	1.125	1.023	1.023	0.079	0.228	1.028	1.060	1.079	0.078	0.063	0.800	0.793	0.993	-0.223	0.171
ARPC1B	0.988	1.116	1.150	0.114	0.229	1.362	1.211	1.141	0.304	0.056	1.281	1.223	1.182	0.296	0.013
LUC7L2	1.031	0.756	0.749	-0.259	0.229	0.591	0.198	0.428	-1.438	0.091	0.545	0.251	0.668	-1.152	0.116
HECTD1	0.742	1.001	0.865	-0.213	0.230	0.440	0.315	1.338	-0.810	0.328	0.597	0.321	1.136	-0.733	0.298
ARPC5	1.013	1.264	1.090	0.160	0.230	1.051	1.144	1.067	0.120	0.087	0.915	0.907	0.862	-0.161	0.026
WDR6	1.153	1.003	1.064	0.100	0.230	0.901	1.067	1.243	0.085	0.590	0.767	0.967	0.851	-0.221	0.149
TDP2	1.021	1.358	1.110	0.207	0.232	0.929	1.065	1.016	0.003	0.966	0.877	0.852	0.888	-0.198	0.008
CDC123	1.008	0.788	0.878	-0.173	0.233	1.099	0.879	0.801	-0.123	0.459	1.091	1.075	1.081	0.114	0.003
ARHGAP5	0.885	0.965	0.988	-0.082	0.234	0.426	0.340	0.582	-1.190	0.034	0.478	0.453	0.550	-1.023	0.007
HEXB	0.850	0.844	1.020	-0.150	0.235	0.717	0.997	0.794	-0.272	0.193	0.828	1.029	0.817	-0.174	0.248

C19orf66	0.586	0.733	1.025	-0.395	0.235	0.712	0.704	0.709	-0.497	0.000	1.239	0.989	0.800	-0.009	0.963
SART3	1.107	1.083	0.990	0.083	0.236	1.058	0.977	0.391	-0.436	0.444	0.834	0.897	0.574	-0.407	0.179
IPO7	0.931	0.907	1.009	-0.077	0.237	0.709	0.912	0.767	-0.337	0.088	0.730	1.053	0.720	-0.284	0.254
ACO1;IRP1	0.897	0.952	1.000	-0.076	0.238	1.222	1.214	1.310	0.320	0.012	1.208	1.363	1.177	0.318	0.039
CCT3	1.019	1.013	1.091	0.057	0.238	1.261	1.310	1.314	0.373	0.003	1.191	1.280	1.178	0.282	0.017
PRDX4	0.796	0.877	1.012	-0.167	0.239	1.675	2.646	2.068	1.065	0.031	2.150	2.956	1.973	1.216	0.021
UBE2H	1.022	0.835	0.849	-0.155	0.240	0.494	0.642	0.428	-0.961	0.030	0.472	0.610	0.497	-0.934	0.014
NUP205	1.052	1.013	1.181	0.110	0.241	1.064	1.130	1.032	0.104	0.113	0.949	0.978	0.851	-0.113	0.204
TANC1	1.214	1.025	1.047	0.127	0.241	1.568	1.320	1.395	0.510	0.020	1.163	1.221	1.245	0.274	0.011
RPL39;RPL39P5	1.004	0.950	0.905	-0.071	0.243	1.020	0.945	0.845	-0.099	0.339	1.007	1.065	0.916	-0.009	0.904
SNX4	1.138	1.341	0.998	0.202	0.243	1.063	0.978	0.834	-0.069	0.571	1.000	0.877	0.790	-0.177	0.214

COPA	0.938	0.963	1.004	-0.047	0.244	1.346	1.302	1.214	0.363	0.014	1.295	1.311	1.225	0.352	0.007
CNN2	1.044	0.697	0.746	-0.293	0.245	0.674	0.535	0.380	-0.955	0.058	0.628	0.706	0.419	-0.810	0.071
DENND4A	1.207	1.010	1.062	0.124	0.246	1.274	1.208	1.383	0.363	0.024	1.087	1.185	1.362	0.270	0.104
LASP1	1.150	1.264	0.983	0.172	0.246	0.775	0.918	0.637	-0.381	0.130	0.645	0.668	0.641	-0.619	0.001
CTNNB1	0.619	0.962	0.876	-0.313	0.247	0.299	0.249	0.733	-1.400	0.101	0.452	0.265	0.927	-1.058	0.181
MIF	1.117	1.054	0.997	0.077	0.247	0.883	0.977	1.013	-0.065	0.388	0.731	0.924	0.882	-0.249	0.137
TUBB3	0.907	0.896	1.015	-0.093	0.247	1.055	1.062	1.095	0.099	0.027	1.018	0.888	1.146	0.017	0.886
DDX17	1.002	0.985	0.977	-0.017	0.248	1.444	1.382	1.314	0.463	0.007	1.402	1.326	1.279	0.416	0.008
SRP68	0.974	0.820	0.960	-0.128	0.249	0.965	0.384	0.676	-0.666	0.228	0.864	0.472	0.744	-0.574	0.160
RPL23	1.055	0.992	1.082	0.060	0.250	1.111	0.969	1.060	0.064	0.387	1.017	0.889	0.996	-0.051	0.488
FN3KRP	2.445	1.310	1.048	0.582	0.252	2.786	1.238	0.855	0.521	0.410	1.153	0.925	0.852	-0.046	0.755
TBCB;CK AP1	1.020	1.000	1.008	0.013	0.255	0.798	0.884	0.904	-0.217	0.060	0.768	0.830	0.897	-0.269	0.053

COPZ1	1.093	0.986	1.151	0.104	0.256	0.830	1.009	0.849	-0.164	0.207	0.736	0.920	0.750	-0.326	0.087
MYO6	0.930	0.971	1.001	-0.048	0.256	1.283	1.459	1.169	0.377	0.055	1.295	1.474	1.138	0.373	0.074
REEP6	1.009	0.904	0.806	-0.147	0.256	0.822	0.785	0.708	-0.377	0.027	0.869	0.893	0.746	-0.263	0.083
SH3GL1	0.945	1.501	1.376	0.322	0.256	0.829	1.021	1.237	0.022	0.909	0.881	0.678	0.660	-0.447	0.078
YWHAG	0.984	1.189	1.457	0.257	0.257	0.818	0.955	0.765	-0.248	0.120	0.655	0.708	0.459	-0.744	0.061
CAPNS1	0.917	1.001	0.793	-0.153	0.258	0.846	0.501	0.352	-0.915	0.130	1.063	0.539	0.374	-0.741	0.235
CAB39	0.768	0.857	1.025	-0.189	0.259	1.068	0.953	1.001	0.009	0.870	1.391	1.076	0.942	0.165	0.422
LGMN	1.238	1.210	3.609	0.811	0.259	0.915	0.881	4.481	0.618	0.508	0.787	0.794	1.153	-0.157	0.477
LIN28B	0.975	0.872	0.982	-0.087	0.260	0.772	0.776	0.786	-0.362	0.000	0.719	0.783	0.751	-0.414	0.007
DENR	0.874	0.933	1.010	-0.094	0.260	0.486	0.525	1.093	-0.614	0.241	0.553	0.621	0.870	-0.581	0.097
BYSL	0.819	0.884	1.021	-0.145	0.260	0.775	0.757	1.225	-0.159	0.556	0.951	0.956	0.986	-0.053	0.083
RPL34	0.914	1.016	0.910	-0.081	0.260	1.103	1.171	1.089	0.164	0.037	0.955	0.876	1.141	-0.022	0.863
41891	0.985	1.083	1.112	0.082	0.261	0.932	1.432	1.262	0.251	0.305	0.898	1.198	1.199	0.122	0.470

LHPP	0.761	1.049	0.767	-0.236	0.262	0.940	0.873	1.004	-0.093	0.250	1.240	0.832	1.290	0.137	0.567
LACTB	0.340	0.877	0.818	-0.679	0.263	1.420	1.138	0.856	0.156	0.539	4.299	1.343	0.882	0.782	0.371
ELP4	0.676	0.958	0.926	-0.246	0.264	0.702	0.731	0.800	-0.428	0.016	0.911	0.853	0.761	-0.253	0.080
MDH2	0.994	1.051	1.033	0.036	0.265	1.072	1.157	1.046	0.125	0.103	1.077	1.053	1.008	0.064	0.148
PSMC3	0.770	1.027	0.861	-0.185	0.265	0.797	0.881	0.673	-0.361	0.087	0.934	0.859	0.679	-0.292	0.167
HIBCH	0.975	1.161	1.329	0.197	0.268	1.281	1.042	1.040	0.158	0.254	1.294	1.135	0.783	0.067	0.786
MRPL34	1.106	0.991	1.055	0.069	0.268	1.066	0.949	0.874	-0.059	0.549	0.867	1.033	0.849	-0.132	0.279
MYH14	0.909	0.906	0.513	-0.414	0.270	0.834	0.942	0.887	-0.174	0.075	0.968	1.048	1.633	0.242	0.410
GSR	1.084	1.161	0.986	0.103	0.270	0.941	1.280	0.894	0.035	0.847	0.875	1.081	0.944	-0.054	0.604
PSMD2	1.025	1.019	1.165	0.095	0.271	1.290	1.248	1.114	0.281	0.048	1.216	1.368	0.958	0.224	0.277
KPNA4	0.998	0.934	0.982	-0.043	0.272	0.553	0.693	0.740	-0.607	0.041	0.553	0.707	0.747	-0.592	0.048
NOP10	0.693	0.903	0.989	-0.231	0.273	0.926	1.019	1.170	0.047	0.677	1.339	1.178	1.167	0.293	0.045
RBM12	1.178	0.968	1.340	0.204	0.274	1.525	0.752	0.870	-0.001	0.997	1.505	0.806	0.619	-0.138	0.752

STAU2	0.959	0.872	0.540	-0.382	0.275	1.324	0.920	0.606	-0.146	0.698	1.203	0.903	1.134	0.100	0.509
HSP90AA1	1.104	0.988	1.061	0.070	0.275	0.704	0.849	0.857	-0.322	0.073	0.613	0.871	0.785	-0.418	0.109
AIMP2	1.101	1.099	0.981	0.082	0.275	1.224	1.268	1.320	0.345	0.008	1.080	1.121	1.261	0.203	0.095
PIP4K2A	1.072	1.316	1.012	0.171	0.276	0.938	0.790	0.759	-0.277	0.098	0.844	0.545	0.687	-0.554	0.093
GOLGA4	0.993	1.033	1.056	0.038	0.276	1.069	1.124	0.859	0.015	0.911	1.140	1.115	0.907	0.069	0.579
DRAP1	1.116	1.047	0.994	0.072	0.276	0.930	1.249	0.929	0.036	0.823	0.742	1.225	0.793	-0.158	0.559
PEG10	1.068	0.730	0.743	-0.262	0.279	0.650	0.567	1.131	-0.420	0.301	0.828	0.870	1.346	-0.015	0.953
FH	0.906	0.750	1.007	-0.182	0.281	0.810	1.084	0.880	-0.124	0.425	1.108	1.308	0.937	0.147	0.401
LDHB	0.989	0.995	0.938	-0.039	0.285	0.909	1.043	0.949	-0.051	0.477	0.940	1.076	1.130	0.065	0.500
GLUD1;GLUD2	1.031	1.223	1.021	0.122	0.286	1.237	1.235	1.284	0.324	0.003	1.276	1.069	1.139	0.212	0.106
PSMD7	0.977	1.150	1.096	0.100	0.287	1.087	1.041	1.212	0.152	0.145	1.105	1.034	0.842	-0.019	0.889

DNAJC2	0.786	0.853	1.041	-0.173	0.288	0.616	0.519	0.894	-0.602	0.121	0.742	0.633	0.601	-0.608	0.022
CAP1	1.045	1.176	1.001	0.100	0.288	0.995	1.110	0.970	0.033	0.632	0.939	0.903	0.993	-0.083	0.173
HNRNPA1 ;HNRNPA 1L2	0.994	0.895	0.978	-0.067	0.288	1.474	1.708	1.637	0.681	0.008	1.348	1.898	1.497	0.646	0.047
CTNND1	1.065	1.175	0.989	0.103	0.289	1.143	1.268	1.877	0.481	0.158	1.110	0.941	1.322	0.155	0.387
ACTR1A; ACTR1B	1.064	1.002	1.262	0.143	0.289	1.161	1.644	1.657	0.554	0.082	1.209	1.543	1.244	0.405	0.068
DDX46	1.115	1.166	0.971	0.112	0.292	1.864	1.339	1.479	0.628	0.047	1.440	1.169	1.543	0.459	0.062
MYL12B; MYL12A; MYL9	0.959	1.170	1.284	0.175	0.294	1.004	1.529	0.988	0.200	0.434	0.983	1.156	0.724	-0.094	0.681
CCT4	1.006	1.019	1.103	0.059	0.294	1.243	1.245	1.268	0.324	0.001	1.238	1.235	1.165	0.278	0.011
ASPH	0.990	1.057	1.037	0.039	0.294	1.197	1.178	1.284	0.285	0.017	1.276	1.100	1.169	0.238	0.061

PTBP3	0.982	1.118	1.070	0.077	0.295	1.256	1.313	1.528	0.445	0.035	1.366	1.182	1.353	0.376	0.031
BTF3L4	0.892	0.751	1.024	-0.182	0.296	0.931	0.846	0.848	-0.194	0.050	0.945	0.890	0.820	-0.178	0.095
NPLOC4	1.183	1.149	0.963	0.130	0.298	1.159	0.955	0.982	0.040	0.691	0.878	0.891	1.010	-0.113	0.220
LSM3	1.175	1.023	1.015	0.096	0.299	0.604	0.631	0.719	-0.622	0.014	0.503	0.636	0.598	-0.795	0.016
RPL29	1.021	0.829	0.920	-0.121	0.300	1.099	0.612	0.712	-0.354	0.296	0.951	0.838	0.776	-0.231	0.114
ALDH18A1	0.900	1.444	1.660	0.370	0.301	2.225	1.950	2.293	1.105	0.004	2.715	1.392	1.353	0.785	0.139
DNAJC10	0.884	1.032	0.894	-0.098	0.305	1.317	1.188	1.223	0.312	0.020	1.315	1.270	1.169	0.322	0.023
ATP6V1G1	1.044	1.222	1.003	0.119	0.305	0.931	0.916	0.827	-0.168	0.088	0.792	0.765	0.743	-0.384	0.005
PIR	1.006	1.350	1.065	0.177	0.306	1.067	1.179	1.093	0.153	0.072	1.040	0.875	0.976	-0.057	0.518
EIF4A3	1.011	0.956	0.888	-0.073	0.307	1.237	1.163	1.021	0.185	0.152	1.129	1.225	1.193	0.241	0.020
EIF2S1	1.047	1.055	0.986	0.041	0.310	1.013	0.974	0.968	-0.022	0.396	1.009	0.929	0.954	-0.054	0.266

TBC1D15	1.020	1.013	1.171	0.091	0.313	0.892	0.998	0.986	-0.062	0.348	0.829	0.930	0.867	-0.194	0.056
CKB	0.958	1.234	1.141	0.144	0.313	0.697	0.866	0.746	-0.384	0.053	0.844	0.693	0.713	-0.421	0.042
PRPF19	0.965	1.011	0.927	-0.048	0.315	1.175	1.151	1.192	0.230	0.004	1.223	1.048	1.208	0.210	0.099
PRKAG1	1.019	0.886	0.943	-0.078	0.316	1.149	1.378	1.038	0.239	0.184	1.185	1.512	1.048	0.303	0.191
PURB	0.931	0.984	0.646	-0.252	0.316	1.023	1.097	0.830	-0.034	0.804	1.124	1.058	1.282	0.203	0.132
TRIP10	0.946	1.328	1.181	0.190	0.317	1.215	1.231	1.054	0.219	0.092	1.102	0.952	0.812	-0.077	0.605
PITRM1	0.982	1.076	1.248	0.133	0.318	1.622	1.485	1.323	0.557	0.023	1.512	1.261	0.955	0.288	0.274
ERI1	1.039	0.790	0.894	-0.149	0.321	0.788	0.831	0.896	-0.256	0.042	0.898	0.899	0.947	-0.129	0.036
NAA25	0.985	0.917	0.999	-0.049	0.322	1.260	1.097	1.035	0.172	0.176	1.201	1.187	1.079	0.207	0.051
KPNA1	1.111	0.964	1.177	0.111	0.323	0.475	0.539	0.631	-0.876	0.018	0.441	0.562	0.581	-0.932	0.018
NAA50	0.986	0.958	1.004	-0.025	0.325	0.970	1.005	0.969	-0.027	0.259	0.955	0.971	0.859	-0.109	0.187
GART	0.598	1.078	0.807	-0.314	0.329	0.731	0.729	0.601	-0.548	0.028	1.000	0.763	0.766	-0.259	0.183
CTNNA1	1.036	1.033	0.989	0.027	0.331	0.925	0.918	0.654	-0.282	0.228	0.820	0.803	0.654	-0.405	0.060

PSMD12	1.038	1.005	1.279	0.139	0.332	1.110	1.224	1.408	0.312	0.089	1.143	1.214	1.089	0.198	0.049
G3BP1	0.994	1.039	1.191	0.100	0.332	0.992	1.150	0.893	0.009	0.939	0.670	0.801	0.650	-0.507	0.033
HNRNPAB	0.969	0.852	1.003	-0.091	0.334	0.817	0.871	0.865	-0.234	0.015	0.887	1.038	0.962	-0.059	0.466
HYPK	0.726	0.955	0.993	-0.179	0.334	0.878	1.032	1.094	-0.004	0.970	1.111	0.941	0.725	-0.133	0.534
UBA6	0.766	0.778	1.088	-0.209	0.334	1.008	1.136	1.566	0.281	0.277	1.276	1.425	1.448	0.466	0.015
PYGB	0.981	1.104	1.051	0.062	0.337	1.095	1.389	1.415	0.368	0.091	1.150	1.178	1.179	0.225	0.003
SAMHD1	1.009	1.136	1.011	0.071	0.337	1.229	0.961	1.039	0.098	0.445	1.146	0.982	0.814	-0.042	0.796
KIF2A	0.953	0.860	1.016	-0.088	0.337	0.811	0.547	0.954	-0.414	0.225	0.860	0.616	0.956	-0.327	0.229
SNRPG	0.992	1.021	1.036	0.023	0.340	1.353	1.374	1.730	0.562	0.039	1.268	1.360	1.490	0.454	0.021
TUBA1C	1.029	0.991	1.117	0.063	0.342	1.185	2.148	2.012	0.786	0.102	1.041	1.976	1.668	0.593	0.166
HNRNPD	0.918	0.936	1.026	-0.061	0.346	0.963	1.031	0.948	-0.029	0.514	1.071	1.141	1.021	0.107	0.148
FAM21A;FAM21C;F	0.817	1.072	0.824	-0.156	0.348	0.843	1.261	0.873	-0.036	0.864	0.968	1.169	0.799	-0.048	0.790

AM21B															
EHD1	0.978	1.320	1.069	0.155	0.349	1.086	1.164	1.119	0.167	0.029	0.918	0.939	1.040	-0.052	0.444
LSM5	1.027	1.039	0.989	0.026	0.351	0.535	0.611	0.573	-0.805	0.005	0.457	0.562	0.566	-0.928	0.012
CARS	1.072	0.978	1.059	0.050	0.352	1.021	0.953	1.030	0.001	0.983	0.925	0.982	0.938	-0.077	0.098
PSMA6	0.984	1.051	1.040	0.035	0.352	0.934	1.129	0.924	-0.013	0.904	1.095	0.949	0.872	-0.048	0.669
UBE2E2;UBE2E3	1.012	1.276	1.020	0.132	0.352	1.251	1.265	1.238	0.324	0.001	1.291	0.907	1.122	0.131	0.470
IQGAP1	1.051	1.017	0.993	0.028	0.353	0.495	0.215	0.440	-1.471	0.059	0.422	0.212	0.449	-1.546	0.047
RAN	1.171	1.327	0.933	0.179	0.353	0.970	1.157	0.987	0.049	0.605	0.858	0.835	1.073	-0.127	0.384
RPP14	1.040	0.917	0.804	-0.128	0.354	1.070	1.064	1.087	0.103	0.008	0.974	1.120	1.104	0.090	0.296
API5	1.106	1.090	0.967	0.074	0.355	1.042	0.947	0.872	-0.072	0.434	0.924	0.935	0.949	-0.096	0.012
DARS2	1.024	1.254	1.004	0.122	0.357	1.266	1.480	1.142	0.366	0.078	1.305	1.133	1.176	0.266	0.049
DICER1	0.677	1.034	0.914	-0.215	0.358	0.471	0.872	0.814	-0.526	0.202	0.726	0.864	0.836	-0.310	0.057

DPP9	0.928	0.972	1.013	-0.043	0.361	0.743	1.091	0.832	-0.190	0.368	0.810	0.978	0.922	-0.151	0.202
RPP40	0.778	0.703	1.117	-0.237	0.364	0.983	0.835	1.543	0.114	0.710	1.331	1.215	1.314	0.362	0.013
RAB10	0.922	1.294	1.202	0.173	0.364	0.778	0.888	0.964	-0.195	0.162	0.873	0.726	0.709	-0.385	0.056
IARS	1.010	0.979	0.955	-0.027	0.366	1.196	1.155	1.285	0.276	0.026	1.189	1.200	1.338	0.311	0.030
MCM5	1.040	1.126	0.981	0.066	0.369	0.828	0.638	0.551	-0.594	0.074	0.742	0.597	0.546	-0.683	0.035
POLR3A	1.064	1.131	0.970	0.074	0.369	0.877	1.497	1.076	0.166	0.537	0.816	1.290	1.158	0.095	0.682
POP1	1.032	0.937	0.901	-0.066	0.372	0.802	0.858	0.672	-0.371	0.072	0.794	0.896	0.687	-0.345	0.090
TMEM167A	0.930	0.907	1.034	-0.066	0.372	0.702	0.754	0.604	-0.548	0.029	0.762	0.857	0.636	-0.423	0.078
PRKDC	1.017	1.171	0.997	0.083	0.375	0.717	0.859	0.708	-0.399	0.047	0.817	0.734	0.761	-0.378	0.014
MRPL33	0.766	0.911	1.051	-0.149	0.375	0.847	1.126	1.294	0.101	0.631	0.956	1.134	0.891	-0.016	0.888
HSP90AB2P	1.056	0.980	1.048	0.039	0.375	0.687	0.884	0.733	-0.389	0.070	0.606	0.937	0.687	-0.453	0.136

RBM28	0.973	0.505	0.974	-0.354	0.378	3.003	1.654	1.659	1.014	0.071	3.200	2.978	1.912	1.396	0.027
NME1	0.903	1.055	0.823	-0.117	0.380	0.893	1.075	1.069	0.012	0.902	0.949	1.056	1.179	0.080	0.467
SNRPA1	0.984	1.009	0.950	-0.028	0.382	1.650	1.714	1.484	0.690	0.008	1.668	1.715	1.394	0.665	0.019
HADH	1.023	0.988	1.091	0.047	0.382	1.150	1.080	1.254	0.213	0.076	1.084	1.093	0.958	0.061	0.425
SRP19	1.077	1.008	0.996	0.038	0.391	0.958	0.941	1.075	-0.015	0.823	0.860	0.887	0.966	-0.147	0.099
PSMA1	1.039	1.234	0.978	0.109	0.392	0.880	0.853	1.368	0.013	0.959	1.006	0.799	1.296	0.020	0.931
DKC1	0.863	1.088	0.745	-0.172	0.392	1.603	1.783	1.528	0.709	0.009	1.808	1.634	1.576	0.740	0.006
RANGAP1	1.229	0.914	1.218	0.151	0.395	0.582	0.527	0.658	-0.770	0.014	0.387	0.584	0.506	-1.043	0.027
C1QBP	0.771	1.961	1.672	0.446	0.396	1.550	1.796	1.630	0.727	0.007	1.667	0.999	0.816	0.147	0.679
PNPT1	0.903	0.762	1.065	-0.150	0.396	1.180	1.323	1.234	0.315	0.022	1.253	2.039	1.134	0.512	0.189
SNRPB2	0.962	0.970	1.016	-0.026	0.401	1.349	1.438	1.552	0.530	0.012	1.319	1.368	1.502	0.479	0.013
SSB	0.991	0.903	1.005	-0.051	0.401	0.698	0.762	0.834	-0.391	0.034	0.736	0.881	0.826	-0.301	0.058
PALLD	1.170	0.992	1.013	0.078	0.407	0.614	0.526	0.395	-0.989	0.034	0.645	0.523	0.385	-0.982	0.045

PTRHD1	0.978	1.016	0.838	-0.088	0.409	0.628	0.494	0.491	-0.904	0.016	0.456	0.420	0.517	-1.112	0.006
RANBP2	0.788	1.059	0.919	-0.127	0.410	1.139	0.876	0.982	-0.010	0.936	1.894	0.983	0.948	0.273	0.488
MCTS1	1.011	0.985	0.947	-0.028	0.412	0.755	0.749	0.859	-0.347	0.032	0.716	0.735	0.827	-0.400	0.025
PUS7L	1.008	0.936	0.990	-0.033	0.415	0.858	0.988	0.818	-0.176	0.164	0.823	1.060	0.847	-0.145	0.334
C14orf126	0.791	1.078	0.890	-0.133	0.415	0.782	0.821	0.801	-0.320	0.004	0.882	0.797	0.801	-0.276	0.029
ARPC3	0.971	1.052	1.077	0.046	0.415	0.956	1.028	0.986	-0.015	0.677	0.867	0.982	0.819	-0.174	0.155
GUSB	0.940	1.410	1.083	0.174	0.417	1.340	1.259	1.130	0.310	0.050	1.483	0.963	1.062	0.200	0.400
DYNC1I2	0.989	1.008	0.763	-0.131	0.418	1.003	1.149	0.630	-0.154	0.617	0.911	1.095	0.791	-0.114	0.491
LARP7	1.169	1.479	0.896	0.211	0.419	1.464	2.357	1.902	0.905	0.045	1.359	1.485	2.599	0.797	0.112
CCNL1	1.116	0.933	1.215	0.113	0.420	1.317	1.329	1.188	0.352	0.021	1.088	1.632	0.984	0.268	0.352
SNRPF	0.990	1.059	1.012	0.028	0.423	1.311	1.366	1.532	0.485	0.019	1.253	1.327	1.412	0.410	0.014
DYNC1H1	1.085	1.024	0.981	0.041	0.427	1.095	1.023	0.976	0.043	0.470	1.089	1.000	1.018	0.050	0.317
A2M	0.918	1.055	0.875	-0.079	0.429	0.494	0.622	0.898	-0.619	0.133	0.538	1.051	1.090	-0.233	0.555

TEX2	0.761	0.806	1.133	-0.175	0.431	1.584	1.522	2.324	0.829	0.051	2.162	1.914	1.734	0.948	0.009
NAA10	0.930	1.061	0.802	-0.113	0.434	0.692	0.641	0.565	-0.665	0.016	0.733	0.623	0.622	-0.606	0.016
ACTR2	0.984	1.135	1.014	0.060	0.437	1.111	1.227	1.113	0.200	0.051	1.119	1.037	1.033	0.087	0.147
EIF2C2	1.010	0.913	0.991	-0.043	0.438	1.101	1.091	1.172	0.165	0.037	1.047	1.140	1.126	0.142	0.066
ZCCHC3	1.085	0.987	1.013	0.039	0.441	1.341	1.376	2.106	0.653	0.090	1.328	1.319	1.835	0.561	0.070
KIF11	1.053	0.961	1.124	0.062	0.443	0.623	0.491	0.447	-0.957	0.021	0.589	0.503	0.362	-1.074	0.035
PTRH2	0.770	1.154	0.768	-0.184	0.446	0.464	0.491	0.583	-0.971	0.010	0.616	0.489	0.673	-0.767	0.030
POP5	1.012	0.995	0.859	-0.070	0.447	1.093	0.990	1.149	0.105	0.238	1.066	1.003	1.174	0.109	0.240
RSU1	0.893	1.099	0.739	-0.155	0.449	0.730	0.888	0.857	-0.282	0.083	0.893	0.819	0.923	-0.189	0.067
ATP6V1A	1.000	1.216	0.991	0.090	0.449	1.170	1.030	0.850	0.012	0.937	1.040	0.857	1.046	-0.034	0.756
SNRPN;SNRPB	0.985	1.021	1.043	0.023	0.449	1.586	1.591	1.742	0.712	0.004	1.606	1.620	1.539	0.667	0.001
TXLNG	0.958	1.133	1.055	0.065	0.449	1.004	1.346	1.180	0.225	0.207	1.078	1.342	1.206	0.268	0.099

LAMA5	0.979	1.036	0.710	-0.158	0.450	0.754	0.783	0.464	-0.623	0.125	0.783	0.883	0.619	-0.408	0.113
FAM98A	0.997	1.163	0.995	0.069	0.453	1.063	1.036	0.941	0.017	0.779	1.159	0.903	0.957	0.001	0.991
NME1-NME2;NME2;NME1	1.011	0.981	0.982	-0.013	0.455	0.978	1.096	1.017	0.041	0.483	0.918	1.021	0.954	-0.054	0.354
NCKAP1	0.965	1.031	0.907	-0.049	0.455	1.175	1.084	0.897	0.064	0.634	1.150	1.072	0.968	0.085	0.359
SMARCA1	1.101	0.929	0.549	-0.278	0.455	1.087	0.932	0.531	-0.298	0.443	0.974	0.982	0.921	-0.061	0.170
PCBP1	1.035	0.951	0.930	-0.043	0.457	1.008	1.017	1.067	0.043	0.234	0.950	1.030	0.975	-0.023	0.576
KIF5B	0.964	1.081	1.057	0.046	0.457	1.197	1.188	1.108	0.219	0.025	1.159	1.128	1.061	0.157	0.053
GTF2E1	1.130	1.092	0.942	0.072	0.465	1.162	1.039	0.939	0.060	0.569	0.904	0.891	0.945	-0.131	0.036
OSBPL3	1.091	0.813	0.894	-0.112	0.466	1.065	0.905	1.158	0.053	0.661	1.014	1.166	1.080	0.117	0.182
GNPNAT1	1.045	1.059	0.971	0.035	0.467	0.786	0.922	0.784	-0.271	0.073	0.904	0.861	0.844	-0.202	0.021
LIMS1;LIMS3	1.056	0.947	1.201	0.088	0.468	0.795	0.938	0.833	-0.228	0.084	0.754	0.996	0.833	-0.225	0.195

HIST2H2AA3;HIST2H2AC	1.048	0.966	1.077	0.042	0.469	1.372	1.431	1.494	0.518	0.005	1.346	1.459	1.341	0.466	0.007
SNRPD1	0.886	1.062	0.919	-0.070	0.471	1.406	1.551	2.512	0.818	0.087	1.468	1.356	3.025	0.863	0.144
USP10	0.971	1.183	1.018	0.075	0.473	1.744	1.515	1.265	0.580	0.049	1.618	1.464	1.268	0.529	0.035
NAMPT;RP11-92J19.4	1.047	0.934	1.428	0.160	0.474	1.010	1.174	1.248	0.189	0.173	0.960	1.297	0.677	-0.082	0.791
AGFG1	0.998	0.985	1.217	0.086	0.476	1.450	1.089	1.166	0.294	0.143	1.292	1.102	0.852	0.093	0.648
POLR2E	1.148	0.933	1.101	0.079	0.476	1.235	2.319	2.416	0.930	0.097	1.074	2.321	0.918	0.398	0.438
PSMC5	1.177	2.009	0.826	0.322	0.479	1.596	1.955	0.226	-0.169	0.881	1.327	0.992	1.301	0.259	0.196
LSM1	1.080	1.012	0.983	0.034	0.480	0.617	0.617	0.647	-0.674	0.001	0.548	0.603	0.564	-0.807	0.003
CHORDC1	1.002	0.799	1.020	-0.097	0.481	1.201	1.059	1.320	0.249	0.113	1.415	1.259	1.174	0.355	0.046

DNAJC1	1.189	1.271	0.882	0.138	0.484	2.203	1.700	1.570	0.852	0.029	1.793	1.164	1.492	0.546	0.094
SRP9	1.026	1.057	0.977	0.028	0.487	1.048	0.966	0.923	-0.032	0.607	0.912	0.864	0.875	-0.179	0.016
THYN1	1.046	0.961	0.864	-0.067	0.488	0.994	0.758	0.835	-0.222	0.191	0.993	0.889	0.906	-0.108	0.162
MRPS34	0.991	0.666	1.053	-0.175	0.488	1.462	1.259	1.308	0.423	0.023	1.564	1.905	1.305	0.653	0.054
BLVRA	0.993	1.020	0.883	-0.054	0.489	0.923	0.847	0.788	-0.233	0.071	0.933	0.997	0.998	-0.035	0.385
HIST2H2BF;HIST1H2BK;H2BFS;HIST1H2BD;HIST1H2BC;HIST1H2BH;HIST1H2BN;HIST1H2BM;HIST1H2BL	0.955	0.912	1.041	-0.047	0.490	1.456	1.463	1.598	0.589	0.005	1.456	1.597	1.451	0.585	0.006

BANF1	0.747	0.816	1.166	-0.164	0.491	1.965	2.463	1.899	1.067	0.012	2.170	2.316	1.536	0.983	0.033
TFCP2	1.090	0.999	0.991	0.037	0.492	1.125	1.055	1.049	0.105	0.084	0.965	1.006	0.939	-0.044	0.265
RALY	0.992	0.906	1.019	-0.042	0.496	1.065	1.330	1.262	0.279	0.102	0.944	1.266	1.333	0.224	0.285
TRIM23	0.952	1.110	1.058	0.054	0.497	1.072	1.215	0.963	0.109	0.379	1.117	1.151	0.883	0.061	0.666
ATP6V1C1	0.885	1.209	1.204	0.122	0.500	0.963	1.113	0.838	-0.051	0.706	1.102	0.823	0.865	-0.117	0.465
ARCN1	1.008	1.214	0.969	0.082	0.500	0.776	0.831	0.761	-0.342	0.012	0.799	0.691	0.718	-0.445	0.019
MAPRE2	1.022	0.952	1.274	0.103	0.500	0.990	1.014	0.941	-0.027	0.482	0.923	0.905	0.719	-0.245	0.168
NIPSNAP1	1.506	0.785	1.399	0.242	0.501	1.496	1.058	1.397	0.381	0.130	1.077	1.288	0.927	0.121	0.473
PUM1	0.873	1.013	1.005	-0.057	0.502	0.904	1.079	1.346	0.131	0.514	1.113	1.121	1.133	0.166	0.002
GPI	0.941	0.955	1.035	-0.035	0.503	1.149	1.229	1.152	0.234	0.018	1.144	1.272	1.077	0.216	0.092
RPP30;RP11-	1.001	1.003	0.974	-0.011	0.506	1.084	1.156	1.131	0.168	0.026	0.964	1.093	1.190	0.109	0.343

320F15.1															
HIST1H2BJ;HIST1H2BO;HIST1H2BB;HIST2H2BE;HIST3H2BB	0.941	0.868	1.066	-0.067	0.521	1.532	1.503	1.498	0.596	0.000	1.510	1.573	1.408	0.581	0.006
C3orf26	1.042	0.907	1.486	0.163	0.522	1.532	2.087	1.556	0.771	0.034	1.417	1.931	0.990	0.480	0.227
RPL35	0.962	1.051	0.879	-0.057	0.523	1.238	1.161	1.297	0.299	0.023	1.146	1.172	1.454	0.322	0.099
SEC31A	0.976	1.078	0.716	-0.136	0.523	0.888	1.006	0.356	-0.551	0.364	0.778	0.857	0.732	-0.346	0.035
URM1	0.994	0.825	1.038	-0.078	0.523	0.733	0.762	0.780	-0.400	0.004	0.602	0.753	0.717	-0.541	0.031
EML4	0.966	1.059	1.044	0.032	0.524	1.009	0.930	0.940	-0.061	0.242	0.996	0.883	0.817	-0.159	0.197
FLNC	1.023	1.000	0.869	-0.056	0.525	0.598	0.602	0.553	-0.776	0.003	0.614	0.591	0.669	-0.681	0.006
FAM82B	0.923	1.135	1.108	0.072	0.525	0.721	0.946	1.213	-0.091	0.716	1.023	0.975	1.101	0.045	0.467

NONO	0.859	0.950	1.064	-0.068	0.526	1.772	1.712	1.748	0.802	0.000	1.970	1.710	1.543	0.793	0.016
DAZAP1	0.826	0.813	1.150	-0.124	0.526	1.603	1.180	1.037	0.324	0.224	1.901	1.487	0.863	0.429	0.331
CAND1	0.952	1.029	0.968	-0.026	0.528	0.900	0.915	0.905	-0.141	0.003	0.893	0.891	0.916	-0.152	0.007
TMEM109	0.959	0.876	1.054	-0.058	0.529	0.668	0.672	0.716	-0.545	0.003	0.586	0.679	0.596	-0.692	0.009
RPS6KA3	1.021	0.968	0.973	-0.019	0.530	1.039	0.986	0.735	-0.137	0.472	0.961	1.000	0.720	-0.177	0.358
COPB1	1.032	0.948	0.964	-0.028	0.532	0.850	0.990	0.730	-0.234	0.206	0.859	0.962	0.762	-0.222	0.149
XRN1	0.466	1.198	0.947	-0.307	0.532	0.518	1.469	0.803	-0.237	0.641	1.085	1.300	0.935	0.133	0.435
RNH1	1.055	0.935	1.176	0.072	0.533	0.643	0.621	0.799	-0.550	0.040	0.668	0.719	0.674	-0.543	0.004
LRPPRC	0.836	1.228	1.332	0.150	0.543	0.921	1.478	1.668	0.395	0.270	0.962	1.298	1.275	0.223	0.251
CCDC124	0.719	1.041	1.028	-0.126	0.545	0.794	0.633	0.753	-0.468	0.042	1.024	0.989	0.651	-0.200	0.441
RRP9	0.741	0.741	1.249	-0.181	0.546	1.277	1.297	1.324	0.378	0.002	1.695	1.517	1.410	0.620	0.015
EIF5A;EIF5AL1	1.031	1.035	0.976	0.020	0.549	0.953	0.966	0.970	-0.055	0.019	0.871	0.919	0.940	-0.137	0.052

ACTR3	0.905	1.012	1.009	-0.038	0.549	1.091	1.153	1.065	0.141	0.053	1.125	1.051	1.019	0.090	0.167
RBM4B;RBM4	0.976	1.078	0.764	-0.106	0.549	1.101	1.397	0.998	0.206	0.290	1.202	1.304	1.262	0.328	0.011
MOB1B;MOB1A	1.046	0.973	0.891	-0.047	0.553	0.882	0.855	1.140	-0.073	0.637	0.837	0.836	1.057	-0.145	0.325
SMC2	0.949	0.946	1.042	-0.032	0.553	1.297	1.271	1.151	0.308	0.029	1.383	1.382	1.224	0.409	0.020
CTSL2	1.004	0.862	1.028	-0.056	0.554	0.880	0.679	0.697	-0.421	0.071	0.680	0.643	0.622	-0.626	0.004
ADAR	1.045	1.192	0.932	0.072	0.555	1.302	1.260	2.025	0.577	0.120	1.175	1.113	2.074	0.480	0.237
GAPDH	1.008	0.995	0.980	-0.008	0.557	0.922	0.901	0.856	-0.165	0.035	0.912	0.890	0.871	-0.167	0.013
TRNT1	1.024	0.921	0.992	-0.032	0.558	0.745	0.855	0.901	-0.267	0.082	0.738	0.861	0.864	-0.289	0.062
SEC23A	0.979	0.997	1.007	-0.008	0.559	1.037	1.024	0.930	-0.006	0.912	0.922	0.955	0.908	-0.107	0.038
PHYH	0.964	1.240	0.989	0.080	0.559	0.941	1.049	0.870	-0.073	0.448	0.883	1.345	0.869	0.015	0.948
GNG12	1.043	0.907	1.343	0.115	0.560	0.858	0.861	0.611	-0.382	0.146	0.751	0.965	0.469	-0.518	0.231

FAM98B	1.019	1.104	0.964	0.039	0.561	0.965	1.004	0.915	-0.058	0.278	0.878	0.978	0.967	-0.089	0.212
HEATR5A	1.207	0.785	0.787	-0.141	0.565	0.732	0.408	0.429	-0.988	0.067	0.467	0.479	0.632	-0.940	0.021
LSM2	1.101	1.016	0.966	0.037	0.566	0.538	0.604	0.559	-0.821	0.004	0.487	0.580	0.554	-0.892	0.007
CROCC	0.963	1.023	1.094	0.036	0.569	1.019	0.939	0.944	-0.049	0.328	0.938	0.915	0.852	-0.151	0.069
USP9X	1.052	0.936	0.941	-0.037	0.574	0.731	0.706	0.642	-0.532	0.011	0.755	0.788	0.722	-0.407	0.008
KATNAL2	0.976	1.054	0.876	-0.050	0.583	0.459	0.637	0.507	-0.919	0.022	0.431	0.593	0.572	-0.925	0.024
SUB1	1.001	0.954	1.195	0.063	0.588	0.595	0.721	1.337	-0.268	0.527	0.620	0.713	0.921	-0.432	0.123
FTSJ1	1.083	0.969	1.013	0.029	0.594	0.706	0.791	0.814	-0.379	0.026	0.654	0.749	0.805	-0.448	0.036
HBS1L	0.986	1.116	0.983	0.038	0.594	1.080	1.065	0.993	0.064	0.233	1.064	0.984	0.996	0.020	0.622
USMG5	0.745	1.250	1.682	0.216	0.594	0.942	1.047	0.874	-0.072	0.443	0.897	0.815	0.393	-0.600	0.252
RPL14	0.989	1.031	0.926	-0.028	0.598	1.961	1.733	1.650	0.829	0.008	1.722	1.652	1.497	0.697	0.007
SNX9	1.078	0.899	0.931	-0.049	0.602	1.118	1.025	1.018	0.074	0.230	1.150	1.086	1.100	0.153	0.026
PRIC285	1.450	0.642	0.657	-0.236	0.603	0.946	0.916	0.353	-0.571	0.346	0.688	1.509	0.624	-0.208	0.657

RPL10;RPL10L	1.311	1.127	0.852	0.111	0.605	1.515	0.814	1.114	0.153	0.614	1.106	0.859	1.425	0.146	0.561
GEMIN5	0.828	1.109	0.935	-0.073	0.610	0.737	0.977	0.814	-0.257	0.164	0.838	0.889	0.815	-0.240	0.023
PPP2R1A	0.869	1.164	1.183	0.086	0.610	0.730	0.799	0.842	-0.342	0.029	0.842	0.737	0.707	-0.396	0.035
NEMF	1.308	0.795	1.285	0.139	0.614	0.717	0.320	0.823	-0.802	0.200	0.511	0.474	0.622	-0.910	0.016
NAA38	1.145	0.918	1.067	0.055	0.616	0.509	0.596	0.669	-0.767	0.022	0.457	0.652	0.564	-0.857	0.029
PTBP1	0.998	1.050	0.987	0.016	0.617	0.925	1.108	1.213	0.105	0.457	0.975	1.040	1.093	0.049	0.410
PKN2	0.985	0.920	1.039	-0.029	0.621	0.537	0.500	0.624	-0.859	0.012	0.486	0.553	0.563	-0.909	0.005
RPRD1B	1.015	0.909	1.017	-0.031	0.625	1.868	1.707	2.001	0.891	0.005	1.821	1.655	1.919	0.844	0.005
SHMT1	1.410	0.906	0.986	0.111	0.628	1.921	0.760	1.116	0.235	0.607	1.312	0.861	1.090	0.100	0.627
TNIK;MINK1	1.062	1.016	0.800	-0.071	0.634	1.041	1.012	0.911	-0.020	0.764	1.133	1.164	1.051	0.157	0.071
CRAT	1.209	0.974	0.961	0.059	0.634	1.217	1.091	0.920	0.096	0.498	0.979	1.154	0.946	0.032	0.753

ANKHD1	0.940	1.101	1.043	0.037	0.635	0.941	0.884	0.904	-0.137	0.036	0.864	0.931	0.984	-0.113	0.174
PTPN11	0.946	1.012	1.150	0.046	0.636	0.852	0.699	1.153	-0.181	0.479	0.800	0.695	0.950	-0.307	0.143
CCT7	1.009	0.990	1.012	0.005	0.640	1.246	1.280	1.258	0.335	0.001	1.230	1.272	1.205	0.305	0.006
PRIM2	0.845	0.937	1.110	-0.063	0.640	1.028	1.224	1.178	0.189	0.132	1.195	1.232	1.054	0.211	0.092
CRYZ	0.967	1.094	0.829	-0.063	0.641	1.055	1.091	0.933	0.034	0.666	1.133	1.121	1.072	0.148	0.025
PSPC1	0.879	0.925	1.101	-0.053	0.643	1.535	1.715	1.889	0.771	0.012	1.966	1.767	1.723	0.861	0.005
FAM136A	1.055	0.957	0.934	-0.029	0.648	0.974	0.985	1.143	0.044	0.617	0.954	0.953	1.046	-0.024	0.643
EEF2	0.985	1.042	1.001	0.013	0.655	0.856	0.779	0.786	-0.310	0.019	0.956	0.861	0.801	-0.200	0.114
GTPBP1	0.961	0.960	1.040	-0.020	0.656	0.637	0.531	1.583	-0.300	0.600	0.537	0.539	1.091	-0.554	0.245
TRMT11	0.864	1.045	1.012	-0.043	0.661	0.784	0.801	0.919	-0.265	0.066	0.863	0.850	1.003	-0.147	0.193
MRPL46	1.013	1.666	0.816	0.154	0.664	2.369	3.373	0.890	0.943	0.243	1.806	1.716	0.593	0.293	0.632
EPRS	1.021	1.002	0.946	-0.016	0.673	1.043	0.989	1.024	0.027	0.357	0.954	0.913	1.054	-0.041	0.569
SRP54	1.040	1.074	0.947	0.027	0.673	1.008	0.994	1.154	0.070	0.419	0.928	0.906	1.131	-0.024	0.832

PDIA3	0.928	1.064	0.954	-0.029	0.675	1.016	1.039	1.005	0.028	0.178	1.059	1.015	1.033	0.050	0.106
C7orf50	1.178	0.732	0.949	-0.096	0.676	1.277	1.621	2.676	0.823	0.120	0.983	2.324	2.487	0.835	0.192
ACP1	1.066	0.958	0.917	-0.031	0.678	0.816	0.777	0.828	-0.310	0.008	0.794	0.797	0.861	-0.292	0.016
GFPT1	0.937	1.015	1.144	0.040	0.679	1.040	0.934	1.055	0.012	0.847	1.058	0.911	0.864	-0.088	0.421
LRPAP1	0.989	1.108	0.967	0.028	0.688	0.494	0.555	0.479	-0.976	0.004	0.523	0.522	0.484	-0.973	0.001
WASF1	1.149	1.316	0.809	0.097	0.690	0.941	1.808	1.324	0.391	0.288	0.864	1.311	1.249	0.167	0.472
COPE	1.033	1.117	0.931	0.035	0.694	1.040	1.018	0.931	-0.007	0.898	0.974	0.904	0.844	-0.143	0.140
TPR	1.280	0.919	0.976	0.066	0.696	0.654	0.812	0.772	-0.429	0.045	0.681	0.742	0.839	-0.412	0.042
TXLNA	0.856	0.966	1.097	-0.046	0.697	0.823	0.727	1.644	-0.008	0.984	0.993	0.896	1.307	0.073	0.699
ANXA2;ANXA2P2	0.937	1.046	1.080	0.028	0.697	0.625	0.626	0.653	-0.656	0.001	0.698	0.595	0.597	-0.671	0.012
MYH9	0.967	0.986	1.113	0.028	0.699	0.947	1.152	0.938	0.011	0.923	1.083	1.152	0.892	0.051	0.689
CLPB	1.140	1.056	0.908	0.043	0.700	1.299	1.316	0.892	0.203	0.386	1.181	1.073	0.812	0.014	0.940

MAP1LC3B2;MAP1LC3B	0.912	1.123	0.885	-0.047	0.703	0.752	0.758	0.631	-0.492	0.030	0.678	0.602	0.656	-0.634	0.006
GGH	1.007	0.969	1.060	0.016	0.705	0.856	0.884	0.852	-0.212	0.006	0.831	0.813	0.777	-0.309	0.008
RBM42	0.721	0.929	1.223	-0.096	0.705	1.206	1.255	1.211	0.291	0.004	1.607	1.398	1.065	0.419	0.138
PTK2	1.120	0.904	0.899	-0.046	0.705	1.693	1.448	0.956	0.409	0.238	1.406	1.369	1.217	0.409	0.024
MLLT4	0.754	0.782	1.333	-0.116	0.705	0.128	0.461	0.776	-1.481	0.195	0.168	0.762	0.620	-1.219	0.216
CCDC25	1.243	0.738	0.894	-0.096	0.706	0.863	0.747	0.554	-0.495	0.119	0.727	0.931	0.651	-0.394	0.123
FTSJ3	0.908	1.157	0.841	-0.060	0.709	2.531	2.528	1.923	1.207	0.012	2.729	2.694	2.264	1.352	0.004
RAB3GAP2	0.889	0.918	1.540	0.110	0.711	2.339	2.592	2.143	1.233	0.004	2.372	2.726	1.311	1.028	0.087
PDIA3	0.971	1.062	1.002	0.016	0.717	1.056	1.098	0.820	-0.025	0.868	1.037	1.059	0.802	-0.061	0.682
EDC4	0.901	1.311	0.661	-0.118	0.719	0.327	0.903	0.131	-1.564	0.192	0.321	0.679	0.170	-1.583	0.111
MAGED2	0.974	1.077	0.891	-0.033	0.721	0.946	0.960	0.811	-0.147	0.199	0.977	1.007	0.881	-0.069	0.360

CHMP5	0.962	1.042	1.028	0.014	0.725	0.952	0.967	0.980	-0.049	0.057	0.904	0.956	0.870	-0.137	0.073
SNRPD2	0.983	0.981	1.021	-0.008	0.726	1.430	1.586	1.858	0.692	0.024	1.349	1.486	1.679	0.583	0.024
SBDS	1.013	1.027	0.923	-0.019	0.727	1.074	1.012	0.981	0.031	0.505	1.106	0.970	0.913	-0.010	0.917
TRPT1	1.106	1.083	0.901	0.037	0.733	1.206	1.079	0.673	-0.064	0.827	1.043	0.959	0.677	-0.188	0.428
GIGYF2	1.091	0.954	0.898	-0.032	0.736	0.612	0.493	0.684	-0.758	0.032	0.569	0.576	0.638	-0.753	0.005
ERC1;ERC2	0.848	1.205	1.104	0.058	0.739	0.870	1.676	0.918	0.140	0.689	0.987	1.724	0.826	0.164	0.660
PPIB	1.032	1.007	0.978	0.008	0.746	0.890	0.966	0.970	-0.087	0.166	0.831	0.918	0.903	-0.179	0.056
BRIX1	0.722	1.019	1.162	-0.076	0.748	1.540	1.777	1.101	0.530	0.122	2.070	1.784	0.885	0.570	0.271
SNUPN	0.908	0.836	1.177	-0.054	0.750	0.763	0.931	0.688	-0.344	0.115	0.934	0.947	0.887	-0.117	0.055
HGD	0.981	1.054	0.990	0.012	0.753	0.985	1.015	0.948	-0.026	0.456	1.064	0.922	0.916	-0.051	0.544
PICALM	0.999	1.089	0.958	0.020	0.753	1.106	1.093	0.925	0.054	0.587	1.045	1.030	1.078	0.071	0.067
UBE2D3;	1.167	1.025	0.905	0.038	0.754	0.974	0.998	0.901	-0.064	0.287	0.822	0.855	0.898	-0.221	0.026

UBE2D2															
PSMD11	0.876	1.056	1.190	0.046	0.755	1.096	1.263	1.637	0.393	0.146	1.173	1.042	1.231	0.196	0.111
UGDH	1.021	1.007	0.951	-0.011	0.760	0.991	1.106	0.973	0.031	0.646	0.910	1.103	1.032	0.017	0.851
SF3B3	1.035	0.965	1.024	0.011	0.765	1.625	1.648	1.772	0.749	0.003	1.635	1.700	1.704	0.748	0.001
SMC1A	0.676	1.303	1.449	0.117	0.766	0.808	0.896	1.042	-0.135	0.332	1.068	0.646	0.760	-0.311	0.283
PUS3	0.954	1.213	0.751	-0.067	0.768	0.721	0.802	3.624	0.356	0.683	0.838	0.637	4.802	0.452	0.669
SLK	0.930	0.979	1.181	0.035	0.770	1.636	1.477	1.715	0.684	0.009	1.544	1.444	1.343	0.528	0.012
EPS8L2	0.904	1.132	1.044	0.032	0.771	0.718	1.031	1.774	0.131	0.762	0.993	0.914	1.316	0.085	0.646
GSPT1	1.042	0.935	1.069	0.020	0.772	0.699	0.553	1.330	-0.320	0.487	0.688	0.686	1.025	-0.349	0.211
ATP6V1B2	0.901	1.014	1.046	-0.022	0.774	0.969	0.908	0.773	-0.186	0.195	0.957	0.797	0.706	-0.297	0.145
LSM6	1.045	1.000	0.976	0.009	0.775	0.549	0.589	0.530	-0.849	0.003	0.464	0.544	0.529	-0.968	0.005

RAB39A;RAB6A;RAB6B	0.969	1.021	1.029	0.009	0.777	1.000	1.211	1.121	0.147	0.209	1.022	1.170	0.860	0.013	0.926
CDC5L	1.187	0.665	1.072	-0.080	0.784	0.849	0.948	1.865	0.195	0.638	0.879	1.893	1.672	0.492	0.288
PUS7	1.008	0.889	1.064	-0.023	0.791	0.689	0.730	0.683	-0.513	0.003	0.709	0.908	0.759	-0.345	0.084
NAA15	0.982	1.004	1.025	0.005	0.793	1.207	1.095	1.010	0.139	0.203	1.197	1.026	0.960	0.080	0.487
HSPA6	1.059	0.901	1.004	-0.020	0.795	0.724	0.796	0.763	-0.395	0.010	0.639	0.850	0.813	-0.393	0.092
BUD31	0.984	0.968	1.084	0.015	0.795	0.568	0.605	0.584	-0.772	0.001	0.561	0.597	0.501	-0.859	0.007
DIS3	0.975	1.194	0.768	-0.054	0.797	1.238	0.905	0.884	-0.005	0.980	1.503	0.700	1.275	0.141	0.715
SRSF1	1.248	0.910	0.780	-0.058	0.799	2.727	2.961	3.439	1.598	0.004	2.411	3.366	4.173	1.694	0.018
GANAB	1.092	0.893	0.975	-0.024	0.800	0.440	0.529	0.490	-1.044	0.005	0.387	0.632	0.531	-0.981	0.042
TUBB8;RP11-631M21.2	0.855	1.208	1.054	0.041	0.806	1.059	1.384	1.113	0.235	0.186	0.980	1.206	1.041	0.099	0.381

CAD	1.149	0.934	0.869	-0.033	0.808	0.759	0.683	0.696	-0.490	0.009	0.844	0.817	0.828	-0.269	0.003
LLGL2	1.119	0.808	1.022	-0.038	0.811	0.743	0.504	0.575	-0.739	0.046	0.752	0.631	0.625	-0.585	0.021
STAU1	0.999	1.057	0.966	0.010	0.817	0.807	1.623	1.241	0.234	0.510	0.959	1.407	1.056	0.170	0.413
HARS2;HARSL	0.898	1.075	1.088	0.024	0.817	1.035	1.136	1.180	0.157	0.107	1.062	1.077	0.987	0.058	0.277
TROVE2	1.066	0.868	1.029	-0.023	0.823	0.882	0.955	0.992	-0.087	0.226	0.830	1.072	0.924	-0.095	0.470
SEC24B	0.775	1.091	1.088	-0.041	0.828	1.187	1.017	0.810	-0.011	0.952	1.551	1.118	0.746	0.124	0.724
EHD4	0.962	0.992	1.073	0.011	0.830	1.946	0.927	2.000	0.617	0.231	2.189	0.959	1.838	0.649	0.215
TRMT112	1.061	0.969	0.948	-0.012	0.831	0.630	0.750	0.785	-0.477	0.039	0.532	0.782	0.737	-0.568	0.081
LMNA	1.271	1.191	0.745	0.058	0.833	1.870	1.738	1.113	0.618	0.118	1.419	1.377	1.338	0.462	0.003
OGFR	0.895	1.349	0.912	0.046	0.834	1.456	1.780	1.781	0.735	0.017	1.643	1.548	1.799	0.731	0.007
PARD6B	1.088	0.928	1.024	0.016	0.837	1.255	1.035	1.477	0.313	0.169	1.001	1.033	0.961	-0.003	0.922
PPP6R3	1.195	0.765	0.999	-0.044	0.837	0.540	0.509	1.067	-0.590	0.228	0.697	0.667	0.884	-0.428	0.077

UXT	1.147	1.267	0.765	0.051	0.839	1.417	1.784	0.766	0.318	0.475	1.241	1.323	0.823	0.145	0.569
TMEM62	1.280	0.907	0.778	-0.048	0.841	1.901	0.841	0.876	0.162	0.713	1.592	0.962	1.004	0.206	0.469
PKP2	0.695	1.125	1.490	0.073	0.841	1.086	1.465	1.747	0.492	0.133	1.313	1.306	1.366	0.409	0.002
SEPHS1	1.184	0.947	0.939	0.025	0.843	1.267	1.352	1.162	0.331	0.035	1.082	1.543	1.213	0.340	0.153
HTATIP2	1.103	0.721	1.430	0.062	0.849	0.769	0.859	1.206	-0.109	0.633	0.688	0.725	0.745	-0.476	0.005
OSTF1	1.028	0.988	0.975	-0.005	0.854	0.779	0.941	0.831	-0.238	0.097	0.667	0.842	0.724	-0.433	0.048
CCNH	0.870	1.252	0.848	-0.038	0.854	0.948	1.657	0.905	0.169	0.608	1.119	1.264	1.177	0.245	0.041
CSE1L	1.034	0.985	0.991	0.004	0.858	1.000	1.078	1.071	0.069	0.183	1.050	1.095	1.086	0.107	0.029
KIF21A	1.118	0.909	0.948	-0.018	0.859	0.458	0.443	0.311	-1.329	0.018	0.536	0.516	0.361	-1.108	0.026
COPS3	0.866	0.999	1.109	-0.020	0.865	0.573	0.742	0.674	-0.601	0.031	0.597	0.758	0.751	-0.519	0.044
NXF1	1.020	1.057	0.946	0.009	0.866	0.589	0.986	1.138	-0.199	0.562	0.817	0.908	1.201	-0.055	0.770
MYL6	0.862	1.022	1.197	0.026	0.869	0.773	1.039	0.832	-0.194	0.269	0.811	1.015	0.683	-0.277	0.236
41884	0.852	0.861	1.267	-0.035	0.869	1.761	1.777	2.237	0.936	0.014	1.945	2.388	1.751	1.008	0.017

USP19	0.894	0.996	1.088	-0.015	0.871	1.656	1.955	1.389	0.723	0.037	1.488	1.995	1.357	0.670	0.057
ARPC2	0.856	1.128	0.995	-0.019	0.883	1.153	1.160	1.014	0.146	0.146	1.181	1.054	1.071	0.138	0.114
FUBP1	1.056	1.022	0.943	0.008	0.885	0.937	0.989	0.887	-0.094	0.174	0.852	0.960	0.894	-0.150	0.094
LSM4	0.987	1.002	1.015	0.002	0.887	0.545	0.619	0.652	-0.728	0.011	0.514	0.634	0.662	-0.737	0.022
ARL1	1.122	1.009	0.910	0.014	0.887	0.909	0.983	0.871	-0.121	0.143	0.771	1.024	1.009	-0.109	0.497
MICU1	1.145	0.953	0.883	-0.018	0.888	1.405	0.855	0.940	0.058	0.816	1.200	0.918	1.078	0.083	0.537
BAIAP2L1	0.905	1.392	0.725	-0.043	0.890	0.859	1.614	0.484	-0.192	0.739	0.847	1.144	0.620	-0.245	0.438
UGP2	1.020	0.955	1.016	-0.005	0.891	0.622	0.646	0.615	-0.672	0.001	0.643	0.677	0.553	-0.685	0.016
IKBKAP	1.076	0.862	1.045	-0.016	0.891	0.996	1.012	0.876	-0.060	0.458	0.771	1.650	0.896	0.063	0.868
OXSR1	0.964	1.049	0.977	-0.006	0.892	0.830	0.711	0.818	-0.351	0.039	0.863	0.833	0.837	-0.245	0.004
EIF3J	0.908	1.032	1.093	0.012	0.896	0.504	0.867	1.634	-0.162	0.772	0.753	0.894	1.205	-0.101	0.662
VPS33B	0.987	1.188	0.813	-0.023	0.897	0.332	0.324	1.608	-0.845	0.385	0.328	0.266	1.984	-0.843	0.456
CACYBP	0.997	1.143	0.904	0.014	0.899	0.877	0.812	0.961	-0.182	0.122	0.908	0.875	0.882	-0.171	0.009

IQGAP2	0.942	1.014	1.063	0.007	0.902	0.389	0.776	0.665	-0.772	0.125	0.563	0.791	0.643	-0.601	0.052
DTD1	1.259	0.900	0.840	-0.024	0.908	1.243	1.117	0.685	-0.024	0.935	0.876	0.869	0.732	-0.281	0.079
DNASE2	0.900	1.046	1.045	-0.008	0.923	0.810	0.920	0.916	-0.183	0.093	0.771	0.837	0.782	-0.329	0.012
CCT5	0.978	0.973	1.043	-0.003	0.928	1.364	1.297	1.260	0.386	0.007	1.336	1.287	1.208	0.351	0.014
THUMPD1	1.054	0.928	1.034	0.006	0.931	0.807	0.840	0.916	-0.229	0.052	0.729	0.839	0.924	-0.274	0.110
TNS3;TNS 1;TENC1	0.738	1.230	1.057	-0.020	0.935	0.758	1.011	0.965	-0.145	0.376	1.001	0.928	0.928	-0.072	0.187
RAB21	1.252	0.896	0.866	-0.014	0.941	1.691	1.176	1.106	0.379	0.185	1.361	1.243	1.244	0.358	0.015
TBCE	0.879	1.081	1.069	0.008	0.943	0.926	1.088	0.992	-0.001	0.994	0.649	0.956	0.888	-0.287	0.236
HSPA14	1.001	1.092	0.925	0.005	0.944	0.741	0.634	0.582	-0.624	0.026	0.686	0.695	0.644	-0.567	0.003
CSNK1A1	1.038	1.077	0.906	0.006	0.946	1.438	1.298	1.043	0.320	0.144	1.296	1.326	1.121	0.315	0.053
PA2G4	1.015	0.983	1.000	-0.001	0.950	1.176	1.025	1.133	0.150	0.127	1.152	1.004	1.114	0.122	0.178
CYFIP2	1.088	0.857	1.091	0.008	0.951	1.120	0.947	1.191	0.112	0.373	1.134	1.108	0.917	0.068	0.556

SRSF2;SFRS2	0.988	1.046	0.964	-0.002	0.953	1.184	1.364	1.362	0.379	0.030	1.187	1.273	1.214	0.292	0.010
GTF2F1	1.140	0.674	1.356	0.020	0.954	0.735	0.627	0.977	-0.384	0.176	0.598	0.672	0.887	-0.496	0.098
SPATS2	0.930	1.051	1.018	-0.003	0.964	1.202	1.134	1.023	0.160	0.144	1.148	1.025	0.930	0.043	0.670
OVCA2	1.216	0.926	0.875	-0.007	0.965	0.959	0.877	0.936	-0.115	0.095	0.705	0.845	0.944	-0.277	0.153
FGA	1.212	0.832	0.976	-0.008	0.965	1.062	1.183	1.001	0.110	0.259	1.004	1.060	0.892	-0.026	0.761
ZNFX1	1.161	0.980	0.889	0.005	0.966	0.500	0.586	0.572	-0.859	0.007	0.525	0.571	0.531	-0.884	0.002
CYCS	0.960	1.041	0.997	-0.002	0.966	0.939	0.951	0.959	-0.075	0.014	0.908	0.818	0.919	-0.184	0.075
NRD1	1.073	0.802	1.147	-0.007	0.970	0.371	0.487	0.522	-1.135	0.017	0.323	0.612	0.482	-1.130	0.052
WASL	0.985	1.074	0.949	0.002	0.971	0.841	0.955	0.836	-0.192	0.092	0.826	0.938	0.859	-0.196	0.069
RAB8B;RAB13	1.105	0.915	0.982	-0.003	0.971	0.584	0.638	0.727	-0.628	0.021	0.577	0.664	0.769	-0.587	0.039
ELAVL1	1.155	0.929	0.923	-0.004	0.972	0.955	0.875	0.857	-0.161	0.079	0.886	0.866	0.802	-0.233	0.033

HNRNPUL1	1.056	0.935	1.009	-0.002	0.972	1.080	1.103	1.081	0.122	0.006	1.109	1.054	1.091	0.117	0.033
MPG	1.145	0.818	1.079	0.005	0.977	1.573	1.560	1.933	0.749	0.018	1.358	1.769	1.697	0.676	0.029
ILKAP	1.216	0.936	0.871	-0.005	0.978	2.703	1.999	1.976	1.139	0.016	1.611	1.758	2.021	0.839	0.013
CSK	0.729	0.986	1.373	-0.006	0.983	1.068	0.956	1.383	0.166	0.404	1.220	0.887	1.005	0.040	0.791
OPA1	0.920	1.132	0.956	-0.002	0.985	0.996	1.126	1.011	0.060	0.393	0.984	0.850	0.924	-0.124	0.181
HK1	1.125	0.858	1.041	0.002	0.985	1.465	0.840	0.808	-0.003	0.992	1.120	1.024	0.881	0.005	0.966
SMG8	1.176	1.110	0.771	0.003	0.988	2.377	2.297	0.852	0.739	0.267	1.933	2.687	1.150	0.859	0.137
SEC24D	0.912	0.989	1.111	0.001	0.989	1.070	1.006	1.145	0.101	0.202	1.105	1.047	1.016	0.077	0.160
DECR1	1.109	1.159	0.773	-0.003	0.989	1.204	1.106	1.114	0.190	0.040	1.158	1.137	1.366	0.282	0.078
NTPCR;C1orf57	0.987	1.001	1.013	0.000	0.992	0.797	0.808	0.849	-0.290	0.009	0.821	0.777	0.738	-0.362	0.015
TOMM34	1.401	0.973	0.733	0.000	1.000	1.990	1.615	1.231	0.662	0.081	1.224	1.626	1.205	0.420	0.096